GRANULAR DYNAMICS OF GAS-SOLID TWO-PHASE FLOWS

PROEFSCHRIFT

ter verkrijging van
de graad van doctor aan de Universiteit Twente,
op gezag van de rector magnificus,
prof.dr. F.A. van Vught,
volgens besluit van het College voor Promoties
in het openbaar te verdedigen
op vrijdag 21 januari 2000, te 16.45 uur.

door

Bob Petrus Bernardus Hoomans

geboren op 2 augustus 1971
te Oldenzaal.

Dit proefschrift is goedgekeurd door de promotoren

prof.dr.ir. J.A.M. Kuipers

prof.dr. W.J. Briels

prof.dr.ir. W.P.M. van Swaaij

Samenstelling promotiecommissie:

prof.dr. W.E. van der Linden, voorzitter	Universiteit Twente
prof.dr.ir. J.A.M. Kuipers, promotor	Universiteit Twente
prof.dr. WJ. Briels, promotor	Universiteit Twente
prof.dr.ir. W.P.M. van Swaaij, promotor	Universiteit Twente
prof.dr. J.P.K. Seville	University of Birmingham, UK
prof.dr.ing. B.H. Hjertager	Aalborg University Esbjerg, DK
prof.ir. C.M. van den Bleek	Technische Universiteit Delft
prof.dr.ir M.M.C.G. Warmoeskerken	Universiteit Twente
prof.dr.ir. G.F. Versteeg	Universiteit Twente

Cover: snapshots of a simulation with a ternary density distribution (Chapter 6)

Second impression august 2001

ISBN 90-3651401

Contents

3. GAS PHASE HYDRODYNAMICS

4. THE EFFECT OF PARTICLE PROPERTIES ON THE HYDRODYNAMICS OF GAS-FLUIDISED BEDS WITH HOMOGENEOUS INFLOW CONDITIONS

5. GRANULAR DYNAMICS SIMULATION OF BUBBLE FORMATION IN A GAS-FLUIDISED BED: HARD-SPHERE VS. SOFT-SPHERE APPROACH

6. GRANULAR DYNAMICS SIMULATION OF SEGREGATION PHENOMENA IN BUBBLING GAS-FLUIDISED BEDS

Summary

Gas-solid two-phase flows are encountered in a wide variety of industrial applications. The complex hydrodynamics of these systems is still not fully understood which renders the scale-up of these units difficult. Therefore the development and validation of fundamental hydrodynamic models is of utmost importance to gain more insight into the complex hydrodynamics.

The study reported in this thesis is concerned with the granular dynamics of gas-solid two-phase flows. In granular dynamics simulations the Newtonian equations of motion are solved for each individual particle in the system while taking into account the mutual interaction between particles and between particles and walls. The gas-phase hydrodynamics is described by the volume averaged Navier-Stokes equations for two-phase flow. The gas-phase flow is resolved on a length scale that is larger than the particle size. Two types of discrete particle models have been developed to be incorporated into the granular dynamics simulations. The first is a (2-D and 3-D) hard-sphere model where the particles are assumed to interact through instantaneous, binary collisions. A sequence of collisions is processed one collision at a time. The second is a (2-D) soft-sphere linear spring/dash-pot model where contact forces between the particles are calculated from the overlap between the particles. This soft-sphere model was chosen since it is the most frequently used model in the literature and hence it is best suited for a comparison with the hard-sphere model. The key collision parameters in both models are the coefficient of restitution ($1 \geq e \geq 0$), the coefficient of friction ($\mu \geq 0$) and the coefficient of tangential restitution ($1 \geq \beta_0 \geq 0$). The linear spring/dash-pot model also requires a spring stiffness to describe the particle interaction. The soft-sphere model is capable of handling multiple particle interactions and can handle static situations in contrast to the hard-sphere model.

The effect of the collision parameters on the bed dynamics in a gas-fluidised bed with homogeneous inflow conditions was investigated. The collision parameters (except for

b_0) turned out to have a profound influence on the fluidisation behaviour. When the collisions were assumed to be fully elastic and perfectly smooth ($e = 1$, $m = 0$) no bubbles were observed and pressure fluctuations inside the bed were rather small. When more realistic values for the collision parameters were used ($e < 1$, $m > 0$) bubbles did appear and the pressure fluctuations were larger. These trends were observed in 2-D simulations as well as in 3-D simulations. The Root Mean Square (RMS) of the pressure fluctuations inside the bed showed an almost linear dependency on the energy dissipation rate by collisions during the simulation at low values of the energy dissipation rate. The influence of a (log-normal) particle size distribution on the bed dynamics was less pronounced than the influence of the collision parameters. When a wider size distribution was taken into account the pressure peaks inside the bed were smaller.

The case of bubble formation at a single central orifice was chosen for a comparison between the (2-D) hard-sphere model and the (2-D) soft-sphere model. Preliminary soft-sphere simulations revealed that a minimum value of the spring stiffness was required to ensure stable simulations. For higher values of the spring stiffness the influence of the value of the spring stiffness on the simulation results was negligible but the required CPU time increased significantly. Incorporation of a (log-normal) particle size distribution improved the agreement between simulation and experiment. Hardly any difference could be observed between the results of the hard-sphere simulations and the soft-sphere simulations indicating that the assumption of binary collisions in the hard-sphere model is not limiting. With both types of models it was found that the assumption of fully elastic and perfectly smooth collisions resulted in much worse agreement between simulation and experiment: hardly any bubble could be observed.

Segregation was successfully simulated with the (2-D) hard-sphere model for systems consisting of particles of equal size but different density as well as for systems consisting of particles of equal density but different size. In the latter case a clear steady state was not reached since the larger particles were continuously transported to the upper layers of the bed in bubble wakes. A statistical analysis showed a rather wide spread in segregation profiles indicating the limited value of a single frame analysis. A simulation assuming

fully elastic and perfectly smooth collisions showed a rapid and almost perfect segregation due to the absence of bubbles in this system. Preliminary experimental validation showed rather poor agreement between simulation and experiment. The simulation predicted segregation at a lower gas velocity than used in the experiment.

The results of simulations of the riser section of a circulating fluidised bed proved to be very sensitive with respect to the collision parameters. In the case of fully elastic and perfectly smooth collisions hardly any clustering of particles could be observed as opposed to the case where these collision parameters were assigned realistic values. Particle-wall collisions turned out to have very little influence on the flow structure. A strong effect of the collision properties on the axial solids profile was found where a pronounced build-up of solids was observed in the simulation with realistic values for the collision parameters. In the simulation assuming fully elastic and perfectly smooth collisions no build-up of solids was observed. This result is supported by experimental findings reported in the open literature. Lift forces acting on the suspended particles turned out to have a slightly redispersive effect on the flow structure which made the radial segregation of the solids a little less pronounced.

The (2-D) hard-sphere model was experimentally validated using the Positron Emission Particle Tracking (PEPT) facility at the University of Birmingham. A quasi 2-D, gas-fluidised bed with homogeneous inflow conditions was used for the validation. In the experiment the motion of a single tracer particle was tracked during one hour. The PEPT data was time-averaged to allow for a comparison with the results of a simulation where 15,000 particles were tracked during 45 seconds. The collision parameters required for the simulation were obtained from independent measurements at the Open University at Milton Keynes. The results showed good agreement between experiment and simulation when the measured values for the collision parameters were used. When the collisions were assumed to be fully elastic and perfectly smooth the agreement was much worse.

Samenvatting

Gas-vast tweefasenstromingen vormen een belangrijk onderdeel van een grote verscheidenheid aan industriële processen. Het opschalen van dergelijke processen wordt bemoeilijkt door de complexiteit van de hydrodynamica van dergelijke systemen. Het is daarom van het grootste belang meer inzicht te krijgen in deze complexe hydrodynamica door het ontwikkelen en valideren van fundamentele hydrodynamische modellen.

Het onderzoek dat ten grondslag ligt aan dit proefschrift houdt zich bezig met de granulaire dynamica van gas-vast tweefasenstromingen. In granulaire dynamica simulaties worden de Newtonse bewegingsvergelijkingen opgelost voor elk individueel granulair deeltje in het systeem waarbij de interactie tussen deeltjes onderling alsmede de interactie tussen deeltjes en systeemwanden wordt verdisconteerd. De hydrodynamica van de gasfase wordt beschreven door de volume-gemiddelde Navier-Stokes vergelijkingen voor tweefasenstroming. De stroming van de gasfase wordt opgelost op een lengteschaal die groter is dan de grootte van een afzonderlijk vaste stof deeltje. Voor de granulaire dynamica simulaties zijn twee soorten discrete deeltjes modellen ontwikkeld. De eerste is een (2-D en 3-D) harde bollen model waar de interactie tussen de deeltjes wordt verondersteld te verlopen via instantane, binaire botsingen. De opeenvolgende botsingen worden hierbij één voor één afgehandeld in chronologische volgorde. Het tweede model is een (2-D) zachte bollen lineaire-veer/smoorpot model waarbij de contactkrachten tussen de deeltjes worden berekend uit hun onderlinge overlap. Dit zachte bollen model is gekozen omdat het het meest gebruikt is in de literatuur en daardoor het best geschikt is voor een vergelijk met het harde bollen model. De belangrijkste botsingsparameters in beide modellen zijn de restitutiecoëfficiënt ($1 \geq e \geq 0$), de frictiecoëfficiënt ($m \geq 0$) en de tangentiele restitutiecoëfficiënt ($1 \geq b_0 \geq 0$). In het lineaire-veer/smoorpotmodel is behalve deze parameters ook nog een veerkonstante vereist om de deeltjesinteractie te beschrijven. In tegenstelling tot het harde bollen model

is het zachte bollen model in staat om meervoudige deeltjesinteractie te verdisconteren en tevens is het geschikt om statische situaties te simuleren.

De invloed van de botsingsparameters op het stromingsgedrag van een gas-gefluidiseerd bed met homogene instroomcondities is onderzocht. De botsingsparameters (met uitzondering van b_0) bleken een grote invloed te hebben op het fluïdisatiegedrag. Als werd aangenomen dat de botsingen volledig elastisch en perfect glad verliepen ($e = 1$, $m = 0$) werden geen bellen waargenomen en waren de drukfluctuaties in het bed klein. Met realistische waarden voor de botsingsparameters ($e < 1$, $m > 0$) werden wel bellen waargenomen en waren de drukfluctuaties in het bed aanzienlijk groter. Deze trend werd zowel in 2-D als in 3-D simulaties waargenomen. De gemiddelde kwadratische waarde van de drukfluctuaties vertoonde een zo goed als lineaire afhankelijkheid van de energiedissipatiesnelheid bij lage waarden van deze laatste. The invloed van een (log-normale) deeltjesgrootteverdeling op het fluïdisatiegedrag was minder groot dan de invloed van de botsingsparameters. Met een bredere deeltjesgrootteverdeling werden de drukpieken in het bed iets lager.

Een vergelijk tussen het (2-D) zachte bollen en het (2-D) harde bollen model werd gemaakt aan de hand van simulaties van belvorming aan een centraal inspuitpunt. Verkennende berekeningen met het zachte bollen model lieten zien dat een minimum waarde van de veerkonstante vereist was om verzekerd te zijn van een stabiele simulatie. Voor hogere waarden van de veerkonstante werd de invloed ervan op de resultaten van de simulaties verwaarloosbaar waarbij echter wel de benodigde rekentijd drastisch toenam. Wanneer een (log-normale) deeltjesgrootteverdeling werd verdisconteerd verbeterde de overeenkomst tussen simulatie en experiment aanzienlijk. Er kon echter nauwelijks enig verschil worden waargenomen tussen de resultaten van het harde bollen model en die van het zachte bollen model. Dit gaf aan dat de aanname van binaire botsingen in het harde bollen model niet beperkend is. Met beide typen modellen werd de overeenkomst tussen simulatie en experiment veel slechter wanneer een simulatie werd uitgevoerd onder de aanname van volledig elastische en perfect gladde botsingen.

Het (2-D) harde bollen model werd met succes ingezet bij het simuleren van segregatie in systemen die bestaan uit deeltjes van gelijke grootte maar verschillende dichtheid alsmede systemen bestaande uit deeltjes van gelijke dichtheid maar verschillende grootte. In dit laatste geval werd geen stationaire toestand bereikt omdat de deeltjes continu omhoog werden getransporteerd in het zog van bellen. Een statistische analyse liet een grote spreiding zien in het segregatieprofiel wat aangeeft dat een analyse op basis van een tijdsopname beperkte waarde heeft. Een simulatie waarbij de botsingen volledig elastisch en perfect glad werden verondersteld liet een zeer snelle en bijna volledige segregatie zien wat toegeschreven kon worden aan de afwezigheid van bellen in dit systeem. Een eerste experimentele validatie liet een matige overeenkomst zien tussen simulatie en experiment. De simulatie voorspelde segregatie bij lagere gassnelheden.

In simulaties van de riser-sectie van een circulerend gefluïdiseerd bed werd gevonden dat het stromingsgedrag sterk afhankelijk is van de botsingsparameters. Clustervorming werd niet of nauwelijks waargenomen als de botsingen volledig elastisch en perfect glad werden verondersteld. Met realistische waarden voor deze parameters kon clustervorming wel degelijk worden waargenomen. De botsingsparameters voor deeltjes-wand botsingen bleken nauwelijks invloed op het stromingsgedrag te hebben. In de simulatie met realistische waarden voor de botsingsparameters werd een duidelijke opbouw van een axiaal vaste stof profiel geconstateerd in tegenstelling tot de simulatie met ideale botsingsparameters. Dit is in overeenstemming met experimenteel waargenomen trends gerapporteerd in de open literatuur. Liftkrachten bleken slechts een klein dispersief effect te hebben wat er toe bij droeg dat de radiële segregatie van de vaste stof wat minder groot was.

Het (2-D) harde bollen model werd experimenteel gevalideerd met behulp van Positron Emission Particle Tracking (PEPT) experimenten uitgevoerd aan de universiteit van Birmingham. Een quasi 2-D gas-gefluïdiseerd bed met homogene instroomcondities werd gebruikt voor de validatie. In het PEPT experiment werd de beweging van een tracer-deeltje gevolgd gedurende een uur. De data van dit experiment werd tijd-gemiddeld om een vergelijk mogelijk te maken met een simulatie waarin 15000 deeltjes werden gevolgd

gedurende 45 seconden. De botsingsparameters benodigd voor de simulatie werden onafhankelijk gemeten aan de Open University in Milton Keynes. De resultaten van een simulatie waarin deze waarden werden gebruikt vertoonde goede overeenstemming met het experiment. De overeenstemming tussen het experiment en een simulatie waarin de botsingen volledig elastisch en perfect glad werden verondersteld was beduidend minder goed.

Chapter 1.

GENERAL INTRODUCTION

Abstract:

In this chapter a brief introduction to fluidisation is presented. The hydrodynamics of gas-fluidised beds is very complex and still not very well understood which renders the scale-up of these units difficult. Therefore fundamental hydrodynamic models are required to gain more insight into the hydrodynamics of gas-fluidised beds. These fundamental models can be classified into three categories based on the level of microscopy featured in the model. In this thesis the focus is on discrete particle models which form the intermediate category in the concept of multi-scale modelling. The position of discrete particle models within the multi-scale modelling concept is explained and the objective of the work presented in this thesis is formulated. Finally the outline of this thesis is presented.

1. Fluidisation

Gas-fluidised beds are widely applied in the chemical process industry (Kunii and Levenspiel, 1991) because of several advantageous properties including isothermal conditions throughout the bed, excellent heat and mass transfer properties and the possibility of continuous operation. Typical applications cover a wide variety of physical and chemical processes such as fluidised bed combustion, catalytic cracking of oil, gas-phase polymerisation of olefins and fluidised bed granulation (detergents, fertilisers) to name a few.

In gas-fluidised beds the gravity force acting on the solid particles is compensated by the drag forces exerted on the particles by the upward flowing gas. The minimum fluidisation velocity (u_{mf}) is defined as the superficial gas velocity at which the gravity force acting on the particles is just counterbalanced by the drag forces exerted on the particles by the gas phase. When operated at gas velocities above u_{mf} several regimes are encountered. The three regimes that are featured in this thesis are presented in Figure 1.1. In this figure the gas velocity increases from left to right.

Figure 1.1. *The three fluidisation regimes featured in this thesis. From left to right: the bubbling regime, the slug flow regime and the fast fluidisation regime.*

At velocities exceeding u_{mf} usually gas bubbles are present in the bed. These bubbles have a decisive influence on the hydrodynamics of a bubbling fluidised bed and hence on its performance as a chemical reactor and/or a heat exchange unit. When the gas velocity is increased further also the size of the bubbles increases. The bubble size may approach the bed diameter in which case the slug flow regime prevails. When the gas velocity is increased beyond the terminal fall velocity of the particles the fast fluidisation regime is encountered. In this regime the particles are entrained with the gas flow and transported upward through the riser. At the top of the riser the particles are separated from the gas in a cyclone and fed back to the bottom of the riser. Such systems are commonly referred to as Circulating Fluidised Beds (CFB's). In between the slug flow and the fast fluidisation regime the turbulent fluidisation regime can be distinguished and when the gas velocity is further increased starting in the fast fluidisation regime the pneumatic transport regime is encountered. In this thesis however, the focus is on the bubbling, slug flow, and fast fluidisation regime.

Although gas-fluidised beds are widely applied, the scale-up of these systems is still very complicated which is mainly due to the complex hydrodynamics of these systems. Therefore it is of crucial importance to develop a thorough understanding of the hydrodynamics of gas-fluidised beds. Together with the development of dedicated experimental techniques the development of fundamental hydrodynamic models is of utmost importance to achieve a better understanding of fluidisation. Eventually this will lead to the improvement of existing processes, improved scale-up and the design of more efficient future processes. In the work presented in this thesis the development of such a fundamental hydrodynamic model is described and the results obtained with it are presented.

2. Hydrodynamic modelling

During the last few decades Computational Fluid Dynamics (CFD) has become a very powerful and versatile tool for the numerical analysis of transport phenomena (Kuipers

and van Swaaij, 1998). With continuously increasing computer power combined with the development of improved physical models CFD has become a very useful tool for chemical engineers. CFD modelling of gas-fluidised beds has proven to be successful and new developments in this area are promising. The majority of studies on modelling of fluidised beds is concerned with the hydrodynamics only. Although attempts have been reported where the hydrodynamics were modelled combined with mass transfer and chemical reaction (Samuelsberg and Hjertager (1996), Gao *et al*., 1999) the results of such attempts depend strongly on how well the hydrodynamics is modelled. Kuipers *et al.* (1998) demonstrated that the predicted performance of a riser reactor in terms of chemical conversion depends strongly on the prevailing flow structure in the riser. If the flow structure is not well captured by the hydrodynamic model a sensible prediction of the reactor performance is impossible. Therefore the development of reliable hydrodynamic models is of utmost importance in order to arrive ultimately at models that are capable of predicting the performance of fluidised beds reactors. Hence, the focus of the present study is on the hydrodynamics only.

2.1 Multi-scale modelling

Due to the complexity of the hydrodynamics of multi-phase flows it has become accepted that a single generalised CFD model cannot cover the wide variety of phenomena encountered in multi-phase flows (Delnoij *et al*. 1997, Kuipers and van Swaaij, 1997). Instead, specific models have to be developed that are tailor made to capture the relevant phenomena occurring at the length scale to which they are applied. By incorporating microscopic information from sub scale models and passing on information to super scale models a multi-scale modelling concept can be established.

Three different classes of fundamental hydrodynamic models (learning models according to van Swaaij, 1985) of gas-fluidised beds can be distinguished. These models can be combined together in a multi-scale concept for fundamental hydrodynamic models of gas-fluidised beds as is schematically represented in Figure 1.2.

In order to model a large (industrial) scale fluidised bed a continuum model, where the gas phase and the solids phase are regarded as interpenetrating continuous media, is the appropriate choice. This Eulerian-Eulerian type of model have been developed and successfully applied over the last two decades (Kuipers *et al*., 1992, Gidaspow, 1994 among many others). These models require closure relations for the solids phase stress tensor and the fluid-particle drag where commonly empirical relations are used in the absence of more accurate closures. Improved closure relations for the solids phase stress tensor can be obtained by using the kinetic theory of granular flow (Sinclair and Jackson, 1989, Nieuwland *et al*., 1996, among many others).

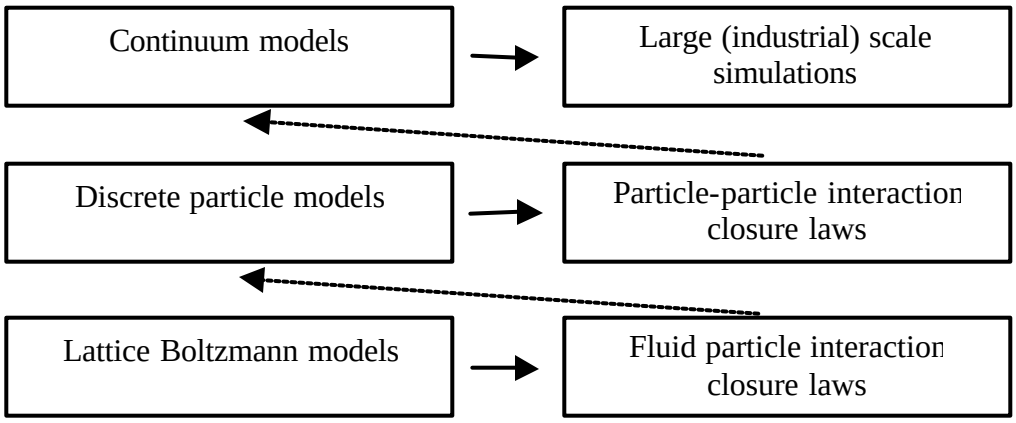

Figure 1.2. *Multi-scale modelling concept for fundamental hydrodynamic models of gas-fluidised beds.*

In discrete particle models the Newtonian equations of motion are solved for each individual solid particle in the system. In this Eulerian-Lagrangian type of model a closure relation for the solids phase rheology is no longer required since the motion of the individual particles is solved directly. However, the number of particles that can be taken into account in this technique is limited ($< 10^{-6}$). Therefore it is not yet possible, even with modern day super computers, to simulate a large (industrial) scale system. However, this type of model can be used to arrive at improved closure equations for continuum models by employing techniques from statistical mechanics. Also assumptions made

within the framework of the kinetic theory of granular flow, as incorporated in advanced continuum models, can be verified. Since discrete particle models are very well suited to study the influence of particle properties on the hydrodynamics of gas-fluidised beds this makes them very useful models within the multi-scale modelling concept. However, discrete particle models still require closure relations for the fluid-particle drag since the gas flow is resolved on a length scale larger than the particle size. In the absence of better closures empirical relations for the fluid-particle drag have to be used.

When the gas flow is resolved on a length scale smaller than the particle size these closure relations for fluid-particle drag are no longer required. Instead they can actually be obtained from the simulations. The Lattice Boltzmann technique seems to be best suited for such simulations because it is very flexible in dealing with complex flow geometries. In Chapter 3 some additional techniques besides Lattice Boltzmann simulations are presented that can be used for the same purpose. It is important to realise that such simulations are limited to systems consisting of a number of particles that is significantly smaller ($<10^{-3}$) than the number of particles that can be taken into account using discrete particle models ($<10^{-6}$).

In short the multi-scale concept as presented in Figure 1.2 consists of three classes of models where more detail of the two-phase flow is resolved going from continuum models to discrete particle models to Lattice Boltzmann models. This goes at the cost of increased computational requirements which necessitates a size reduction of the simulated system. The model capable of simulating a larger system is fed with a closure relation obtained from a more microscopic simulation. In return the results of these simulations can be used to pass on information to models capable of simulating the flow on a larger scale. Before such a connection between separate scales can be established the individual simulation techniques must be well developed, verified and experimentally validated. In the work presented in this thesis the focus is on the development and the use of discrete particle models.

3. Discrete particle modelling

In granular dynamics simulations of gas-fluidised beds the Newtonian equations of motion are solved for each individual solid particle by using a discrete particle model. For the fluid-particle interaction empirical relations have to be used since the hydrodynamics of the gas-phase is resolved on a length scale larger than the particle size.

The discrete particle approach for gas-fluidised beds was pioneered by Tsuji *et al.* (1993) who developed a two-dimensional soft-sphere discrete particle model of a gas-fluidised bed based on the work of Cundall and Strack (1977). Kawaguchi *et al.* (1998) extended this model to three dimensions as far as the motion of the particles is concerned. Hoomans *et al*. (1996) presented a hard-sphere approach in their two-dimensional discrete particle model of a gas-fluidised bed. Ouyang and Li (1998) developed a slightly different version of this model. Xu and Yu (1997) presented a hybrid simulation technique that features elements from both hard-sphere and soft-sphere techniques. Mikami *et al*. (1998) extended the model originally developed by Tsuji *et al*. (1993) to include cohesive forces between the particles. Recent developments in this area include the (2-D) simulation of fluidised bed with internals (Rong *et al*., 1999) and the (2-D) simulation of gas-phase olefin polymerisation (Kaneko *et al*., 1999) where energy balances and chemical reaction rates were taken into account.

As far as particle interaction is concerned a multi-scale modelling concept can be distinguished as is schematically presented in Figure 1.3. As mentioned in the previous section continuum models require closure relations for the solids phase rheology (*i.e.* viscosity, solids phase pressure). These relations can be obtained from discrete particle models by employing techniques from statistical mechanics. Discrete particle models can also be used to verify assumptions made in the kinetic theory of granular flow which is used in most of the recently developed continuum models.

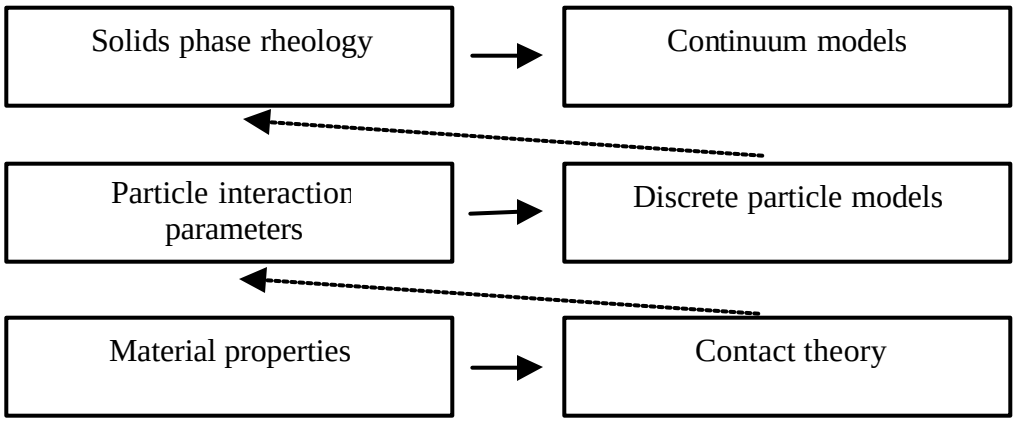

Figure 1.3. *Multi-scale modelling concept for models involving particle interaction.*

The particle interaction parameters required for the discrete particle models can be obtained from experiments as was the case in the work presented in this thesis. However, it is important to realise that these parameters can also be obtained from microscopic particle interaction models. By using the appropriate contact theory the particle interaction parameters can be obtained using only material properties as input. In this way a multi-scale concept for particle-interaction models arises. Transport properties for the solids-phase in a continuum model are obtained from discrete particle models and the particle interaction parameters required in discrete particle models are obtained from contact theory based on material properties.

4. Outline of this thesis

The objective of the work presented in this thesis is to study the influence of particle properties on the dynamics of gas-solid two-phase flows using discrete particle models. In chapters 2 and 3 the theoretical framework of the granular dynamics simulations of gas-fluidised beds will be presented and in the chapters 4, 5, 6, 7 and 8 several applications and experimental validation of these models will be discussed.

Chapter 2 deals with granular dynamics. The two types of discrete particle models used in this work, the hard-sphere and the soft-sphere model, are presented in detail. The hard-sphere model has been developed both in 2-D and in 3-D whereas the soft-sphere linear spring/dash-pot model has been developed in 2-D only. The two types of models are thoroughly discussed and a comparison will be presented. Furthermore an experimental technique to measure the collision parameters required in both types of models is presented. Finally the external forces acting on a single (Lagrangian) particle in a gas-fluidised bed are presented.

In Chapter 3 the gas phase dynamics is discussed for which the Eulerian approach was adopted. Alternative techniques will be discussed briefly. The volume averaged continuity and momentum conservation equations are presented together with the closure equations. Special attention is paid to the two-way coupling between the motion of the solid particles and the motion of the continuous gas-phase.

In Chapter 4 the hard-sphere model is applied to gas-fluidised beds with homogenous inflow conditions. The dependency of the bed dynamics on the collision parameters will be investigated. Furthermore the influence of the incorporation of a (log-normal) particle size distribution on the bed dynamics is studied. Finally the results obtained with the 2D model are compared with the results obtained with the 3D model.

In Chapter 5 the hard-sphere model is compared with the soft-sphere model. The formation of a single bubble at a central orifice will be used as a test case for the comparison. The dependency of the results of the soft-sphere model on the value of the spring stiffness is investigated and the influence of the incorporation of a (log-normal) particle size distribution will be studied. The results of the hard-sphere and soft-sphere model will be compared with each other and with experimental data. Finally the influence of the collision parameters on the bubble formation process will be investigated.

Chapter 6 deals with segregation phenomena in bubbling gas-fluidised beds. Simulations of systems consisting of particles of equal size but different density and systems consisting of particles of equal density but different size will be presented. Both the hard-sphere (2-D) and the soft-sphere models are used. Segregation will be demonstrated for each of these systems and a statistical analysis of the segregation dynamics is presented for the system consisting of particles of equal density but different size. For the latter system the influence of the collision parameters on the segregation is investigated. Finally an experimental validation is performed using a specially designed set-up.

In Chapter 7 the hard-sphere model is applied to riser flow. The model is modified to allow for a continuous transport of particles throughout the riser duct. The influence of the collision parameters on the flow structure in the riser will be investigated. The formation of clusters is studied and radial and axial solids profiles are obtained after time averaging of the data. The results will be compared with experimental data available in the open literature.

Finally in Chapter 8 experimental validation of granular dynamics simulations of a gas-fluidised bed with homogeneous inflow conditions is performed using the Positron Emission Particle Tracking (PEPT) facility at the University of Birmingham. In the PEPT experiment the motion of a single radioactive tracer particle is tracked during one hour. The time averaged data obtained from the experiment will be compared with the results of a simulation where 15,000 particles are tracked during 45 seconds. The results will be compared on the basis of velocity maps, occupancy plots and speed histograms. The results of a simulation where independently measured collision parameters are used will be compared with the results of a simulation assuming fully elastic, perfectly smooth collisions and the results of the PEPT experiment.

References

Delnoij, E., Kuipers, J.A.M. and van Swaaij W.P.M., (1997). Computational fluid dynamics applied to gas-liquid contactors, *Chem. Engng Sci*. **52**, 3623.

Gao, J., Xu, C., Lin, S., Tang, G. and Guo, Y., (1999). Advanced model for turbulent gas-solid flow and reaction in FCC riser reactors, *AIChE J*., **45**, 1095.

Hoomans, B.P.B., Kuipers, J.A.M., Briels, W.J. and van Swaaij, W.P.M., (1996). Discrete particle simulation of bubble and slug formation in a two-dimensional gas-fluidised bed: a hard-sphere approach, *Chem. Engng Sci*., **51**, 99.

Hoomans, B.P.B., Kuipers, J.A.M., Briels, W.J. and van Swaaij, W.P.M., (1998). Comments on the paper "Numerical simulation of the gas-solid flow in a fluidized bed by combining discrete particle method with computational fluid dynamics" by B.H. Xu and A.B. Yu, *Chem. Engng Sci*., **53**, 2645.

Kaneko, Y., Shiojima, T. and Horio, M., (1999). DEM simulation of fluidized beds for gas-phase olefin polymerization, *Chem. Engng Sci*., **54**, 5809.

Kawaguchi, T., Tanaka, T. and Tsuji, Y., (1998). Numerical simulation of two-dimensional fluidized beds using the discrete element method (comparison between the two- and three-dimensional models), *Powder Technol*. **96**, 129.

Kuipers, J.A.M., van Duin K.J., van Beckum, F.P.H. and van Swaaij, W.P.M., (1992). A numerical model of gas-fluidized beds, *Chem. Engng Sci*., **47,** 1913.

Kuipers, J.A.M. and van Swaaij, W.P.M., (1997). Application of computational fluid dynamics to chemical reaction engineering, *Rev. Chem Eng*., **13**, No 3, 1.

Kuipers, J.A.M. and van Swaaij, W.P.M., (1998). Computational fluid dynamics applied to chemical reaction engineering, *Adv. Chem Eng*., **24**, 227.

Kunii, D. and Levenspiel, O., (1991). *Fluidization engineering*, 2nd edition, Butterworth-Heinemann, Boston, USA.

Mikami, T., Kamiya, H. and Horio, M., (1998). Numerical simulation of cohesive powder behavior in a fluidized bed, *Chem. Engng Sci.* **53**, 1927.

Ouyang, J. and Li, J. (1999). Particle-motion-resolved discrete model for simulating gas-solid fluidization, *Chem. Engng Sci.*, **54**, 2077.

Rong, D., Mikami, T. and Horio, M., (1999). Particle and bubble movements around tubes immersed in fluidized beds – a numerical study, *Chem. Engng Sci*., **54**, 5737.

Samuelsberg, A.E. and Hjertager, B.H., (1996). Computational fluid dynamic simulation of an oxy-chlorination reaction in a full-scale fluidized bed reactor, in *Proceedings of the 5th Int. Conf. Circulating Fluidized beds, Beijing (China), May 28- June 1, 1996.*

van Swaaij, W.P.M., (1985)., Chemical reactors, in *Fluidisation*, 2nd edition p. 595, Davidson, J.F., Clift, R. and Harrison, D. (Eds), Academic Press, London, UK.

Tsuji, Y., Kawaguchi, T. and Tanaka, T., (1993). Discrete particle simulation of two dimensional fluidized bed, *Powder Technol.* **77**, 79.

Xu, B.H. and Yu, A.B., (1997). Numerical simulation of the gas-solid flow in a fluidized bed by combining discrete particle method with computational fluid dynamics, *Chem. Engng Sci*. **52**, 2785.

Chapter 2.

GRANULAR DYNAMICS

Abstract:

In this chapter a review is presented of the various granular dynamics simulation techniques available in the literature. The approaches can be divided into three groups: hard-particle techniques, soft-particle techniques and Monte Carlo techniques. These three types of simulation are discussed with emphasis on their application to simulation of gas-solid two-phase flow. In this work two types of models were developed. The first is a hard-sphere model where the particles are assumed to interact through instantaneous, binary collisions. A sequence of collisions is processed one collision at a time. The second is a soft-sphere linear spring/dash-pot model where contact forces between the particles are calculated from the overlap between the particles. Both models are described in detail. The key parameters in these models to describe a collision are the coefficient of restitution (e), the coefficient of friction (μ) and the coefficient of tangential restitution (β_0). The effect of these parameters on a single collision is demonstrated. A comparison between the hard-sphere and the soft-sphere model is presented. The soft-sphere model is capable of simulating static situations unlike the hard-sphere technique. However in the soft-sphere model special care must be taken in the choice of time step and the spring stiffness required for the calculation of the repulsive force. It is shown that the spring stiffness of the tangential spring should not be taken equal to the stiffness of the normal spring in order to avoid unrealistic behaviour. Experiments are described that enable measurement of the three collision parameters by careful observation of single impacts. Finally the external forces acting on the particles used in the simulations of gas-fluidised beds in this work are presented.

Parts of this chapter are based on the paper:

B.P.B. Hoomans, J.A.M. Kuipers, W.J. Briels and W.P.M. van Swaaij, (1996). Discrete particle simulation of bubble and slug formation in two-dimensional gas-fluidised beds: a hard-sphere approach, *Chem. Engng Sci.*, **51**, 99.

1. Introduction

Measured by tons granular matter is after water the most manipulated material in the world (de Gennes, 1999). However, roughly 40% of the capacity of industrial plants is wasted due to problems related to transport of granular matter (Knowlton *et al*., 1994). Therefore it is not surprising that Granular Dynamics (GD) has attracted the interest of a large number and a wide variety of researchers over the last decades. The interest not only originates from industrial needs but there is also an increasing interest in granular media from a more fundamental perspective. Phenomena like heap formation and arching provide both theoreticians and experimentalists with challenging problems concerning the statics of granular matter (de Gennes, 1999). However the greatest challenge is provided by the dynamics of this material which unveils a wealth of phenomena, such as standing waves in vibrated beds, segregation, clustering and inelastic collapse, that we are just beginning to understand (Jaeger *et al*., 1996). In this work the focus will be on the granular dynamics of gas-solid two-phase flow which is a field of research that has gained an increasing amount of attention over the last decade.

The systems considered in this work are all operated in the grain inertia regime according to Bagnold (1954) which implies that particle-particle and particle-wall interactions are dominated by inertia rather than viscous forces. This holds for gas-solid flow with rather coarse particles which is the subject of study in this work. In the case of liquid-solid fluidised beds lubrication forces have to be taken into account (Schwarzer, 1995) and for liquid-solid systems with smaller particles (< 100 μm) direct particle interaction does not even occur. Such systems can be studied by means of Stokesian dynamics simulations (Ichiki and Hayakawa, 1995). The modelling approaches adopted in Granular Dynamics can be roughly divided into two groups: soft particle and hard particle approaches. Before the two approaches adopted in this work (hard-sphere and soft-sphere linear-spring/dash-pot) will be described in detail in the preceding paragraphs a short review of the different approaches that are available in the literature will be presented. These approaches can be divided into three types of simulations: hard-particle approaches, soft-particle approaches

and Monte-Carlo approaches. Hard-particle simulations can be typified as *event driven* because the interaction times are small compared to free flight times. In *event driven* simulations the progression depends on the number of collisions that occurs. Soft-particle simulations can be typified as *time driven* because the interaction times are large compared to free flight times. In *time driven* simulations a constant time step is used to progress through the dynamics of the system.

1.1 Hard-Particle Approaches

The hard-sphere simulation technique was first presented by Alder and Wainwright (1957) in order to study phase transitions in molecular systems by means of numerical simulations. In a later paper (Alder and Wainwright, 1959) the technique was presented in more detail including a way to deal with a square well interaction potential apart from merely hard-sphere interaction. In hard-sphere simulations the particles are assumed to interact through instantaneous, binary collisions. A sequence of collisions is processed one collision at a time in order of occurrence. For this purpose a list of future collisions is compiled and updated when necessary. For a comprehensive introduction to this type of simulation the reader is referred to Allen and Tildesley (1990). A lot of effort has been put into the further optimisation and development of this *event driven* type of simulation technique (Marin *et al.*, 1993). Over two decades after the publications by Alder and Wainwright the hard-sphere approach was discovered as a useful tool for granular dynamics simulations (Campbell, 1985). The dissipative particle interaction in granular media makes these systems significantly different from molecular systems where energy is always conserved. Hence energy has to be continuously supplied to a granular system in order to keep the particles in motion. This can for instance be achieved by applying a shear rate through a proper choice of boundary conditions (Campbell, 1985). In granular dynamics simulations of gas-solid two-phase flow there is a constant stream of energy supplied to the particles through gravity and the drag force exerted on the particles by the gas-phase. For the remainder of this paragraph the focus will be on the various techniques used in granular dynamics simulations of gas-solid two-phase flow.

Tsuji *et al.* (1987) presented a hard-sphere granular dynamics model for dilute gas-solid flow in a horizontal channel. They neglected the particle-particle interaction but instead focussed on particle-wall interaction where an irregular bouncing model was used. This can be justified since the solids fraction in their system was very low ($\varepsilon_s < 0.01$). Sommerfeld (1990) and Frank *et al.* (1992) presented similar approaches where also attention was paid to experimental validation.

For denser flows the particle-particle interaction can no longer be neglected. The problem in these simulations is not so much the description of the particle-particle interaction itself since accurate collision models are available. The main problem is the large number of particles and hence the large number of collisions that have to be detected and processed. A technique that takes particle-particle interaction into account without detecting and processing every single collision that occurs in the system is the Direct Simulation Monte Carlo (DSMC) technique that was originally developed by Bird (1976) for molecular simulations. This technique was employed by Yonemura *et al.* (1993) in their simulations of gas-solid flow in a vertical channel. A more detailed description of this technique was presented by Tsuji *et al.* (1998). The particles tracked in this simulation technique are not actual particles but 'sample' particles that represent several 'real' particles. The DSMC method can therefore be regarded as a coarse grained model of the actual dynamics. The occurrence of a collision as well as the geometry of a collision (*i.e.* the collision coordinate system) are determined by a random number generator where the probability of a collision depends on the local solids fraction (the greater the solid fraction the greater the probability of a collision). However one should be careful when applying this technique since the modified Nanbu method used by Tsuji *et al.* (1998) does not guarantee exact conservation of energy in the absence of dissipative terms (Frezzoti, 1997). Oesterlé and Petitjean (1993) presented a technique that resembles the DSMC technique strongly but differs in the sense that the particles in their simulations are 'real' particles instead of 'sample' particles.

Hopkins *et al*. (1991) developed a type of hard-particle simulation technique where collisions were detected at constant time intervals. Although they did not apply it directly to gas-solid flow the technique is worthwhile mentioning here since Ge and Li (1997) and Ouyang and Li (1999) adopted this approach in their simulations of gas-fluidised beds. In this computational strategy the particles are assumed to interact as hard-spheres but the motion update is performed at constant time steps. After each time step the whole system is scanned for overlap between particles and when this is detected the particles involved are assumed to have collided during that time step and subsequently their new velocities are calculated. This technique works fine for relatively dilute systems when the time step is chosen relatively small. For denser systems overlap may be found between more than two particles which gives rise to incorrect dynamics. In the case of larger time steps it may be possible that collisions are overlooked. Hogue and Newland (1994) used a similar strategy in their simulations where a technique was used that was especially designed to handle non-spherical (*i.e.* polygonal) particles. In addition to the model of Hogue and Newland, Müller and Liebling (1995) presented a triangulation technique that enables a sequence of collisions between polygonal particles to be correctly processed.

Hoomans *et al*. (1996) presented a true hard-sphere type of simulation technique for gas-fluidised beds. This was the first time that this technique was developed and applied with success to such a dense system as a bubbling gas-fluidised bed. In this two-dimensional model a sequence of collisions is processed proceeding from one collision to the next by using a collision list that is compiled and updated in a highly efficient manner. In the following chapter this technique will be explained in detail. Lun and Liu (1997) presented a three-dimensional hard-sphere model for a more dilute gas-solid flow where they used a granular dynamics model presented earlier by Lun (1996).

1.2 Soft-Particle Approaches

The *Distinct Element Method* (DEM) developed by Cundall and Strack (1979) was the first granular dynamics simulation technique published in the open literature. They used a

two-dimensional soft particle model where the particles were allowed to overlap slightly. The contact forces were subsequently calculated from the deformation history of the contact using a linear spring/dash-pot model. This method allowed for multiple particle overlap although the net contact force was obtained from pair-wise interactions. Soft-particle approaches differ in the choice of force scheme used to calculate the inter-particle forces. A review of various popular schemes for repulsive inter-particle forces is presented by Schäfer *et al.* (1996). Before the various soft-particle approaches used in fluidised bed simulations will be discussed, two alternatives to the Cundall and Strack model are briefly outlined here.

Walton and Braun (1986) presented a model that uses two different spring constants to model energy dissipation instead of a dash-pot. The spring constant for the compression phase (loading) of the constant is taken to be lower than the constant used for the restitution phase (unloading). The coefficient of restitution can be related to the ratio of the two spring constants. This model was used by McCarthy and Ottino (1998) and Wightman *et al*. (1998) in their studies of granular mixing in a rotating container.

Langston *et al.* (1994) presented a force scheme that was based on a continuous potential of an exponential form containing two unknown parameters, the stiffness of the interaction and an interaction constant. In a later paper (Langston *et al*., 1995) they presented a three-dimensional version of this model. The repulsive force was obtained by taking the gradient of this potential while the stiffness parameter was chosen in such a way that particle overlap could not become too high without requiring too small a time step. The interaction constant was chosen in such a way that the net force would be zero when a particle would rest on top of another particle in a gravity field. One should be careful when applying this model since it features rather unrealistic behaviour when using a cut-off distance greater than the particle diameter. When two particles that do not touch each other are positioned at the same height within the cut-off distance of the potential they will still experience a repulsive force. This is not physically correct behaviour for dry granular material.

The soft-sphere approach was first applied to gas-fluidised beds by Tsuji *et al*. (1993). In their two-dimensional model the particle interaction was calculated using a soft-sphere interaction model similar to the one presented by Cundall and Strack (1979). Previously Tsuji *et al.* (1992) presented a three-dimensional model (as far as the particles were concerned) for gas-solid flow in a horizontal pipe. However, in this model the gas-phase dynamics was represented by a one-dimensional model with hardly any dynamic features. A three-dimensional version of their fluidised bed model was presented by Kawaguchi *et al*. (1998). In that model the particle motion was resolved in full 3-D whereas the gas-phase dynamics was still calculated in 2-D. This can be justified because the system used in their simulations was a rather flat (quasi 2-D) fluidised bed. In such a system the motion of the gas-phase in the third dimension can be neglected.

Schwarzer (1995) presented a two-dimensional model of a liquid-fluidised bed. Apart from the inter-particle forces, for which the Cundall and Strack model was used, also lubrication forces were taken into account. These lubrication forces can be neglected for gas-fluidised beds but play an important role in liquid-fluidised beds. Also a Gaussian particle size distribution was taken into account in these simulations although the effect of the size distribution on the flow behaviour was not investigated.

Xu and Yu (1997) presented a two-dimensional model of a gas-fluidised bed that was based on the model developed by Tsuji *et al.* (1993). However in their simulations a collision detection algorithm that is normally found in hard-sphere simulations was used to determine the first instant of contact precisely. The spring constants used in their simulations were much higher than the ones used by Tsuji *et al.* (1993). Unfortunately no results were reported that could show the importance of the detection algorithm for the overall simulation results.

Mikami *et al*. (1998) extended the model developed by Tsuji *et al*. (1993) by incorporating liquid bridge forces to simulate cohesive particle fluidisation. The particles used in their simulations are still Geldart D particles but due to the liquid bridge forces the fluidisation behaviour resembles the behaviour of Geldart C particles strongly.

Mikami (1998) was also the first to present full 3-D simulations (also with respect to the gas-phase) where no less than 500,000 particles were used.

1.3 Monte Carlo techniques

Another popular method to study many particle systems is the Monte Carlo technique (Frenkel and Smit 1996). This method has been applied to granular systems by Rosato *et al.* (1986). In their Monte Carlo simulations a new overlap-free particle configuration is generated at each step. The change in the system energy is then calculated and if this change is negative the new configuration is accepted. If the system energy has increased the new configuration is accepted with a probability obtained from Boltzmann distribution based on the change in energy. Using this method Rosato *et al.* were able to simulate segregation phenomena in shaken or vibrated systems where effects due to an interstitial fluid were neglected. It is important to realise that time is not a variable in Monte Carlo simulations. A Monte Carlo step can only be linked to an actual time step by means of calibration but this is not a straightforward task. Therefore this method is not capable of simulating the dynamics of a granular system without the input of a-priory knowledge.

The Monte Carlo technique is capable of predicting steady state (*i.e.* equilibrium) conditions and for that purpose it has certain advantages over dynamic simulations. Seibert and Burns (1998) were able to predict segregation phenomena in liquid-fluidised beds using an extended version of their previously developed model (Seibert and Burns, 1996). In their model they used a net force (calculated from gravity and fluid drag) to calculate the change of energy involved with a particle movement. Although the results compared rather well with experimental data no statement was made about the time scale over which the phenomena occurred. This is of course to be expected for this type of simulation technique.

2. Hard-Sphere approach

In the hard sphere model used in this work the particles are assumed to interact through binary, quasi-instantaneous collisions where contact occurs at a point. The particles are perfect, homogeneous spheres and the interaction forces are impulsive. In between collisions the particles are in free flight. First the collision model will be presented and then the computational strategy and some optimisation techniques will be described. Since the hard-sphere model was developed in 3-D as well as in 2-D the collision model will be presented in vector notation. For the 2-D version the z-component of the position and velocity vectors are zero and only rotation about the z-axis is considered.

2.1 Collision model

In the collision model it is assumed that the interaction forces are impulsive and therefore all other finite forces are negligible during collision. The original 2-D collision model was mapped after the model presented by Wang and Mason (1992). In this work however we will mainly adopt the notation used by Foerster *et al.* (1994) since that is more widely accepted (see for example Lun, 1997 and Tsuji *et al.* 1998). The coordinate systems used in our model are defined in Figure 2.1.

Consider the two colliding spheres a and b in Figure 2.1 with position vectors $\mathbf{r}_a$ and $\mathbf{r}_b$. The normal unit vector can now be defined:

$$\mathbf{n} = \frac{\mathbf{r}_a - \mathbf{r}_b}{\left|\mathbf{r}_a - \mathbf{r}_b\right|}. \tag{2.1}$$

Hence the normal unit vector points in the direction from the centre of particle b to the centre of particle a. The point of origin is the contact point. Prior to collision, the spheres with radii R_a and R_b and masses m_a and m_b have translation velocity vectors $\mathbf{v}_a$ and $\mathbf{v}_b$ and

rotational velocity vectors ω_a and ω_b (clockwise rotation is negative by definition). Velocities prior-to-collision are indicated by the subscript $_0$.

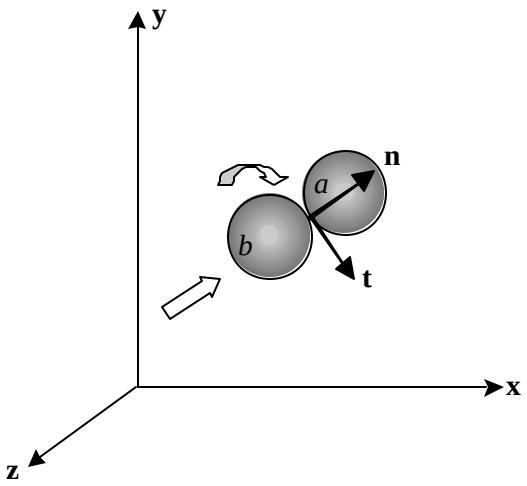

Figure 2.1. *Definition of the coordinate systems.*

For a binary collision of these spheres the following equations can be derived by applying Newton's second and third laws:

$$m_a(\mathbf{v}_a - \mathbf{v}_{a,0}) = \mathbf{J} \tag{2.2}$$

$$m_b(\mathbf{v}_b - \mathbf{v}_{b,0}) = -\mathbf{J} \tag{2.3}$$

$$I_a(\omega_a - \omega_{a,0}) = -(R_a\mathbf{n})\times\mathbf{J} \tag{2.4}$$

$$I_b(\omega_b - \omega_{b,0}) = R_b\mathbf{n}\times(-\mathbf{J}) \tag{2.5}$$

$$m_a(\mathbf{v}_a - \mathbf{v}_{a,0}) = -m_b(\mathbf{v}_b - \mathbf{v}_{b,0}) = \mathbf{J} \tag{2.6}$$

$$\frac{I_a}{R_a}(\omega_a - \omega_{a,0}) = \frac{I_b}{R_b}(\omega_b - \omega_{b,0}) = -\mathbf{n}\times\mathbf{J} \tag{2.7}$$

$$I = \frac{2}{5}mR^2. \tag{2.8}$$

The impulse vector **J** is defined as follows:

$$\mathbf{J} = \int_{t=0}^{t=t_c} \mathbf{F}_{ab}\, dt\,, \tag{2.9}$$

where t_c stands for the contact time (*i.e.* the duration of the contact).

From equations 2.6 and 2.7 it is clear that the post-collision velocities of both particles can be calculated when the impulse vector **J** is known. If the force $\mathbf{F}_{ab}$ in equation 2.9 were known as a function of all the parameters involved, the impulse **J** could be calculated directly. Thornton (1997) demonstrated that based on a simplified theoretical model for the normal interaction between elastic-perfectly plastic spheres an analytical solution could be obtained for the rebound velocity. Walton (1992) used two types of finite element codes (DYNA2D and NIKE2D) to simulate the collision process in detail on a sub-particle level. The only input parameters necessary in these calculations are material properties although assumptions have to be made about the deformation behaviour (elastic/plastic) of the material. In simulations of gas-fluidised beds a large number of collisions (typically 10^6-10^9) have to be processed and therefore the actual physics of a binary collision has to be simplified to some extent and constitutive relations have to be introduced.

Before these constitutive relations will be introduced first the relative velocity at the contact point ($\mathbf{v}_{ab}$) has to be defined:

$$\mathbf{v}_{ab} \equiv (\mathbf{v}_{a,c} - \mathbf{v}_{b,c})\ . \tag{2.10}$$

$$\mathbf{v}_{ab} = (\mathbf{v}_a - \omega_a \times R_a \mathbf{n}) - (\mathbf{v}_b + \omega_b \times R_b \mathbf{n})\ . \tag{2.11}$$

$$\mathbf{v}_{ab} = (\mathbf{v}_a - \mathbf{v}_b) - (R_a \omega_a + R_b \omega_b) \times \mathbf{n}\ . \tag{2.12}$$

From this relative velocity, the tangential unit vector can be obtained since the normal unit vector is already defined in equation 2.1:

$$\mathbf{t} = \frac{\mathbf{v}_{ab,0} - \mathbf{n}(\mathbf{v}_{ab,0} \cdot \mathbf{n})}{\left|\mathbf{v}_{ab,0} - \mathbf{n}(\mathbf{v}_{ab,0} \cdot \mathbf{n})\right|} \ . \tag{2.13}$$

Equations 2.6 and 2.7 can now be rearranged using $(\mathbf{n}\times\mathbf{J})\times\mathbf{n} = \mathbf{J} - \mathbf{n}(\mathbf{J}\cdot\mathbf{n})$ and equation 2.12 to obtain:

$$\mathbf{v}_{ab} - \mathbf{v}_{ab,0} = B_1\mathbf{J} - (B_1 - B_2)\mathbf{n}(\mathbf{J}\cdot\mathbf{n}) \ , \tag{2.14}$$

where

$$B_1 = \frac{7}{2}\left(\frac{1}{m_a} + \frac{1}{m_b}\right) \tag{2.15}$$

and

$$B_2 = \frac{1}{m_a} + \frac{1}{m_b} . \tag{2.16}$$

At this point constitutive relations are required to close the set of equations. Through these constitutive relations three parameters enter the model. The first parameter is the coefficient of (normal) restitution, $(0 \le e \le 1)$:

$$\mathbf{v}_{ab}\cdot\mathbf{n} = -e(\mathbf{v}_{ab,0}\cdot\mathbf{n}) \ . \tag{2.17}$$

For non-spherical particles this definition can lead to energy inconsistencies (Stronge, 1990) but for spherical particles this definition holds. The second parameter is the coefficient of (dynamic) friction, $(m \ge 0)$:

$$\left|\mathbf{n}\times\mathbf{J}\right| = -m(\mathbf{n}\cdot\mathbf{J}) \ . \tag{2.18}$$

The third parameter is the coefficient of tangential restitution, $(0 \le b_0 \le 1)$:

$$\mathbf{n}\times\mathbf{v}_{ab} = -b_0\left(\mathbf{n}\times\mathbf{v}_{ab,0}\right) . \tag{2.19}$$

Notice that this relation does not affect the components parallel to **n** and that the components orthogonal to **n** are related by a factor $-b_0$. Although it is accepted that these coefficients depend on particle size and impact velocity this is not taken into account in this model. The only exception is made for the coefficient of normal restitution where collisions occurring at a normal impact velocity less than a threshold value *'MINC0'* (typically 10^{-4} m/s) are assumed to be perfectly elastic (e = 1.0).

Combining equations 2.14 and 2.17 yields the following expression for the normal component of the impulse vector:

$$J_n = -(1+e)\frac{\mathbf{v}_{ab0}\cdot\mathbf{n}}{B_2} \tag{2.20}$$

For the tangential component two types of collisions can be distinguished that are called *sticking* and *sliding*. If the tangential component of the relative velocity is sufficiently high in comparison to the coefficients of friction and tangential restitution that gross sliding occurs throughout the whole duration of the contact, the collision is of the *sliding* type. The non-sliding collisions are of the *sticking* type. When b_0 is equal to zero the tangential component of the relative velocity becomes zero during a *sticking* collision. When b_0 is greater than zero in such a collision, reversal of the tangential component of the relative velocity will occur. The criterion to determine the type of collision is as follows:

$$\mu < \frac{(1+b_0)\mathbf{v}_{ab0}\cdot\mathbf{t}}{J_n B_1} \qquad \textit{sliding} \tag{2.21}$$

$$\mu \geq \frac{(1+b_0)\mathbf{v}_{ab0}\cdot\mathbf{t}}{J_n B_1} \qquad \textit{sticking} \tag{2.22}$$

For collisions of the *sticking* type, the tangential impulse is given by:

$$J_t = -(1+b_0)\frac{\left|\mathbf{n}\times\mathbf{v}_{ab,0}\right|}{B_1} = -(1+b_0)\frac{\mathbf{v}_{ab0}\cdot\mathbf{t}}{B_1} \ . \tag{2.23}$$

For collisions of the *sliding* type, the tangential impulse is given by:

$$J_t = -m \ J_n \ . \tag{2.24}$$

The total impulse vector is then simply obtained by addition:

$$\mathbf{J} = J_n\mathbf{n} + J_t\mathbf{t} \ . \tag{2.25}$$

The post-collision velocities can now be calculated from equations 2.6 and 2.7.

In particle-wall collisions the mass of particle b (*i.e.* the wall) is infinitely large which makes all terms $1/m_b$ equal to zero. It is possible to implement a moving/rotating wall through the velocity vectors $\mathbf{v}_b$ and ω_b but in the simulations performed for this work these velocities are all set equal to zero.

The energy dissipated during a collision can be obtained by solving the following integral over the duration of the collision:

$$E_{dsp,tot} = \int v_{ab,n}\,dJ_n + \int v_{ab,t}\,dJ_t \ . \tag{2.26}$$

The energy dissipated by the normal component in a collision is:

$$E_{dsp,n} = \frac{v_{ab,n0}^2}{2B_2}\left(1-e^2\right). \tag{2.27}$$

For the energy dissipated by the tangential component the two types of collision have to be distinguished again. If the collision is of the *sticking* kind, the dissipated energy is:

$$E_{dsp,t} = \frac{v_{ab,t0}^2}{2B_1}\left(1 - b_0^2\right), \tag{2.28}$$

and if the collision is of the *sliding* type, the dissipated energy is:

$$E_{dsp,t} = -m\mathrm{J}_n\left(\mathbf{v}_{ab,0}\cdot\mathbf{t} - \frac{1}{2}mB_1\mathrm{J}_n\right). \tag{2.29}$$

The total amount of energy dissipated in a collision is then obtained by adding the tangential and normal contributions:

$$E_{dsp,tot} = E_{dsp,n} + E_{dsp,t}. \tag{2.30}$$

2.2 Key parameters of the collision model

Since the three key parameters of the collision model are of crucial importance for the remainder of this work the effect of each of the three will now be highlighted. The system considered here is a particle that collides with a flat wall under the influence of gravity (**g**). For all these examples the particles do not experience any friction of the gas phase. In Figure 2.2 the effect of the coefficient of restitution is illustrated.

When a particle collides perfectly elastically, without any energy dissipation (e = 1) with a horizontal flat wall it will bounce back to the same height as it was initially released from. No energy is dissipated in this process and the particle will eternally continue to bounce. When e < 1, which is always the case for granular material, energy is dissipated in the collision and the particle will not bounce back to the same height as it was initially released from. Eventually the particle will come to rest on the wall.

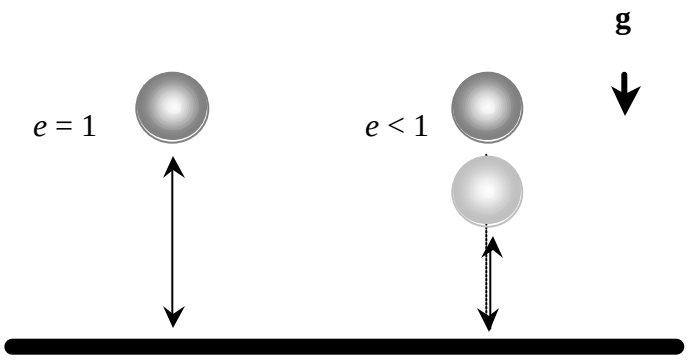

Figure 2.2. *The effect of the coefficient of restitution (e).*

The effect of the coefficient of friction (m) is demonstrated in Figure 2.3. Consider the same case as before but now the particle initially rotates as well ($b_0 = 0$). In the case of a perfectly smooth particle ($m = 0$) this rotation does not affect the translation motion of the particle after collision. No energy is dissipated in this case. When the particle is not perfectly smooth ($m > 0$), which is always the case for granular material, the rotation does affect both the translation and the rotation after collision as illustrated. In this case energy is dissipated during the collision. For *sticking* collisions this effect is much more pronounced than for *sliding* collisions.

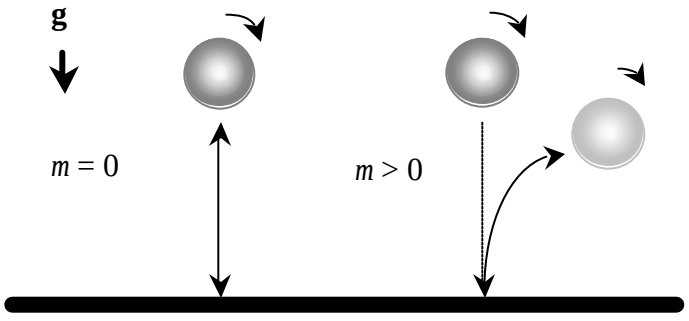

Figure 2.3. *The effect of the coefficient of friction (m).*

The effect of the coefficient of tangential restitution is demonstrated in Figure 2.4. The case is identical to the one above for the coefficient of friction except that now the coefficient of friction is high enough to ensure that the collision is of the *sticking* type.

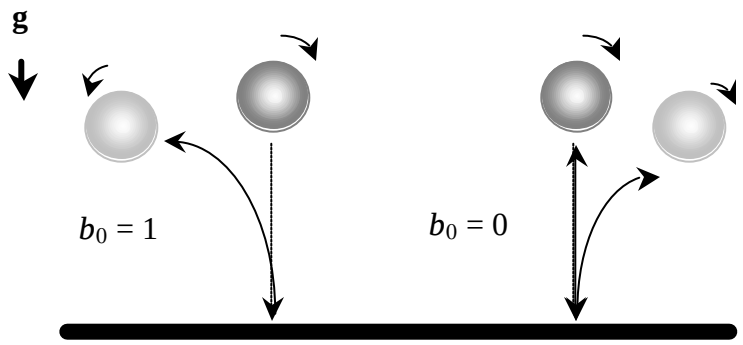

Figure 2.4. *The effect of the coefficient of tangential restitution (b_0).*

In the case of $b_0 = 0$ the result is identical to the case described above provided the collision is of the *sticking* type. The tangential component of the relative velocity at the contact point is equal to zero at the end of the collision and energy is dissipated. However, when $b_0 = 1$ the tangential component of the relative velocity at the contact point reverses and the particle bounces back in the opposite direction. No energy is dissipated in this case.

In section 5 experiments are described that enable determination of these collision parameters from careful observation of single impacts.

2.3 Sequence of collisions

In the hard-sphere model a constant time step *DT* is used to take the external forces acting on the particles into account. Within this time step *DT* the velocities are assumed to change only due to collisions and a sequence of collisions is processed one collision at a time like in a regular hard-sphere simulation in Molecular Dynamics. So in fact a separate MD hard-sphere simulation is performed within each time step. To do so it is necessary to

determine what pair of particles will collide first which requires the determination of the collision times of all relevant collision pairs. The collision time t_{ab} of a pair of particles (a,b) is defined as the time remaining until these particles will collide. It can be calculated from the initial positions and velocities of both particles.

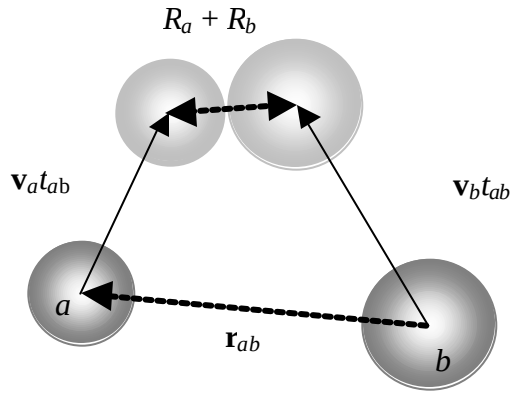

Figure 2.5. *Determination of the collision time t_{ab}.*

When particles a and b collide the distance between the two centres of mass is equal to the sum of the two radii as is shown in Figure 2.5. This yields a quadratic equation in t_{ab} the smallest solution of which corresponds to collision (Allen and Tildesley, 1990):

$$t_{ab} = \frac{-\mathbf{r}_{ab} \cdot \mathbf{v}_{ab} - \sqrt{(\mathbf{r}_{ab} \cdot \mathbf{v}_{ab})^2 - v_{ab}^2 \left(r_{ab}^2 - (R_a + R_b)^2\right)}}{v_{ab}^2} , \qquad (2.31)$$

where $\mathbf{r}_{ab} \equiv \mathbf{r}_a - \mathbf{r}_b$ and $\mathbf{v}_{ab} \equiv \mathbf{v}_a - \mathbf{v}_b$ (in this definition of $\mathbf{v}_{ab}$ the particle rotation is not taken into account unlike in equation 2.12). Note that if $\mathbf{r}_{ab} \cdot \mathbf{v}_{ab} > 0$ the particles are moving away from each other and will not collide.

In case of a collision with a wall the collision time follows simply from the distance to the wall and the normal velocity component toward that wall which leads for a vertical wall to the following expression:

$$t_{a,wall} = \frac{(|x_{wall}| + R_a) - |\mathbf{r}_{x,a}|}{v_{x,a}} \ . \tag{2.32}$$

The algorithm used to process a sequence of collisions within a constant time step *DT* is presented in Figure 2.6.

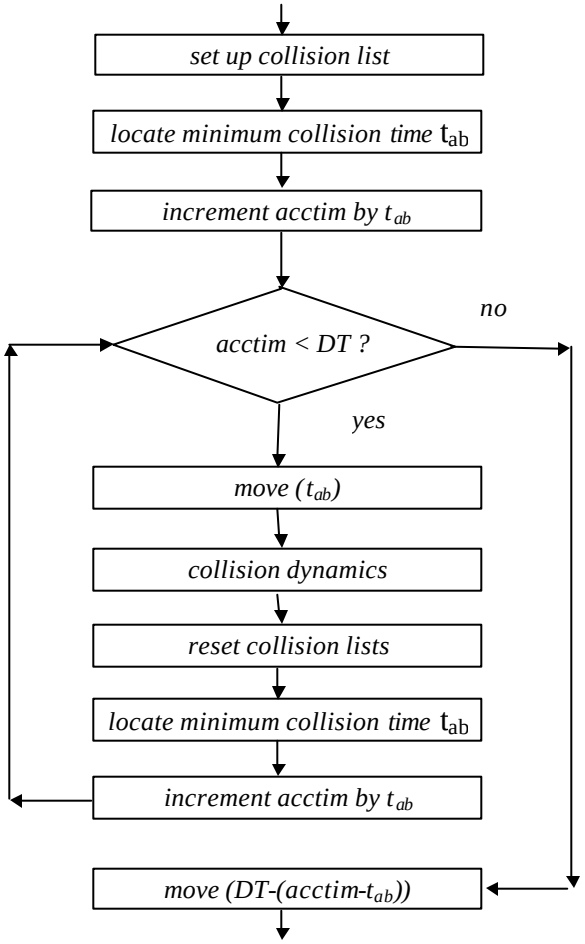

Figure 2.6. *Computational strategy of a hard-sphere simulation within a time step DT.*

First the collision lists are initialised in which for each particle a collision partner and a corresponding collision time are stored. For each particle the smallest collision time is determined by scanning all relevant collision partners. The variable *acctim* (accumulated time) keeps track of the time spent since the beginning of the time step. In the routine *move(*t_{ab}) the collision times of all particles are reduced with t_{ab} and the particle positions are updated using a first order explicit integration:

$$\mathbf{r}_a(t+t_{ab}) = \mathbf{r}_a(t) + \mathbf{v}_a t_{ab} \ . \tag{2.33}$$

The calculation of the collision dynamics involves the collision model presented in the previous paragraph. Subsequently the routine *reset collision lists* is entered where new collision times and partners have to be found all the particles involved in the collision. This does not only effect the particles *a* and *b* but also the particles that were about to collide with either *a* or *b*. Finally a new collision pair has to be detected and *acctim* can be incremented with the new collision time t_{ab}. As soon as a minimum collision time is found that after addition to *acctim* is greater than the time step *DT*, the loop is finished. After the loop is finished the particles have to be moved forward until *acctim* equals *DT*. During this motion no collision occurs.

2.4 Optimisation

To perform simulations of relatively large systems for relatively long times it is essential to optimise the hard-sphere computational strategy. The first step to achieve this is to minimise the number of particles that have to be scanned for a possible collision by employing a neighbour list. In the neighbour list of particle *a* all the particles that are found within a square of size D_{nblist} with particle *a* located at the centre, are stored. When looking for a collision partner for particle *a* only the particles in the neighbour list need to be scanned. In Figure 2.7 particle *a* is coloured black and its neighbour particles are shaded. The neighbour lists are updated at each time step dt_{nblist}.

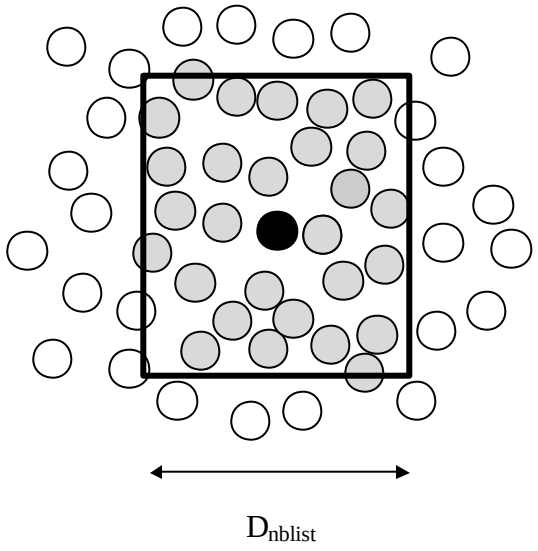

Figure 2.7. *The neighbour list principle: all shaded particles are stored in the neighbour list of the black particle.*

When updating the neighbour list it is still not necessary to scan all particles. The solution of the gas flow field (Chapter 3) requires the computational domain to be divided into cells; for each cell the particles whose centre can be found in that cell are stored in a list. When updating the neighbour list, only the cell where the particle's centre is found and the three nearest adjacent cells are scanned for possible neighbours.

With the implementation of the neighbour lists substantial speed up has been achieved and simulations with over 1,000 particles are easily possible. The search for collision partners (*set up collision lists* and *reset collision lists* in Figure 2.6) is no longer the most CPU time consuming routine in the algorithm. Instead the update of the particle motion (*move* in Figure 2.6) takes up 50 % of the CPU time in a typical fluidised bed simulation. This can be optimised by applying a more efficient motion update strategy. In the original version of the code all particles were moved to their new positions before each collision. This implies $N_{particles}*N_{collisions}$ motion updates per time step which means that particles that do not collide are moved over a straight line in far too many steps as illustrated in Figure 2.8.

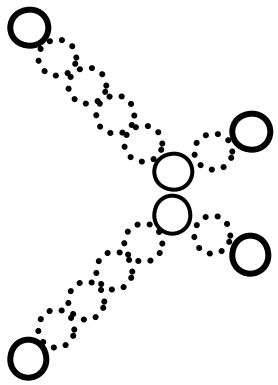

Figure 2.8. *Efficient motion update.*

Since the particles in Figure 2.8 collide only once, two motion updates will suffice for both particles. In the previous version the particles were moved to their new position in a total of seven steps for this specific example, that is five motion updates too many. This does not only slow down the algorithm but also gives rise to numerical errors. In typical fluidised bed simulations the total number of collisions per time step is of the same order as the total number of particles (*i.e.* 10^4-10^5) indicating that the total number of unnecessary motion updates is of the same order as the total number of particles. In the new algorithm special care must be taken when looking for new collision partners for particles that just collided, since the positions stored in memory for the particles not involved in that collision are not their actual positions. This causes some overhead for the new algorithm but nonetheless the speed gain is substantial since the routine *move(*t_{ab}*)* in Figure 2.6 went down from 50% to less than 1% of the total amount of CPU time.

After optimising the motion update strategy the search for the smallest collision time (*locate minimum collision time* in Figure 2.6) is the main CPU time consumer in the hard-sphere routine. This search has to be performed after each collision and in the old version all particles were scanned and the smallest collision time was stored. In the new strategy advantage is taken of the fact that the computational domain is already divided into cells as illustrated in Figure 2.9. This figure is rather idealised for clarity but on average a typical grid cell can contain up to 100 particles.

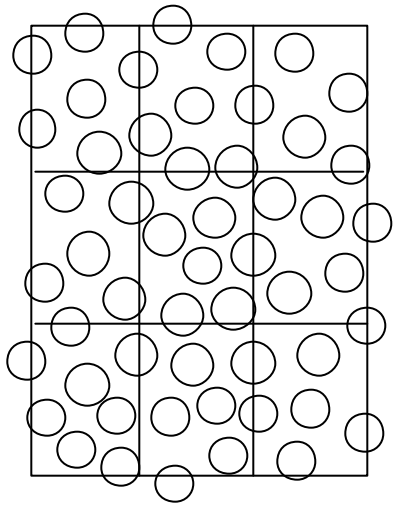

Figure 2.9. *Efficient search for smallest collision times using grid cells*.

When for each grid cell the smallest collision time is stored it is not necessary to scan all particles after each collision. Instead all the grid cells are scanned and since the total number of grid cells is at least one order of magnitude smaller than the total number of particles (*i.e.* 2,340 cells vs. 40,000 particles for the bubble formation simulations in Chapter 5) this is much faster. Of course a new smallest collision time has to be found in the grid cells containing particles that were involved in the last collision but this causes negligible overhead.

After implementation of these optimised routines the main CPU time consumer is again the search for possible collisions even though this search is performed only within the neighbour list! A suitable choice of the size of the neighbour list and the time step for updating the neighbour list is now critical. These choices however depend on the sort of system that is simulated. For instance in bubbling beds (Chapters 4 and 5) a relatively small neighbour list ($D_{nblist} = 3\ D_p$) can be used that is updated every second time step. For risers (Chapter 7) however a larger neighbour list has to be used ($D_{nblist} = 8\ D_p$) since the velocity differences between the particles are larger as well. If a neighbour list is chosen to be too small it is possible that a collision is not detected and overlap between

particles can occur. This cannot be tolerated in hard-sphere simulations and if such an overlap is detected in our code the simulation is stopped immediately. On the other hand if the neighbour list is chosen to be rather large all collisions will be detected but this will go at cost of the computational speed.

A hard-sphere simulation is an *event driven* simulation which implies that the amount of collisions to be processed per time step depends on the dynamics of the system. The number of collisions to be processed can be considerably higher in a dense region of the bed than in a dilute region. Hence the CPU time required to progress a time step can vary significantly. It is therefore not straightforward to benefit from parallel computing with a highly optimised *event driven* code.

3. Soft-Sphere approach

Although the hard-sphere model was used for the majority of the simulations in this work also a soft-sphere model was implemented. It was not the objective to select the best soft-sphere model available but the aim was to compare the results obtained with the most popular soft-sphere model for fluidisation simulations with the results obtained with the hard-sphere model. The linear spring/dash-pot model (Cundall and Strack, 1979) is the most popular soft-sphere granular dynamics model since it was used by Tsuji *et al.* (1993), Schwarzer (1995), Xu and Yu (1997), Kawaguchi *et al.* (1998) and Mikami *et al.* (1998). For a review of various contact force models used in soft-sphere simulations the reader is referred to Walton (1992) or Schäfer *et al.* (1996).

The soft-sphere model was implemented in 2-D. In the vector notation employed in the preceding paragraphs the z-component of the position and velocity vectors is equal to zero and only rotation about the z-axis is considered. The notation and some definitions can differ somewhat from the ones used for the hard-sphere model. Unfortunately there is no standard notation in Granular Dynamics (yet) and therefore it was attempted here to stay close to the notations used in the references above.

3.1 The linear spring/dash-pot model

In soft-sphere models the following equations of motion are used:

$$m\frac{d^2\mathbf{r}}{dt^2} = \mathbf{F}_{contact} + \mathbf{F}_{external}, \tag{2.34}$$

$$I\frac{d\omega}{dt} = \mathbf{T}, \tag{2.35}$$

where $\mathbf{r}$ is the position vector of the centre of the particle, m is the mass of the particle, $\mathbf{F}_{contact}$ is the contact force acting on the particle, $\mathbf{F}_{external}$ is the external force acting on the particle, ω is the rotation velocity, $\mathbf{T}$ is the torque acting on the particle and I is the moment of inertia of the particle as defined in equation 2.8. In this section the focus will be on the contact forces between the particles, the external forces will be discussed in section 6.

The particle velocities are updated using the accelerations from equations 2.34 and 2.35 by means of a first order explicit integration:

$$\mathbf{v} = \mathbf{v}_0 + \dot{\mathbf{v}}_0 DT, \tag{2.36}$$

$$w = w_0 + \dot{w}_0 DT. \tag{2.37}$$

The new particle positions are subsequently also obtained from a first order explicit integration:

$$\mathbf{r} = \mathbf{r}_0 + \mathbf{v}DT, \tag{2.38}$$

where the subscript $_0$ denotes the value at the previous time step.

The interaction forces between particles in contact are modelled with a spring, a dash-pot and a friction slider, as shown in Figure 2.10.

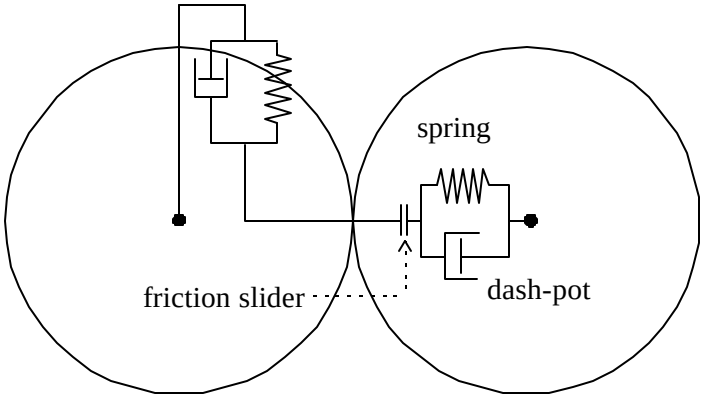

Figure 2.10. *The linear spring/dash-pot model.*

The contact forces are evaluated from the overlap between the particles and their relative velocities. Two particles *a* and *b* are in contact (*i.e.* have mutual overlap) if the distance between their centres is less than the sum of their radii:

$$\left|\mathbf{r}_b - \mathbf{r}_a\right| < R_{p,a} + R_{p,b} \tag{2.39}$$

The repulsive force acting on the particles is divided into a normal ($\mathbf{F}_n$) and a tangential ($\mathbf{F}_t$) component. The procedure of evaluating these contact forces starts with defining a normal unit vector, pointing from the mass centre of particle *a* to the mass centre of particle *b* as is presented in Figure 2.11.

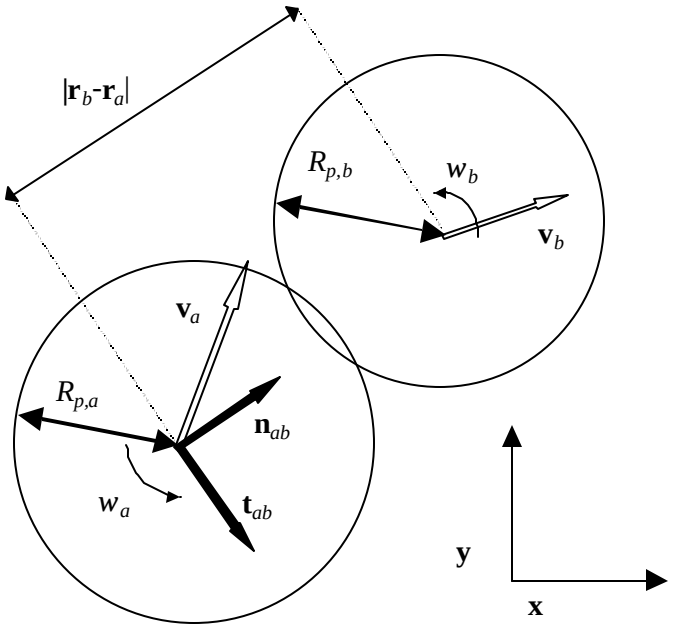

Figure 2.11. *Definition of the coordinate system used in the soft-sphere model*

Note that this definition differs from equation 2.1 used in the hard-sphere model:

$$\mathbf{n}_{ab} = \frac{\mathbf{r}_b - \mathbf{r}_a}{|\mathbf{r}_b - \mathbf{r}_a|} \,. \tag{2.40}$$

The relative velocity of particle *a* with respect to *b* is given by:

$$\mathbf{v}_{ab} = (\mathbf{v}_a - \mathbf{v}_b) + (R_a \omega_a + R_b \omega_b) \times \mathbf{n}_{ab} \,. \tag{2.41}$$

The normal component of the relative velocity is given by:

$$\mathbf{v}_{n,ab} = (\mathbf{v}_{ab} \cdot \mathbf{n}_{ab}) \mathbf{n}_{ab} \,. \tag{2.42}$$

The tangential relative velocity, or slip velocity of particle *a* with respect to *b* can now be obtained as follows:

$$\mathbf{v}_{t,ab} = \mathbf{v}_{ab} - \mathbf{v}_{n,ab} \tag{2.43}$$

The tangential unit vector is defined as follows:

$$\mathbf{t}_{ab} = \frac{\mathbf{v}_{t,ab}}{\left|\mathbf{v}_{t,ab}\right|}. \tag{2.44}$$

By defining the tangential unit vector this way the vector is always pointing in the direction of the slip velocity.

The overlap in the normal direction can immediately be calculated as the difference between the sum of the particle radii and the distance between the particles:

$$x_n = \left(R_a + R_b\right) - \left|\mathbf{r}_a - \mathbf{r}_b\right| \tag{2.45}$$

The tangential displacement that has been established since the beginning of the contact is obtained by integrating the relative velocities with respect to time:

$$x_t(t) = \int_{t_0}^{t} \mathbf{v}_{t,ab}\, dt \tag{2.46}$$

The contact forces are now given by:

$$\mathbf{F}_{n,ab} = -k_n x_n \mathbf{n}_{ab} - h_n \mathbf{v}_{n,ab} \tag{2.47}$$

$$\mathbf{F}_{t,ab} = -k_t \mathbf{?}_t - h_t \mathbf{v}_{t,ab} \tag{2.48}$$

If however the following relation is satisfied:

$$\left|\mathbf{F}_{t,ab}\right| > m\left|\mathbf{F}_{n,ab}\right|, \tag{2.49}$$

then sliding occurs and the tangential force is given by:

$$\mathbf{F}_{t,ab} = -m\left|\mathbf{F}_{n,ab}\right|\mathbf{t}_{ab}. \tag{2.50}$$

For contacts between particles and walls, the walls are assumed to be non-moving and of infinite mass just like in the hard-sphere model.

The energy dissipated during contact between particles a and b can be calculated by solving the following integral over the duration of the contact:

$$E_{dsp,ab} = -\int \mathbf{F}_{ab} \cdot \mathbf{v}_{ab} dt. \tag{2.51}$$

Particle a can be in contact with several particles at the same time. Therefore the resulting force and torque acting on particle a are obtained by summation of the forces with respect to b:

$$\mathbf{F}_{contact,a} = \sum_b \left(\mathbf{F}_{n,ab} + \mathbf{F}_{t,ab}\right), \tag{2.52}$$

$$\mathbf{T}_a = \sum_b \left(R_a \mathbf{n}_{ab} \times \mathbf{F}_{t,ab}\right). \tag{2.53}$$

Since the contact forces are in general at least an order of magnitude larger than the external forces a separation of time scales was introduced. At each time step DT the external forces were taken into account while at $0.1DT$ the equations of motion were solved by taking only the contact forces into account.

It should be stressed here once again that the contact force model presented above was used because it is the most popular model for fluidised bed simulations. Therefore it is

the most useful model for a comparison with the hard-sphere model. However, it is not necessarily the best contact force available. In fact, the expression for the tangential contact force (equation 2.48) can lead to very unrealistic behaviour if no special measures are taken as will be demonstrated in the following paragraph.

3.2 Model parameters

The linear spring/dash-pot model features three key parameters that will be discussed here. The first is the spring stiffness (k) for both the linear normal and the linear tangential spring. Measurements by Mullier *et al*. (1991) for 6 mm diameter cellulose acetate spheres showed a linear dependency of the normal load upon the normal displacement apart from a short initial stage (Walton, 1992). Therefore the use of the linear spring can be justified for this type of material although it is one of the simplest models available. For a more elaborate discussion on contact theory the reader is referred to Johnson (1985). In most simulations the value of the spring stiffness is chosen rather low for computational convenience. Tsuji *et al.* (1993), Kawaguchi *et al*. (1998) and Mikami *et al*. (1998) all used a spring stiffness of 800 N/m for aluminum particles whereas Xu and Yu (1997) used a much higher value of 50,000 N/m in their simulations. The measurements by Mullier *et al*. (1991) suggest a value of about 400,000 N/m for the spring stiffness of the 6 mm diameter cellulose acetate spheres. It is likely that the values for the spring stiffness of 4 mm diameter aluminum spheres used in the work mentioned above are even higher. At higher values for the spring stiffness the duration of the contact becomes smaller and this requires a smaller time step to ensure numerical stability. From equation 2.47 (harmonic oscillator with (weak) damping) a solution for the displacement and relative velocity as a function of time can be obtained using the initial conditions ($\xi_n = 0$ at $t = 0$, and $v_n = v_{n0}$ at $t = 0$):

$$x_n(t) = \frac{v_{n0}}{\sqrt{B_2 k_n - (0.5 h B_2)^2}} \sin\left(\sqrt{B_2 k_n - (0.5 h B_2)^2}\, t\right) \exp(-0.5 h B_2 t), \qquad (2.54)$$

From this solution the (normal) contact time between two particles can be found using $\xi_n = 0$ at $t = t_{contact,\,n}$, and $v_n = -e\,v_{n0}$ at $t = t_{contact,\,n}$:

$$t_{contact,n} = \sqrt{\frac{p^2 + (\ln e)^2}{B_2 k_n}} \quad , \tag{2.55}$$

where B_2 is defined in equation 2.16 and e is the normal coefficient of restitution defined in equation 2.17. In a similar way a relation for the normal damping coefficient h_n can be obtained:

$$h_n = \frac{-2\ln e}{B_2 t_{contact,n}} . \tag{2.56}$$

Note that this result differs from the result presented by Mikami *et al*. (1998) which is only valid for a particle-wall contact.

In the case of ($e = 0$) the system is a critically damped harmonic oscillator and the contact time will be infinite. In that case the following relation should be used to obtain the damping coefficient h_n:

$$h_n = 2\sqrt{\frac{k_n}{B_2}} . \tag{2.57}$$

Xu and Yu (1997) presented a trial and error method to obtain the value of the damping coefficient that is far less elegant. They simulated a particle wall collision similar to the case presented in Figure 2.2 and adjusted the damping coefficient until the rebound height of the particle matched the expected value for that particular coefficient of restitution.

Another important issue is the difference between the normal and the tangential spring stiffness. In all soft-sphere simulations of fluidised beds reported in the literature the tangential spring stiffness is chosen to be equal to the normal spring stiffness. This can lead to energy inconsistencies as will be demonstrated here.

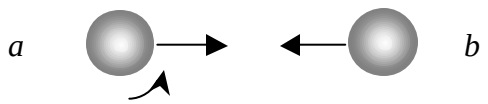

Figure 2.12. *Binary collision between rough spheres.*

Consider the case of a binary collision between rough particles (no sliding occurs) where there is a significant tangential component of the relative velocity as depicted in Figure 2.12 (see also Figure 2.13a). When applying the same analysis as for the normal contact time starting from equation 2.48 the following expression is found for the tangential contact time:

$$t_{contact,t} = \sqrt{\frac{p^2 + (\ln b_0)^2}{B_1 k_t}}, \tag{2.58}$$

where B_1 is defined in equation 2.15 and b_0 is the coefficient of tangential restitution defined in equation 2.19. Since B_1 and B_2 are not equal and e and b_0 are not necessarily equal as well, the following relation must be satisfied to ensure that the normal and tangential contact times are equal:

$$k_t = \frac{2}{7}\left(\frac{p^2 + (\ln b_0)^2}{p^2 + (\ln e)^2}\right) k_n . \tag{2.59}$$

If this relation is not satisfied the tangential spring will still be loaded at the instant of detachment. This implies that energy is stored in the spring that causes a defect in the

energy balance over the contact period. In the following section this will be demonstrated.

For the tangential damping coefficient the following result is obtained:

$$\eta_t = \frac{-2 \ln \beta_0}{B_1 t_{contact,t}}. \tag{2.60}$$

Note that also the tangential damping coefficient differs from the normal damping coefficient. This has never been addressed before in any of the soft-sphere simulations of gas-fluidised beds presented in the literature.

In the case of ($\beta_0 = 0$) the system is a critically damped harmonic oscillator and the contact time will be infinite. In that case the following relation should be used to obtain the tangential damping coefficient η_t:

$$\eta_t = \frac{4}{7}\sqrt{\frac{k_t}{B_1}}. \tag{2.61}$$

The coefficient of friction (μ) plays the same role in the linear spring/dash-pot model as it does in the hard-sphere model. It can be obtained from experiments as will be explained in section 5.

4. Hard-Sphere vs. Soft-Sphere

For the majority of the simulations presented in this work the hard-sphere model is used. However, there are certain cases where a soft-sphere model is to be preferred. In the following paragraphs the key differences between the two approaches will be highlighted.

4.1 Static situations

For dynamic systems in general a hard-sphere simulation is computationally faster than a soft-sphere simulation as long as there is sufficient motion in the system and the void fraction does not become too low. Severe problems are encountered when static situations like for example de-fluidisation occur. The particles become very closely packed with very low relative velocities. The number of collisions then increases exponentially whilst the impulse concerned with a single collision becomes negligible. Despite of the double precision accuracy used in the simulations the particles eventually overlap (although this overlap is far smaller than the atomic length scale) due to number loss and the algorithm breaks down. A soft-sphere model has no problems in dealing with static situations and is therefore to be preferred for simulations where such situations can occur. This includes systems where attractive forces between particles (like for example the liquid bridge forces in the simulations by Mikami *et al*. 1998) play an important role.

4.2 Spring stiffness

In the limit of an infinitely high value of the spring stiffness the soft-sphere model meets the hard-sphere model. However the soft-sphere model cannot be run at very high values of the spring stiffness due to computational limitations. The assumption of instantaneous collisions in the hard-sphere model does not capture the whole physics of the collision process but neither does the assumption of using an artificially low value for the spring stiffness in the soft-sphere model. It is important to realise that where a soft-sphere model in principle is capable of predicting the contact time between particles (which is of great importance for studying heat and mass transfer phenomena in gas-fluidised beds) these predictions have no value when an artificially low spring stiffness is used.

Furthermore there is the issue of the tangential spring stiffness versus the normal spring stiffness. In the vast majority of the linear spring/dash-pot soft-sphere models presented in the literature the tangential spring stiffness is chosen to be equal to the normal spring stiffness. This can lead to energy inconsistencies as will be demonstrated here. Consider the case presented in Figure 2.12. where two particles collide perfectly elastically and

perfectly rough (e = 1, b_0 = 1 and m is large enough to ensure a *sticking* collision). Particle *a* moves at a velocity of 0.01 m/s and a rotation velocity of 1.0 1/s toward particle *b* which does not rotate and moves at a velocity of –0.01 m/s. In Figure 2.13a the rotation velocity of particle a is plotted as a function of time for three cases: a hard-sphere simulation, a soft-sphere simulation with a tangential spring stiffness (k_t) at 2/7 of the normal spring stiffness (k_n) and a soft-sphere simulation with $k_t = k_n$.

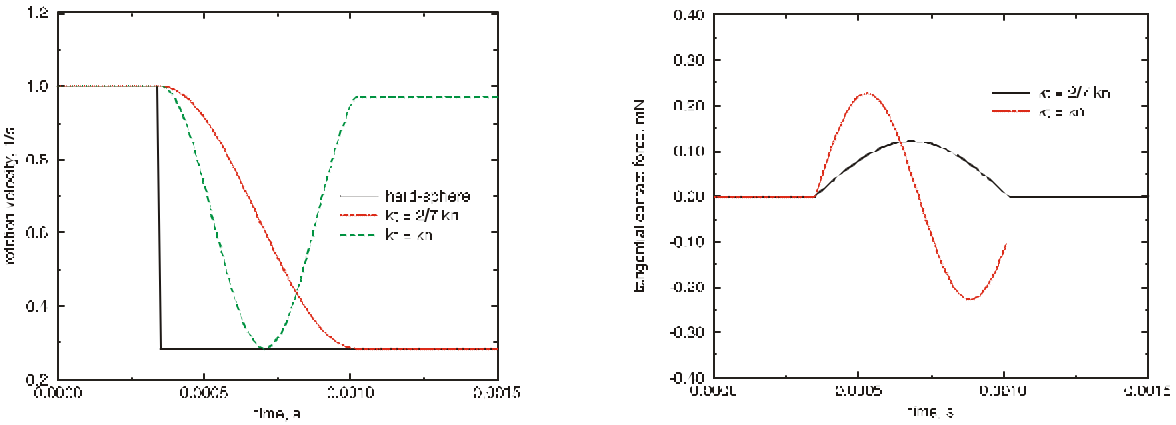

Figure 2.13. *a) Rotation velocity of particle a as a function of time. b) Tangential contact forces as a function of time.*

It is clear that in the case where $k_t = k_n$ the rotation velocity after collision is not predicted correctly. From Figure 2.13b) it can be seen that the tangential contact force is non-zero at the end of collision implying that not all the energy that is put into the spring is recovered. Hence energy inconsistencies can arise when k_t is chosen to be equal to k_n. It should be noted however that these inconsistencies are rather small since in general the rotation energy is two orders of magnitude smaller than the kinetic energy.

The particles in these simulations were 4 mm diameter aluminium spheres (r = 2700 kg/m^3) as previously used by Tsuji *et al*. (1993) and a value of 1000 kg/m was used for the normal spring stiffness. A time step of 10^{-7} s was used for the numerical integration.

4.3 Energy considerations

The main advantage of the hard-sphere model is that there is an analytical solution available for the collision model. Given the velocities of the particles prior to collision together with the particle properties the post-collision velocities can be calculated exactly. Hence numerical errors cannot cause any problems concerning energy conservation. This is not guaranteed for soft-sphere models where the accuracy of the solution depends on the time step used for the numerical integration. The time step should always be chosen carefully in such simulations to avoid energy inconsistencies. Consider the same case as in the previous paragraph (see Figure 2.12) but now none of the particles do rotate. A spring stiffness of 800 kg/m was chosen in order to match the parameter settings used by Tsuji *et al*. (1993) and Kawaguchi *et al.* (1998). For this binary head-on collision with the coefficient of (normal) restitution (*e*) set equal to 0.9 a contact time of 7.47 10^{-4} s can be calculated using equation 2.55. Tsuji *et al.* (1993) and Kawaguchi *et al*. (1998) used a time step of 2 10^{-4} s in their simulations with these particles. Mikami *et al*. (1998) performed simulations of a different system but used the same ratio between contact time and time step of 3.7. In Figure 2.14 the effect of the time step on the resolution of the normal contact force as a function of time is presented.

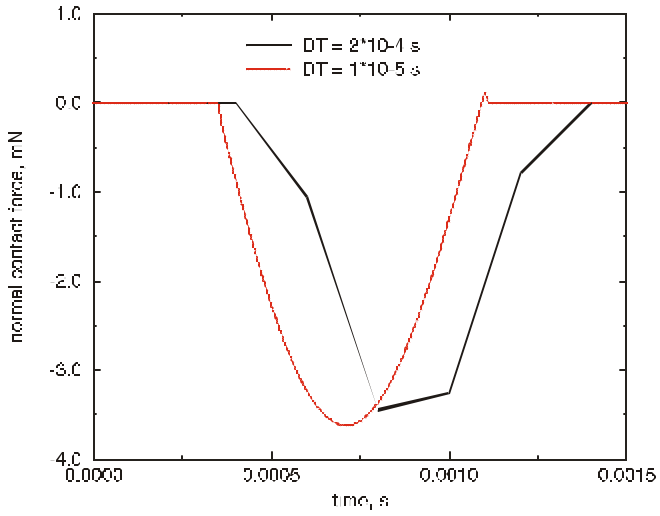

Figure 2.14. *The normal contact force as a function of time for a binary head-on collision at two different time steps (e = 0.9).*

It can be seen that the curve for the case with biggest time step (2 10^{-4} s) is by far not as smooth as the curve for the case with the smallest time step (1 10^{-5} s). However this results in a relative error in the energy balance that is surprisingly low (1.64 % for the 2 10^{-4} s case and 0.05% for the 1 10^{-5} s case). Nonetheless one should keep in mind that in a typical fluidised bed simulation a lot of collisions occur and this error can accumulate quite rapidly. Another typical feature of the linear spring/dash-pot model can be observed in this figure as well: in the final stage the contact force becomes attractive instead of repulsive ($DT = 10^{-5}$ s). This is due to the damping term in equation 2.47: at the end of the contact, when the overlap approaches zero, the relative velocity increases and hence the damping term causes the contact force to become negative (*i.e.* attractive).

Another error arises due to the determination of contact between particles at a constant time step. In Figure 2.14 this can be observed very well since the time at which the particles first come into contact is not the same for both time steps. The strategy used by Xu and Yu (1997) who determine the instant of first contact precisely by employing a collision search algorithm from hard-sphere simulations would prevent this. However the additional search for first contact goes at a cost of the computational speed whereas the actual integration is still performed at a rather large time step. Improvements can be achieved by employing higher order numerical schemes.

4.4 Multiple particle interactions

A drawback of the hard-sphere model is the assumption that the particles interact via instantaneous binary collisions. Consider the case presented in Figure 2.15 where a particle approaches two other particles at constant velocity in the absence of an external force. The particles are positioned in such a way that a three body collision should occur. The collision times for both pairs of particles are identical. In the hard-sphere routine one of the two possible collisions is detected as the first collision to occur and this binary collision (in this case a perfectly elastic, perfectly smooth collision) is processed first. The second collision is processed immediately afterwards where the post-collision

velocity of the first collision is used as the initial velocity for the second collision. This renders the rebound pattern shown in Figure 2.15. which is physically not correct.

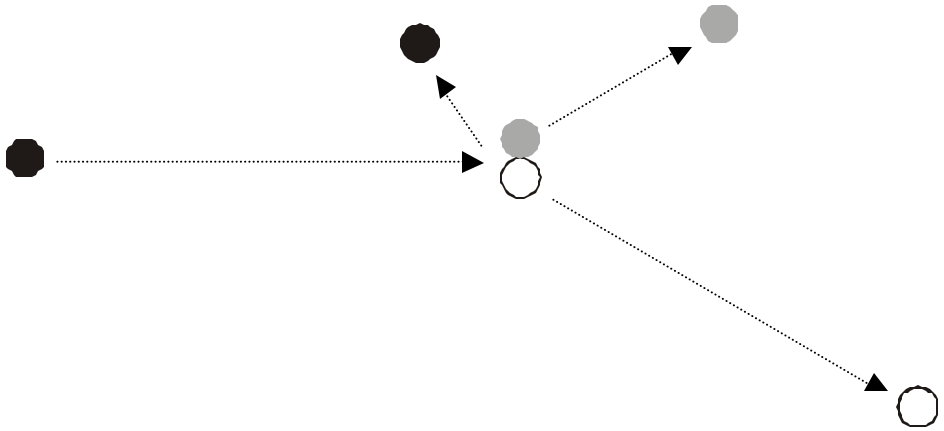

Figure 2.15. *Three-body collision simulated with a hard-sphere model.*

When the same case is repeated with the soft-sphere model the result presented in Figure 2.16 is obtained.

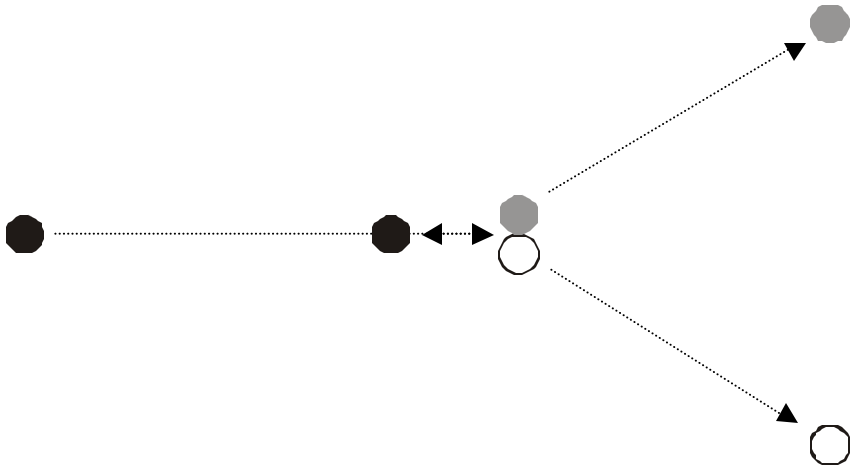

Figure 2.16. *Three-body collision simulated with a soft-sphere model.*

Because the soft-sphere model is capable of handling multiple particle interactions the rebound pattern is predicted correctly here. It should be noted that this specific test case

was carefully selected to demonstrate the effect of the assumption of instantaneous, binary collisions.

5. Measurement of collision parameters

In the hard-sphere model used in this work three parameters are required to describe to describe a collision: the coefficient of restitution (e), the coefficient of tangential restitution (b_0) and the coefficient of friction (m). These three parameters are also required for the linear spring/dash-pot model besides the spring stiffness. Unfortunately experimental data for these collision parameters are scarce in the open literature. This is rather surprising since rigid-body impact was already a research subject in the days of Galilei (1638) and the concept of the coefficient of restitution was introduced by Newton (1686) accompanied by the first experimental data. The book by Goldsmith (1960) provides a good review of both theory and experiments concerning impacts. Measurements of the coefficient of restitution are reported there as well including the dependency of this parameter upon impact velocity and particle size. In more recent years the attention was focussed on the impact of particles on flat plates (Maw *et al.*, 1981 and Sondergaard *et al.*, 1990) where more detailed data was obtained.

It was not until the last decade that also particle-particle collisions became a subject of experimental investigations. Foerster *et al*. (1994) presented a method to obtain the three collision parameters (e, m and b_0) by careful experimentation and image processing. The difficulty in these experiments lies in the control of the geometry of the impact. Lorenz *et al*. (1997) presented a refinement of this technique together with additional data for more types of particles then the cellulose acetate and soda lime glass spheres used by Foerster *et al*. 1994). Bernasconi *et al*. (1997) presented an advanced image processing technique employing three synchronised CCD cameras that enables accurate measurements of the particle position as well as the orientation of the particles. Labous *et al*. (1997) presented an experimental technique to measure collisional properties of spheres using high-speed video analysis. They studied the dependency of the coefficient of restitution on impact

velocity and particle mass. Despite the fact that quite a number of research groups are capable of measuring collision properties there is still a lack of collision data in the literature.

The Impact Research Group of the Open University at Milton Keynes has developed an accurate technique to measure collision properties. The collision properties of the glass particles used in simulations reported in Chapters 6 and 8 were measured at this facility. The technique to measure particle impact parameters accurately was first developed for particle impacts on flat plates and is described in detail by Kharaz *et al*. (1999). This set-up was used to measure the particle-wall impact parameters used for a simulation reported in Chapter 6. To enable measurement of particle-particle impact parameters some adjustments to the set-up were required that are reported by Gorham and Kharaz (1999) and will be briefly outlined here. The set-up used for the measurements is schematically represented in Figure 2.17.

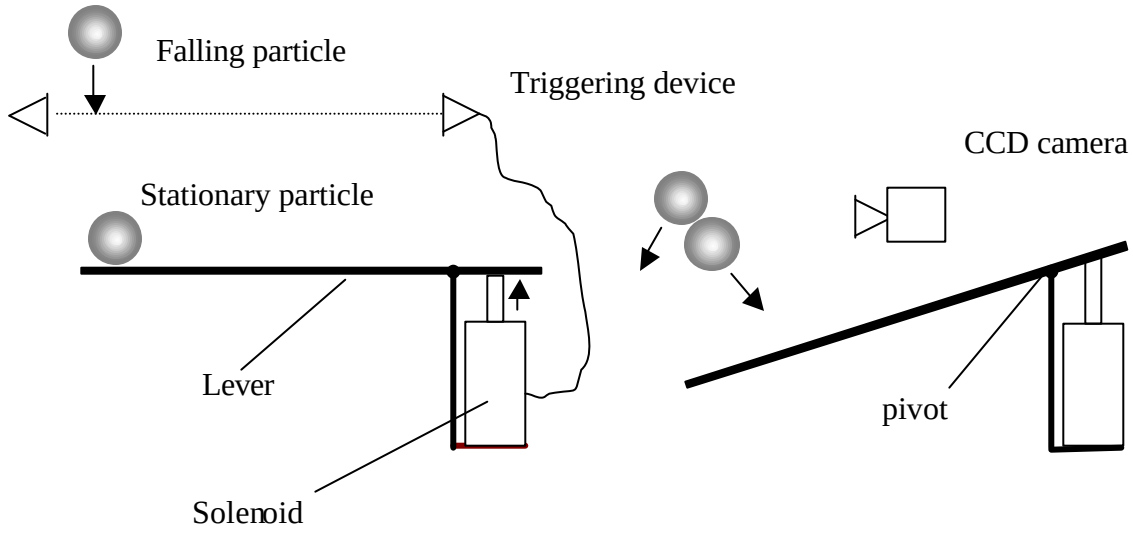

Figure 2.17. *Schematic representation of the experimental set-up used for the measurement of particle-particle collision properties: a) before collision b) after collision.*

A particle is released from a vacuum nozzle with zero rotation. It then falls through an optical-fibre triggering device which generates a sequence of pulses to control the CCD camera, the strobe light and the solenoid (Figure 2.17a). The lever-arm is then quickly moved away at 0.3 ms before collision leaving the stationary particle entirely free and in the correct position for a collision (Figure 2.17b). By following this procedure the particle can be assumed to be non-moving, non rotating and still at the same initial position. The collision is then recorded on a single frame of the CCD camera using strobe flashes that are timed in such a way that particle images do not overlap. This is required for accurate determination of the particle positions from the recording by digital image processing which finally yields the particle velocities before and after collision.

The coefficient of restitution (e) can easily be obtained from the normal components of the relative velocity before and after impact. Since the particles do not rotate before collision it is not necessary to know the particle rotation after impact since the velocity after impact ($\mathbf{v}_{ab}$), which includes a rotation contribution, can be calculated using equations 2.6 and 2.14. The two other collision parameters can now be obtained from a plot of Ψ_{after} as a function of Ψ_{before} that are defined as follows:

$$\Psi_{after} = \frac{-\left(\mathbf{v}_{ab} \cdot \mathbf{t}\right)}{\left(\mathbf{v}_{ab,0} \cdot \mathbf{n}\right)} , \tag{2.62}$$

$$\Psi_{before} = \frac{-\left(\mathbf{v}_{ab,0} \cdot \mathbf{t}\right)}{\left(\mathbf{v}_{ab,0} \cdot \mathbf{n}\right)} . \tag{2.63}$$

Such a plot is schematically represented in Figure 2.18. Each data point represents one collision measurement where the impact velocity was about 1.0 m/s.

Two straight lines are fitted through the data points: one for the *sticking* regime and one for the *sliding* regime. The coefficient of tangential restitution can be obtained from the slope of the *sticking* line:

$$\Psi_{before} = -b_0 \Psi_{after} , \tag{2.64}$$

and the coefficient of friction can be obtained from the intercept of the *sliding* line:

$$\Psi_{before} = \Psi_{after} - \frac{7}{2}(1+e)m \ . \tag{2.65}$$

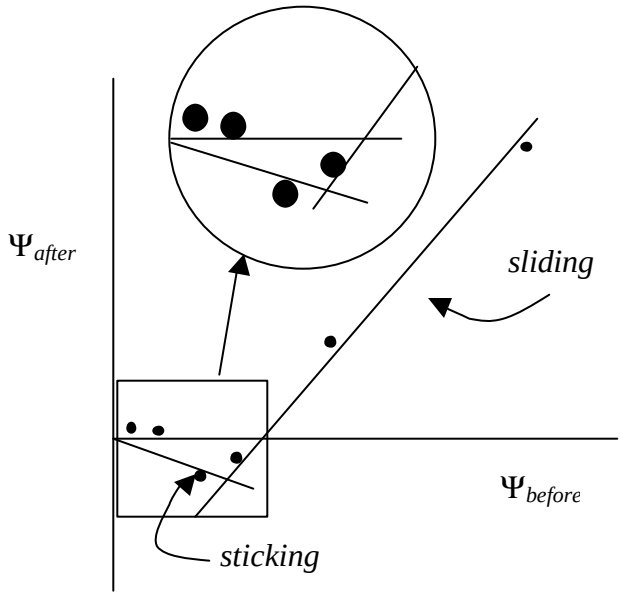

Figure 2.18. *Schematic representation of a plot of* Ψ_{after} *vs.* Ψ_{before} *for a typical result of a measurement.*

Each individual measurement yields either a value for e and $b_{0,}$ or e and m depending on the collision regime. Nevertheless a series of measurements is required to obtain the two linear fits that determine the two regimes. Typical results obtained with this technique for glass particles show the following values for the collision parameters: e = 0.97 ±0.01, m = 0.1 ±0.01 and b_0 = 0.33 ±0.05. For nearly head-on collisions (low values of Ψ_{before}) the measurements show positive values of Ψ_{after}. This phenomenon is referred to as *micro-slip* and cannot be explained by our hard-sphere model. The model developed by Maw *et al*. (1976) however is capable of predicting this phenomenon. Nevertheless it is believed

that the three-parameter hard-sphere collision model contains sufficient physics to be capable of reliable predictions.

6. External Forces

The incorporation of external forces differs somewhat from the approach followed by Hoomans *et al*. (1996). In this work the external forces are used in accordance with those implemented in the two-fluid model presented by Kuipers *et al.* (1992) where, of course, the forces now act on a single particle:

$$m_p \frac{d\mathbf{v}_p}{dt} = m_p \mathbf{g} + \frac{V_p b}{(1-e)}\left(\mathbf{u} - \mathbf{v}_p\right) - V_p \nabla p \tag{2.66}$$

where m_p represents the mass of a particle, $\mathbf{v}_p$ its velocity, $\mathbf{u}$ the local gas velocity and V_p the volume of a particle. A similar equation of motion was used by Kawaguchi *et al*. (1998). In equation 2.66 the first term on the right hand side is due to gravity. The second term is due to the drag force where b represents an inter-phase momentum exchange coefficient as it usually appears in two-fluid models. For low void fractions (e < 0.80) b is obtained from the well-known Ergun equation:

$$b = 150\frac{(1-e)^2}{e}\frac{m_g}{D_p^2} + 1.75(1-e)\frac{r_g}{D_p}\left|\mathbf{u} - \mathbf{v}_p\right| \tag{2.67}$$

where D_p represents the particle diameter, m_g the viscosity of the gas and r_g the density of the gas. For high void fractions (e ≥ 0.80) the following expression for the inter-phase momentum transfer coefficient has been used which is basically the correlation presented by Wen and Yu (1966) who extended the work of Richardson and Zaki (1954):

$$b = \frac{3}{4} C_d \frac{e(1-e)}{D_p} r_g \left| \mathbf{u} - \mathbf{v}_p \right| e^{-2.65} \tag{2.68}$$

The drag coefficient C_d is a function of the particle Reynolds number:

$$C_d = \begin{cases} \dfrac{24}{\mathrm{Re}_p}\left(1 + 0.15\mathrm{Re}_p^{0.687}\right) & \mathrm{Re}_p < 1000 \\ 0.44 & \mathrm{Re}_p \geq 1000 \end{cases} \tag{2.69}$$

where the particle Reynolds number in this case is defined as:

$$\mathrm{Re}_p = \frac{e r_g \left| \mathbf{u} - \mathbf{v}_p \right| D_p}{m_g} \quad . \tag{2.70}$$

The pressure gradient in the third term on the right hand side of equation 2.66 is calculated by using a first order approximation. The local value was obtained from an area weighted averaging technique using the values of the pressure gradients at the four surrounding grid nodes. This technique is also used to obtain local gas velocities and local void fractions at the position of the centre of the particle. The area weighted averaging technique used to obtain the local averaged value $\overline{Q}$ of a quantity Q(i,j) from the four surrounding computational nodes is shown in Figure 2.19. The local averaged value is calculated as follows:

$$\overline{Q} = \frac{A_{i,j} Q_{i,j} + A_{ii.j} Q_{ii,j} + A_{ii,jj} Q_{ii,jj} + A_{i,jj} Q_{i,jj}}{DXDY} \tag{2.71}$$

where:

$$\begin{aligned} A_{i,j} &= \left(DX - d_x\right)\left(DY - d_y\right) \\ A_{ii,j} &= d_x\left(DY - d_y\right) \\ A_{ii,jj} &= d_x d_y \\ A_{i,jj} &= \left(DX - d_x\right) d_y \end{aligned} \tag{2.72}$$

The distances d_x and d_y, necessary in this averaging technique, are calculated from the position of the particle in the staggered grid.

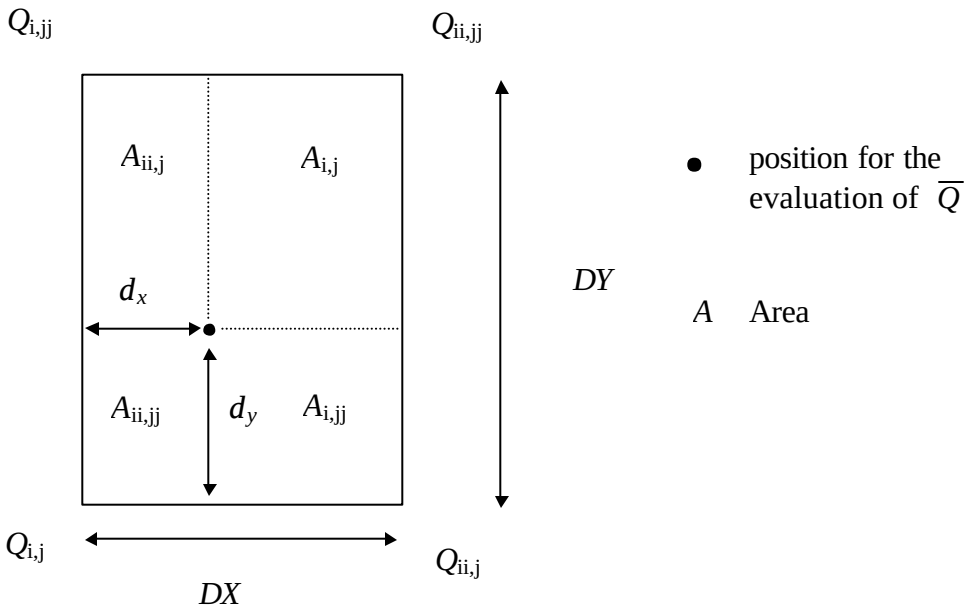

Figure 2.19. *Area weighted averaging.*

For the integration of equation 2.66 an explicit first order scheme is used to update the velocities and the positions of the particles. Other external forces than the ones included in equation 2.66 can be taken into account as well. In Chapter 7 simulations of more dilute flows in the riser section of a circulating fluidised bed are presented where lift forces were also taken into account.

Notation

B_1, B_2	collision constants, 1/kg
C_d	drag coefficient, [-]
D_{nblist}	diameter of neighbour square

D_p	particle diameter, m
dt_{nblist}	time step for neighbour list update, s
DT	time step, s
e	coefficient of restitution, [-]
E	energy, J
$\mathbf{F}$	force, N
$\mathbf{g}$	gravitational acceleration, m/s^2
I	moment of inertia, kgm^2
$\mathbf{J}$	impulse vector, kgm/s
k	spring stiffness, N/m
m	particle mass, kg
$\mathbf{n}$	normal unit vector, [-]
n_{tot}	total number of particles, [-]
n_{coll}	total number of collisions, [-]
R_p	particle radius, m
$\mathbf{r}$	position, m
$\mathbf{T}$	torque, Nm
$\mathbf{t}$	tangential unit vector, [-]
t	time, s
t_{ab}	collision time, s
$\mathbf{u}$	gas phase velocity, m/s
$\mathbf{v}$	velocity, m/s

Greek symbols

b	volumetric inter-phase momentum transfer coefficient, kg/(m^{3}s)
b_0	coefficient of tangential restitution, [-]
d	distance, m
e	void fraction, [-]
m_g	gas shear viscosity, kg/(ms)
m	friction coefficient, [-]
h	damping coefficient, Ns/m

r	density, kg/m^3
w	angular velocity, 1/s
x	displacement, m
Ψ	defined in equations 2.62 and 2.63, [-]

Subscripts

0	initial condition
a,b	particle indices
av	average
cp	contact point
dsp	dissipated
gyr	gyration
nblist	neighbour list
p	particle
w	wall

References

Alder, B.J. and Wainwright, T.E., (1957). Phase Transition for a Hard-Sphere System, *J. Chem. Phys*. **27**, 1208.

Alder, B.J. and Wainwright, T.E., (1959*).* Studies in Molecular Dynamics. I. General Method, *J. Chem. Phys*. **31**, 459.

Allen, M.P. and Tildesley, D.J., (1990). *Computer simulations of liquids*, Oxford Science Publications, Oxford, UK.

Bagnold, R.A., (1954). Experiments on a gravity-free dispersion of large solid particles in a Newtonian fluid under shear, *Proc. R. Soc. Lond.*, **A225**, 49.

Bernasconi, D.J., Fandrich, M.E. and Hogue, C., (1997). Experimental 3-D Impact Analysis. *Multibody System Dynamics*, **1**, 361.

Bird, G.A., (1976). *Molecular Gas Dynamics and Direct Simulation of Gas Flows*, Oxford University Press, Oxford, UK.

Campbell, C.S. and Brennen, C.E., (1985). Computer simulations of granular shear flows, *J.Fluid. Mech.* **151**, 167.

Cundall, P.A. and Strack, O.D.L., (1979). A discrete numerical model for granular assemblies. *Géotechnique*, **29**, 47.

de Gennes, P.G., (1999). Granular matter: a tentative view, *Rev. Mod. Phys*., **71**, S374.

Foerster, S.F., Louge, M.Y., Chang, H. and Allia, K., (1994). Measurements of the collision properties of small spheres. *Phys. Fluids*, **6** (3), 1108.

Frank, Th., Schade, K.-P. and Petrak, D., (1992). Numerical simulation and experimental investigation of a gas-solid two-phase flow in a horizontal channel, *Int. J. Multiphase Flow*, **19**, 187.

Frenkel, D. and Smit, B., (1996*). Understanding Molecular Simulation, from Algorithms to Applications*, Academic Press, Inc., San Diego, USA.

Frezzotti, A., (1997). A particle scheme for the numerical solution of the Enskog equation, *Phys. Fluids*, **9** (5), 1329.

Galilei, G., (1638). Unterredungen und Demonstrationen über zwei neue Wissenszweige, *Oswald's Klassiker* **25**, 38, Leipzig, W. Engelmann, 1890-91.

Ge, W. and Li, J., (1997). Pseudo-Particle Approach to Hydrodynamics of Gas/Solid Two-Phase Flow, In *Proceedings of the 5th Int. Conf. Circulating Fluidized beds, Beijing (China), May 28- June 1, 1996*, DT8, 1.

Goldsmith, W., (1960). *Impact, the theory and physical behaviour of colliding solids*, E. Arnold Pub., London.

Gorham, D.A. and Kharaz, A.H., (1999). Results of particle impact tests, Impact Research Group Report IRG 13, The Open University, Milton Keynes, UK.

Hogue, C. and Newland, D., (1994). Efficient computer simulation of moving granular particles, *Powder Technol.* **78**, 51.

Hoomans, B.P.B., Kuipers, J.A.M., Briels, W.J. and van Swaaij, W.P.M., (1996). Discrete particle simulation of bubble and slug formation in a two-dimensional gas-fluidised bed: a hard-sphere approach, *Chem. Engng Sci*., **51**, 99.

Hopkins, M.A. and Louge, M.Y., (1991). Inelastic microstructure in rapid granular flows of smooth disks, *Phys. Fluids* **A 3**(1), 47.

Ichiki, K. and Hayakawa, H., (1995). Dynamical simulation of fluidized beds: hydrodynamically interacting granular particles, *Phys. Rev. E*. **52**, 658.

Jaeger, H.M., Nagel, S.R. and Behringer, R.P., (1996). Granular solids, liquids and gases, *Rev. Mod. Phys*., **68**, 1259.

Johnson, K.L., (1985). *Contact Mechanics*, Cambridge University Press, Cambridge, UK.

Kawaguchi, T., Tanaka, T. and Tsuji, Y., (1998). Numerical simulation of two-dimensional fluidized beds using the discrete element method (comparison between the two- and three-dimensional models), *Powder Technol*. **96**, 129.

Kharaz, A.H., Gorham, D.A., and Salman, A.D., (1999). Accurate measurement of particle impact parameters, *Measurement Science and Technology* **10**, 31.

Knowlton, T.M., Carson, J.W., Klinzing, G.E. and Yang, W.C., (1994). The importance of storage, transfer and collection, *Chem. Eng. Progress*. **90** (4), 44.

Kuipers, J.A.M., van Duin K.J., van Beckum, F.P.H. and van Swaaij, W.P.M., (1992). A numerical model of gas-fluidized beds, *Chem. Engng Sci*., **47,** 1913

Labous, L., Rosato, A.D. and Dave, R.N., (1997). Measurements of collisional properties of spheres using high-speed video analysis, *Phys. Rev. E*. **56**, 5717.

Langston, P.A., Tüzün U. and Heyes, D.M., (1994). Continuous potential discrete particle simulations of stress and velocity fields in hoppers transition from fluid to granular flow, *Chem. Engng Sci.* **49**, 1259.

Langston, P.A., Tüzün, U. and Heyes, D.M., (1995). Discrete element simulation of granular flow in 2D and 3D hoppers: dependence of discharge rate and wall stress on particle interactions. *Chem. Engng Sci*. **50**, 967.

Lorenz, A., Tuozzolo, C. and Louge, M.Y., (1997). Measurement of impact properties of small, nearly spherical particles. *Exp. Mech*. **37**, 292.

Lun, C.C.K., (1996). Granular dynamics of slightly inelastic spheres in Couette flow, *Phys. Fluids* **8**, 2868.

Lun, C.C.K., and Liu, H.S., (1997). Numerical simulation of dilute turbulent gas-solid flows in horizontal channels, *Int. J. Multiphase Flow* **23**, 575.

Marin, M., Risso, D. and Cordero, P., (1993). Efficient algorithms for many-body hard particle molecular dynamics, *J. Comput. Phys.* **109**, 306.

Maw, N., Barber, J.R. and Fawcett, J.N., (1976). The oblique impact of elastic spheres, *Wear* **38**, 101.

Maw, N., Barber, J.R. and Fawcett, J.N., (1981). The role of elastic tangential compliance in oblique impact, *Trans. ASME: J. Lubrication Tech*. **103**, 74.

McCarthy, J.J., and Ottino, J.M., (1998). Particle dynamics simulation: a hybrid technique applied to granular mixing, *Powder Technol.* **97**, 91.

Mikami, T., Kamiya, H. and Horio, M., (1998). Numerical simulation of cohesive powder behavior in a fluidized bed, *Chem. Engng Sci.* **53**, 1927.

Mikami, T., (1998). Agglomeration fluidization of liquid/solid bridging particles an its control, PhD thesis, Tokyo University of Agriculture and Technology, Department of Chemical Engineering, Japan.

Müller, D. and Liebling, Th.M., (1995). Detection of collisions of polygons by using a triangulation, In *Contact Mechanics* (M. Raous, M. Jean and J.J. Moreau eds.), proceedings of the 2nd Contact Mechanics International Symposium, September 19-23, Carry-le–Rouet, France, p. 369.

Mullier, M. Tüzün, U. and Walton, O.R., (1991). A single-particle friction cell for measuring contact frictional properties of granular materials, *Powder Technol.* **65**, 61.

Newton. I., (1686). *Philosophiae naturalis principia mathematica,* (Translated into English by A. Motte). New York, D. Adee, 1848.

Oesterlé, B. and Petitjean, A., (1993). Simulation of particle-to-particle interactions in gas-solid flows, *Int. J. Multiphase flow* **19**, 191.

Ouyang, J. and Li, J. (1999). Particle-motion-resolved discrete model for simulating gas-solid fluidization, *Chem. Engng Sci.* **54**, 2077.

Richardson, J.F. and Zaki, W.N., (1954). Sedimentation and fluidization: part I. *Trans. Inst. Chem. Eng*. **32**, 35.

Rosato, A., Prinz, F., Standburg, K.J. and Swendsen, R., (1986). Monte Carlo Simulation of particulate matter segregation, *Powder Technol*. **49**, 59.

Schäfer, J., Dippel, S. and Wolf, D.E., (1996). Force schemes in simulations of granular materials, *J. Phys. I France* **6**, 5.

Schwarzer, S., (1995). Sedimentation and flow through porous media: Simulating dynamically coupled discrete and continuum phase, *Phys. Rev. E.* **52**, 6461.

Seibert, K.D. and Burns, M.A., (1996). Simulation of fluidized beds and other fluid-particle systems using statistical mechanics, *AIChE J*. **42**, 660.

Seibert, K.D. and Burns, M.A., (1998). Simulation of structural phenomena in mixed-particle fluidized beds, *AIChE J*. **44**, 528.

Sommerfeld, M., (1990). Numerical simulation of the particle dispersion in turbulent flow: the importance of particle lift forces ad particle/wall collision models, In *Numerical Methods for Multiphase Flows*, Vol. **91**. ASME, New York.

Sondergaard, R., Chaney, K. and Brennen, C.E., (1990). Measurements of solid spheres bouncing off flat plates, *J. Appl. Mech*. **57**, 694.

Stronge, W.J., (1990). Rigid body collisions with friction, *Proc. R. Soc. Lond. A.* **431**, 169.

Thornton, C., (1997). Coefficient of restitution for collinear collisions of elastic-perfectly plastic spheres, *J. Appl. Mech*. **64**, 383.

Tsuji, Y., Morikawa, Y., Tanaka. T., Nakatsukasa, N. and Nakatani, N., (1987). Numerical simulation of gas-solid two-phase flow in a two-dimensional horizontal channel, *Int. J. Multiphase Flow* **13**, 671.

Tsuji, Y., Tanaka, T. and Ishida, T., (1992). Lagrangian numerical simulation of plug flow of cohesionless particles in a horizontal pipe, *Powder Technol.* **71**, 239.

Tsuji, Y., Kawaguchi, T. and Tanaka, T., (1993). Discrete particle simulation of two dimensional fluidized bed, *Powder Technol.* **77**, 79.

Tsuji, Y., Tanaka, T. and Yonemura, S., (1998). Cluster patterns in circulating fluidized beds predicted by numerical simulation (discrete particle model versus two-fluid model), *Powder Technol.* **95**, pp. 254-264.

Walton, O.R. and Braun, R.L., (1986). Viscosity and temperature calculations for assemblies of inelastic frictional disks, *Journal of Rheology* **30**, 949.

Walton, O.R., (1992). Numerical simulation of inelastic, frictional particle-particle interactions, in *Particulate Two-Phase Flow, Part I,* edited by M.C. Roco, Butterworth-Heinemann, Boston, 884.

Wang, Y. and Mason, M.T., (1992). Two-dimensional rigid-body collisions with friction. *J. Appl. Mech*. **59**, 635.

Wen, C.Y. and Yu, Y.H., (1966). Mechanics of fluidization. *Chem. Eng. Prog. Symp. Ser*. **62** (62), 100.

Wightman, C., Moakher, M., Muzzio, F.J. and Walton, O., (1998). Simulation of flow and mixing of particles in a rotating and rocking cylinder, *AIChE J*. **44**, 1266.

Xu, B.H. and Yu, A.B., (1997). Numerical simulation of the gas-solid flow in a fluidized bed by combining discrete particle method with computational fluid dynamics. *Chem. Engng Sci*. **52**, 2785.

Yonemura, S., Tanaka, T. and Tsuji, Y., (1993). Cluster formation in gas-solid flow predicted by the DSMC method, In *Proc. ASME/FED Symp*. No. **166**, ASME, New York, USA, 303.

Chapter 3.

GAS PHASE HYDRODYNAMICS

Abstract:

In this chapter the model for the gas phase hydrodynamics is presented. The two-dimensional model is based on the volume averaged Navier-Stokes equations for two-phase flow and is solved on a scale larger than the particle size. This requires the drag force exerted on the particles by the gas phase to be incorporated in the model through empirical relations. A short review of techniques that allow the flow around each individual particle to be calculated, and thus do not require any empirical input concerning fluid-particle drag, is presented as well. The numerical solution technique and the applied boundary conditions are briefly outlined. Two-way coupling between the motion of the particles and the motion of the gas-phase is established via the void fraction and a source term in the momentum conservation equation for the gas phase. A detailed description of the calculation of the void fraction from both the 2-D and the 3-D granular dynamics model is presented. The incorporation of the momentum source term in the gas phase hydrodynamics model is explained as well.

Parts of this chapter are based on the papers:

B.P.B. Hoomans, J.A.M. Kuipers, W.J. Briels and W.P.M. van Swaaij, (1996). Discrete particle simulation of bubble and slug formation in two-dimensional gas-fluidised beds: a hard-sphere approach, *Chem. Engng Sci.*, **51**, 99.

B.P.B. Hoomans, J.A.M. Kuipers, W.J. Briels and W.P.M. van Swaaij, (1998). Comments on the paper 'Numerical simulation of the gas-solid flow in a fluidized bed by combining discrete particle method with computational fluid dynamics' by B.H. Xu and A.B. Yu, *Chem. Engng Sci.*, **54**, 2645.

1. Introduction

The drag force exerted on a particle by the gas phase requires the velocity of the gas phase at the position of the particle. In the approach used in this work the gas phase hydrodynamics is resolved on a length scale that is larger than the particle size. Hence empirical relations are required to determine the drag force exerted on the particles by the gas phase. This implies that special care has to taken to achieve correct two-way coupling. The technique adopted in this work is reminiscent of the Particle-Source-In Cell method developed by Crowe *et al*. (1977). An alternative for this method was presented by Pan and Banerjee (1996) where the particle effects on the fluid motion were fed back by calculating the velocity disturbance caused by the particles assuming that the flow around them is locally Stokesian. This technique is however rather expensive in terms of CPU time and is limited to rather dilute flows of particles that are slightly heavier than fluid.

The approach followed in this work is described in the preceding sections. However, it is worthwhile to discuss some techniques here that are capable of solving the flow field around each individual particle and therefore enable the calculation of the force exerted on the particle by the fluid without any empirical input. This can provide improved closure relations for the drag force that can be used in Eulerian Lagrangian simulations where the flow field is resolved on a scale larger than the particle diameter.

1.1 Direct solution of the Navier-Stokes equations

When the flow around a particle is solved using a no-slip boundary condition on the particle surface, the drag force exerted on the particle can be obtained by integration of the stress tensor over the particle surface. There are several methods available to solve the Navier-Stokes equations in such a complex geometry. Guj and de Matteis (1986) presented a technique to solve the two-dimensional flow field around an arrangement of particles using boundary fitted co-ordinates. Hu (1996) used a finite element technique

based on moving unstructured grids to simulate the two-dimensional motion of solid particles in a liquid. Kalthoff *et al.* (1997) developed a technique where a finite difference Navier-Stokes solver is used to solve the two-dimensional liquid motion. Since the grid size is smaller than the particle diameter a forcing technique was used to ensure no-slip boundary conditions on the particle surface. The drag force exerted on a particle was then obtained by numerical integration of the stress tensor over the particle surface using an analytical expansion of the fluid field.

Although these techniques provide a lot of detail without requiring any empirical input, the number of particles that can be used in these simulations is still limited (10^2 -10^3). Furthermore these are still two-dimensional simulations and hence three-dimensional models would put even higher demands on computing power.

1.2 Lattice Boltzmann simulations

A flow simulation technique that has become very popular in recent years is the lattice Boltzmann technique pioneered by McNamara and Zanetti (1988). In this technique a one-particle velocity distribution function rather than 'real particles' (as in lattice gas cellular automata as described by Frisch *et al.*, 1986) is transported on a carefully selected lattice. A time step in a lattice Boltzmann simulation consists of two phases: a collision phase and a propagation phase. The transport properties of the system (for example the viscosity) are defined by the eigenvalues of the collision operator used in the collision phase. This technique is capable of dealing with complex geometries which is important for the majority of flows encountered in industry. Eggels and Somers (1995) extended the technique by including a turbulent stress tensor as well as a scalar transport equation. Eggels (1996) used this model to perform large-eddy simulations of baffled stirred tank reactors in full 3-D.

The lattice Boltzmann technique is also capable of performing simulations of multiphase systems. Ladd (1994) used this technique to simulate colloidal systems. In these 3-D simulations special attention was paid to ensure no-slip boundary conditions on the

particle-fluid boundaries. In principle this method can also be applied to gas-solid systems as encountered in gas-fluidised beds. However the system should be of limited size (several solid particles instead of thousands) due to computational limitations. The method is therefore very well suited to obtain improved closure relations for the gas-particle drag force on the length scale at which it is applied in granular dynamics simulations of gas-fluidised beds as described in this work.

1.3 Dissipative Particle Dynamics

A somewhat similar approach to flow simulations is the dissipative particle dynamics technique originally developed by Koelman and Hoogerbrugge (1992). Hoogerbrugge and Koelman (1993) applied this technique to perform 3-D simulations of hard-sphere suspensions under steady shear. This technique is based on the dynamics of particles that should be regarded as momentum carriers rather than physical particles. Unlike in lattice Boltzmann simulations these particles are not restricted to lattice sites. The dynamics of these particles consists of a collision phase, where the interaction between the particles is taken into account, and a propagation phase, where the particles are moved according to an equation of motion that contains contributions of a random and a dissipative force. Español and Warren (1995) have shown that the dissipative force as used by Hoogerbrugge and Koelman (1993) needs to be modified in order to obey the fluctuation-dissipation theorem. Simulations of suspensions are possible by local freezing of particles that are found within the volume defined by the suspended particle. By summation of the forces experienced by all the particles that constitute the suspended particle, the net force exerted on the suspended particle is obtained. The DPD technique is capable of handling complex geometries and has been used to study colloidal systems. It seems however that the DPD technique is limited to low Reynolds number flow and therefore its use for inertia dominated systems, like gas-fluidised beds, is doubtful.

Ge and Li (1997) presented a technique that resembles DPD in the sense that the gas-phase is represented by discrete particles rather than the Navier-Stokes equations. Despite the fact that this method is rather original it leaves quite some questions unanswered. For

example it is not clear how physical properties of the gas are incorporated into the model. Furthermore it is not clear what equation of motion is used for the gas particles. It would be helpful if it could be demonstrated that this model is capable of predicting key fluidisation phenomena such as the minimum fluidisation velocity and the terminal velocity of a particle falling under the influence of gravity in a quiescent gas.

2. Governing Equations

The calculation of the gas-phase hydrodynamics mainly follows the lines presented by Kuipers *et al.* (1992). It is based on the numerical solution of the following set of partial differential equations that can be seen as a generalised form of the Navier-Stokes equations for a gas interacting with a solid phase as originally derived by Anderson and Jackson (1967).

Continuity equation gas phase:

$$\frac{\partial\left(\varepsilon_g \rho_g\right)}{\partial t} + \left(\nabla \cdot \varepsilon_g \rho_g \mathbf{u}\right) = 0 . \tag{3.1}$$

Momentum equation gas phase:

$$\frac{\partial\left(\varepsilon_g \rho_g \mathbf{u}\right)}{\partial t} + \left(\nabla \cdot \varepsilon_g \rho_g \mathbf{u}\mathbf{u}\right) = -\varepsilon \nabla p - \mathbf{S}_p - \left(\nabla \cdot \varepsilon \tau_g\right) + \varepsilon_g \rho_g \mathbf{g} \ . \tag{3.2}$$

In this work isothermal, two-dimensional motion is considered which implies that three basic variables have to be specified. The three basic variables in the model are the pressure (p) and the two velocity components of the gas-phase (u_x and u_y). The void fraction (ε) and the momentum exchange source term ($\mathbf{S}_p$) are obtained from the discrete

particle model as will be explained in section 6. All remaining variables have to be specified in terms of the three basic variables and/or the variables obtained from the discrete particle model through constitutive equations.

3. Constitutive Equations

3.1 Gas phase density

The gas phase density (r_g) is related to the pressure (p) and the gas phase temperature (T) by the ideal gas law:

$$?_g = \frac{M_g}{RT} p \ , \tag{3.3}$$

where R is the gas constant (8.314 J/(mol K)). The average molecular weight of air (M_g = 28.8 10^{-3} kg/mol) was used and the temperature was set to a constant value of T = 293 K.

3.2 Gas phase stress tensor

The viscous stress tensor t_g is assumed to depend only on the gas motion. The general form for a Newtonian fluid (Bird *et al*., 1960) has been implemented:

$$\mathrm{t}_g = - \left[\left(l_g - \frac{2}{3} m_g \right) (\nabla \cdot \mathbf{u}) \mathbf{I} + m_g \left((\nabla \mathbf{u}) + (\nabla \mathbf{u})^T \right) \right] . \tag{3.4}$$

In the simulations the bulk viscosity of the gas phase l_g was set equal to zero which is allowed for gases (Bird *et al*., 1960) whereas for the gas phase shear viscosity a constant value of m_g = 1.8 10^{-5} kg/ms was used. **I** denotes the unit tensor.

Note that no turbulence modelling was taken into account. For bubbling beds this can be justified since the turbulence is damped out in the bed due to the very high solids fraction.

4. Numerical Solution

The numerical solution follows the lines of Kuipers *et al.* (1993) and will not be discussed in detail here. A finite difference technique, employing a staggered grid to ensure numerical stability, is used to solve the gas-phase conservation equations 3.1 and 3.2. This implies that the scalar variables (p and e) are defined at the cell centre and that the velocity components are defined at the cell faces as is shown in Figure 3.1.

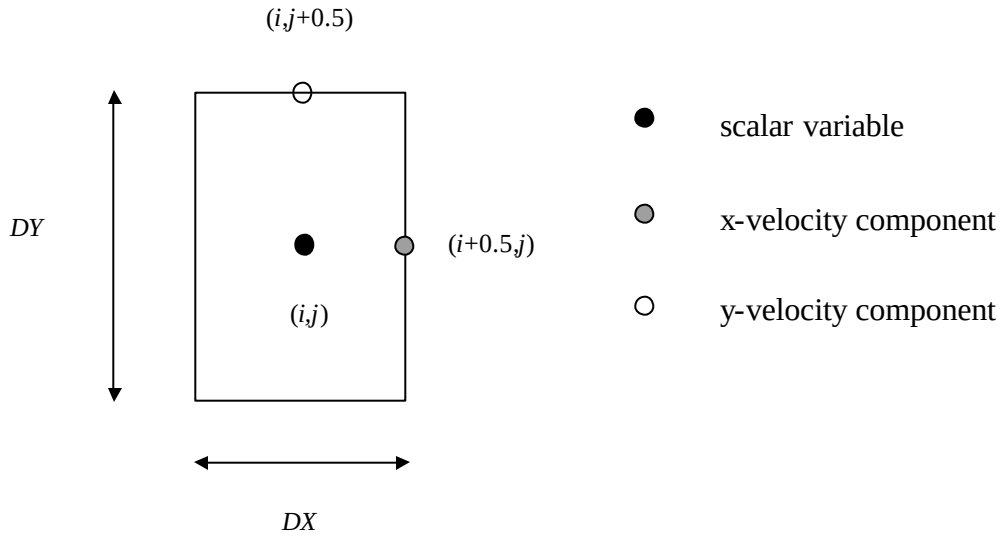

Figure 3.1. *Lay out of the staggered grid*.

A pressure correction technique was employed to solve the set of partial differential equations. The model is capable of performing transient two-dimensional calculations in a Cartesian or an axi-symmetrical geometry. In the simulations reported in this work only the Cartesian option was used.

5. Boundary Conditions

For the incorporation of the boundary conditions a flag matrix is used which allows boundary conditions to be specified for each single cell. A variety of boundary conditions can be applied by specification of the value of the cell flag fl(*i*,*j*) which is associated with the relevant boundary condition for that cell(*i*,*j*). The typical set of boundary conditions used in the simulations performed in this study is shown in Figure 3.2.

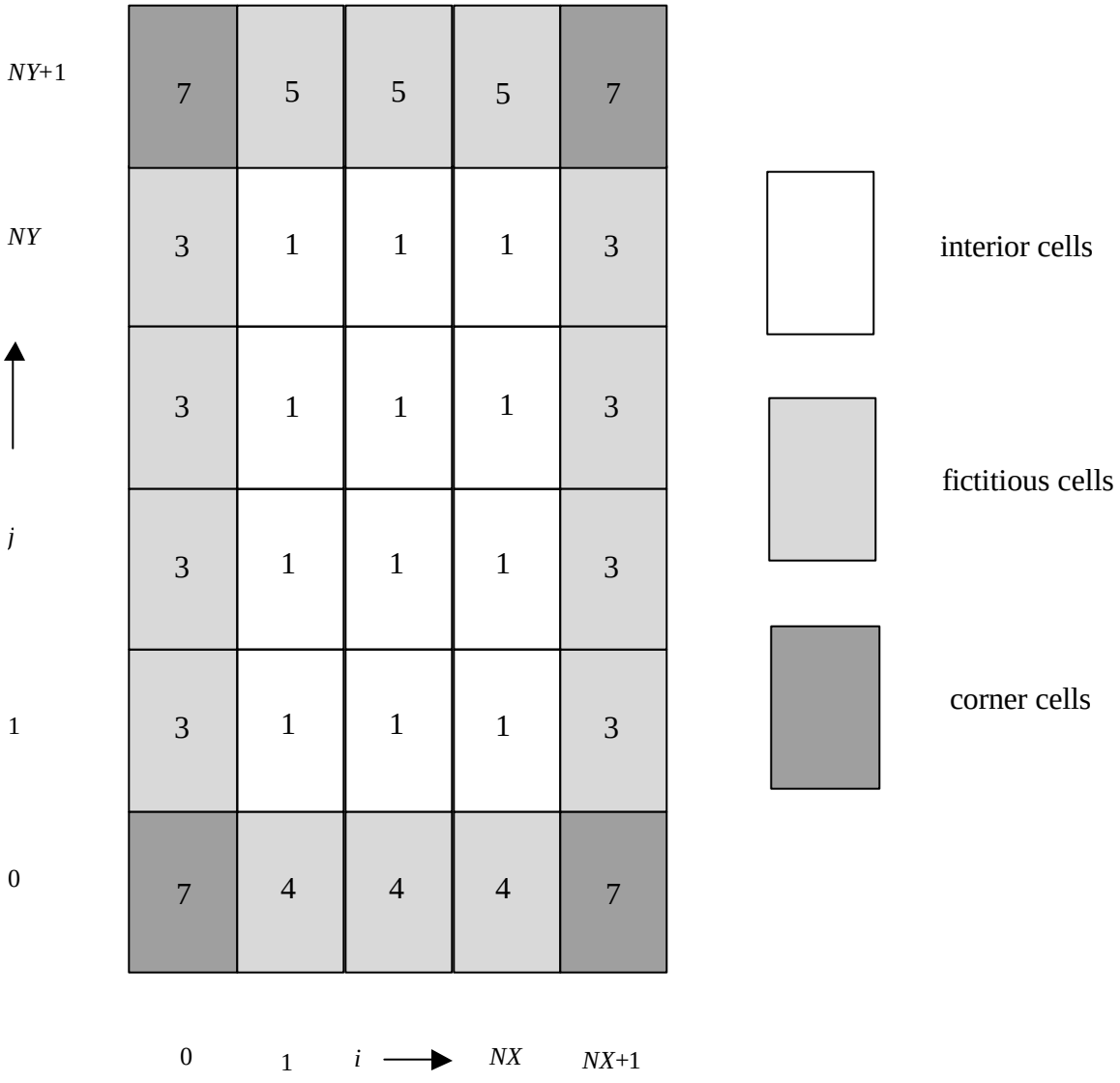

Figure 3.2. *Cell flags for the boundary conditions for the hydrodynamic model*

The cell flags and the corresponding boundary conditions that are featured in the present code are listed in Table 3.1.

Table 3.1. *Cell flags and corresponding cell types.*

fl(*i,j)*	Cell type of cell(*i,j*)
1	Interior cell, no boundary conditions have to be specified
2	Impermeable wall, free slip boundaries
3	Impermeable wall, no slip boundaries
4	Influx cell, velocities have to be specified
5	Prescribed pressure cell, free slip boundaries
6	Continuous outflow cell, free slip boundaries
7	Corner cell, no boundary conditions have to be specified

To mimic a distributor plate the void fraction in the influx cells (fl(*i,j*) = 4) was set to a constant value of 0.4.

6. Two-way coupling

An important issue in granular dynamics simulations of two-phase flow is the two-way coupling. The calculation of the drag force is based on empirical relations and therefore not exact. Hence it is required that two-way coupling is achieved in such a way that the model is capable to predict typical fluidisation phenomena such as the pressure drop over the bed at minimum fluidisation conditions. This pressure drop, multiplied by the cross sectional area, should balance the force exerted by gravity on the particles. Xu and Yu (1997) used a technique similar to the one used by Schwarzer (1995) where the total drag force exerted on a particle was fed back to the gas phase with a minus sign. With this technique the pressure drop over the bed at minimum fluidisation conditions in the simulations of Xu and Yu (1997) was over predicted by a factor 1.5 (Hoomans *et al*., 1998). Therefore special care has to be taken in order to select a two-way coupling technique that ensures the key fluidisation features to be incorporated correctly.

Two-way coupling is achieved via the calculation of the void fraction and the incorporation of an interaction term in the momentum conservation equation for the gas-phase (equation 3.2). In the following paragraphs it is explained how two-way coupling is achieved in the model used in this work.

6.1 Void fraction

6.1.1 Calculation of the void fraction in 2-D

The solution of equations 3.1 and 3.2 requires specification of the void fraction (e) which can be obtained from the discrete particle model. Since the particle positions are known the void fraction $e(i,j)$ can be calculated based on the area occupied by the particles in that cell i,j. Since the void fraction is an important parameter which considerably influences the motion of the gas phase, a detailed check for overlap was performed in which multiple cell overlap was taken into account as illustrated in Figure 3.3. In this figure a case is presented where a particle overlaps four different grid cells. The distances from the particle centre to the nearest boundaries of the grid cells are indicated by d_1 and d_2.

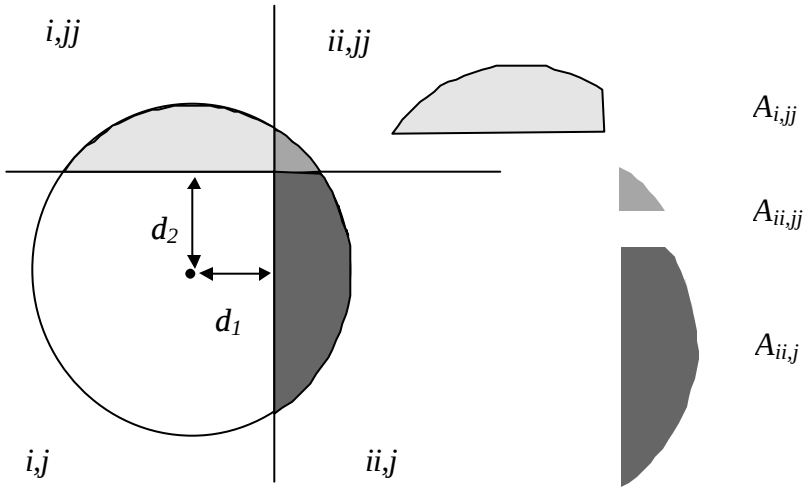

Figure 3.3. *Multiple particle-cell overlap*.

The smallest overlapping area of the particle $A_{ii,jj}$ can be calculated as follows:

$$A_{ii,jj} = d_1 d_2 - \frac{1}{2} R_p \left[d_1 \sqrt{1 - \left(\frac{d_1}{R_p} \right)^2} + d_2 \sqrt{1 - \left(\frac{d_2}{R_p} \right)^2} - R_p \left(\arccos\left(\frac{d_1}{R_p} \right) - \arcsin\left(\frac{d_2}{R_p} \right) \right) \right] . \quad (3.5)$$

For the area A_{jj} overlapping with the upper two cells in Figure 3.3 the following relation can be obtained:

$$A_{jj} = A_{i,jj} + A_{ii,jj} = R_p \left(R_p \arccos\left(\frac{d_2}{R_p} \right) - d_2 \sqrt{1 - \left(\frac{d_2}{R_p} \right)^2} \right) . \quad (3.6)$$

Keeping in mind that:

$$A_{i,j} + A_{i,jj} + A_{ii,jj} + A_{ii,j} = pR_p^2 , \quad (3.7)$$

all four areas can now be calculated using basic subtractions. In the case where a particle overlaps with only two cells the area of overlap can simply be obtained from equation 3.6.

However, the void fraction calculated in this way is based on a two-dimensional analysis that is inconsistent with the applied empiricism in the calculation of the drag force exerted on a particle (Chapter 2, section 6). To correct for this inconsistency the void fraction calculated on the basis of area (e_{2D}) is transformed into a three-dimensional void fraction (e_{3D}) using the following equation:

$$e_{3D} = 1 - \frac{2}{\sqrt{p\sqrt{3}}} \left(1 - e_{2D} \right)^{3/2} . \quad (3.8)$$

This equation has been derived on the basis of a comparison between a two-dimensional hexagonal lattice and a three-dimensional FCC unit cube assuming equal inter-particle distances. It ensures that the closest packing in the 2-D hexagonal lattice is transformed into the closest packing in the 3-D FCC case. Ouyang and Li (1999) used a transformation similar to equation 3.8 but used the square root of 2 instead of 2 in the second term on the right hand side. This renders void fractions that in general are too high.

Tsuji *et al*. (1993), Xu and Yu (1997), Kawaguchi *et al*. (1998) and Mikami *et al*. (1998) all used a different approach. They calculated the void fraction on the basis of volumes assuming that the system consists of one particle layer. Hence the third dimension is equal to the particle diameter. This method yields void fractions that are in general too high as well. Using this method the closest packing can never be obtained and therefore it is not a correct representation for a three-dimensional system.

6.1.2 Calculation of the void fraction in 3-D

In the 3-D model the problem with the conversion of a 2-D void fraction to a 3-D void fraction no longer exists. Since the gas phase hydrodynamics is still resolved in 2-D each particle can still have overlap with four cells at maximum. Consider Figure 3.3 but now read volumes instead of areas. The main difficulty in the 3-D void fraction calculation is to obtain an expression for the volume $V_{ii,jj}$. Since there is no analytical expression available for this volume an approximation has to be used. When a particle overlaps with two cells the volume of a spherical cap can be calculated exactly by:

$$V_{cap} = \frac{p\left(R_p - d_1\right)^2}{3}\left(2R_p + d_1\right), \tag{3.9}$$

with d_1 being the distance from the centre of the particle to the cell boundary. $V_{ii,jj}$ can now be approximated by:

$$V_{ii,jj} = \left(\frac{V_{ii,jj} + V_{i,jj}}{V_p} \right) \left(\frac{V_{ii,jj} + V_{ii,j}}{V_p} \right) V_p \,. \tag{3.10}$$

Since $V_{ii,jj}+V_{i,jj}$ and $V_{ii,jj}+V_{ii,j}$ are sphere caps, these volumes can be calculated using equation 3.9. Each of the 4 volumes can subsequently be obtained using basic subtractions.

6.2 Momentum transfer

The method used in this work is based on Newton's third law and was also used by Delnoij *et al.* (1997). It differs from the technique used by Hoomans *et al.* (1996). The reaction force to the drag force exerted on a particle per unit volume is included in the momentum conservation equation 3.2 via a source term $\mathbf{S}_p$ that has the dimension N/m^3:

$$\mathbf{S}_p = -\frac{1}{V} \int \sum_{a=0}^{Npart} \frac{V_p \, b}{(1-e)} \; (\mathbf{u} - \mathbf{v}_a) d \;\; (\mathbf{r} - \mathbf{r}_a) dV \tag{3.11}$$

The d-function ensures that the reaction force acts as a point force at the position of the particle in the system. In the numerical implementation this force-per-volume term is distributed to the four nearest grid nodes using the area weighted averaging technique described in Chapter 2, section 6, where also the expression for the volumetric momentum exchange coefficient b can be found. A mixed explicit implicit numerical treatment was applied similar to the one used by Kuipers *et al.* (1993) to solve the gas phase conservation equations.

Since the source term $\mathbf{S}_p$ has the dimension of force per unit volume the force exerted on the particles has to de divided by the volume of a grid cell. In the 3-D model this is straightforward since the third dimension is determined by the depth of the bed. In the 2-D model a virtual third dimension has to be introduced. This virtual third dimension is

estimated based on the same calculation as the conversion from e_{2D} to e_{3D}. In the 2-D simulations the volume of a computational cell was chosen to be:

$$V_{cell} = 2DRDZ\,3^{-0.75}D_p, \tag{3.12}$$

in which the third dimension is slightly less than the particle diameter. Note that this volume depends on the particle size and hence is not a constant in simulations where a particle size distribution is taken into account.

Tsuji *et al.* (1993), Kawaguchi *et al.* (1998) and Mikami *et al.* (1998) use a technique where the coupling was achieved in a similar way as in two-fluid models. This technique was also employed by Hoomans *et al.* (1996). A two-fluid model requires averaged values of particle velocities and these can be obtained by averaging over all the particles in a computational cell. However, this technique is limited to systems consisting of particle of uniform size and therefore the technique used in this work was preferred.

Notation

A	area, m^2
D_p	particle diameter, m
DX	horizontal computational cell dimension, m
DY	vertical computational cell dimension, m
$fl(i,j)$	cell flag [-], defined in Table 1
$\mathbf{g}$	gravitational acceleration, m/s^2
$\mathbf{I}$	unity tensor, [-]
i,j	cell indices, [-]
M	molecular weight, kg/mol
NX	number of computational cells in x-direction, [-]
NY	number of computational cells in y-direction, [-]
p	pressure, Pa

r	particle position vector, m
R_p	particle radius, m
R	gas constant, J/mol K
$\mathbf{S}_p$	source term defined in equation 3.11
t	time, s
T	temperature, K
u	gas phase velocity, m/s
V	volume, m^3
v	velocity, m/s

Greek symbols

b	volumetric interphase momentum transfer coefficient, $kg/(m^3s)$
d	distance, m
e	void fraction, [-]
l_g	gas bulk viscosity, kg/(m.s)
m_g	gas shear viscosity, kg/(m.s)
r	density, kg/m^3
t	gas phase stress tensor, kg/ms^2

Subscripts

g	gas phase
i,j	cell indices
p	particle
x	x-component
y	y-component

Superscripts

T	transposed

References

Anderson, T.B. and Jackson, R., (1967). A fluid mechanical description of fluidized beds (equations of motion), *Ind. Eng. Chem., Fundam.,* **6**, 527.

Bird, R.B., Stewart, W.E. and Lightfood, E.N., (1960). *Transport phenomena*, John Wiley & Sons, New York.

Crowe, C.T., Sharma, M.P. and Stock, D.E., (1977). The Particle-Source-In Cell (PSI-CELL) model for gas-droplet flows, *ASME Trans. J. Fluids Eng*., 325.

Delnoij, E., Lammers, F.A., Kuipers, J.A.M. and van Swaaij W.P.M., (1997). Dynamic simulation of dispersed gas-liquid two-phase flow using a discrete bubble model, *Chem. Engng Sci*., **52**, 1429.

Eggels, J.G.M., and Somers, J.A., (1995). Numerical simulation of free convective flow using the lattice-Boltzmann scheme, *Int. J. Heat and Fluid Flow*, **16**, 357.

Eggels, J.G.M., (1996). Direct and large-eddy simulation of turbulent and fluid flow using the lattice-Boltzmann scheme, *Int. J. Heat and Fluid Flow*, **17**, 307.

Español, P. and Warren, P., (1995). Statistical mechanics of dissipative particle dynamics, *Europhys. Lett.,* **30**, 191.

Ge, W. and Li, J., (1997). Pseudo-Particle Approach to Hydrodynamics of Gas/Solid Two-Phase Flow, In *Proceedings of the 5th Int. Conf. Circulating Fluidized beds, Beijing (China), May 28- June 1, 1996,* DT8, 1.

Guj, G. and de Matteis, G., (1986). Fluid-particles interaction in particulate fluidized beds: numerical and experimental analysis, *Phys. Chem. Hydrodynamics,* **7**, 145.

Hoogerbrugge, P.J. and Koelman, J.M.V.A., (1992). Simulating microscopic hydrodynamic phenomena with dissipative particle dynamics, *Europhys. Lett*., **19**, 155.

Hoomans, B.P.B., Kuipers, J.A.M., Briels, W.J. and van Swaaij, W.P.M., (1996). Discrete particle simulation of bubble and slug formation in a two-dimensional gas-fluidised bed: a hard-sphere approach, *Chem. Engng Sci*., **51**, 99.

Hoomans, B.P.B., Kuipers, J.A.M., Briels, W.J. and van Swaaij, W.P.M., (1998). Comments on the paper "Numerical simulation of the gas-solid flow in a fluidized bed by combining discrete particle method with computational fluid dynamics" by B.H. Xu and A.B. Yu, *Chem. Engng Sci*., **53**, 2645.

Hu, H.H., (1996). Durect simulation of flows of solid-liquid mixtures, *Int. J. Multiphase Flow*, **22**, 335.

Kalthoff, W., Schwarzer, S. and Hermann, H.J., (1997). Algorithn for the simulation of particle suspensions with inertia effects, *Phys. Rev. E*, **56**, 2234.

Kawaguchi, T., Tanaka, T. and Tsuji, Y., (1998). Numerical simulation of two-dimensional fluidized beds using the discrete element method (comparison between the two- and three-dimensional models), *Powder Technol*., **96**, 129.

Koelman, J.M.V.A. and Hoogerbrugge, P.J., (1993). Dynamics simulations of hard-sphere suspensions under steady shear, *Europhys. Lett*., **21**, 363.

Kuipers, J.A.M., van Duin K.J., van Beckum, F.P.H. and van Swaaij, W.P.M., (1992). A numerical model of gas-fluidized beds, *Chem. Engng Sci*., **47,** 1913.

Kuipers, J.A.M., van Duin K.J., van Beckum, F.P.H. and van Swaaij, W.P.M., (1993). Computer simulation of the hydrodynamics of a two-dimensional gas-fluidized bed, *Comput. Chem. Engng*, **17**, 839.

Ladd, A.J.C., (1994). Numerical simulations of particulate suspensions via a discretized Boltzmann equation. Part 1. Theoretical foundation, *J. Fluid Mech*., **271**, 185.

McNamara, G.R. and Zanetti, G., (1988). Use of the Boltzmann equation to simulate latice-gas automata, *Phys. Rev. Lett*., **61**, 2332.

Mikami, T., Kamiya, H. and Horio, M., (1998). Numerical simulation of cohesive powder behavior in a fluidized bed, *Chem. Engng Sci*., **53**, 1927.

Ouyang, J. and Li, J. (1999). Particle-motion-resolved discrete model for simulating gas-solid fluidization, *Chem. Engng Sci.*, **54**, 2077.

Pan, Y. and Banerjee, S., (1995). Numerical simulation of particle interactions with wall turbulence, *Phys. Fluids*, **8**, 2733.

Schwarzer, S., (1995). Sedimentation and flow through porous media: Simulating dynamically coupled discrete and continuum phase, *Phys. Rev. E.*, **52**, 6461.

Tsuji, Y., Kawaguchi, T. and Tanaka, T., (1993). Discrete particle simulation of two dimensional fluidized bed, *Powder Technol.*, **77**, 79.

Xu, B.H. and Yu, A.B., (1997). Numerical simulation of the gas-solid flow in a fluidized bed by combining discrete particle method with computational fluid dynamics, *Chem. Engng Sci*., **52**, 2785.

Chapter 4.

THE EFFECT OF PARTICLE PROPERTIES ON THE HYDRODYNAMICS OF GAS-FLUIDISED BEDS WITH HOMOGENOUS INFLOW CONDITIONS

Abstract:

A hard-sphere Granular Dynamics model was used to study the influence of particle properties on the hydrodynamics of gas-fluidised beds with homogeneous inflow conditions. In the model the Newtonian equations of motion are solved for each solid particle while taking into account the particle-particle and particle-wall collisions. The gas phase hydrodynamics is described by the spatially averaged Navier-Stokes equations for two-phase flow. The hydrodynamics of a homogeneously fluidised bed (0.5 m height, 0.15 m width, 2400 particles of 4 mm diameter, $\rho = 2700\ kg/m^3$, $u_{gas} = 1.5\ u_{mf}$) was strongly affected by the collision parameters (i.e. the coefficients of restitution and friction): the more energy is dissipated in collisions the more bubbling and slugging could be observed. The Root Mean Square (RMS) of the pressure fluctuations inside the bed showed an almost linear dependency on the energy dissipation rate by collisions during the simulation for low dissipation rates. The effect of a particle size distribution on the bed hydrodynamics was studied as well. Pressure peaks inside the bed decreased with increasing geometric standard deviation of the log-normal size distribution. Simulations with a three-dimensional model (as far as the particles are concerned) required a minimum depth of the bed of five particle diameters for stable simulations. The results of the three-dimensional simulations confirmed the trends observed in the two-dimensional simulations concerning the effect of the collision parameters on the bed hydrodynamics. Time series of the pressure inside the bed showed a lower frequency and a lower RMS value in the 3-D simulations. The particle-wall interaction had a more pronounced influence on the hydrodynamics in the 3-D simulations than in the 2-D simulations.

Parts of this chapter are based on the papers:

B.P.B. Hoomans, J.A.M. Kuipers, W.J. Briels and W.P.M. van Swaaij, (1996). Discrete particle simulation of bubble and slug formation in two-dimensional gas-fluidised beds: a hard-sphere approach, *Chem. Engng Sci.*, **51**, 99.

B.P.B. Hoomans, J.A.M. Kuipers and W.P.M. van Swaaij, (1998). The influence of a particle size distribution on the granular dynamics of dense gas-fluidized beds: a computer simulation study, *AIChE Symp. Ser. No. 318*, **Vol. 94**, 15.

B.P.B. Hoomans, J.A.M. Kuipers and W.P.M. van Swaaij, (1998). The influence of particle properties on pressure signals in dense gas-fluidised beds: a computer simulation study, *World Congress on Particle Technology 3*, July 7-9, Brighton, UK.

1. Introduction

With increasing computer power Granular Dynamics simulations have become a very useful and versatile research tool to study the dynamics of dense gas-particle flows. In these models the Newtonian equations of motion are solved for each individual granular particle in the system. The mutual interactions between particles and the interaction between particles and walls are taken into account directly. Applications of this type of models are very diverse ranging from agglomerate dynamics (Thornton *et al.*, 1996) to hopper flow (Langston *et al.*, 1995) and gas-fluidised beds (Hoomans *et al.*, 1996).

In fluidisation simulations the Granular Dynamics models have a clear advantage over continuum models since the particle interactions are taken into account directly and consequently the necessity to specify closure relations for the solids-phase stress tensor, as encountered in continuum models (Kuipers *et al.*, 1992 among many others), is circumvented. Furthermore a discrete particle model is very well suited to take an arbitrary particle size distribution into account which is far more complex, if not impossible, in case a continuum modelling approach is adopted.

Tsuji *et al.* (1993) developed a two-dimensional soft-sphere discrete particle model of a gas-fluidised bed based on the work of Cundall and Strack (1977). In this approach the particles are allowed to overlap slightly and this overlap is subsequently used to calculate the contact forces. Kawaguchi *et al.* (1998) extended the model developed by Tsuji *et al.* (1993) to three-dimensions as far as the motion of the particles is concerned. Hoomans *et al.* (1996) used a hard-sphere approach in their two-dimensional discrete particle model of a gas-fluidised bed which implies that the particles interact through binary, instantaneous, inelastic collisions with friction. Xu and Yu (1997) used a two-dimensional soft-sphere model similar to the one used by Tsuji *et al.* (1993) in their fluidised bed simulations but they also employed techniques from hard-sphere simulations in order to determine the instant when the particles first come into contact precisely. Mikami *et al.* (1998) presented a two-dimensional soft-

sphere model of a gas-fluidised bed where cohesive forces between the particles were taken into account. A more detailed discussion of the models mentioned above is presented in Chapter 2.

In Granular Dynamics simulations particle-particle and particle-wall interactions are taken into account directly which is a clear advantage over continuum models. Collision parameters like the coefficient of restitution can be included in continuum models by employing the kinetic theory of granular flow to arrive at improved closure relations for the solids-phase stress tensor (Sinclair and Jackson (1989), Gidaspow (1994), Nieuwland *et al.* (1996)). However, these improved closures rely on a one-parameter collision model, do not take particle rotation into account and more importantly show an extreme and non-realistic sensitivity of the overall bed hydrodynamics to very small deviations from one for the coefficient of restitution (Hrenya and Sinclair, 1997). Within the framework of a discrete particle model the collision parameters are included in a more natural way and therefore this type of model is to be preferred when investigating the influence of particle parameters on the bed hydrodynamics.

Hoomans *et al.* (1996) have shown that the dynamics of a fluidised bed depends strongly on the collision parameters (*i.e.* coefficients of restitution (e) and friction (μ)). In the case where no energy is dissipated (*i.e.* $e = 1$ and $\mu = 0$) no bubble or slug formation was observed and the bed showed a rather homogeneous fluidisation behaviour. In the case where the impact parameters were given more realistic values (i.e. $e = 0.9$ and $\mu = 0.3$) and hence energy is dissipated in collisions, bubble formation was observed and the bed behaviour appeared to be in much better agreement with that observed in reality. Van den Bleek and Schouten (1993) already showed that the coefficient of restitution has an effect on the dynamics of a fluidised bed. They used a one-dimensional five-particle-array model to generate time series of particle position and voidage which is described in more detail by Schouten and van den Bleek (1992). These time series were subsequently analysed by applying techniques from deterministic chaos theory. They found that for increasing values of the coefficient of restitution (up to 0.9) the bed dynamics became less chaotic. The coefficient of

restitution was varied over a range from 0.0 to 0.9, which is unfortunately not the most interesting range. Typical values for this parameter of granular material generally used in fluidisation are found within 0.8 and 1.0. However, it is clear that despite the fact that this five-particle-array model is a rather crude representation of the dynamics of a fluidised bed, it does capture the essential feature that the collision parameters have a pronounced effect on the bed hydrodynamics.

Experimental studies on the influence of particle interaction parameters on the dynamics of gas-fluidised beds are unfortunately rather scarce. For example the Geldart (1974) classification of the fluidisation behaviour of powders does not include any particle interaction parameters. Thiel and Potter (1977) reported an influence of the particle-particle interaction on the dynamics of slugging fluidised beds. They characterised this interaction through the *angle of internal friction* (Zenz and Othmer, 1960). This is a bulk property rather than a particle property but in general it can be assumed that the rougher the particles the lower the angle of internal friction. Chen *et al.* (1997a and 1997b) investigated the influence of solid frictional interactions on pressure fluctuations in fluidised beds. They also characterised the particle interaction through the angle of internal friction. For relatively shallow beds they found larger root mean square (RMS) values for the pressure fluctuations in beds consisting of particles with lower angles of internal friction. They also reported a negligible influence of the wall roughness on the RMS values of the measured pressure fluctuations. Chang and Louge (1992) studied the hydrodynamics in a riser where they applied a coating to glass particles in order to make them smoother and hence obtain a lower coefficient of friction. Although this system is operated in a completely different regime compared to those prevailing in the experiments mentioned above and the simulations presented in this chapter, the experimental results obtained by Chang and Louge (1992) are worthwhile mentioning here. For the coated particles a completely different axial pressure profile was measured than for the regular glass particles. In the case of the coated particles (*i.e.* lower coefficient of friction) the solids hold-up in the riser section (and thus the axial pressure gradient) was a lot smaller. Since the only difference between the two experiments was the use of the coated particles instead of the regular glass particles their experiments indicate that particle-particle interaction has a significant effect on the flow structure in the riser.

In this chapter the dependency of the hydrodynamics of a gas-fluidised bed with homogeneous inflow conditions on the collision parameters is investigated in more detail using the hard-sphere model. Furthermore the model was used to study the influence of a particle size distribution on the hydrodynamics of gas-fluidised beds with homogeneous inflow conditions. The majority of the simulations was performed with the two-dimensional model, but also simulations with the three-dimensional model were performed.

2. Model

Since a detailed description of the model is presented in Chapter 2 and Chapter 3, the key features will be summarised briefly here.

2.1 Granular dynamics

The collision model as originally developed by Wang and Mason (1992) is used to describe a binary, instantaneous, inelastic collision with friction. The key parameters of the model are the coefficient of restitution ($0 \leq e \leq 1$) and the coefficient of friction ($m \geq 0$). Foerster *et al.* (1994) have shown that also the coefficient of tangential restitution ($0 \leq b_0 \leq 1$) should be used in order to describe the collision dynamics more accurately. These three collision parameters are all included in the model.

In the hard-sphere approach a sequence of binary collisions is processed. This implies that a collision list is compiled in which for each particle a collision partner and a corresponding collision time is stored. A constant time step is used to take the external forces into account and *within* this time step the prevailing collisions are processed sequentially. In order to reduce the required CPU time neighbour lists are used. For each particle a list of neighbouring particles is stored and only for the particles in this list a check for possible collisions is performed.

2.2 External forces

The incorporation of external forces differs somewhat from the approach followed by Hoomans *et al*. (1996). In this work the external forces are used in accordance with those implemented in the two-fluid model presented by Kuipers *et al.* (1992) where, of course, the forces now act on a single particle:

$$m_p \frac{d\mathbf{v}_p}{dt} = m_p \mathbf{g} + \frac{V_p \beta}{(1-\varepsilon)}\left(\mathbf{u} - \mathbf{v}_p\right) - V_p \nabla p \quad , \tag{4.1}$$

where m_p represents the mass of a particle, $\mathbf{v}_p$ its velocity, $\mathbf{u}$ the local gas velocity and V_p the volume of a particle. In equation (4.1) the first term is due to gravity and the third term is the force due to the pressure gradient. The second term is due to the drag force where β represents an inter-phase momentum exchange coefficient as it usually appears in two-fluid models. For low void fractions (ε < 0.80) β is obtained from the well-known Ergun equation:

$$\beta = 150 \frac{(1-\varepsilon)^2}{\varepsilon} \frac{\mu_g}{D_p^2} + 1.75(1-\varepsilon)\frac{\rho_g}{D_p}\left|\mathbf{u} - \mathbf{v}_p\right| \quad , \tag{4.2}$$

where D_p represents the particle diameter, μ_g the viscosity of the gas and ρ_g the density of the gas. For high void fractions ($\varepsilon \geq 0.80$) the following expression for the inter-phase momentum transfer coefficient has been used which is basically the correlation presented by Wen and Yu (1966) who extended the work of Richardson and Zaki (1954):

$$\beta = \frac{3}{4} C_d \frac{\varepsilon(1-\varepsilon)}{D_p} \rho_g \left|\mathbf{u} - \mathbf{v}_p\right| \varepsilon^{-2.65} \, . \tag{4.3}$$

The drag coefficient C_d is a function of the particle Reynolds number and given by:

$$C_d = \begin{cases} \dfrac{24}{\mathrm{Re}_p}\left(1 + 0.15\mathrm{Re}_p^{0.687}\right) & \mathrm{Re}_p < 1000 \\ 0.44 & \mathrm{Re}_p \geq 1000 \end{cases}, \tag{4.4}$$

where the particle Reynolds number (Re_p) in this case is defined as follows:

$$\mathrm{Re}_p = \frac{e\, r_g \left|\mathbf{u} - \mathbf{v}_p\right| D_p}{m_g} \quad . \tag{4.5}$$

For the integration of equation (4.1) a simple explicit first order scheme was used to update the velocities and positions of the particles.

2.3 Gas phase hydrodynamics

The calculation of the gas phase hydrodynamics mainly follows the lines presented by Kuipers *et al.* (1992). It is based on the numerical solution of the following set of partial differential equations that can be seen as a generalised form of the Navier-Stokes equations for a gas interacting with a solid phase as originally derived by Anderson and Jackson (1967).

Continuity equation gas phase:

$$\frac{\P\left(e r_g\right)}{\P t} + \left(\nabla \cdot e r_g \mathbf{u}\right) = 0 \ . \tag{4.6}$$

Momentum equation gas phase:

$$\frac{\P\left(e r_g \mathbf{u}\right)}{\P t} + \left(\nabla \cdot e r_g \mathbf{u}\mathbf{u}\right) = -e\nabla p - \mathbf{S}_p - \left(\nabla \cdot e\mathrm{t}_g\right) + e r_g \mathbf{g} \ . \tag{4.7}$$

In this work transient, two-dimensional, isothermal (T = 293 K) flow of air at atmospheric conditions is considered. The constitutive equations can be found in Chapter 3. There is one important modification with respect to the model presented by Hoomans *et al*. (1996) and that deals with the way in which the two-way coupling between the gas-phase and the dispersed particles is established. In the present model the reaction force to the drag force exerted on a particle per unit of volume is fed back to the gas phase through the source term $\mathbf{S}_p$ which has the dimension of force per unit of volume N/m^3.

3. Effects of collision parameters

A large number of simulations was performed in order to investigate the influence of the collision properties on the bed dynamics. As a test system the same system as used before by Tsuji *et al.* (1993), Hoomans *et al.* (1996) and Xu and Yu (1997) was chosen. The most important system parameters are summarised in table 4.1.

Table 4.1. *Parameter settings for all simulations*

Particles		Bed	
Shape	Spherical	Width	0.15 m
Diameter, D_p	4.0 mm	Height	0.50 m
Material	Aluminium	Number of x-cells	15
Density, ρ	2700 kg/m^3	Number of y-cells	25
Number, N_{part}	2400		

In all simulations the minimum fluidisation conditions were used as initial conditions while the values for the coefficients of restitution (e) and friction (μ) were varied. A time step of 10^{-4} seconds was used in all simulations and the gas inflow at the bottom was set equal to 1.5 u_{mf} for the whole width of the bed (u_{mf} = 1.78 m/s). The simulations were continued for 8 seconds real time and during the simulations the pressure in the bed 0.2 m above the centre of the bottom plate was monitored.

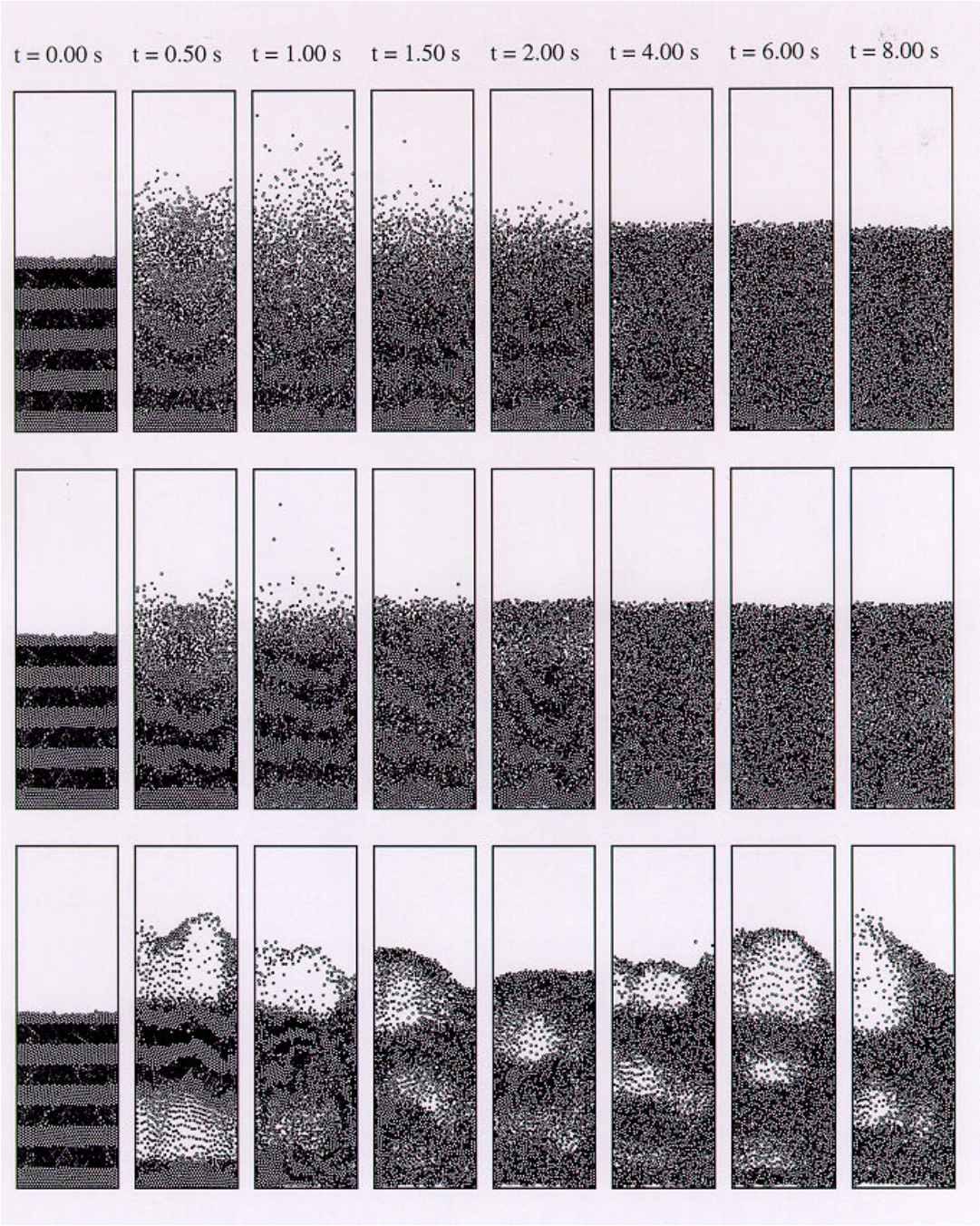

Figure 4.1. *Snapshots of particle configurations for three simulations with* $u_g = 1.5\ u_{mf}$. *Upper:* $e = 1$, $m = 0$, *middle:* $e = 0.99$, $m = 0$, *bottom:* $e = 0.9$, $m = 0.3$.

A typical (non-ideal) run takes about 6 minutes of CPU-time per simulated second on a Silicon Graphics Origin200 server (R10000 processor, 180 MHz). Snapshots of the particle configurations for three different simulations are presented in Figure 4.1. The two extreme cases (e = 1.0, m = 0.0 (ideal) and e = 0.9, m = 0.3 (non-ideal)) are shown there together with a simulation where e = 0.99 and m = 0.0. A number of particle layers was marked by colour at t = 0 s in order to visualise the induced particle mixing during the fluidisation process. It can be seen that in the ideal case barely any bubbles or slugs are being formed which enables the initial structure to remain intact for quite some time. In the non-ideal case the formation of bubbles and slugs can be observed clearly and due to these instabilities the particle mixing in the bed is much better. After 2 seconds the initial structure can still be observed in the ideal case whereas it has completely disappeared in the non-ideal case. The simulation with e = 0.99 resembles the ideal case very much although the particle mixing appears to be slightly better. This is a much more natural dependency than the one reported for instance by Hrenya and Sinclair (1997). They reported simulations of riser flow using a two-fluid model that incorporates the kinetic theory for granular flow a change in e from 1.0 to 0.99 completely changed the hydrodynamic behaviour.

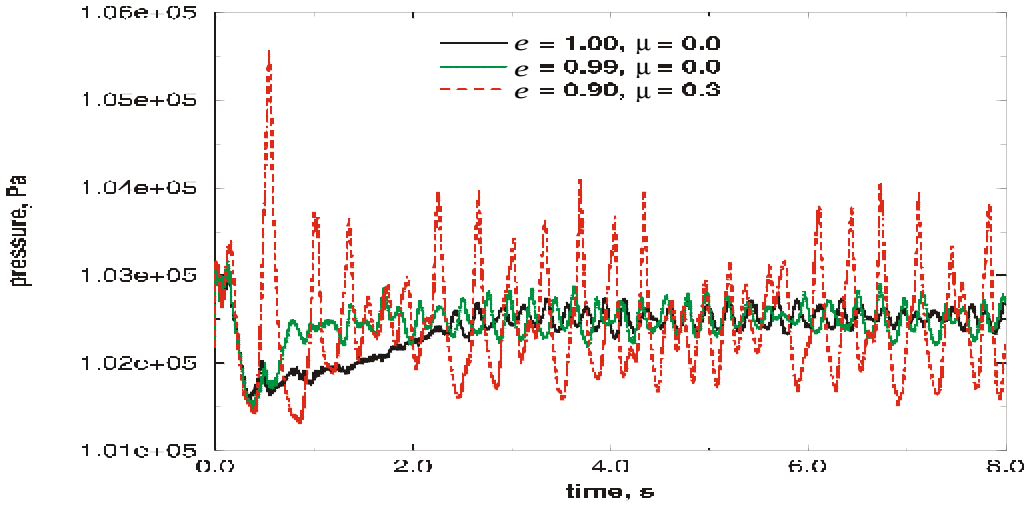

Figure 4.2. *Pressure at 0.2 m above the centre of the distributor plate as a function of time.*

However, it should be noted that these simulations were concerned with a different hydrodynamic regime than encountered in the simulations reported here and therefore a direct comparison may not be justified.

The computed pressure signals at 0.2 m above the centre of the bottom plate for the three simulations are presented in Figure 4.2. It can be observed that the pressure fluctuations in the non-ideal case are much stronger than in the ideal case. In fact the pressure fluctuations turn out to depend strongly on the collision parameters. In Figure 4.3 the root mean square (RMS) of the pressure signals is presented as a function of the coefficient of restitution (e).

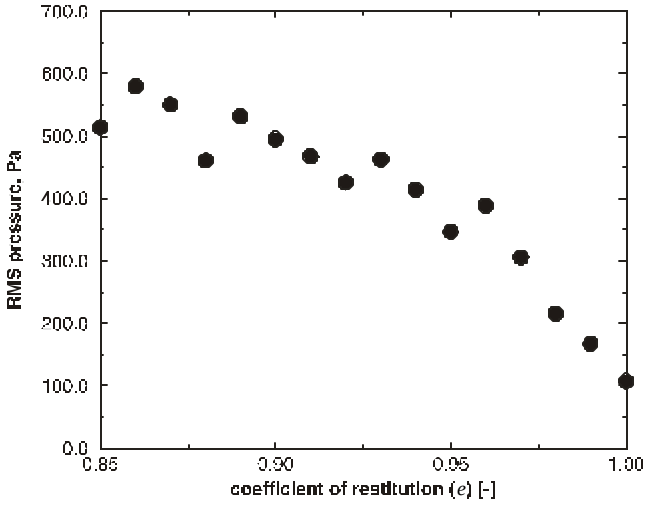

Figure 4.3. *Root Mean Square (RMS) of the pressure fluctuations as a function of the coefficient of restitution.*

It can clearly be observed that the RMS increases with decreasing value of e. The fact that, for instance, the RMS value for the simulation with e = 0.96 is higher than that for the simulation with e = 0.95 is due to the different dynamics. Despite of the lower value for the coefficient of restitution a higher amount of energy is dissipated in collisions during the simulation. Because the total number of collisions in these simulations is about the same (8.3 million) the average impact velocity was apparently higher in the case of e = 0.96. With a slightly different initial condition this might change which is due the complex (i.e. chaotic) nature of the system's dynamics. In all the simulations that were performed in order to obtain the RMS values presented in

Figure 4.3, the coefficient of friction was set equal to zero. In the calculation of the RMS the initial stages of the simulation (approximately 2 s) were not taken into account in order to avoid start-up effects from influencing the results.

In Figure 4.4 the RMS is presented as a function of the value of the coefficient of friction (μ). For all the simulations that were performed in order to obtain the RMS values presented in Figure 4.4 the coefficient of restitution (e) was set equal to 1.0.

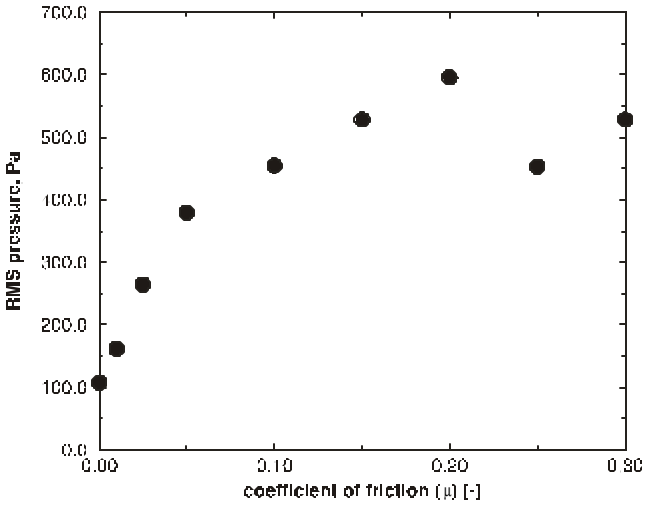

Figure 4.4. *Root Mean Square (RMS) of pressure fluctuations as a function of the coefficient of friction.*

Here it can be observed that the RMS increases with increasing value for the coefficient of friction. In Figure 4.4 the value for the RMS is lower for the simulation with $\mu = 0.25$ than for the simulations with $\mu = 0.2$ which is not expected. However the amount of energy dissipated in collisions for both simulations is not the same; in fact more energy is dissipated in the simulation with $\mu = 0.2$ than in the simulation with $\mu = 0.25$. In the latter case fewer collisions occurred and apparently the collisions that occurred had less impact.

Also the influence of the coefficient of tangential restitution (b_0) was investigated. However, this parameter turned out to have little influence on the overall bed hydrodynamics. This is probably due to the low (but realistic) values used for the coefficient of friction (μ). When the coefficient of friction was increased ($\mu = 1000$)

to ensure that all collisions were of the *sticking* type the influence of b_0 was much more pronounced. With e =1.0, m = 1000 and b_0 = 1.0 similar results were obtained as for the case with e = 1.0, m = 0.0 and b_0 = 0.0. However, the influence of the coefficient of tangential restitution for realistic values of the coefficient of friction (m < 1.0) was negligible.

In all simulations mentioned above the values of the collision parameters for particle-wall collisions were taken to be equal to the values for particle-particle collisions. The influence of the particle-wall interaction on the overall bed hydrodynamics was investigated as well. This influence was found to be negligible. The particle-particle interaction is very much dominant over the particle-wall interaction in the 2-D model used here. A simulation with ideal particle-particle interaction (e = 1.0, m = 0.0) but non-ideal particle-wall interaction (e_w = 0.9 , m_w = 0.3) showed very similar results as in the fully ideal case.

In Figure 4.5 the RMS of the pressure is plotted as a function of the energy dissipation rate by collisions during the simulation. All simulations performed in this study are included in this figure.

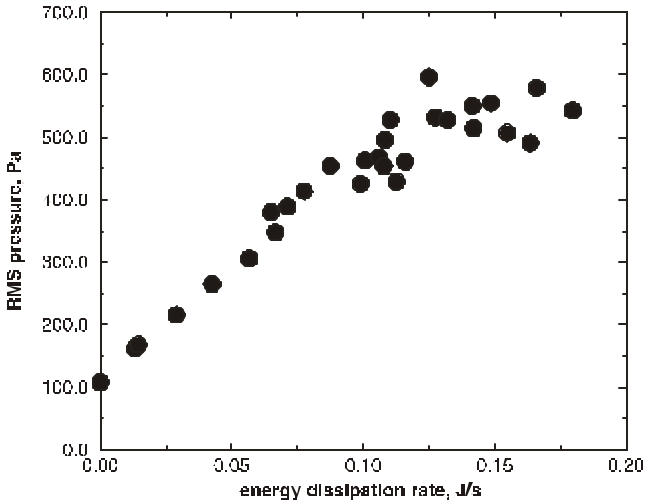

Figure 4.5. *Root Mean Square (RMS) of pressure fluctuations as a function of the energy dissipation rate by collisions during the simulation*.

It can be seen that the RMS increases almost linearly with the energy dissipation rate by collisions in the system. For higher values of the dissipation rate (*i.e.* lower coefficients of restitution and/or higher coefficients of friction) the data points show some scatter. This is due to the richer dynamics of the system (*i.e.* more vigorous bubbling and slugging which causes a more irregular pressure signal) at higher dissipation rates which requires longer simulation times than the 8 seconds employed here in order to obtain better statistics.

4. Energy conservation

Since the amount of energy dissipated in collisions turns out to have a profound influence on the bed hydrodynamics the energy housekeeping during a simulation was investigated in more detail. The energies concerned with the particle positions and velocities (*i.e.* kinetic energy, potential energy and rotation energy) can be calculated (instantaneously) as follows:

$$E_{kin} = \frac{1}{2}\sum_{k}^{Npart} m_k v_k^2 , \tag{4.8}$$

$$E_{pot} = \sum_{k}^{Npart} m_k g r_{y,k} , \tag{4.9}$$

$$E_{rot} = \frac{1}{2}\sum_{k}^{Npart} I_k w_k^2 \quad . \tag{4.10}$$

The energy dissipated in collisions is calculated using the equations presented in Chapter 2. This dissipated energy is taken to be positive by definition. The energy that the particles receive from the interaction with the gas phase can be obtained as follows:

$$E_{drag} = \sum_{k}^{Npart} \int \left(\frac{V_{p,k}\, b}{(1-e)} (\mathbf{u} - \mathbf{v}_k) - V_{p,k} \nabla p \right) \cdot \mathbf{v}_k \, dt \quad . \tag{4.11}$$

All the five different energies mentioned above are calculated independently. Since the dissipated energy is taken to be positive by definition the sum of the potential,

kinetic, rotation and dissipated energy should equal the amount of energy that the particles receive from the interaction with the gas phase. The total amount of energy in the system can now be obtained as follows:

$$E_{tot} = E_{pot} + E_{kin} + E_{rot} + E_{disp} - E_{drag}, \tag{4.12}$$

and this amount should remain constant during a simulation.

In Figure 4.6 the energy housekeeping during a simulation with non-ideal collision parameters (e = 0.9, m = 0.3) is presented. It can be observed that the potential energy is larger than the kinetic energy. The rotation energy is about 2 orders of magnitude smaller than the potential energy and therefore appears to be zero in this figure. The energy dissipated in collisions increases almost linearly with time and its behaviour is closely followed by the energy supplied by the drag force. In Figure 4.7 the energy housekeeping during a simulation with ideal collision parameters (e = 1.0, m = 0.0) is presented. It should be stressed that the only differences between the system in Figure 4.6 and 4.7 are the values of the collision parameters.

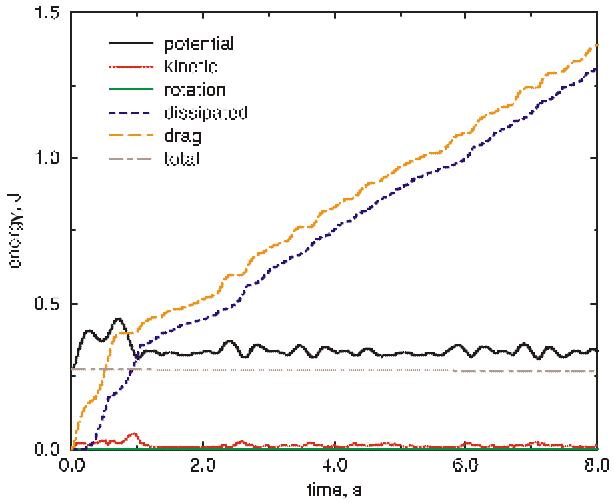

Figure 4.6. *Energy housekeeping for a simulation with non-ideal collision parameter settings (e = 0.9, m = 0.3) with a homogenous gas-inflow velocity $u_{gas} = 1.5\ u_{mf}$.*

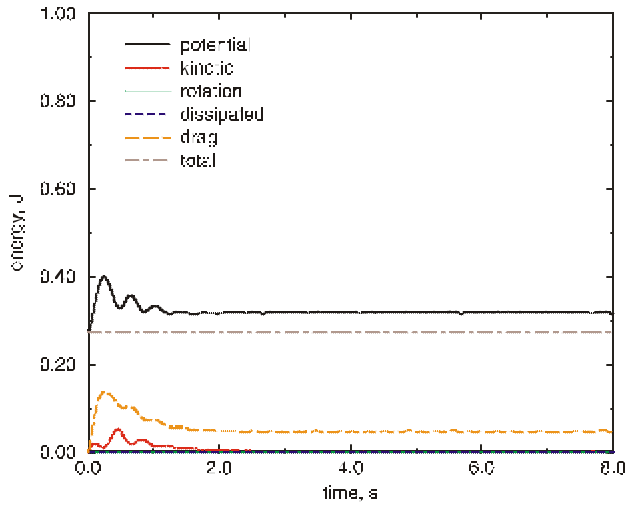

Figure 4.7. *Energy housekeeping for a simulation with ideal collision parameter settings (e = 1.0, μ = 0.0) with a homogenous gas-inflow velocity u_g = 1.5 u_{mf}.*

In Figure 4.7 it can be observed that the amount of energy dissipated in collisions remains zero throughout the whole simulation. The energy put into the system by drag force remains constant after a short initial stage (2 seconds). This is the amount of energy required for the expansion of the bed. Note that in both the non-ideal and the ideal cases the total energy remains constant throughout the whole simulation as required. It can also be observed that the potential energy in the non-ideal case (Figure 4.6) fluctuates more strongly than in the ideal case (Figure 4.7) which is obviously due to the bubbling and slugging in the non-ideal case. Due to this vigorous bubbling and slugging the pressure fluctuations in the bed are stronger than in the ideal case as reported in the previous section. The energy required for these stronger fluctuations is supplied by the drag force which puts a lot more energy into the system in the non-ideal case (Figure 4.6) than in the ideal case (Figure 4.7).

5. Influence of a particle size distribution

Hardly any distribution of particle size encountered in fluidisation studies is symmetrical, most of them are skewed to larger diameters (Seville *et al.* (1997)). A symmetrical size distribution like a normal or a Gaussian distribution is therefore not representative for particles used in laboratory or industrial practice. In this work the particle diameters are obtained from a log-normal distribution which is asymmetrical and can be represented in mathematical terms as follows:

$$\mathrm{d}f = \frac{1}{\sqrt{2\pi}\, D_p \ln s_g} \exp\left[-\frac{\left(\ln D_p - \ln D_{p,CM}\right)^2}{2\left(\ln s_g\right)^2} \right] \mathrm{d}D_p \quad , \tag{4.13}$$

where df is the fraction of particles having diameters whose logarithms lie between ln D_p and ln D_p + d(ln D_p). In equation 4.13 $D_{p,CM}$ is the count median diameter and s_g is the geometric standard deviation. When creating the particle size distribution all the diameters which are smaller than $D_{p,CM} \cdot s_g$ or larger than $D_{p,CM} \cdot s_g$ are rejected to mimic the effects of sieving. An example of a particle size distribution generated with this method is represented in a (discrete) frequency histogram in Figure 4.8.

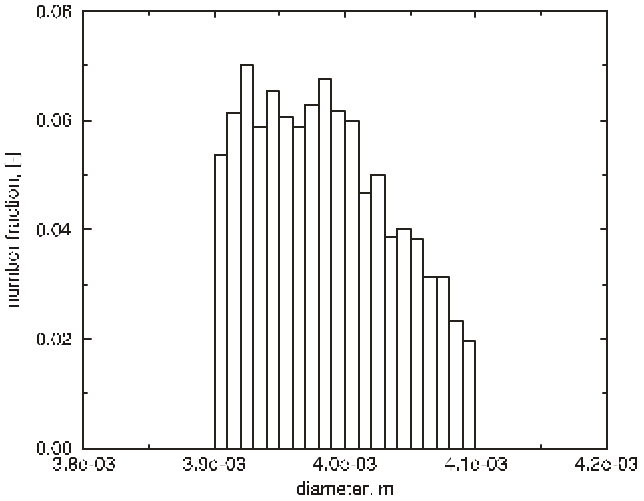

Figure 4.8. *Frequency histogram of a log-normal particle size distribution with a count median diameter of 4.0 mm and a geometric standard deviation (GSD or s_g) of 0.1 mm.*

The influence of the distribution width on the bed hydrodynamics at homogeneous inflow conditions was studied. Simulations were performed using the parameter settings presented in table 4.1 where the particle diameter of 4 mm is now the mean particle diameter. A time step of 10^{-4} s was used and all simulations were run for 10 s. The coefficient of restitution (e) was set equal to 0.9 and the coefficient of friction (m) was set equal to 0.3 for both particle-particle and particle-wall collisions. The initial configurations were obtained by placing the particles in the system and allowing them to fall under the influence of gravity while the homogeneous gas inflow was set equal to u_{mf}. Simulations were performed for a system consisting of particles of uniform size and systems consisting of particles with a log-normal size distribution with a geometric standard deviation s_g = 0.1, 0.5 and 1.0 mm respectively. A homogeneous gas inflow at 1.5 u_{mf} was specified at the bottom of the system.

In Figure 4.9 the pressure fluctuations inside the bed at 0.2 m above the centre of the bottom plate are presented for all the four cases.

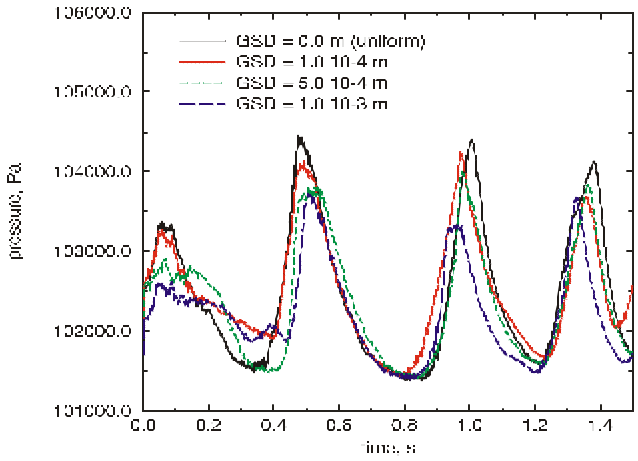

Figure 4.9. *Pressure at 0.2 m above the centre of the distributor plate as a function of time for the four cases, GSD = Geometric Standard Deviation (s_g).*

It can be observed that the pressure peaks decrease with increasing geometric standard deviation of the size distribution. This can be explained by the lower void fraction in the uniform case due to the closer packing which results in a higher force acting on

the particles which in turn causes the higher pressure peaks. After the first 1.5 s the differences become less pronounced which indicates that especially in situations where close packing can occur, such as at minimum fluidisation conditions, it is important to take poly-dispersity into account.

6. 3-D simulations

A three-dimensional version of the hard-sphere model was developed. Similar to the model presented by Kawaguchi *et al.* (1998), the gas phase hydrodynamics is still resolved in two dimensions. This can be justified since the simulated system is a flat fluidised bed with a depth of 22 mm where the motion of the gas phase in the third dimension can be neglected. The 3-D bed is schematically represented in Figure 4.10.

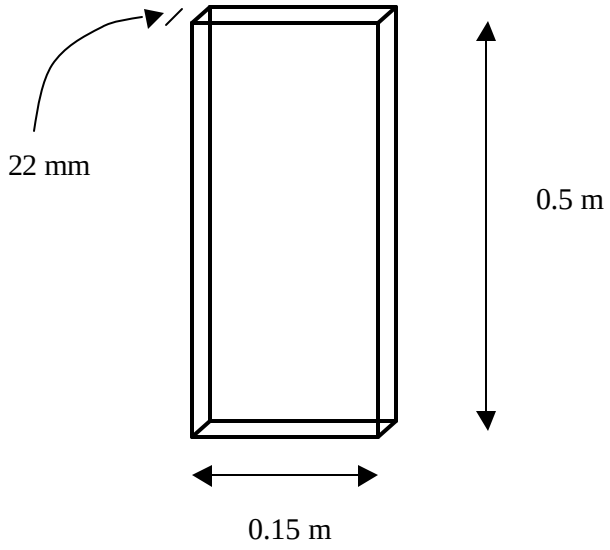

Figure 4.10. *Schematic representation of the 3-D bed.*

All other parameter settings are the same as used for the two-dimensional system presented in table 4.1. In preliminary tests it became clear that a minimum depth of 5 particle diameters was required to ensure stable simulations. At smaller depths the particles get stuck between the front and back walls and the hard-sphere algorithm breaks down. Eventually the simulation crashes due to particle overlap. With a depth

of 22 mm (5.5 particle diameters) such problems did not occur and therefore this depth was used in the simulations. The number of particles used in the 3-D simulations was 14,000 in order to match initial bed height in the 2-D simulations.

6.1 Influence of collision parameters

The collision parameters turned out to have a key influence in the two-dimensional simulations and therefore their influence was also investigated using the three-dimensional model. The set-up of the 3-D simulations was the same as for the 2-D simulations. The bed was homogeneously fluidised with a gas inflow of 1.5 u_{mf}.

In Figure 4.11 snapshots obtained from three different 3-D simulations are presented. A simulation with non-ideal collision parameters ($e = e_w = 0.9$, $m = m_w = 0.3$) was performed as well as a simulation with ideal collision parameters ($e = e_w = 1.0$, $m = m_w = 0.0$). A simulation with ideal particle-particle interaction but non-ideal particle-wall interaction ($e = 1.0$, $e_w = 0.9$, $m = 0.0$, $m_w = 0.3$) was also carried out. The snapshots presented in this figure are front views similar to the snapshots of the 2-D simulations in Figure 4.1. A number of particle layers was marked by colour based on the position at $t = 0$ s in order to visualise the induced particle mixing during the fluidisation process. For the 3-D case it should be noted that the bed is 5.5 particle diameters deep and this affects the visualisation: the particles near the front wall dominate the image.

The trends observed in the 2-D simulations are clearly confirmed in the 3-D simulations. In the ideal case no bubbles are observed and after a vigorous expansion the bed remains rather homogeneously fluidised. In the non-ideal case bubbles are observed and the bed height is continuously fluctuating. In the snapshots this may not be very clear due to the visualisation technique employed here, but this fluctuating motion could clearly be observed in animations. Also the potential energy of the system showed these fluctuations in the non-ideal case.

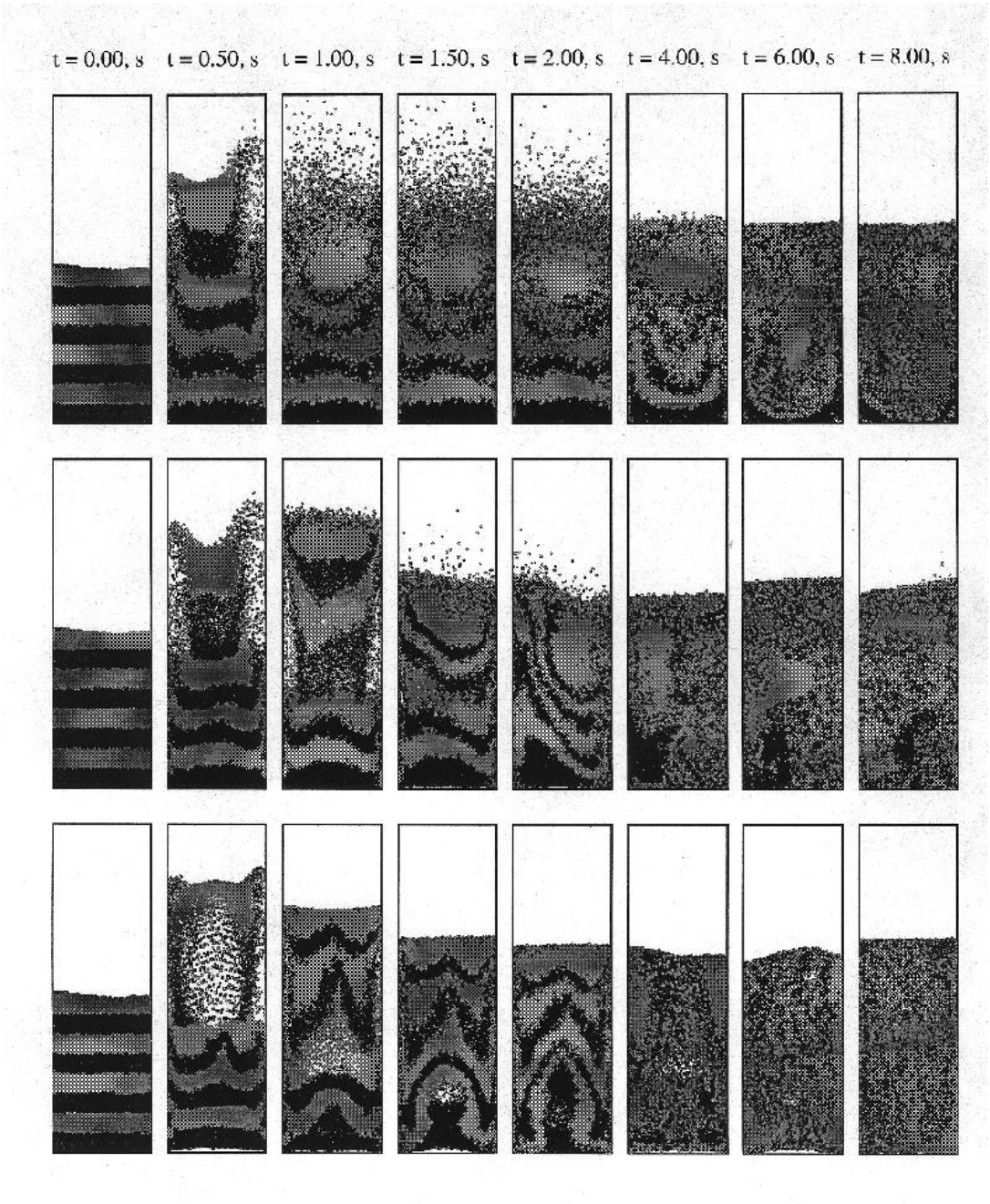

Figure 4.11. *Snapshots of particle configurations for three 3-D simulations with u_g = 1.5 u_{mf}. Upper: $e = e_w = 1.0$, $m = m_w = 0.0$, middle: $e = 1.0$, $e_w = 0.9$, $m = 0.0$, $m_w = 0.3$ bottom: $e = e_w = 0.9$, $m = m_w = 0.3$.*

The particle-wall interaction has a significant influence on the hydrodynamics. In the snapshots this can be observed especially during the initial stages of the simulation. Also the potential energy of this system shows stronger fluctuations than the ideal system.

6.2 2-D versus 3-D

The snapshots of the 3-D non-ideal simulation in Figure 4.11 show less bubbling and slugging than the snapshots in the 2-D equivalent in Figure 4.1. This can be partially due to the visualisation technique employed here but also the pressure fluctuations inside the bed are less strong and have a lower frequency (2.3 Hz in 3-D vs. 3.3 Hz in 2-D for the non-ideal case).

In Figure 4.12 the pressure 0.2 m above the centre of the distributor plate is plotted as a function of time for the 2-D and 3-D simulation with ideal values for the collision parameters.

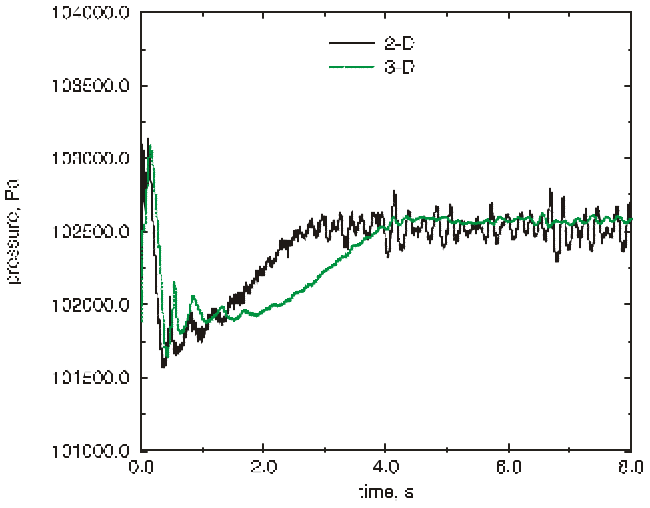

Figure 4.12. *Pressure 0.2 m above the centre of the distributor plate as a function of time ($e = e_w = 1.0$, $m = m_w = 0.0$): 2-D simulations compared to 3-D simulations*

Although in both the 2-D and the 3-D simulations the fluctuations are not very strong, the fluctuations in the 2-D case are more pronounced compared to the 3-D case. The

RMS value is about 70 Pa higher for the 2-D simulation. The same difference was found for the non-ideal case. These differences may be explained in terms of improved statistics since the number of particles in a computational cell is much higher in the 3-D case. Also the absence of a degree of freedom of motion in the 2-D case can cause the system to show a more constrained behaviour and hence cause stronger fluctuations.

In Figure 4.13 the pressure fluctuations in the 2-D and 3-D simulations are compared for the case with ideal particle-particle interaction and non-ideal particle-wall interaction (e = 1.0, e_w = 0.9, m = 0.0, m_w = 0.3).

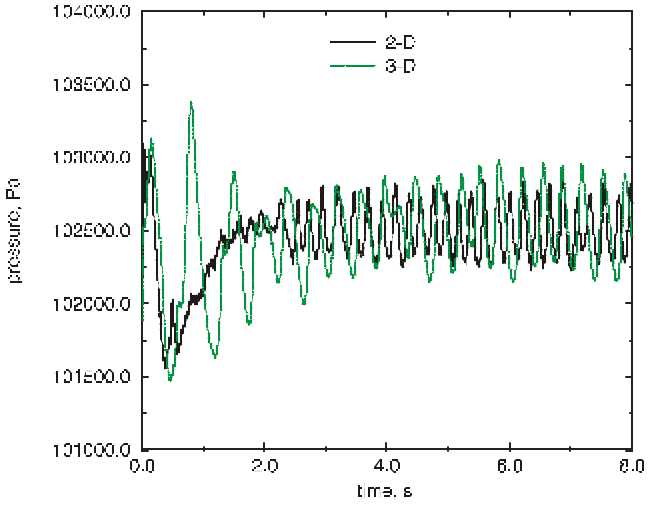

Figure 4.13. *Pressure 0.2 m above the centre of the distributor plate as a function of time (e_w = 0.9, m = 0.0, m_w = 0.3): 2-D simulations compared to 3-D simulations.*

For this case the fluctuations are stronger in the 3-D simulation. The RMS value of the fluctuations was 60 Pa higher in the 3-D case. Baring in mind that in the other cases the fluctuations in the 2-D simulations were stronger than in the 3-D simulations it can be concluded that the particle-wall interaction has a more pronounced effect on the hydrodynamics in 3-D simulations than in 2-D simulations. This is obviously due to the presence of the front and the back wall in the 3-D simulations of the 'flat' bed

which renders a much higher number of particle-wall collisions than in the 2-D simulations.

The 3-D simulations are much more computational intensive than the 2-D simulations. It takes 6 minutes of CPU time per simulated second on a Silicon Graphics Origin200 server (R10000 processor, 180 MHz) with the 2-D model (2400 particles) whereas it takes 220 minutes per second to perform the same (non-ideal) simulation with the 3-D model (14,000 particles).

7. Conclusions

A hard-sphere Granular Dynamics model was used to study the effect of the particle properties on the hydrodynamics of gas-fluidised beds with homogeneous inflow conditions. The bed dynamics is strongly affected by the values of the collision parameters (*i.e.* the coefficients of restitution (e) and friction (m)). When ideal particle interaction was assumed (e = 1.0, m = 0.0, *i.e.* no energy is dissipated in collisions) non-realistic bed dynamics is observed: no bubble or slug formation occurs and particle mixing is poor. When realistic particle interaction was assumed (e = 0.9, m = 0.3) bubble and slug formation are observed and the fluidisation behaviour is in much better accordance with that inferred from experimental observations. The coefficient of tangential restitution (b_0) has little influence on the overall behaviour. The particle-particle interaction parameters turned out to be much more important than the particle-wall interaction parameters in the two-dimensional simulations. Pressure fluctuations inside the bed are much stronger in the non-ideal case than in the ideal case. With intermediate values for the collision parameters the behaviour also changes gradually with pressure fluctuations becoming less strong when the coefficients are changed toward their ideal values. It turned out to be more convenient to determine the root mean square (RMS) of the pressure fluctuations as a function of the energy dissipation rate since this is affected both by the collision parameters and the system dynamics. The RMS values of the fluctuations show an almost linear increase with the energy dissipation rate during a simulation. The higher the energy dissipation rate the more energy was put into the system by the drag force.

Two-dimensional simulations have been performed with particles which diameters have been obtained from a log-normal distribution. The main influence of the poly-dispersity could be observed when the particles were in a rather close packing. Pressure peaks inside a slugging fluidised bed decreased with increasing geometric standard deviation of the log-normal size distribution during the initial stages of a simulation starting from minimum fluidisation conditions. This indicates that it is especially important to take a particle size distribution into account in systems where locally very dense particle configurations can occur.

Also a three-dimensional model (as far as the particles are concerned) was developed. A minimum depth of the bed of 5 particle diameters was required to ensure stable simulations. The 3-D model confirmed the trends observed in the 2-D model with respect to the dependency of the overall bed hydrodynamics on the collision parameters. Time series of the pressure inside the bed showed a lower frequency and a lower RMS value in the 3-D simulations than in the 2-D case. The particle-wall interaction had a more pronounced influence on the hydrodynamics in the 3-D simulations than in the 2-D simulations. As anticipated the 3-D simulations required considerably more CPU time than the 2-D simulations.

Notation

C_d	drag coefficient, [-]
e	coefficient of restitution, [-]
D_p	particle diameter, m
$\mathbf{g}$	gravitational acceleration, m/s^2
m_p	particle mass, kg
p	pressure, Pa
$\mathbf{r}$	position vector, m
$\mathbf{S}_p$	momentum source term N/m^3
T	temperature, K
t	time, s

$\mathbf{u}$	gas velocity vector, m/s
$\mathbf{v}_p$	particle velocity vector, m/s
V_p	particle volume, m^3

Greek symbols

b	volumetric interphase momentum transfer coefficient, $kg/(m^3s)$
b_0	coefficient of tangential restitution, [-]
e	void fraction, [-]
m	coefficient of friction, [-]
m_g	gas viscosity, kg/ms
t	gas phase stress tensor, kg/ms^2
r	density, kg/m^3
s_g	Geometric Standard Deviation (GSD), m

Subscripts

CM	Count Median
dsp	dissipated
drg	drag
GSD	Geometric Standard Deviation
g	gas phase
kin	kinetic
mf	minimum fluidisation
p	particle
pot	potential
rot	rotation
tot	total
w	wall

References

Anderson, T.B. and Jackson, R., (1967). A fluid mechanical description of fluidized beds (equations of motion), *Ind. Eng. Chem., Fundam.*, **6**, 527.

Bleek, van den, C.M., and Schouten, J.C., (1993). Can deterministic chaos create order in fluidized-beds scale-up ?, *Chem. Engng Sci.*, **48**, 2367.

Chang, H. and Louge, M.Y., (1992), Fluid dynamic similarity of circulating fluidized beds, *Powder Technol.*, **70**, 259.

Chen, Z., Gibilaro, L.G., and Foscolo, P.U., (1997a). Fluid pressure loss in slugging fluidised beds, *Chem. Engng Sci*., **52**, 55.

Chen, Z., Di Felice, R., Gibilaro, L.G., and Foscolo, P.U., (1997b). Effects of solid frictional interactions on the applicability of the fluid-dynamic scaling rules for fluidisation, *Chem. Eng. Comm*., **157**, 205.

Cundall, P.A. and Strack, O.D.L., (1979). A discrete numerical model for granular assemblies. *Géotechnique*, **29**, 47.

Foerster S.F., Louge, M.Y., Chang,H. and Allia, K. (1994). Measurements of the collision properties of small spheres. *Phys. Fluids,*, **6**, 1108.

Geldart, D., (1973). Types of gas fluidization, *Powder Technol*., **7**, 285.

Gidaspow, D. (1994). *Multiphase Flow and Fluidization*, Academic Press, Boston, USA.

Hoomans, B.P.B., Kuipers, J.A.M., Briels, W.J. and van Swaaij, W.P.M., (1996). Discrete particle simulation of bubble and slug formation in a two-dimensional gas-fluidised bed: a hard-sphere approach, *Chem. Engng Sci.*, **51**, 99.

Hrenya, C.M. and Sinclair, J.L. (1997). Effects of particle-phase turbule nce in gas-solid flows, *AIChE J.*, **43**, 853.

Kuipers, J.A.M., van Duin K.J., van Beckum, F.P.H. and van Swaaij, W.P.M., (1992). A numerical model of gas-fluidized beds, *Chem. Engng Sci.*, **47,** 1913

Langston, P.A., Tüzün, U. and Heyes, D.M., (1995). Discrete element simulation of granular flow in 2D and 3D hoppers: dependence of discharge rate and wall stress on particle interactions. *Chem. Engng Sci.*, **50**, 967.

Kawaguchi, T., Tanaka, T. and Tsuji, Y., (1998). Numerical simulation of two-dimensional fluidized beds using the discrete element method (comparison between the two- and three-dimensional models), *Powder Technol.*, **96**, 129.

Mikami, T., Kamiya, H. and Horio, M., (1998). Numerical simulation of cohesive powder behavior in a fluidized bed, *Chem. Engng Sci.*, **53**, 1927.

Nieuwland, J.J., van Sint Annaland, M., Kuipers, J.A.M. and van Swaaij, W.P.M., (1996), Hydrodynamic modelling of gas-particle flows in riser reactors, *AIChE J.*, **37**, 1009.

Richardson, J.F. and Zaki, W.N., (1954). Sedimentation and fluidization: part I. *Trans. Inst. Chem. Eng*., **32**, 35.

Schouten, J.C. and Bleek, van den, C.M., (1992). Chaotic hydrodynamics of fluidization: consequences for scaling and modeling of fluid bed reactors, *AIChE Symp. Ser.*, No. 289 **Vol. 88**, 70.

Seville, J.P.K., U. Tüzün, and R. Clift, (1997). *Processing of Particulate Solids*, Blackie Academic & Professional.

Sinclair, J.L. and Jackson, R. (1989). Gas-particle flow in a vertical pipe with particle-particle interactions, *AIChE J.*, **35**, 1473.

Thiel, W.J. and Potter, O.E., (1977). Slugging in Fluidized beds, *Ind. Eng. Chem,, Fundam*. **16**, 242.

Thornton, C., K. K. Yin, and M. J. Adams, 1996, Numerical simulation of the impact fracture and fragmentation of agglomerates, *J, Phys. D: Appl. Phys.*, **29**, 424.

Tsuji, Y., Kawaguchi, T. and Tanaka, T., (1993). Discrete particle simulation of two dimensional fluidized bed, *Powder Technol.* **77**, 79.

Wang, Y. and Mason, M.T., (1992). Two-dimensional rigid-body collisions with friction. *J. Appl. Mech.*, **59**, 635.

Wen, C.Y. and Yu, Y.H., (1966). Mechanics of fluidization. *Chem. Eng. Prog. Symp. Ser*., **62** (62), 100.

Xu, B.H. and Yu, A.B., (1997). Numerical simulation of the gas-solid flow in a fluidized bed by combining discrete particle method with computational fluid dynamics. *Chem. Engng Sci*. **52**, 2785.

Zenz, F.A. and Othmer D.F., (1960). *Fluidisation and fluid-particle systems*, Reinhold Publishing Corp. New York, USA.

Chapter 5.

GRANULAR DYNAMICS SIMULATION OF BUBBLE FORMATION IN A GAS FLUIDISED BED: HARD-SPHERE VS. SOFT-SPHERE APPROACH

Abstract:

Two types of Granular Dynamics models have been developed to study bubble formation in a gas-fluidised bed. For each individual particle the Newtonian equations of motion are solved taking into account the external forces (i.e. gravity and drag). In the hard-sphere simulations a sequence of binary, instantaneous collisions is processed one collision at a time while a collision model is used to describe the inelastic collisions with friction. In the soft-sphere model the particle-particle and particle-wall interactions are taken into account through a linear spring/dash-pot contact force model. The gas phase hydrodynamics is described by the spatially averaged Navier-Stokes equations for two-phase flow. Bubble formation at a central jet in a bed of 0.2 m width and 0.3 m height with 40,000 glass ballotini particles of 850 mm diameter was chosen as a test case for the simulations. Preliminary simulations with the soft-sphere model revealed that the results are rather insensitive to the time step used for the integration of the contact forces as well as the value of the spring stiffness. The agreement between simulation and experiment was improved by incorporation of a log-normal particle size distribution. Hardly any difference could be observed between the results of the hard-sphere and the soft-sphere simulations that both compared well with the experiment. The computational efficiency of the hard-sphere simulations depends strongly on the dynamics of the system in contrast to the computational efficiency of the soft-sphere simulations. The collision parameters turned out to have a key influence in both types of simulations. When the collisions were assumed to be fully elastic and perfectly smooth the agreement with the experiment was much worse.

Parts of this chapter are based on the papers:

B.P.B. Hoomans, J.A.M. Kuipers, W.J. Briels and W.P.M. van Swaaij, (1996). Discrete particle simulation of bubble and slug formation in two-dimensional gas-fluidised beds: a hard-sphere approach, *Chem. Engng Sci.*, **51**, 99.

J.A.M. Kuipers, B.P.B. Hoomans and W.P.M. van Swaaij, (1998). Hydrodynamic models of gas-fluidized beds and their role for design and operation of fluidized bed chemical reactors, in *Fluidization IX*, L.-S. Fan and T.M. Knowlton (eds), 15.

B.P.B. Hoomans, J.A.M. Kuipers and W.P.M. van Swaaij, (1998). The influence of a particle size distribution on the granular dynamics of dense gas-fluidized beds: a computer simulation study, *AIChE Symp. Ser. No. 318*, **Vol. 94**, 15.

1. Introduction

Due to increasing computer power Granular Dynamics simulations have become a very useful and versatile research tool to study the hydrodynamics of gas-fluidised beds. In these simulations the Newtonian equations of motion for each individual particle in the system are solved. Particle-particle and particle-wall interactions are taken into account directly which is a clear advantage over two-fluid models which require closure relations for the solids-phase stress tensor (Gidaspow (1994), Sinclair and Jackson (1989) and Kuipers *et al.* (1992) among others). Furthermore a discrete particle model is very well suited to take an arbitrary particle size distribution into account which is far more complex, if not impossible, in case a continuum modelling approach is adopted.

Tsuji *et al.* (1993) developed a soft-sphere discrete particle model of a gas-fluidised bed based on the work of Cundall and Strack (1977). In their approach the particles are allowed to overlap slightly and from this overlap the contact forces are subsequently calculated. Kawaguchi *et al.* (1998) extended the model developed by Tsuji *et al.* (1993) to three-dimensions as far as the motion of the particles is concerned. Hoomans *et al.* (1996) used a hard-sphere approach in their discrete particle model of a gas-fluidised bed which implies that the particles interact through binary, instantaneous, inelastic collisions with friction. Xu and Yu (1997) used a two-dimensional soft-sphere model similar to the one used by Tsuji *et al.* (1993) in their fluidised bed simulations but they also employed techniques from hard-sphere simulations in order to determine the instant when the particles first come into contact precisely. Mikami *et al.* (1998) presented a two-dimensional soft-sphere model of a gas-fluidised bed where the model developed by Tsuji *et al.* (1993) was extended in order to take cohesive forces between the particles into account.

In all the soft-sphere models used for fluidised bed simulations a linear-spring/dash-pot model is used to describe the normal contact forces. In these simulations the value of the

spring stiffness is chosen artificially low for computational convenience. It is assumed that this is allowed but it has never been demonstrated that the simulation results are not affected by the value of the spring stiffness. In order to investigate the effect of the spring stiffness on the simulation results and to allow for a comparison with hard-sphere simulations, a soft-sphere linear spring/dash-pot model was developed. Since for both types of models the gas phase hydrodynamics and the two-way coupling was incorporated in exactly the same manner it is possible to make a direct comparison that highlights only the effects due to the choice of model. The formation of a single bubble at a central orifice in a gas-fluidised bed was chosen as a test case because of the availability of a well defined experiment (Hoomans *et al*., 1996) that allows for validation.

2. Models

Since a detailed description of the models is presented in Chapter 2 and Chapter 3, the key features will be summarised only briefly here.

2.1 Hard-sphere granular dynamics

The collision model as originally developed by Wang and Mason (1992) is used to describe a binary, instantaneous, inelastic collision with friction. The key parameters of the model are the coefficient of restitution ($0 \leq e \leq 1$) and the coefficient of friction ($m \geq 0$). Foerster *et al.* (1994) have shown that also the coefficient of tangential restitution ($0 \leq b_0 \leq 1$) should be used in order to describe the collision dynamics more accurately. These three collision parameters are all included in the model.

In the hard-sphere approach a sequence of binary collisions is processed. This implies that a collision list is compiled in which for each particle a collision partner and a corresponding collision time is stored. A constant time step is used to take the external forces into account and *within* this time step the prevailing collisions are processed sequentially. In order to reduce the required CPU time neighbour lists are used. For each

particle a list of neighbouring particles is stored and only for the particles in this list a check for possible collisions is performed.

2.2 Soft-sphere granular dynamics

The linear spring/dash-pot model (Cundall and Strack, 1979) is the most popular soft-sphere granular dynamics model since it was used by Tsuji *et al.* (1993), Schwarzer (1995), Xu and Yu (1997), Kawaguchi *et al.* (1998) and Mikami *et al.* (1998). For a review of various contact force models used in soft-sphere simulations the reader is referred to Walton (1992) or Schäfer *et al.* (1996).

In soft-sphere models the following equations of motion are used:

$$m\frac{d^2\mathbf{r}}{dt^2} = \mathbf{F}_{contact} + \mathbf{F}_{external}, \tag{5.1}$$

$$I\frac{d\omega}{dt} = \mathbf{T}, \tag{5.2}$$

where $\mathbf{r}$ is the position vector of the centre of the particle, m is the mass of the particle, $\mathbf{F}_{contact}$ is the contact force acting on the particle, $\mathbf{F}_{external}$ is the net external force acting on the particle, ω is the rotation velocity, $\mathbf{T}$ is the torque acting on the particle and I is the moment of inertia of the particle. In this paragraph the focus will be on the contact forces between the particles, the external forces will be discussed in the following paragraph.

The contact forces are given by:

$$\mathbf{F}_{n,ab} = -k_n x_n \mathbf{n}_{ab} - h_n \mathbf{v}_{n,ab} \tag{5.3}$$

$$\mathbf{F}_{t,ab} = -k_t \mathbf{?}_t - h_t \mathbf{v}_{t,ab} \tag{5.4}$$

If however the following relation is satisfied:

$$\left|\mathbf{F}_{t,ab}\right| > m\left|\mathbf{F}_{n,ab}\right|, \tag{5.5}$$

then sliding occurs and the tangential force is given by:

$$\mathbf{F}_{t,ab} = -m\left|\mathbf{F}_{n,ab}\right|\mathbf{t}_{ab}. \tag{5.6}$$

For contacts between particles and walls, the walls are assumed to be non-moving and of infinite mass just like in the hard-sphere model.

The resulting force and torque for particle a are now simply obtained by adding the pair wise contributions of all the particles that are in contact with a:

$$\mathbf{F}_{contact,a} = \sum_b \left(\mathbf{F}_{n,ab} + \mathbf{F}_{t,ab}\right), \tag{5.7}$$

$$\mathbf{T}_a = \sum_b \left(R_a \mathbf{n}_{ab} \times \mathbf{F}_{t,ab}\right). \tag{5.8}$$

Since the contact forces are in general at least an order of magnitude larger than the external forces a separation of time scales was introduced. By default at each time step DT the external forces were taken into account while at $0.1DT$ the equations of motion were solved by taking only the contact forces into account. Hence the external forces remain constant during a time step DT.

2.3 External forces

The incorporation of external forces differs somewhat from the approach followed by Hoomans *et al*. (1996). In this work the external forces are used in accordance with those implemented in the two-fluid model presented by Kuipers *et al.* (1992) where, of course, the forces now act on a single particle:

$$m_p \frac{d\mathbf{v}_p}{dt} = m_p \mathbf{g} + \frac{V_p b}{(1-e)}\left(\mathbf{u} - \mathbf{v}_p\right) - V_p \nabla p \quad , \tag{5.9}$$

where m_p represents the mass of a particle, $\mathbf{v}_p$ its velocity, $\mathbf{u}$ the local gas velocity and V_p the volume of a particle. In equation (5.9) the first term is due to gravity and the third term is the force due to the pressure gradient. The second term is due to the drag force where b represents an inter-phase momentum exchange coefficient as it usually appears in two-fluid models. For low void fractions ($e < 0.80$) b is obtained from the well-known Ergun equation:

$$b = 150\frac{(1-e)^2}{e}\frac{m_g}{D_p^2} + 1.75(1-e)\frac{r_g}{D_p}\left|\mathbf{u} - \mathbf{v}_p\right| \quad , \tag{5.10}$$

where D_p represents the particle diameter, m_g the viscosity of the gas and r_g the density of the gas. For high void fractions ($e \geq 0.80$) the following expression for the inter-phase momentum transfer coefficient has been used which is basically the correlation presented by Wen and Yu (1966) who extended the work of Richardson and Zaki (1954):

$$b = \frac{3}{4}C_d \frac{e(1-e)}{D_p} r_g \left|\mathbf{u} - \mathbf{v}_p\right| e^{-2.65} \quad . \tag{5.11}$$

The drag coefficient C_d is a function of the particle Reynolds number and given by:

$$C_d = \begin{cases} \dfrac{24}{\mathrm{Re}_p}\left(1 + 0.15\mathrm{Re}_p^{0.687}\right) & \mathrm{Re}_p < 1000 \\ 0.44 & \mathrm{Re}_p \geq 1000 \end{cases} , \tag{5.12}$$

where the particle Reynolds number (Re_p) in this case is defined as follows:

$$\mathrm{Re}_p = \frac{\varepsilon_g \rho_g \left| \mathbf{u} - \mathbf{v}_p \right| D_p}{\mu_g} \quad . \tag{5.13}$$

For the integration of equation (5.9) a simple explicit first order scheme was used to update the velocities and positions of the particles.

2.4 Gas phase hydrodynamics

The calculation of the gas phase hydrodynamics mainly follows the lines presented by Kuipers *et al.* (1992). It is based on the numerical solution of the following set of partial differential equations that can be seen as a generalised form of the Navier-Stokes equations for a gas interacting with a solid phase as originally derived by Anderson and Jackson (1967).

Continuity equation gas phase:

$$\frac{\partial \left(\varepsilon_g \rho_g \right)}{\partial t} + \left(\nabla \cdot \varepsilon_g \rho_g \mathbf{u} \right) = 0 \, . \tag{5.14}$$

Momentum equation gas phase:

$$\frac{\partial \left(\varepsilon_g \rho_g \mathbf{u} \right)}{\partial t} + \left(\nabla \cdot \varepsilon_g \rho_g \mathbf{u}\mathbf{u} \right) = -\varepsilon \nabla p - \mathbf{S}_p - \left(\nabla \cdot \varepsilon \tau_g \right) + \varepsilon_g \rho_g \mathbf{g} \, . \tag{5.15}$$

In this work transient, two-dimensional, isothermal (T = 293 K) flow of air at atmospheric conditions is considered. The constitutive equations can be found in Chapter 3. There is one important modification with respect to the model presented by Hoomans *et al.* (1996) and that deals with the way in which the two-way coupling between the gas phase and the dispersed particles is established. In the present model the reaction force to the drag force

exerted on a particle per unit of volume is fed back to the gas phase through the source term $\mathbf{S}_p$ which has the dimension of force per unit of volume N/m^3.

3. Preliminary simulations

At first several preliminary simulations were performed using the soft-sphere model to investigate the influence of the spring stiffness on the simulations results. The formation of a bubble at a central orifice was chosen as a test case. The parameter settings for these simulations are presented in table 5.1.

Table 5.1. *Parameter settings bubble formation simulations*

Particles:		Bed:	
Shape	spherical	width	195 mm
diameter, D_p	850 μm	height	300 mm
Material	ballotini glass	orifice diameter, d_o	15 mm
density, ρ_p	2930 kg/m^3	cell width, *DX*	5 mm
e	0.96	cell height, *DY*	5 mm
e_w	0.86	number x-cells, *NX*	39
μ	0.15	number y-cells, *NY*	60
μ_w	0.15		
Number, N_p	40,000	time step, *DT*	10^{-4} s

The values of the collision parameters are taken from Hoomans *et al.* (1996). The coefficient of tangential restitution (β_0) is assumed to be equal to zero. Unless indicated otherwise a time step $DT = 10^{-4}$ s is used while $DT_{contact} = 0.1\ DT$. At the side walls no-slip boundary conditions were applied and at the upper boundary cells a prescribed pressure was chosen. At the bottom row of cells the gas inflow velocity was set equal to the minimum fluidisation velocity of the glass particles (u_{mf} = 0.5 m/s). In the three central cells the gas velocity was set equal to 5 u_{mf} during the first 0.2 s of the simulation to generate a single bubble.

The effect of the spring stiffness was studied for a system consisting of particles of uniform size. The contact time for such particles within the framework of the linear spring/dash-pot model can be calculated as follows:

$$t_{contact} = \sqrt{\frac{m_p\left(p^2 + \ln^2 e\right)}{2k_n}} \quad . \tag{5.16}$$

The values of the spring stiffness were varied from 1 to 10,000 N/m. The contact times for these values of the spring stiffness are presented in table 5.2. Unless indicated otherwise the value of the stiffness of the tangential spring was chosen as 2/7 times the normal spring stiffness (k_t = 2/7 k_n). Note that the contact times in the linear spring/dash-pot model do not depend on the impact velocity.

Table 5.2. *Contact times and results of simulations[*] for various values of the normal spring stiffness. In all cases DT = 10^{-4} s.*

k_n N/m	$t_{contact}$ s	$DT_{contact}$. 10^{-4} s	$DT_{contact}$. 10^{-5} s	$DT_{contact}$. 10^{-6} s
1	$3.05\ 10^{-3}$	*No*	*No*	*No*
10	$9.64\ 10^{-4}$	*Yes*	*Yes*	*Yes*
100	$3.05\ 10^{-4}$	*No*	*Yes*	*Yes*
1000	$9.64\ 10^{-5}$	*No*	*Yes*	*Yes*
10000	$3.05\ 10^{-5}$	*No*	*No*	*Yes*

[*] *No: simulation not completed successfully, Yes: simulation completed successfully*

With a normal spring stiffness of 1 N/m no successful simulations could be performed. The repulsive force is simply not strong enough compared to the external forces (gravity and drag) to prevent the particles from excessive overlap. During the simulation this leads to extremely low local void fractions (e < 0.2) which eventually causes the simulation to crash. With a spring stiffness of 10 N/m or higher such problems were not encountered.

However, at higher values of the spring stiffness the time step for the numerical integration of the contact forces should be chosen sufficiently small in comparison with the contact time in order to perform stable simulations. It turned out that in the case of k_n = 100 N/m ($t_{contact}$ = 3.05 10^{-4} s) a time step of 10^{-4} s was not sufficiently small to perform a stable simulation. However, when a time step of 5 10^{-5} s was used, the simulation was successfully completed. Hence the ratio of the contact time and the time step should at least be greater than 3 ($t_{contact}/DT_{contact}$ > 3) to ensure the stability of the simulation. In Figure 5.1 the sum of the potential energy of all the particles in the system is plotted as a function of time for several time steps ($DT_{contact}$).

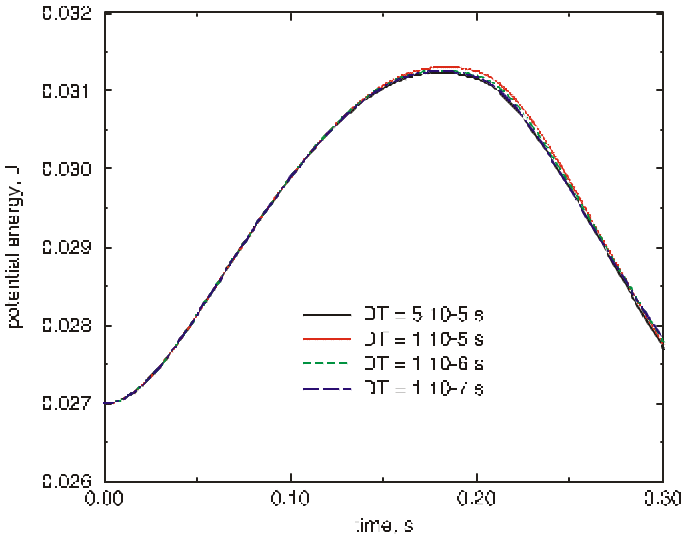

Figure 5.1. *The potential energy of the system as a function of time for several time steps. In all cases k_n = 100 N/m.*

From Figure 5.1 it can be observed that there is hardly any influence of the time step used for the integration of the contact forces on the overall results of the simulation which is rather surprising. Snapshots of the simulations do not reveal a significant difference either. There is however a big difference in CPU time because a simulation requires nearly 10 times as much CPU time when the time step is reduced by a factor 10. In the simulations presented by Tsuji *et al.* (1993), Kawaguchi *et al.* (1998) and Mikami *et al.* (1998) a time step was used that was 3.7 times smaller than the contact time for the particles used in their systems. In the simulations presented by Xu and Yu (1997) the

ratio of the contact time and the time step was 6.2. Although a ratio of 3.7 appears to be rather close to the stability limit the results presented in Figure 5.1 suggest that it is not required to choose a very small time step. This result is somewhat surprising since in Chapter 2, Figure 2.14, it was demonstrated that the effect of the time step on the time resolution of the contact force was rather large. However, the error in the energy balance over the collision was rather low in that particular case. This could explain the minor influence of $DT_{contact}$ on the simulation results. The results presented in Figure 5.1 also indicate that the technique employed by Xu and Yu (1997) to determine the precise instant of first contact within a time step does not improve the results of a simulation.

Additional simulations were performed using the hard-sphere model where the overall time step (DT) for the integration of the external forces was varied ($DT = 10^{-3}$ s, $DT = 10^{-4}$ s, $DT = 10^{-5}$ s). In all these cases $DT_{contact} = 10^{-5}$ s. For all three time steps very similar results were obtained. The simulation with $DT = 10^{-5}$ s was significantly slower in terms of CPU time than the simulation with $DT = 10^{-4}$ s but the difference between the simulations with $DT = 10^{-3}$ s and $DT = 10^{-4}$ s was remarkably small. This is due to the fact that in the simulation with $DT = 10^{-3}$ s a larger neighbour list was required since this list could only be updated at every time step.

In Figure 5.2 snapshots at $t = 0.2$ s are presented for simulations with various values of the spring stiffness: $k_n = 10$ N/m, $k_n = 100$ N/m and $k_n = 10000$ N/m. A simulation with $k_n = 1000$ N/m was not included in the figure but showed very similar results. By default the value for the tangential spring stiffness is set equal to 2/7 times the value of normal spring stiffness ($k_t = 2/7\ k_n$) for reasons discussed in Chapter 2. In Figure 5.2 a snapshot at $t = 0.2$ s is included of a simulation where the value for the tangential spring stiffness is set equal to the value of normal spring stiffness ($k_t = k_n = 100$ N/m).

All snapshots in Figure 5.2 appear to be surprisingly identical. Apparently the value of the spring stiffness has a negligible effect on the simulation results as long as it is high enough compared to the net external force to prevent the particles from overlapping too much (more than roughly 10% of the particle diameter). However, the choice of spring

stiffness does affect the CPU time required for a simulation significantly since the time step used for the integration of the contact forces should at least be three times smaller than the contact time corresponding to the spring stiffness used in the simulation.

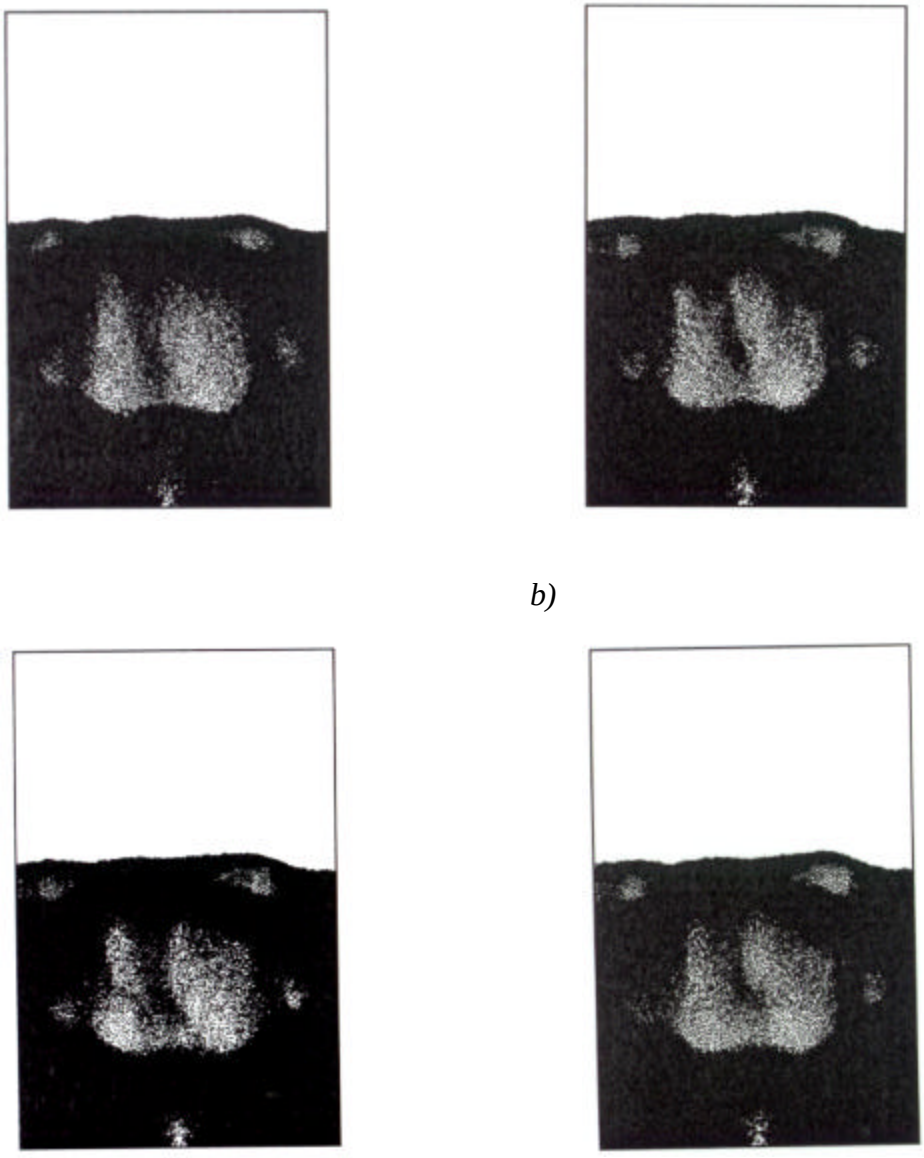

a) *b)*

c) *d)*

Figure 5.2. *Snapshots of particle configurations at t = 0.2 s for various values of the spring stiffness a) k_n = 10 N/m b) k_n = 10000 N/m c) k_n = 100 N/m d) k_n = k_t = 100 N/m.*

In Chapter 2 it was demonstrated that the value of the tangential spring stiffness should be set equal to 2/7 times the value of normal spring stiffness (k_t = 2/7 k_n) in order to ensure equal normal and tangential contact times. From the snapshot in Figure 5.2*d* (k_t = k_n = 100 N/m) hardly any difference can be observed with the snapshot in Figure 5.2*c* (k_n = 100 N/m, k_t = 2/7 k_n). This is however not surprising because of the low value of the coefficient of friction (μ) that causes a considerable amount of *sliding* contacts. For the same reason the coefficient of tangential restitution (β_0) had a negligible influence on the simulation results (compared to the coefficients of normal restitution (e) and friction) presented in Chapter 4. Furthermore the effect is most pronounced for *sticking* contacts with a coefficient of tangential restitution equal to one (β_0 = 1.0) while in the simulation presented in Figure 5.2 the coefficient of tangential restitution is set equal to zero (β_0 = 0.0). However, an additional simulation with β_0 = 1.0 showed very similar results and hence the effect due to the low coefficient of friction is dominant.

4. Experimental validation

The hard-sphere and the soft-sphere codes were compared with each other and validated using data of a bubble formation experiment obtained from the experimental set-up described below.

4.1 Experimental

The set-up used for the experiment is shown schematically in Figure 5.3 (Nieuwland, 1994). The primary fluidising gas was introduced into the bed through two equally sized distribution chambers. From these distribution chambers the primary fluidisation gas was introduced into the fluidised bed section through a porous sintered stainless steel plate with a mean pore diameter of 10 μm. This porous plate, which served as the main distributor of the primary fluidising gas, was equipped with a central rectangular pipe (internal dimensions: 15.0 x 15.0 mm) to inject secondary fluidising gas. This rectangular

jet was covered with a piece of stainless steel gauze to prevent the particles from entering it.

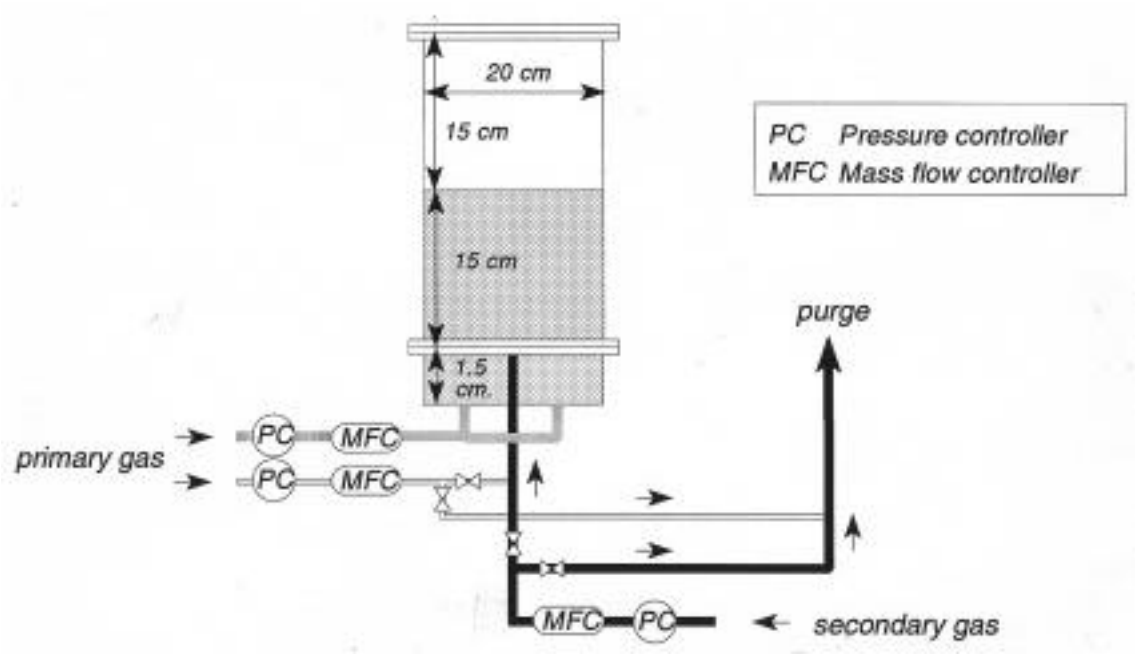

Figure 5.3. *Schematic representation of the experimental set-up.*

During the experiments three different gas flow rates were adjusted independently by means of calibrated thermal mass flow controllers: a gas flow through the distributor section to keep the bed at incipient fluidisation conditions, a gas flow through the rectangular orifice to fluidise the particles above the orifice and a gas flow for the bubble formation at the orifice. Prior to bubble injection, the secondary gas was purged, while the primary gas flowed through the gas distributor and the orifice to keep the bed at minimum fluidisation conditions. Rapidly responding, computer controlled, magnetic valves were used to inject secondary gas through the orifice into the bed to form a bubble and to purge the primary gas during the period of injection. In the experiment the primary gas was introduced at a superficial velocity of 0.5 m/s (u_{mf}) and during a period of 0.2 s secondary gas was injected through the central orifice at a superficial velocity of 2.5 m/s (5 u_{mf}). An S-VHS video camera was used to observe the bed during the whole process

of bubble formation. A sieve fraction of glass ballotini particles (r_p = 2930 kg/m^3) with diameters between 800 and 900 μm was used.

4.2 Influence of a particle size distribution

In order to test whether the simulation results were improved by taking a particle size distribution into account, a simulation with particles of uniform size was compared with a simulation where a log-normal particle size distribution was taken into account (Hoomans *et al.*, 1998). The results of these simulations were validated using data of a bubble formation experiment obtained from the experimental set-up described above.

The main parameter settings for the simulations are presented in Table 5.1. Apart form a simulation with particles of a uniform diameter of 850 μm a simulation was performed where the particle diameters were obtained from a log-normal distribution with a count median average of 850 μm and a geometric standard deviation of 50 μm. The particle size distribution employed in the simulation is presented in Figure 5.4.

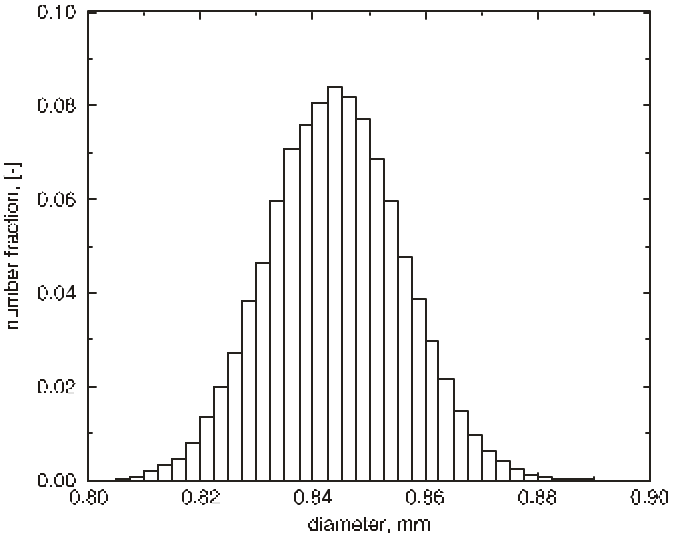

Figure 5.4. *Particle size distribution for the bubble formation simulations*

Snapshots at t = 0.2 s of the two simulations and corresponding video images of the experiment are presented in Figure 5.5. The simulations presented here were performed using the hard-sphere code.

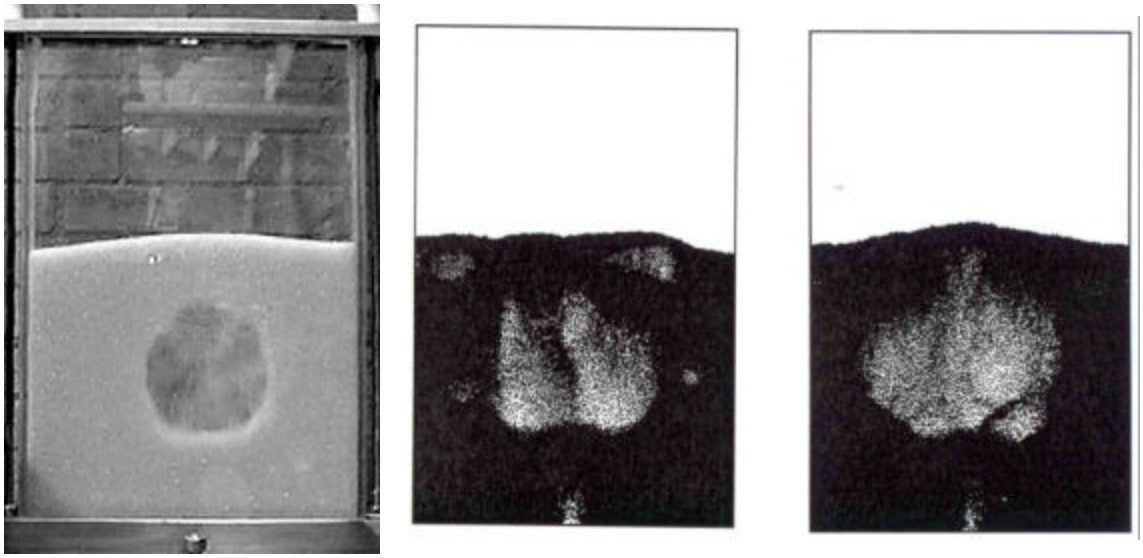

a) *b)* *c)*

Figure 5.5. *Snapshots at t = 0.2 s of: a) experiment, b) simulation with uniform particles, c) simulation with log-normal particle size distribution.*

It can be observed that in the system with particles of uniform size small 'satellite' bubbles appear above and alongside the main bubble. This is not observed in the experiment nor in the simulation with the poly-disperse particle assembly. These 'satellite' bubbles are probably due to locally low void fraction due to close packing. In a system consisting of particles of uniform size such locally low void fractions can occur since it is possible for an assembly of particles to gather in a lattice-like structure. When locally low void fractions prevail the drag force (which depends strongly on the void fraction) can become strong enough to generate a bubble. The size of the main bubble agrees reasonably well with the experiment for both of the (2-D) simulations which is rather encouraging especially since the model parameters were obtained on beforehand and independently.

4.3 Hard-sphere vs. soft-sphere

The simulations were performed using the parameter settings presented in Table 5.1. For the soft-sphere simulations a normal spring stiffness (k_n) of 100 N/m was used and the time step for the integration of the contact forces ($DT_{contact}$) was set equal to 10^{-5} s. In both simulations the particle size distribution presented in Figure 5.4 is taken into account. In Figure 5.6 snapshots of the hard-sphere (middle) and the soft-sphere (right) simulations are presented together with the corresponding pictures of the experiment (left). The initial conditions were identical in both simulations and hence there was no overlap between particles at t = 0 s. which is required for the hard-sphere simulation.

In the snapshots presented in Figure 5.6 it can be observed that the bubble is being formed at the central orifice during the first 0.1 s which is in good agreement with the experiment. After 0.1 s the bubble detaches from the distributor plate and starts to rise in the bed. Since the jet remains active during the first 0.2 s the formation of a second bubble is initiated but the jet does not remain active long enough for this second bubble to grow to full size. After 0.1 s the shape of the bubble predicted in the simulations starts to deviate from the bubble shape observed in the experiment although the main bubble size as well as the position of the bubble in the bed is fairly well predicted. The bubble shape observed in the experiment is more round and the gas-solid boundary appears to be sharper than in the simulations. This can be very well due to the two-dimensional nature of the simulations. Although the experimental set-up was quasi two-dimensional the bed was still more than 17 particle diameters deep (16 mm) which is a significant difference with the simulations where the particle motion is restricted to two dimensions. In addition a higher order numerical scheme for the convective fluxes in the gas phase momentum conservation equations is known to yield results with sharper bubble boundaries in Eulerian simulations. The use of such a higher order scheme (like for instance the Barton scheme) may also improve the bubble definition in (already 2-D) Lagrangian simulations.

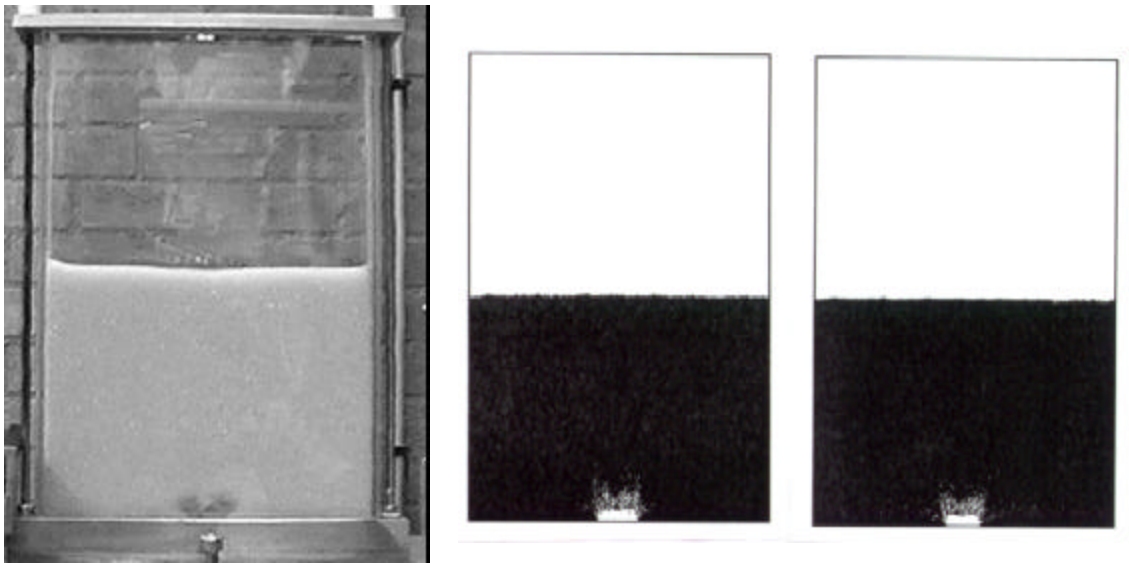

a) *t = 0.05 s*

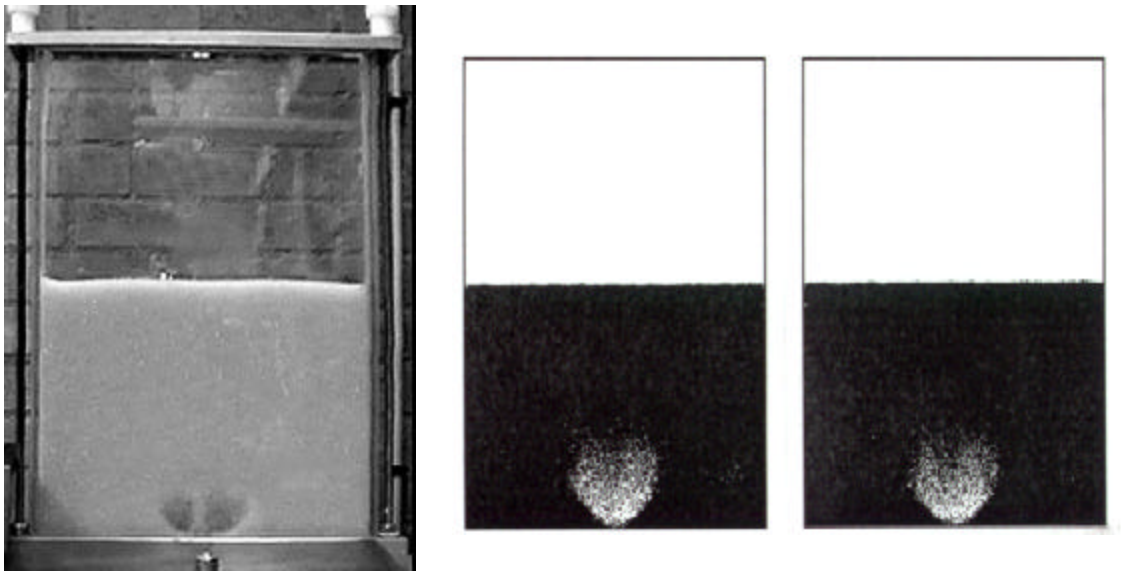

b) *t = 0.10 s*

Figure 5.6. *Snapshots of bubble formation simulations compared with an experiment. From left to right: experiment, hard-sphere simulation and soft-sphere simulation, a) t = 0.05 s b) t = 0.10 s…*

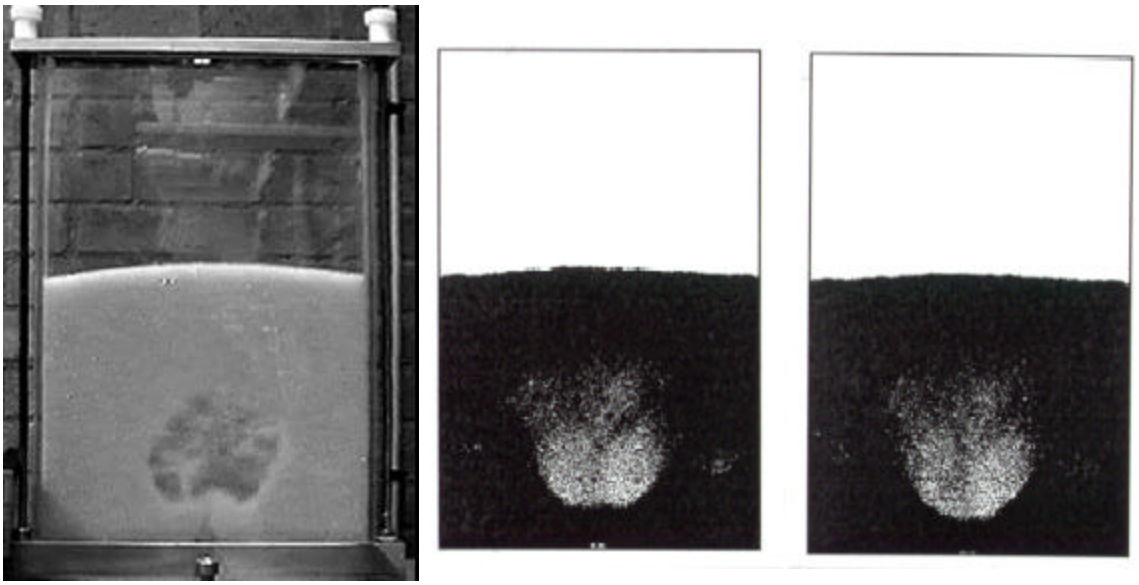

c) *t = 0.15 s*

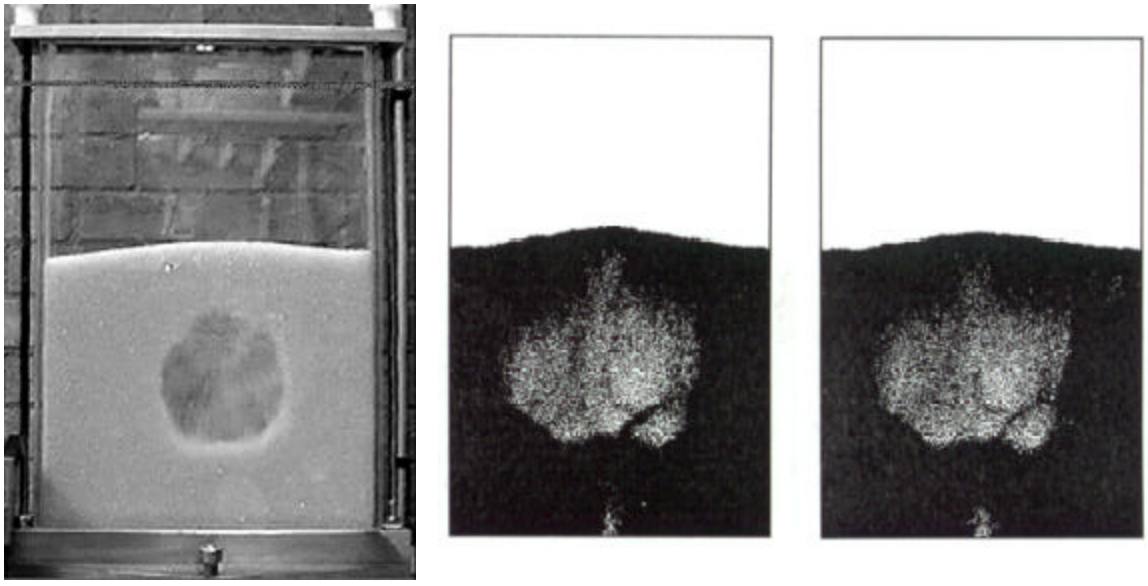

d) *t = 0.20 s*

Figure 5.6. *(…continued) Snapshots of bubble formation simulations compared with an experiment. From left to right: experiment, hard-sphere, soft-sphere c) t = 0.15 s d) t = 0.20 s.*

It is remarkable however that hardly any difference can be observed between the results of the hard-sphere and the soft-sphere simulations. The snapshots appear to be almost identical. In the hard-sphere all collisions are assumed to be binary whereas the soft-sphere code is able to handle multiple contacts. Since the results show hardly any difference it can be concluded that the assumption in the hard-sphere code that all collisions are binary is not limiting. There was however a difference in computational efficiency between the two simulations. The hard-sphere simulation required about 220 minutes of CPU time on a Silicon Graphics Origin200 server with a R10000 processor (180 MHz, 1Mb cache memory) for a simulation of 0.3 s whereas the soft-sphere simulation required 250 minutes of CPU time on the same machine. The main difference between the two simulations is that the soft-sphere simulation progresses in time at a rather constant speed whereas this is certainly not the case in the hard-sphere simulation. In the hard-sphere simulation the first 0.2 s (with an active jet) only require 30% of the total amount of CPU time. This is due to the strong increase in the number of collisions after 0.2 s when the jet is no longer active. From t = 0.0 s to t = 0.2 s a total number of 37,8 million collisions was processed whereas from t = 0.2 s to t = 0.3 s the respectable number of 110 million collisions was processed. Hence the computational efficiency of a hard-sphere simulation depends strongly on the dynamics of the system.

4.4 Effect of collision parameters

Kuipers *et al.* (1998) demonstrated the effect of the collision parameters on bubble formation at a single, central orifice using a hard-sphere simulation. When the collisions were assumed to be fully elastic and perfectly smooth (e = 1.0, μ = 0.0, also referred to as *ideal* collision parameters) no bubble could be observed after 0.2 s. The difference with the simulation where realistic values for the collision parameters were specified (e = 0.96, μ = 0.15, also referred to as *non-ideal* collision parameters) was tremendous. This simulation was repeated here using the soft-sphere code with, apart from the collision parameters, the same parameter settings as used for the simulation in the previous paragraph. Snapshots of both the hard-sphere and the soft-sphere simulations are presented in Figure 5.7 together with video images of the experiment.

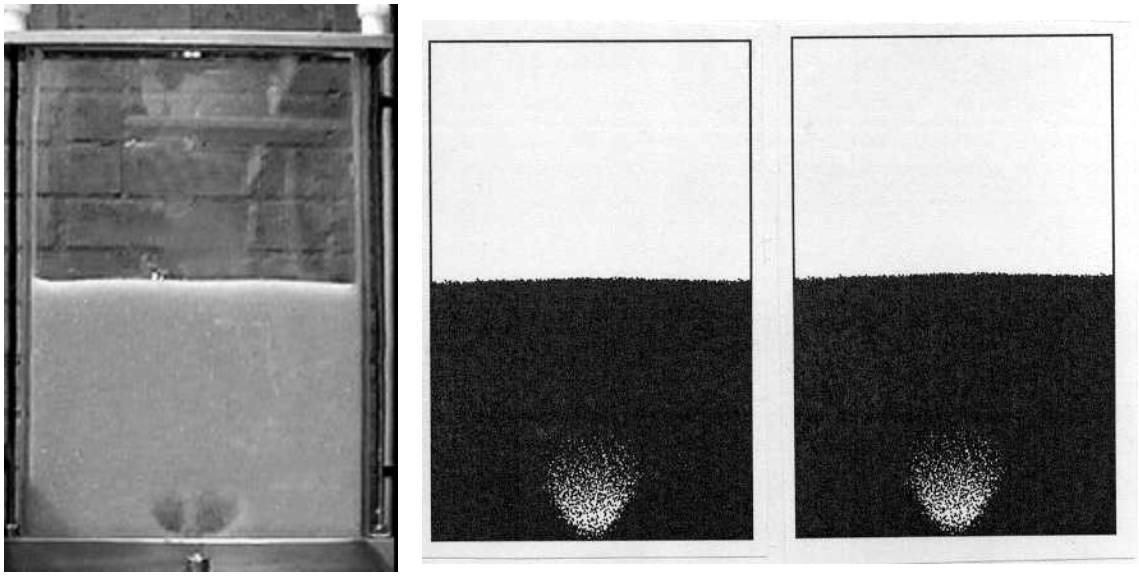

a) *t = 0.1 s*

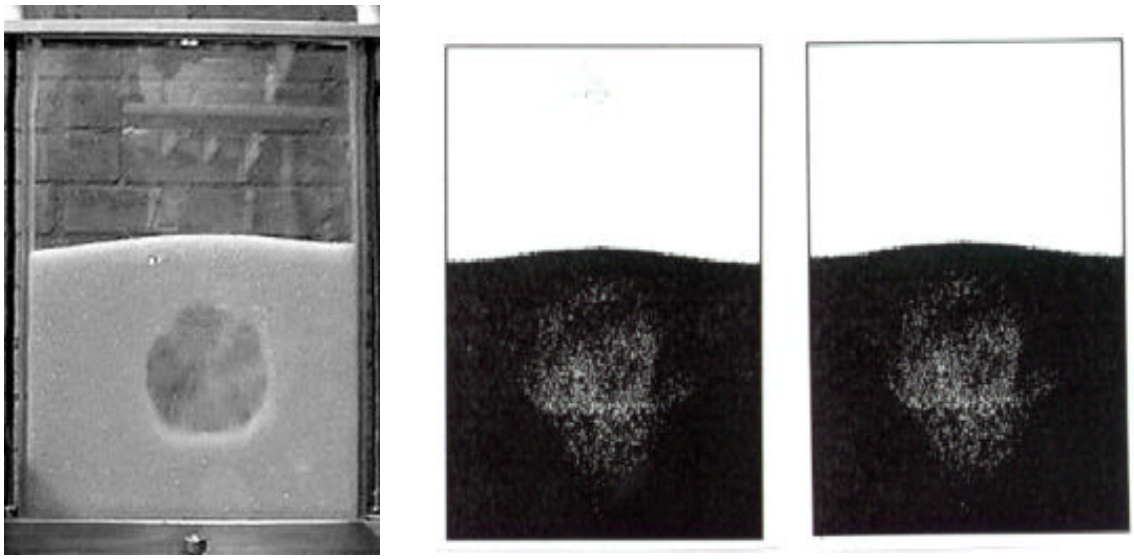

b) *t = 0.2 s*

Figure 5.7. *Snapshots of bubble formation simulations with ideal collision parameter settings (e = 1.0, m = 0.0, b_0 = 0.0) compared with an experiment. From left to right: experiment, hard-sphere, soft-sphere a) t = 0.1 s b) t = 0.2 s.*

In Figure 5.7 it can clearly be observed that the result presented earlier by Kuipers *et al.* (1998) obtained with a hard-sphere code is reproduced here with a soft-sphere code. The snapshot at t = 0.1 s is still quite similar to the snapshot of the simulation with the non-ideal collision parameters presented in Figure 5.6 as well as the experiment. But in the snapshot at t = 0.2 s in Figure 5.7 the bubble seems to have disappeared which is not in agreement with the snapshot at t = 0.2 s in Figure 5.6 and more importantly the experiment. This stresses the importance of the collision parameters in granular dynamics simulations of gas-fluidised beds. When non-realistic values for the collision parameters are specified non-realistic behaviour is predicted. This is found in both the hard-sphere and soft-sphere granular dynamics simulations.

5. Conclusions

A hard-sphere and a soft-sphere granular dynamics model of a gas-fluidised bed have been developed. These two-dimensional models were compared with each other and validated experimentally using the formation of a single bubble at a central orifice as a test case. Preliminary simulations with the soft-sphere code revealed that the time step used for the integration of the contact forces should be more than 3 times smaller than the contact time. The results of the simulations did not change significantly when the time step for the integration of the contact forces was decreased. The results of the simulations were also rather insensitive to the value of the normal spring stiffness. The value of the normal spring stiffness should be high enough compared to the net external force in order to prevent the particles from overlapping too much (more than roughly 10% of their diameter). Although the use of very high values for the spring stiffness does not change the results significantly it requires more CPU time since smaller time steps have to be used. A simulation were the value of the tangential spring stiffness was set equal to the value of the normal spring stiffness ($k_t = k_n$) showed hardly any difference with the default simulations where $k_t = 2/7\ k_n$.

The incorporation of a particle size distribution turned out to improve the agreement between simulation and experiment. In a bubble formation simulation with particles of uniform size small 'satellite' bubbles appeared above and alongside the main bubble. This could not be observed in the experiment nor in the simulation where a log-normal particle size distribution was taken into account.

A hard-sphere and a soft-sphere simulation where a log-normal particle size distribution was taken into account were compared with each other and with an experiment. Both simulations agreed rather well with the experiment especially during the initial stages. The main bubble size and the position of the bubble in the bed were found to be in good agreement with the experiment. The shape of the bubble observed in the experiment was more round than the one observed in the simulations. Also the gas-solid boundary appeared to be sharper in the experiment than in the simulations. This is probably due to the two-dimensional nature of the simulations. Further improvement can be achieved by extending the model to three dimensions because although the bed used in the experiment was quasi two-dimensional it was still 16 mm deep. However, a full 3-D system simulation of this system would require about 750,000 particles which is extremely challenging even for state of the art computing resources of today. Applying periodic boundary conditions in the z-direction would reduce the total number of particles required in the simulation but in that case the influence of the front and back walls would be eliminated as well. Another improvement can be achieved by employing a higher order numerical scheme for the convective fluxes in the gas phase momentum equations that suffer less from numerical diffusion. Results of Eulerian simulations with such higher order schemes show sharper bubble boundaries and that could also be the case for Lagrangian simulations. The results of both the hard-sphere and the soft-sphere simulation were nearly identical. Therefore it can be concluded that the assumption in the hard-sphere code that all collisions are binary is not limiting. However, there was a difference in computational efficiency. Where the soft-sphere simulation progresses through the simulation at a rather constant speed the computational efficiency of the hard-sphere simulation depends strongly on the dynamics of the system. The more collisions

occur the slower the progress. The overall CPU time requirements of the two codes were very similar for a simulation of 0.3 s.

The collision parameters (*i.e.* coefficients of restitution and friction) turned out to have a key influence on the bubble formation process. When the collisions were assumed to be fully elastic and perfectly smooth (e = 1.0, m = 0.0) no bubble could be observed after 0.2 s. This result was obtained with both the hard-sphere and the soft-sphere model.

Notation

C_d	drag coefficient, [-]
D_o	orifice width, m
D_p	particle diameter, m
DT	time step, s
DX	horizontal computational cell dimension, m
DY	vertical computational cell dimension, m
e	coefficient of restitution, [-]
$\mathbf{F}$	force, N
$\mathbf{g}$	gravitational acceleration, m/s^2
I	moment of inertia, kgm^2
k	spring stiffness, N/m
m	particle mass, kg
N_p	number of particles, [-]
NX	number of computational cells in x-direction, [-]
NY	number of computational cells in y-direction, [-]
$\mathbf{n}$	normal unit vector, [-]
p	pressure, Pa
R_p	particle radius, m
$\mathbf{r}$	position vector, m
$\mathbf{S}_p$	momentum source term, N/m^3

T	torque, Nm
T	temperature, K
t	time, s
u	gas velocity vector, m/s
v	particle velocity vector, m/s
V_p	particle volume, m^3

Greek symbols

b	volumetric interphase momentum transfer coefficient, $kg/(m^3s)$
b_0	coefficient of tangential restitution, [-]
e	void fraction, [-]
m	coefficient of friction, [-]
m_g	gas viscosity, kg/ms
h	damping coefficient, Ns/m
t	gas phase stress tensor, kg/ms^2
r	density, kg/m^3
x	displacement, m

Subscripts

g	gas phase
mf	minimum fluidisation
p	particle
w	wall

References

Anderson, T.B. and Jackson, R., (1967). A fluid mechanical description of fluidized beds (equations of motion), *Ind. Eng. Chem., Fundam.*, **6**, 527.

Cundall, P.A. and Strack, O.D.L., (1979). A discrete numerical model for granular assemblies. *Géotechnique*, **29**, 47.

Foerster S.F., Louge, M.Y., Chang,H. and Allia, K. (1994). Measurements of the collision properties of small spheres. *Phys. Fluids,*, **6**, 1108.

Gidaspow, D. (1994). *Multiphase Flow and Fluidization*, Academic Press, Boston, USA.

Hoomans, B.P.B., Kuipers, J.A.M., Briels, W.J. and van Swaaij, W.P.M., (1996). Discrete particle simulation of bubble and slug formation in a two-dimensional gas-fluidised bed: a hard-sphere approach, *Chem. Engng Sci*., **51**, 99.

Hoomans, B.P.B., Kuipers, J.A.M. and van Swaaij, W.P.M., (1998). The Influence of a Particle Size Distribution on the Granular Dynamics of Dense Gas-Fluidized beds: a Computer Simulation Study", *AIChE Symp. Ser. No. 318*, **94**, 15.

Kuipers, J.A.M., van Duin K.J., van Beckum, F.P.H. and van Swaaij, W.P.M., (1992). A numerical model of gas-fluidized beds, *Chem. Engng Sci*., **47,** 1913

Kuipers, J.A.M., Hoomans, B.P.B. and van Swaaij, W.P.M., (1998). Hydrodynamic Models of Gas-Fluidized Beds and their Role for Design and Operation of Fluidized Bed Chemical Reactors", in *Fluidization IX*, L.-S. Fan and T.M. Knowlton eds., 15.

Kawaguchi, T., Tanaka, T. and Tsuji, Y., (1998). Numerical simulation of two-dimensional fluidized beds using the discrete element method (comparison between the two- and three-dimensional models), *Powder Technol*., **96**, 129.

Mikami, T., Kamiya, H. and Horio, M., (1998). Numerical simulation of cohesive powder behavior in a fluidized bed, *Chem. Engng Sci*., **53**, 1927.

Nieuwland, J.J., (1994). *Hydrodynamic modelling of gas-solid two-phase flows*, PhD Thesis, University of Twente, The Netherlands.

Richardson, J.F. and Zaki, W.N., (1954). Sedimentation and fluidization: part I. *Trans. Inst. Chem. Eng*., **32**, 35.

Schäfer, J., Dippel, S. and Wolf, D.E., (1996). Force schemes in simulations of granular materials, *J. Phys. I France* **6**, 5.

Schwarzer, S., (1995). Sedimentation and flow through porous media: Simulating dynamically coupled discrete and continuum phase, *Phys. Rev. E.* **52**, 6461.

Sinclair, J.L. and Jackson, R. (1989). Gas-particle flow in a vertical pipe with particle-particle interactions, *AIChE J*., **35**, 1473.

Tsuji, Y., Kawaguchi, T. and Tanaka, T., (1993). Discrete particle simulation of two dimensional fluidized bed, *Powder Technol.* **77**, 79.

Walton, O.R., (1992). Numerical simulation of inelastic, frictional particle-particle interactions, in *Particulate Two-Phase Flow, Part I,* edited by M.C. Roco, Butterworth-Heinemann, Boston, 884.

Wang, Y. and Mason, M.T., (1992). Two-dimensional rigid-body collisions with friction. *J. Appl. Mech*., **59**, 635.

Wen, C.Y. and Yu, Y.H., (1966). Mechanics of fluidization. *Chem. Eng. Prog. Symp. Ser*., **62** (62), 100.

Xu, B.H. and Yu, A.B., (1997). Numerical simulation of the gas-solid flow in a fluidized bed by combining discrete particle method with computational fluid dynamics. *Chem. Engng Sci*. **52**, 2785.

Chapter 6.

GRANULAR DYNAMICS SIMULATION OF SEGREGATION PHENOMENA IN BUBBLING GAS-FLUIDISED BEDS

Abstract:

Granular dynamics simulations of gas-fluidised beds were performed in order to simulate segregation phenomena in systems consisting of particles of different size and density. In the model the gas-phase hydrodynamics is described by the spatially averaged Navier-Stokes equations for two-phase flow. For each solid particle the Newtonian equations of motion are solved taking into account the particle-particle and particle-wall interactions. The (2-D) model was applied to a system consisting of particles of three different densities but equal size and to systems consisting of particles of two different sizes but equal density. In the different density system segregation was observed over a time scale of several seconds. In the different size systems segregation was also observed but a clear steady state was not reached since the larger particles were continuously transported to the upper regions of the bed in bubble wakes. A statistical analysis of the segregation in terms of mass fraction distributions is presented. When the particle-particle and particle-wall interactions were assumed to be fully elastic and perfectly smooth, segregation occurred very fast and was almost complete due to the absence of bubbles. Preliminary experimental validation showed rather poor agreement between simulation and experiment. The simulation predicts segregation at a lower gas velocity than used in the experiment.

Parts of this chapter are based on the following papers:

B.P.B. Hoomans, J.A.M. Kuipers and W.P.M. van Swaaij, (1998). Discrete Particle Simulation of Segregation Phenomena in Dense Gas-Fluidized Beds, in *Fluidization IX*, L.S. Fan and T.M. Knowlton (eds),485.

B.P.B. Hoomans, J.A.M. Kuipers and W.P.M. van Swaaij, (1999). Granular Dynamics Simulation of Segregation Phenomena in Dense Gas-Fluidised beds, *Powder Technology* (in press).

1. Introduction

Segregation phenomena can play an important role in fluidised systems consisting of particles of different size and/or density. Typical examples of such processes are fluidised bed polymerisation and fluidised bed granulation among others. In order to improve the performance of these processes detailed knowledge about the distribution of the different solids species throughout the bed in different operating conditions is required. In a system consisting of particles of equal density but different size the bigger (heavier) particles tend to reside at the bottom of the bed if the fluidisation velocity does not exceed the minimum fluidisation velocity (u_{mf}) of the big particles. The big particles are in this case referred to as *jetsam*. The smaller (lighter) particles show the tendency to float and reside at the bed surface. These particles are referred to as *flotsam*. At gas velocities much higher than the u_{mf} of the jetsam better mixing is normally achieved. In case of a system consisting of particles of equal size but different density the denser particles are referred to as jetsam whereas the lighter particles are referred to as flotsam.

Segregation phenomena in gas-fluidised beds have been the subject of several experimental studies reported in the literature. Nienow *et al.* (1987), Hoffmann *et al.* (1993) and Wu and Baeyens (1998) studied systems consisting of particles of equal density but different size. Nienow and Naimer (1980) performed experiments on systems consisting of particles of equal size but different density. Rowe *et al.* (1972) presented experimental results for both types of systems. In general the different density systems tend to segregate more easily than the poly-disperse systems.

Due to increasing computer power discrete particle models have become a very useful and versatile research tool in order to study the hydrodynamics of gas-fluidised beds. In these models the Newtonian equations of motion for each individual particle are solved. Particle-particle and particle-wall interactions are taken into account directly which is a clear advantage over two-fluid models that require closure relations for the solids-phase

stress tensor (Kuipers *et al.* (1992) and Gidaspow (1994) among many others). When simulating gas-fluidised beds with particles of different size and/or particles of different density multi-fluid models can be used (Gidaspow *et al.*, 1990) but several difficulties are encountered due to the fact that large sets of continuum equations have to be solved. In addition, and more fundamentally, significant problems arise when closure laws for the mutual interaction of particles belonging to different classes have to be formulated. Although the Kinetic Theory of Granular Flow (KTGF) offers a theoretical framework to overcome this problem this approach is not very flexible and the computational cost increases dramatically with each additional solid phase. Kumaran and Koch (1993) and Manger (1996) applied this theory to binary mixtures and recently Mathiesen *et al.* (1998) extended the work of Manger (1996) in order to handle three solid phases. A discrete particle approach offers a more natural way to overcome these problems since each individual particle in the simulation is tracked. Hence discrete particle models are very useful in order to study segregation phenomena in gas-fluidised beds consisting of particles of different size and/or density in detail. Moreover they can be used to generate data which can subsequently be used to develop closure models for continuum models. However the number of particles that can be taken into account in a simulation is limited (typically $< 10^6$) which implies that currently the method can only be applied to rather small systems consisting rather coarse particles.

The discrete particle approach for gas-fluidised beds was pioneered by Tsuji *et al.* (1993) who developed a soft-sphere discrete particle model based on the work of Cundall and Strack (1979). In this approach the particles are allowed to overlap slightly and this overlap is subsequently used to calculate the contact forces. Recently Kawaguchi *et al.* (1998) presented results for a three-dimensional version of this model. Schwarzer (1995) used a model similar to that of Tsuji *et al.* (1993) to simulate liquid fluidised beds in which lubrication forces were also taken into account. Hoomans *et al.* (1996) were the first to present a hard-sphere granular dynamics model of a gas-fluidised bed. In this discrete particle model the particles interact through binary, instantaneous, inelastic collisions with friction. Xu and Yu (1997) presented a hybrid technique where they used a contact force model in order to determine the inter-particle forces and a collision detection

algorithm in order to determine the precise instant at which the particles first come into contact. Mikami *et al.* (1998) recently extended the model of Tsuji *et al*. (1993) in order to include cohesive forces between the particles. Seibert and Burns (1998) were able to predict segregation phenomena in liquid fluidised beds using a Monte Carlo simulation technique. However, the Monte Carlo technique is only capable of predicting a certain steady state and is not suitable to simulate the dynamics of segregation.

In this chapter two-dimensional granular dynamics simulations will be used to study segregation phenomena in bubbling gas-fluidised beds. The majority of the simulations is concerned with systems consisting of particles of equal density but different size but also a system consisting of particles of uniform size but different density is included.

2. Models

Since a detailed description of the models is presented in Chapter 2 and Chapter 3, the key features will be summarised only briefly here.

2.1 Hard-sphere granular dynamics

The collision model as originally developed by Wang and Mason (1992) is used to describe a binary, instantaneous, inelastic collision with friction. The key parameters of the model are the coefficient of restitution ($0 \leq e \leq 1$) and the coefficient of friction ($m \geq 0$). Foerster *et al.* (1994) have shown that also the coefficient of tangential restitution ($0 \leq b_0 \leq 1$) should be used in order to describe the collision dynamics more accurately. These three collision parameters are all included in the model.

In the hard-sphere approach a sequence of binary collisions is processed. This implies that a collision list is compiled in which for each particle a collision partner and a corresponding collision time is stored. A constant time step is used to take the external

forces into account and *within* this time step the prevailing collisions are processed sequentially. In order to reduce the required CPU time neighbour lists are used. For each particle a list of neighbouring particles is stored and only for the particles in this list a check for possible collisions is performed. When simulating a binary system of particles of different size two cut off distances are used as schematically shown in Figure 6.1.

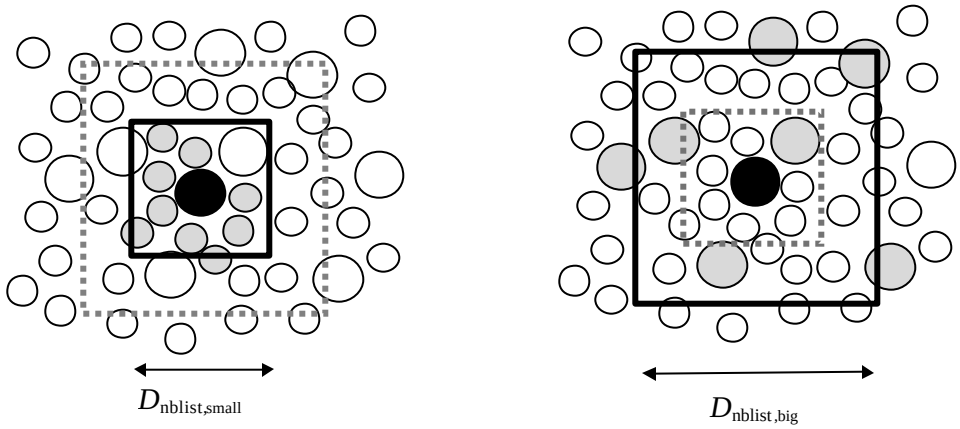

Figure 6.1. *The neighbour list principle using two cut off distances. The shaded particles are stored in the neighbour list of the black one.*

The neighbour list consists of all the small particles which are found within the small square (coloured grey) and the big particles which are found within the big square (coloured grey). By using this approach the number of particles in the neighbour list will never become too high which significantly reduces both CPU time and memory space requirements.

2.2 Soft-sphere granular dynamics

Although the majority of the simulations presented in this chapter were performed with the hard-sphere code also a simulation with the soft-sphere code was performed and therefore that model is described briefly here as well.

In soft-sphere models the following equations of motion are used:

$$m\frac{d^2\mathbf{r}}{dt^2} = \mathbf{F}_{contact} + \mathbf{F}_{external}, \tag{6.1}$$

$$I\frac{d\omega}{dt} = \mathbf{T}, \tag{6.2}$$

where $\mathbf{r}$ is the position vector of the centre of the particle, m is the mass of the particle, $\mathbf{F}_{contact}$ is the contact force acting on the particle, $\mathbf{F}_{external}$ is the net external force acting on the particle, ω is the rotation velocity, $\mathbf{T}$ is the torque acting on the particle and I is the moment of inertia of the particle. In this paragraph the focus will be on the contact forces between the particles, the external forces will be discussed in the following paragraph.

The contact forces are given by:

$$\mathbf{F}_{n,ab} = -k_n x_n \mathbf{n}_{ab} - h_n \mathbf{v}_{n,ab} \tag{6.3}$$

$$\mathbf{F}_{t,ab} = -k_t \mathbf{?}_t - h_t \mathbf{v}_{t,ab} \tag{6.4}$$

If however the following relation is satisfied:

$$\left|\mathbf{F}_{t,ab}\right| > m\left|\mathbf{F}_{n,ab}\right|, \tag{6.5}$$

then sliding occurs and the tangential force is given by:

$$\mathbf{F}_{t,ab} = -m\left|\mathbf{F}_{n,ab}\right|\mathbf{t}_{ab}. \tag{6.6}$$

For contacts between particles and walls, the walls were assumed to be non-moving and of infinite mass just like in the hard-sphere model.

The resulting force and torque for particle a are now simply obtained by adding the pair wise contributions of all the particles that are in contact with a:

$$\mathbf{F}_{contact,a} = \sum_b \left(\mathbf{F}_{n,ab} + \mathbf{F}_{t,ab} \right) \quad , \tag{6.7}$$

$$\mathbf{T}_a = \sum_b \left(R_a \mathbf{n}_{ab} \times \mathbf{F}_{t,ab} \right). \tag{6.8}$$

Since the contact forces are in general at least an order of magnitude larger than the external forces a separation of time scales was introduced. By default at each time step *DT* the external forces were taken into account while at 0.1*DT* the equations of motion were solved by taking only the contact forces into account.

2.3 External forces

The incorporation of external forces differs somewhat from the approach followed by Hoomans *et al*. (1996). In this work the external forces are used in accordance with those implemented in the two-fluid model presented by Kuipers *et al.* (1992) where, of course, the forces now act on a single particle:

$$m_p \frac{d\mathbf{v}_p}{dt} = m_p \mathbf{g} + \frac{V_p b}{(1-e)} \left(\mathbf{u} - \mathbf{v}_p \right) - V_p \nabla p \quad , \tag{6.9}$$

where m_p represents the mass of a particle, $\mathbf{v}_p$ its velocity, $\mathbf{u}$ the local gas velocity and V_p the volume of a particle. In equation (6.9) the first term is due to gravity and the third term is the force due to the pressure gradient. The second term is due to the drag force where b represents an inter-phase momentum exchange coefficient as it usually appears in two-fluid models. For low void fractions ($e < 0.80$) b is obtained from the well-known Ergun equation:

$$b = 150 \frac{(1-e)^2}{e} \frac{m_g}{D_p^2} + 1.75(1-e) \frac{r_g}{D_p} \left| \mathbf{u} - \mathbf{v}_p \right| \quad , \tag{6.10}$$

where D_p represents the particle diameter, μ_g the viscosity of the gas and ρ_g the density of the gas. For high void fractions ($\varepsilon \geq 0.80$) the following expression for the inter-phase momentum transfer coefficient has been used which is basically the correlation presented by Wen and Yu (1966) who extended the work of Richardson and Zaki (1954):

$$\beta = \frac{3}{4} C_d \frac{\varepsilon(1-\varepsilon)}{D_p} \rho_g \left|\mathbf{u} - \mathbf{v}_p\right| \varepsilon^{-2.65} \quad . \tag{6.11}$$

The drag coefficient C_d is a function of the particle Reynolds number and given by:

$$C_d = \begin{cases} \dfrac{24}{\mathrm{Re}_p}\left(1 + 0.15\mathrm{Re}_p^{0.687}\right) & \mathrm{Re}_p < 1000 \\ 0.44 & \mathrm{Re}_p \geq 1000 \end{cases}, \tag{6.12}$$

where the particle Reynolds number (Re_p) in this case is defined as follows:

$$\mathrm{Re}_p = \frac{\varepsilon \rho_g \left|\mathbf{u} - \mathbf{v}_p\right| D_p}{\mu_g} \quad . \tag{6.13}$$

For the integration of equation (6.9) a simple explicit first order scheme was used to update the velocities and positions of the particles.

2.4 Gas phase hydrodynamics

The calculation of the gas phase hydrodynamics mainly follows the lines presented by Kuipers *et al.* (1992). It is based on the numerical solution of the following set of partial differential equations that can be seen as a generalised form of the Navier-Stokes equations for a gas interacting with a solid phase as originally derived by Anderson and Jackson (1967).

Continuity equation gas phase:

$$\frac{\partial\left(\varepsilon_g \rho_g\right)}{\partial t} + \left(\nabla \cdot \varepsilon_g \rho_g \mathbf{u}\right) = 0 . \tag{6.14}$$

Momentum equation gas phase:

$$\frac{\partial\left(\varepsilon_g \rho_g \mathbf{u}\right)}{\partial t} + \left(\nabla \cdot \varepsilon_g \rho_g \mathbf{u}\mathbf{u}\right) = -\varepsilon \nabla p - \mathbf{S}_p - \left(\nabla \cdot \varepsilon \tau_g\right) + \varepsilon_g \rho_g \mathbf{g} . \tag{6.15}$$

In this work transient, two-dimensional, isothermal (T = 293 K) flow of air at atmospheric conditions is considered. The constitutive equations can be found in Chapter 3. There is one important modification with respect to the model presented by Hoomans *et al*. (1996) and that deals with the way in which the two-way coupling between the gas phase and the dispersed particles is established. In the present model the reaction force to the drag force exerted on a particle per unit of volume is fed back to the gas phase through the source term $\mathbf{S}_p$ which has the dimension of force per unit of volume N/m^3. For the calculation of the void fraction (ε) the technique described in Chapter 3 was used. No special modifications were made to take the effect of the particle size distribution into account.

3. Ternary density distribution

A simulation was performed of a system that consisted of three types of particles of uniform size but of different density using the hard-sphere code. The system was filled with 800 particles with a density of 2700 kg/m^3 (u_{mf} = 1.79 m/s), 800 particles with a density of 1800 kg/m^3 (u_{mf} = 1.42 m/s) and 800 particles with a density of 900 kg/m^3 (u_{mf} = 0.98 m/s). The main parameter settings for this simulation can be found in table 6.1. The

gas inflow velocity was set equal to the minimum fluidisation velocity of the densest (r_p = 2700 kg/m^3) particles (u_{mf} = 1.79 m/s).

Table 6.1. *Parameter settings for the simulation with a different density mixture*

Particles:		Bed:	
shape	spherical	width	0.15 m.
diameter	4.0 mm	height	0.50 m
r_p = 2700 kg/m^3	N_p = 800	number x-cells, *NX*	15
r_p = 1800 kg/m^3	N_p = 800	number y-cells, *NY*	25
r_p = 900 kg/m^3	N_p = 800	cell width, *DX*	10 mm
$e = e_w$	0.9	cell height, *DY*	10 mm
$m = m_w$	0.3		
$N_{p,total}$	2400	time step, *DT*	10^{-4} s

The coefficients of tangential restitution were assumed to be equal to zero. The bed was fluidised at the minimum fluidisation velocity of the densest particles (u_g = 1.79 m/s) for 15 s starting from perfectly mixed initial conditions. In Figure 6.2 snapshots of the particle configurations are presented.

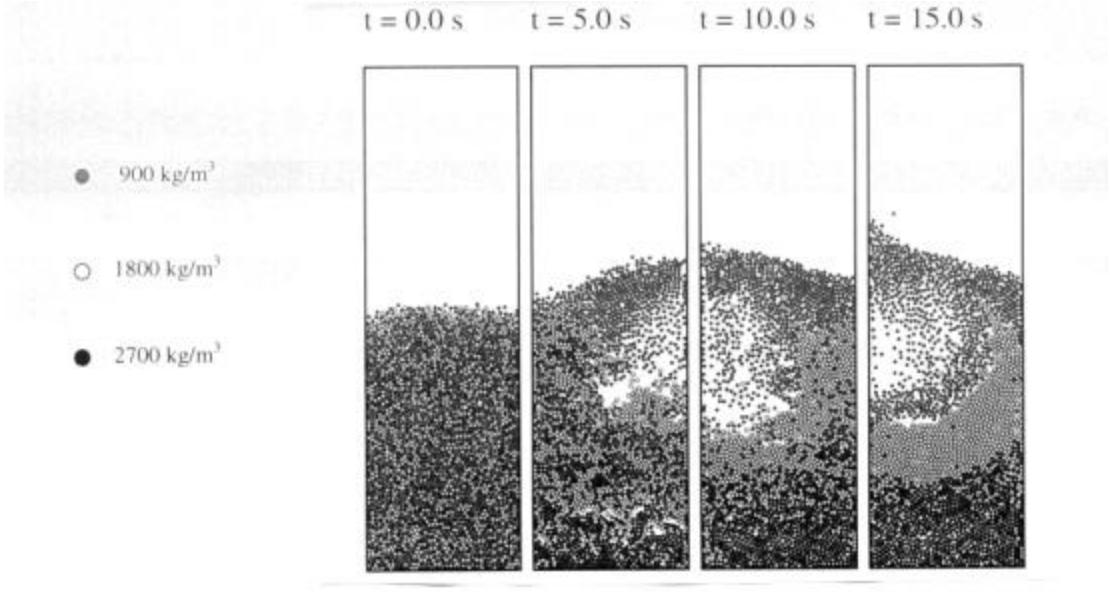

Figure 6.2. *Snapshots of the particle configurations in a system with a ternary density distribution.*

In Figure 6.2 the segregation effect can clearly be observed. After only 15 seconds three distinct layers can be identified. In Figure 6.3 the mass fractions are plotted as a function of the bed height at t = 15 s. The mass fractions are obtained by averaging over the full width of a bed section of 0.05 m height. In this figure it can be observed that the mass fraction of the jetsam particles (r_p = 2700 kg/m^3) is nearly one in the bottom region where the mass fraction of the flotsam particles (r_p = 900 kg/m^3) is zero. In the upper regions of the bed the mass fraction jetsam is zero whereas the mass fraction flotsam approaches one. The middle section of the bed clearly shows a peak in the mass fraction of the particles with r_p = 1800 kg/m^3.

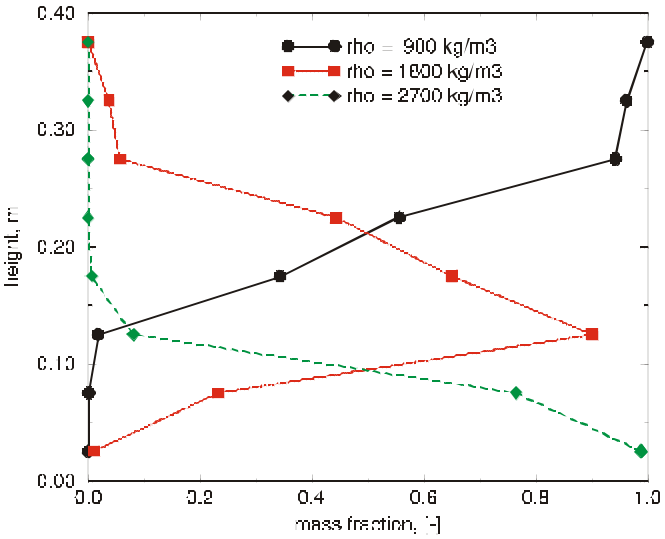

Figure 6.3. *Mass fractions as a function of the bed height at t = 15 s for the simulation with a ternary density distribution.*

It is remarkable that even though the two less dense types of particles are both fluidised well above their u_{mf} there is a clear segregation effect between these two layers as well. Even though the fluidisation velocity is 1.3u_{mf} of the particles with r_p = 1800 kg/m^3, the segregation between the upper two layers is rather clear. However, this is in agreement with the experimental observations by Rowe *et al.* (1972) who reported that different

density systems still show segregation above the u_{mf} of the jetsam particles. Since the particle size is rather large in this relatively small system wake effects due to bubbles are less pronounced. A dispersive mechanism was therefore not dominantly present and this may have enhanced the segregation.

4. Binary size distribution

4.1 Base case

A simulation was performed of a system that consisted of two types of particles of different size but equal density using the hard-sphere code. A homogeneous mixture of 250 particles of 4.0 mm diameter and 4750 particles of 1.5 mm diameter (50/50 wt.) was fluidised at the minimum fluidisation velocity of the bigger particles ($u_{mf,big}$ = 1.7 m/s). The simulation was run for 50 seconds using the parameter settings presented in table 6.2. The collision parameters for the glass particles were obtained from Hoomans *et al*. (1996).

Table 6.2. *Parameter settings for the simulations with a binary size distribution*

Particles:		Bed:	
shape	spherical	width	0.15 m.
density, r_p	2480 kg/m^3	height	0.25 m
D_p = 1.5 mm	N_p = 4750	number x-cells, *NX*	15
D_p = 4.0 mm	N_p = 250	number y-cells, *NY*	25
e	0.96	cell width, *DX*	10 mm
e_w	0.86	cell height, *DY*	10 mm
$m = m_w$	0.15		
$N_{p,total}$	5000	time step, *DT*	10^{-4} s

The coefficients of tangential restitution were assumed to be equal to zero. Snapshots of particle configurations are shown in Figure 6.4. In this figure it can be observed that segregation does occur with the bigger particles accumulating at the bottom of the bed.

However, this is a very dynamic situation as could be observed in animations where it became clear that the bigger particles are continuously transported to the upper regions of the bed in the wake of a bubble and descend again in the denser regions. This process continued throughout the simulation.

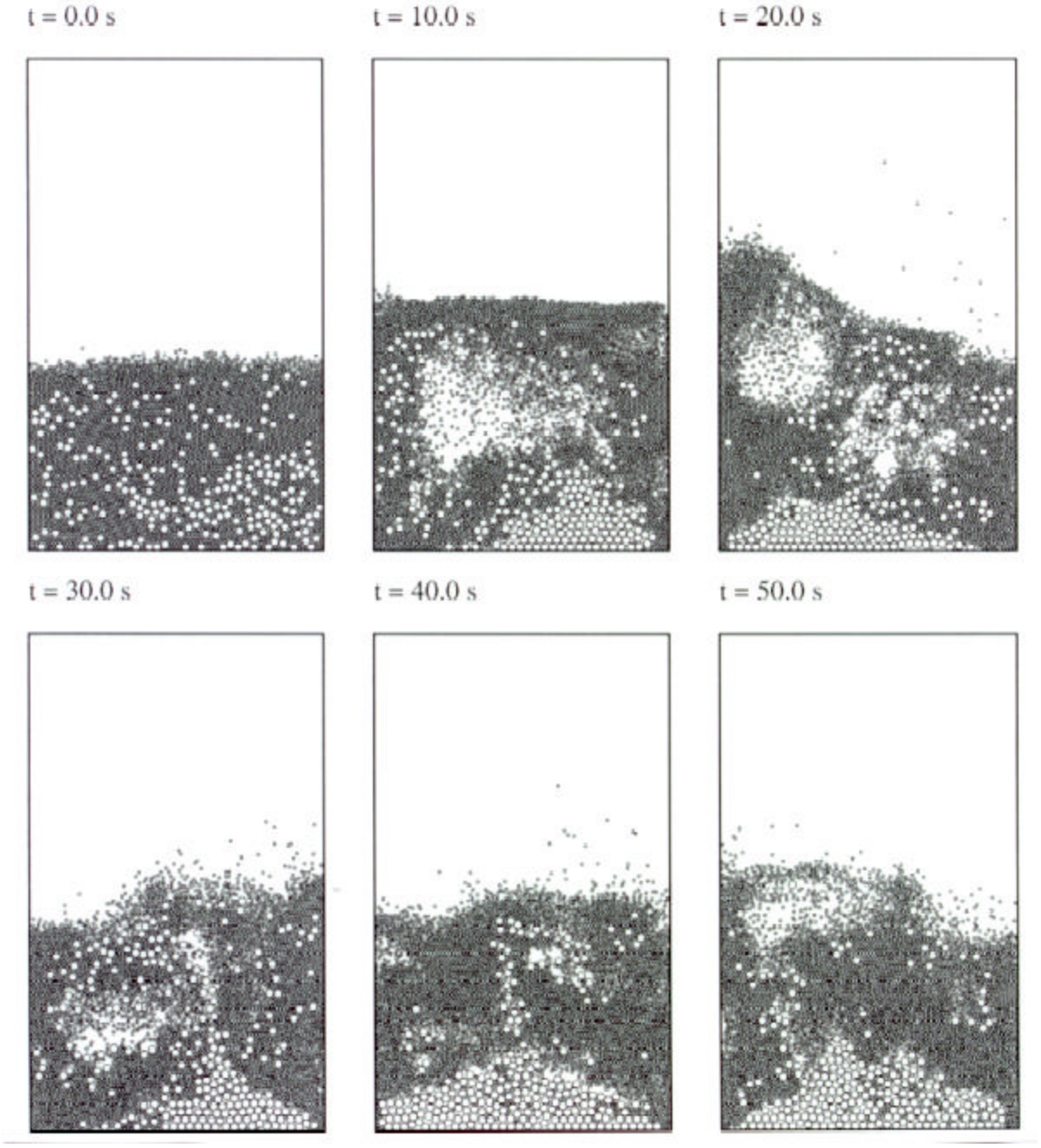

Figure 6.4. *Snapshots of the particle configurations for a binary system of particles of different size.*

A typical simulation took about 25 minutes of CPU time per simulated second on a Silicon Graphics Power Challenge with a 196 MHz R10000 processor. In Figure 6.5 the mass fraction jetsam at t = 20 s is plotted as a function of the height in the bed. Since all particle positions are known at each instant during a simulation such a plot can be calculated instantaneously. In experiments normally the gas supply is first shut off after which the bed is sectioned and each section is analysed separately. In the figure an additional line at the average mass fraction of 0.5 is included to guide the eye.

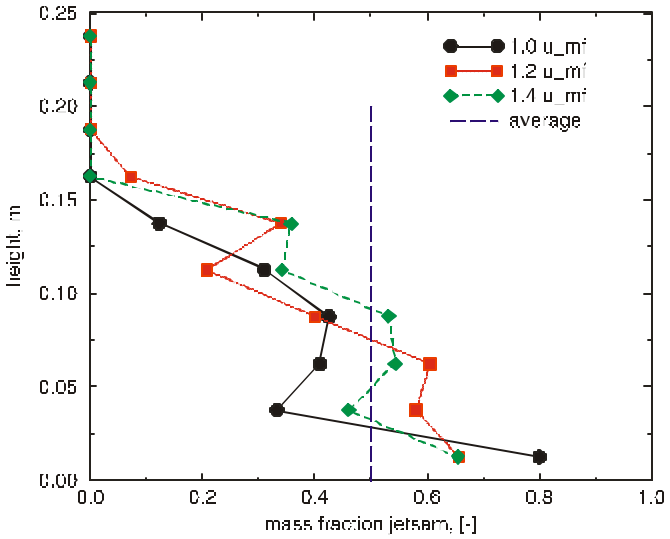

Figure 6.5. *Mass fraction jetsam as a function of the bed height at t = 20 s for the simulations with a binary size distribution at three different gas velocities (u_mf refers to the u_{mf} of the big particles)*

It can be observed that the mass fraction jetsam is indeed higher in the lower part of the bed although the fraction does not become one. This is not surprising since it could already be observed from the snapshots in Figure 6.4 that there is no pure layer of jetsam particles being formed on the bottom of the bed. The common knowledge that different density systems tend to segregate more easily than different size systems (Rowe *et al.*, 1972) is confirmed here when Figure 6.5 is compared with Figure 6.3. In Figure 6.5 also results for higher gas velocities are included from which it can be observed that the solids mixing is better at increased gas velocities.

4.2 Statistical analysis of segregation

Although segregation could be observed in the base case simulation presented in the previous paragraph the system remained very dynamic. Therefore an analysis based on a single frame, as was presented for the base case simulation, does not provide a complete understanding of the segregation phenomenon. A similar problem is encountered in segregation experiments where segregation profiles are determined after the gas supply is abruptly shut off and the bed is subsequently divided in sections that are separately analysed (Hoffmann *et al.* (1993), Wu and Baeyens (1998)). By repeating the experiments the reliability of the results can be improved which is however rather time consuming. In granular dynamics simulations the positions of all the particles in the system are known at each instant. This enables the determination of segregation profiles by averaging over a large number of particle configurations, also referred to as *frames*. For the results presented in Figure 6.6 an average segregation profile was obtained using the particle configurations at each 0.01 seconds for a total duration of 50 seconds. Hence a reliable average and a corresponding variance could be obtained from 5000 frames. A line indicating the average mass fraction jetsam is included to guide the eye.

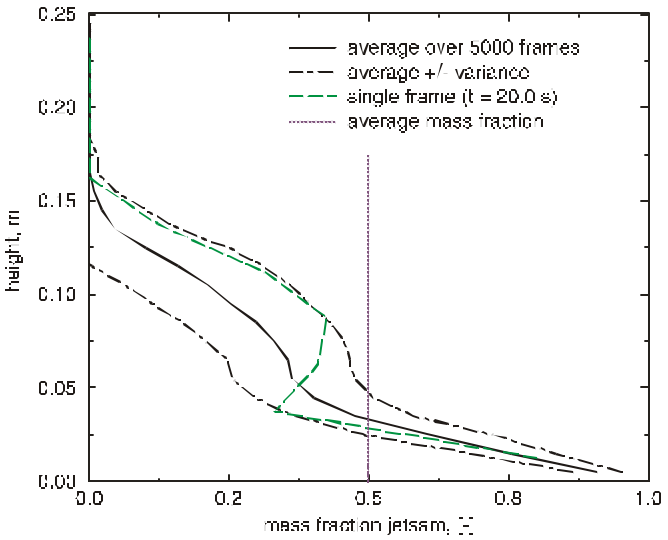

Figure 6.6. *Segregation profiles obtained from both single- and multiple frame analysis*

In this figure a segregation profile obtained from a single frame analysis (t = 20.0 s) is included as well. Since this profile differs significantly from the average profile it clearly shows that one has to be careful with the application of single frame analysis. It only gives an impression of an instantaneous situation and therefore does not provide a complete understanding of the segregated state of the system.

In Figure 6.7 the probability distribution of the mass fraction jetsam at a bed height of 0.075 m obtained over the full duration of the simulation is presented.

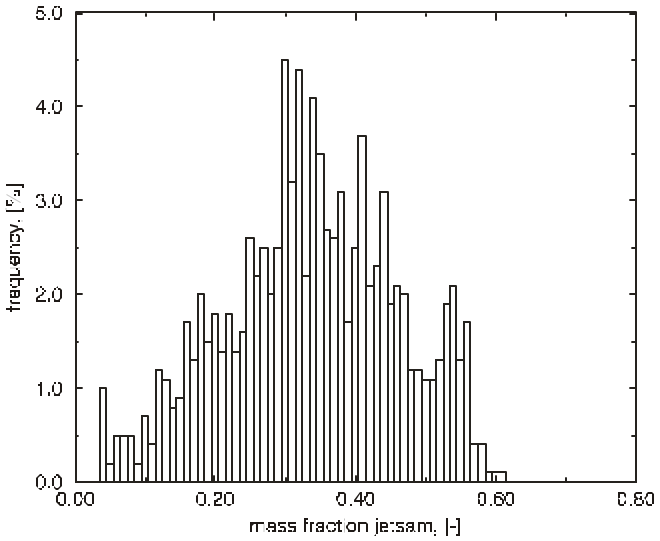

Figure 6.7. *Probability distribution of the jetsam mass fraction at 0.075 m above the distributor plate obtained over 50 seconds*

The wide spread in this distribution again emphasises that a single frame analysis may lead to an incomplete understanding of the segregated state of the system. It is important to note that the segregation profiles obtained from the simulation are based on the actual positions of the particles during fluidisation while in experiments the gas supply is always shut off before the collapsed bed is sectioned and analysed. The segregation profiles obtained in such experiments are therefore based on the particle positions in a collapsed bed rather than a bed in a fluidised state.

4.3 Effects of collision parameters

Since the collision parameters turned out to have a significant influence on the bed hydrodynamics in all the simulations presented in the previous chapters an additional simulation was performed assuming fully elastic (e = 1) and perfectly smooth (m = 0) collisions. All other parameters were set to the same values as presented in table 6.2. Snapshots of this simulation are presented in Figure 6.8.

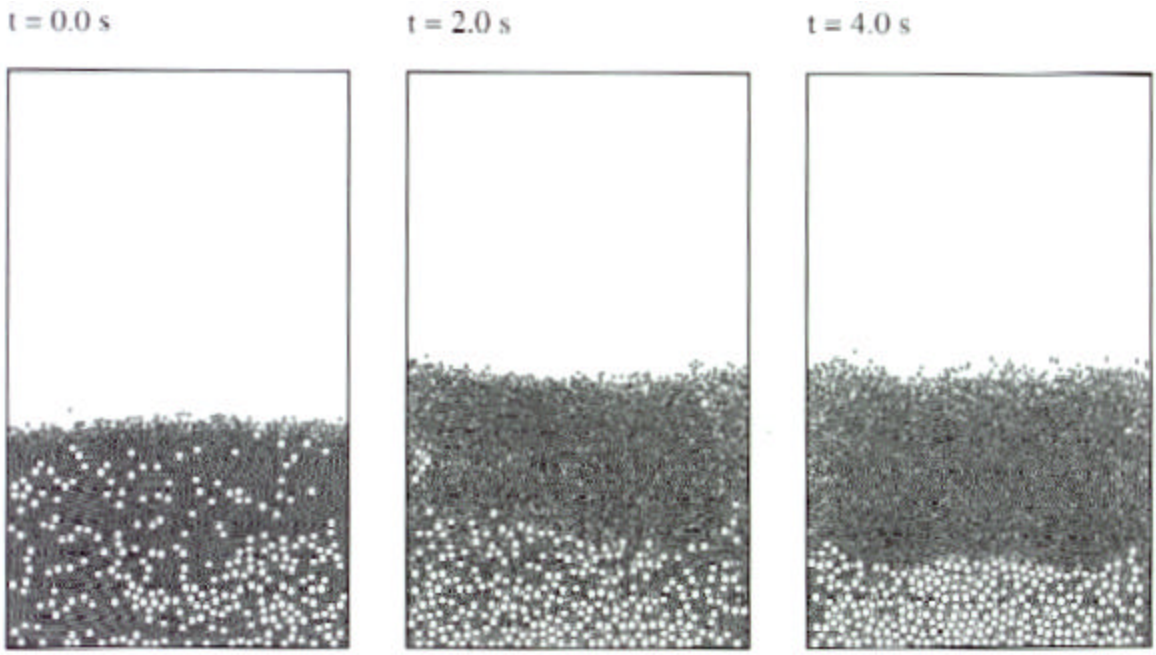

Figure 6.8. *Snapshots of particle configurations for the simulation with ideal collision parameters (e = 1.0, m = 0.0)*

The result is striking, a segregated state is reached after a few seconds and this situation does not change significantly anymore. Due to the absence of bubbles there is no mechanism present to transport the bigger particles to the upper regions of the bed, which stresses the crucial role of bubbles for solids mixing in fluidised beds. The simulation was

continued for 20 seconds and an average segregation profile over 2000 frames was obtained. This average segregation profile is presented in Figure 6.9.

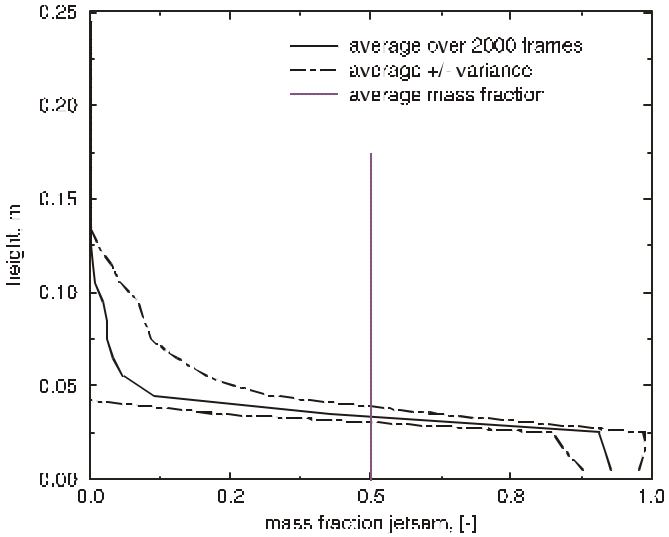

Figure 6.9. *Segregation profiles obtained from both single- and multiple frame analysis for the simulation with ideal collision* parameters (*e = 1.0, m = 0.0)*

In this figure it can be observed that the segregation is far more pronounced than in the base case simulation (Figure 6.6) with non-ideal collision parameters (e = 0.96, m = 0.15) and that the variance is a lot less as well.

5. Experimental validation

5.1 Experimental

For the purpose of experimental validation of the segregation simulations a set-up was designed and constructed that is schematically represented in Figure 6.10.

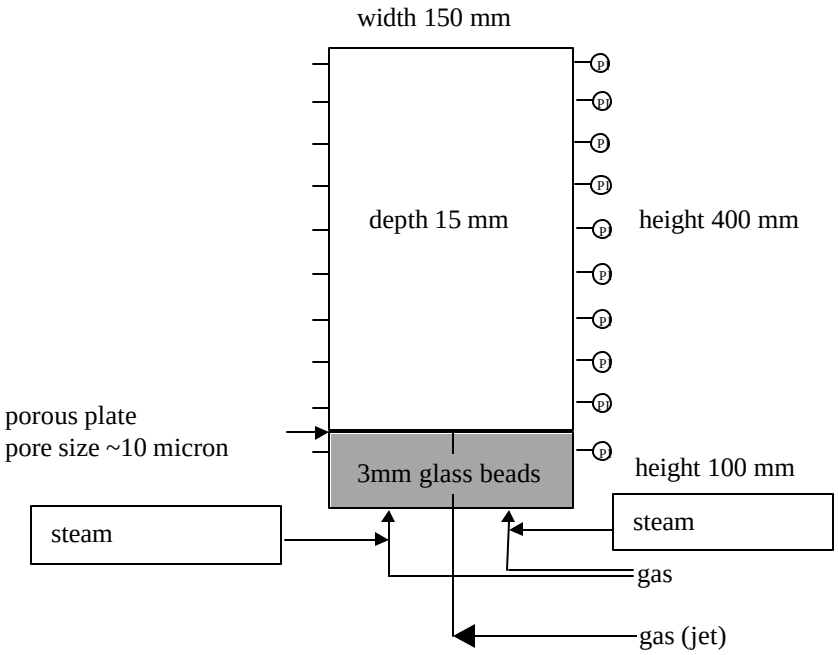

Figure 6.10. *Schematic representation of the experimental set-up*

In this quasi two-dimensional set-up the particles can be observed with a video camera during the fluidisation process since glass was used as the material for the construction of the bed. Coloured glass particles obtained from *Worf Glaskugeln GmbH* in Mainz, Germany were used that can easily be distinguished by visual observation. The biggest particles were coloured red and had a diameter of 2.5 mm, the smallest were coloured yellow and had a diameter of 1.5 mm. Since homogeneous gas inflow conditions were used during the segregation experiments the option to invoke a jet was not used. Instead, the gas velocity in the jet was set equal to the uniform inflow velocity. A 50/50 wt. particle mixture was used for the validation with an initial bed height of 0.15 m. The fluidising gas (air at ambient conditions) was humidified in order to minimise the influence of electrostatic forces. In preliminary measurements the minimum fluidisation velocities were determined separately for both types of particles. For the 1.5 mm diameter particles a minimum fluidisation velocity (u_{mf}) of 0.92 m/s was found whereas for the 2.5 mm diameter particles a u_{mf} of 1.28 m/s was found. For a 50/50 wt.% mixture the

segregation turned out to be most pronounced when the gas inflow velocity was chosen equal to 1.3 m/s.

5.2 Results

The parameter settings used for the simulations that were to be compared with the experiment are presented in table 6.3.

Table 6.3. *Parameter settings for the simulation duplicating the experiment*

Particles:		Bed:	
Shape	Spherical	Width	0.15 m.
density, r_p	2525 kg/m^3	Height	0.40 m
$D_{p,small}$ = 1.5 mm	N_p = 6481	number x-cells, *NX*	15
$D_{p,big}$ = 2.5 mm	N_p = 1400	number y-cells, *NY*	40
		cell width, *DX*	10 mm
k_n	1000 N/m	cell height, *DY*	10 mm
$N_{p,total}$	7881	time step, *DT*	10^{-4} s

The collision parameters for the particles used in the experiment were measured at the Open University at Milton Keynes using the facility of the Impact Research group that is described in Chapter 2. In the simulations presented in the previous paragraphs the collision parameters for particle-particle collisions were identical: no distinction was made between collisions of particles of different types. For the simulation presented here the code was extended to take the various collision parameters into account. The values of the collision parameters that were obtained from the measurements at the Open University are presented in table 6.4 (Gorham and Kharaz, 1999).

Table 6.4. *Collision parameters obtained by Gorham and Kharaz (1999)*

	big-big	*big-small*	*small-small*	*big-wall*	*small-wall*
e	0.97	0.97	0.97	0.97	0.97
m	0.11	0.10	0.15	0.09	0.10
b_0	0.33	0.33	0.33	0.33	0.33

At first a simulation was run with a homogeneous gas inflow velocity of 1.3 m/s using the hard-sphere code. However, after 60 seconds still no segregation could be observed which is not in agreement with the results of the experiment. At lower gas velocities segregation was observed but for these simulations the hard-sphere code could not be used due to stability problems. The hard-sphere approach is not able to handle static zones in the bed and at gas velocities below u_{mf} such static zones cannot be avoided. Therefore the soft-sphere code was used to perform a simulation with a homogeneous gas inflow velocity of 0.9 m/s. For this simulation the soft-sphere code was extended to take the various collision parameters into account. The normal spring stiffness was set equal to 1000 N/m for all sorts of contacts and a time step of 10^{-5} s was used for the integration of the contact forces.

Video images of the experiment and snapshots of the simulation are presented together in Figure 6.11. It can clearly be observed that the segregation is more pronounced and faster in the experiment than in the simulation. In the video images of the experiment bubbling appears to be far more pronounced than in the simulation. In the simulation with a gas inflow velocity of 1.3 m/s the bubbling was also much more pronounced but in that particular simulation segregation did not occur.

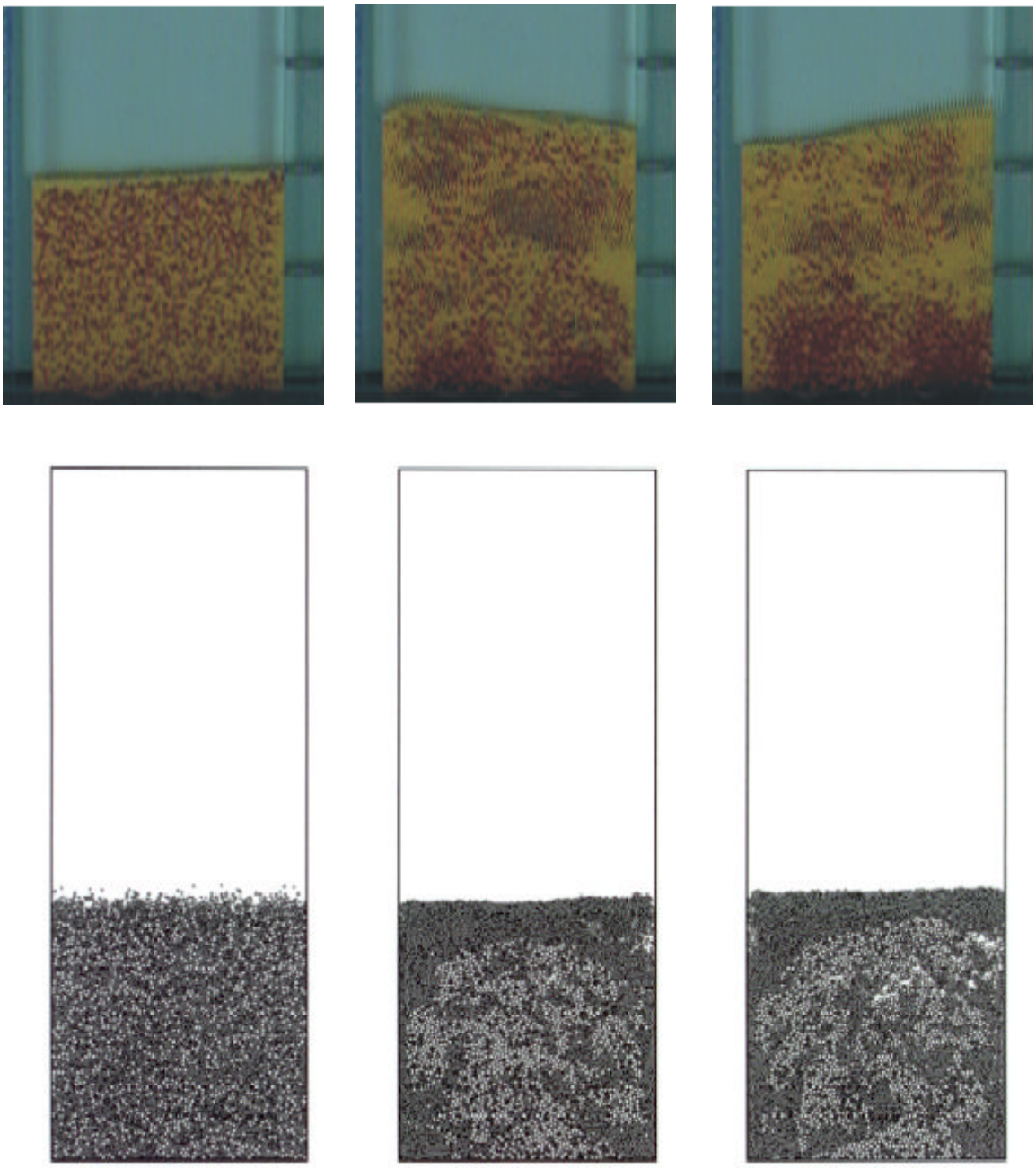

t = 0 s *t* = 20 s*t* = 40 s

Figure 6.11. *Snapshots of the simulation compared with video images of the experiment*

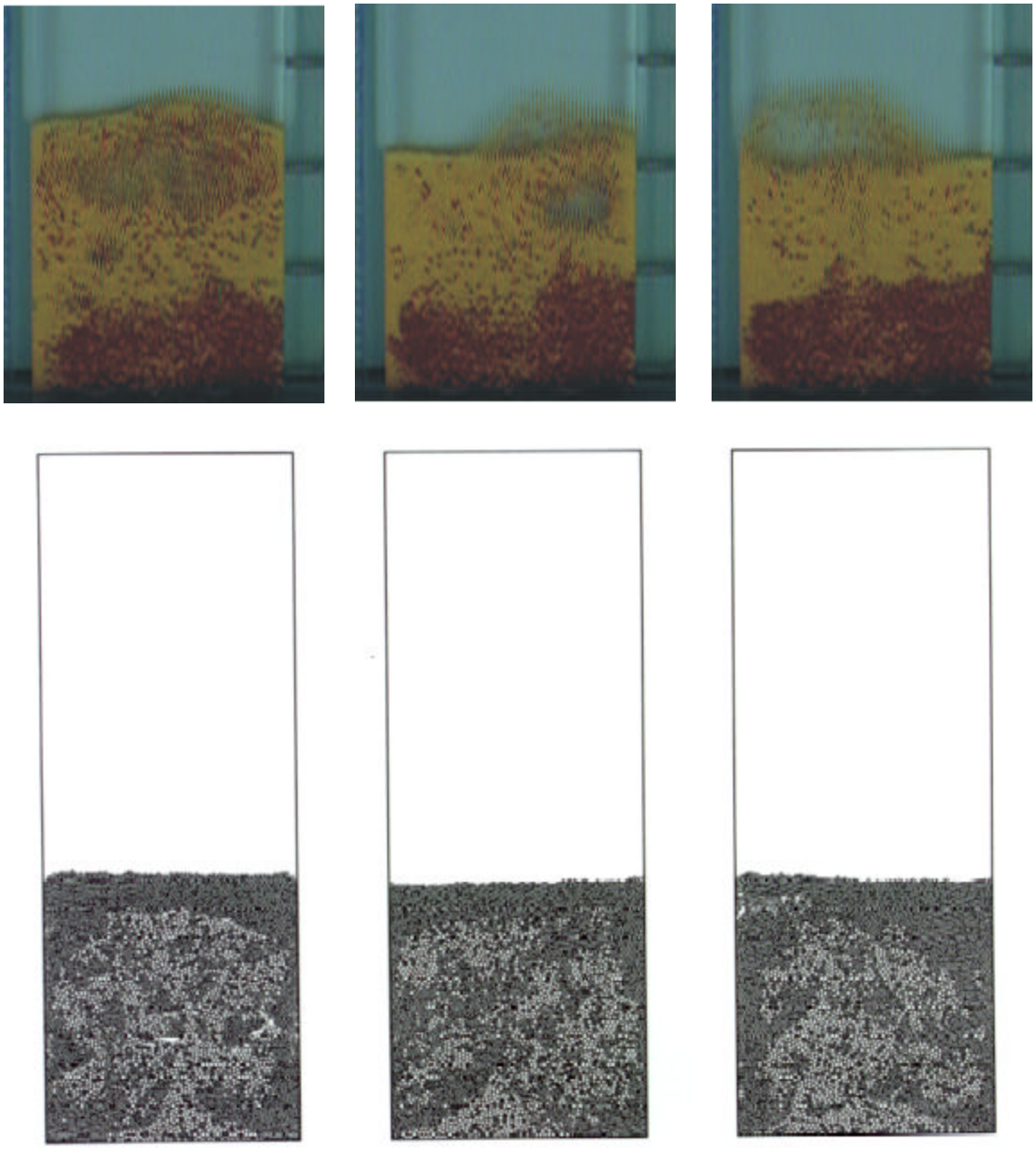

t = 60 s*t* = 80 s*t* = 100 s

Figure 6.11. *(continued) Snapshots of the simulation compared with video images of the experiment*

At t = 100 s the segregation was almost complete in the experiment whereas this was by far not the case in the simulation. Therefore the simulation was continued in order to check whether the segregation would become more complete. In Figure 6.12 snapshots of the simulation at t = 150 s and t = 200 s are presented.

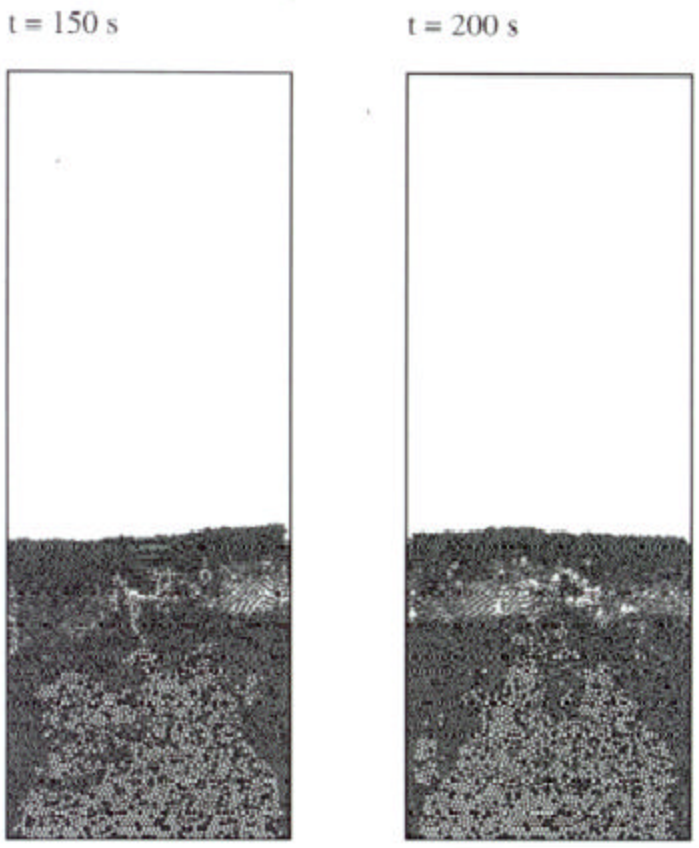

Figure 6.12. *Snapshots of the simulation at t = 150 s and t = 200 s*

Indeed the segregation is more pronounced than it was at t = 100 s but still not as complete as it was in the experiment. Also the bigger particles tend to accumulate in the centre of the bed whereas in the experiment there is a sharper horizontal division between the two particle layers. Since the simulation was very time consuming (280 minutes of CPU time per simulated second on a Silicon Graphics Origin200 server with a R10000 processor, 225 MHz, 2 Mb cache) the simulation was not repeated at different gas velocities.

Although the soft-sphere model is capable of predicting segregation for this system it is clear that the agreement with the experiment is rather poor. This is most likely due to the fact that the motion of the particles is restricted to two dimensions in the simulation. Also the particle sizes used in the experiment do not differ so much (1.5 vs. 2.5 mm). Segregation is expected to be more pronounced in the case of a larger size difference as was used in the simulation in the previous paragraph (1.5 vs. 4.0 mm). However the use of 4.0 mm diameter particles in a bed of 15 mm depth is questionable. On the other hand particles of 1.0 mm diameter could be used instead of 1.5 mm diameter but this would increase the number of particles in the simulation and hence the computational cost.

It is important to realise that in the present code the hydrodynamics of the gas phase is still resolved on a length scale that is larger than the particle size. This affects the two-way coupling between the particle dynamics and the gas phase hydrodynamics. In Figure 6.13 two computational cells are schematically represented with each a different particle configuration but identical void fraction.

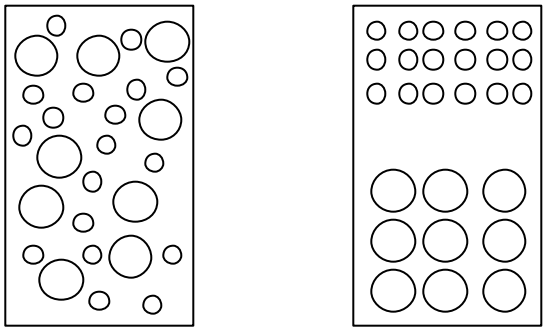

Figure 6.13. *Schematic representation of two computational cells with identical void fraction but different solids distribution*

In the present code these two configurations are treated in exactly the same manner as far as the two-way coupling is concerned, assuming that the particle velocities are identical in both cases. It is however to be expected that when the gas flow is solved on a length scale

smaller than the particle size these two configurations will show different results in terms of two-way coupling. In Chapter 3 some techniques are discussed that are capable of solving the gas phase hydrodynamics on this sub-particle scale. Using for instance the Lattice Boltzmann technique the effects of the sub-grid particle configuration on the flow behaviour can be studied on a length scale smaller than the particle size. Such microscopic simulations can subsequently be used to improve the two-way coupling in the Eulerian-Lagrangian simulations by for instance an improved correlation for the drag force acting on a particle. This can eventually lead to improved agreement between simulation and experiment for the case presented in this section.

6. Conclusions

Gas-fluidised beds consisting of particles of different size and density were simulated using a hard-sphere discrete particle model. Segregation was observed in the case of a binary system of particles of different size as well as in the case of a ternary system consisting of particles of different density. In the latter case the segregation effect was more pronounced which is in agreement with experimental findings reported in the literature. Using realistic values for the collision parameters (e = 0.96, μ = 0.15) segregation was observed on a time scale of several seconds although the system never reached a clear steady state. The bigger (jetsam) particles were continuously transported to the upper regions of the bed by the bubbles and then moved down again in the denser regions. An average segregation profile was determined using 5000 frames (every 0.01 second for a total duration of 50 seconds). The results showed a rather large variance. An analysis based on a single frame was found to lead to an incomplete understanding of the segregated state. When the collisions were assumed to be perfectly elastic and perfectly smooth (e = 1.0, m = 0.0) a completely different behaviour was observed. Due to the absence of bubbles segregation became almost complete after only a few seconds and this situation did not change significantly anymore during the remainder of the simulation. This stresses the important role of bubbles in the mixing of solids in fluidised beds.

Finally an experimental set-up was designed and constructed for the purpose of experimental validation. At a gas inflow velocity of 1.3 m/s segregation was observed in the experiments over a time scale of less than a minute but in the simulations no segregation could be observed over the same time scale. At a lower gas inflow velocity (0.9 m/s) segregation was observed in the simulations. For these simulations the soft-sphere code had to be used due to the presence of static zones. However the time scale over which the segregation occurred and the final segregation pattern were in poor agreement with the experimental results. This is most likely due to the fact that the motion of the particles in the simulation is restricted to two dimensions in contrast with the experiment. Furthermore the difference in the particle sizes used for the validation is rather small (1.5 mm vs. 2.5 mm diameter) which renders a tough test for the model.

Notation

C_d	drag coefficient, [-]
D_{nblist}	width of neighbour list square, m
D_p	particle diameter, m
DT	time step, s
DX	horizontal computational cell dimension, m
DY	vertical computational cell dimension, m
e	coefficient of restitution, [-]
$\mathbf{F}$	force, N
$\mathbf{g}$	gravitational acceleration, m/s^2
I	moment of inertia, kgm^2
k	spring stiffness, N/m
m	particle mass, kg
N_p	Number of particles, [-]
NX	number of computational cells in x-direction, [-]
NY	number of computational cells in y-direction, [-]

n	normal unit vector, [-]
p	pressure, Pa
R_p	particle radius, m
r	position vector, m
$\mathbf{S}_p$	momentum source term, N/m^3
T	torque, Nm
T	temperature, K
t	tangential unit vector, [-]
t	time, s
u	gas velocity vector, m/s
v	particle velocity vector, m/s
V_p	particle volume, m^3

Greek symbols

b	defined in Eqs () and (), kg/m^3s
b_0	coefficient of tangential restitution, [-]
e	void fraction, [-]
m	coefficient of friction, [-]
m_g	gas viscosity, kg/ms
h	damping coefficient, Ns/m
t	gas-phase stress tensor, kg/ms^2
r	density, kg/m^3
w	angular velocity, s^{-1}
x	displacement, m

Subscripts

g	gas phase
mf	minimum fluidisation
n	*normal*

nblist	neighbour list
p	particle
t	tangential
w	wall

References

Anderson, T.B. and Jackson, R., (1967). A fluid mechanical description of fluidized beds (equations of motion), *Ind. Eng. Chem., Fundam.*, **6**, 527.

Cundall, P.A. and Strack, O.D.L., (1979). A discrete numerical model for granular assemblies. *Géotechnique*, **29**, 47.

Foerster S.F., Louge, M.Y., Chang, H. and Allia, K. (1994). Measurements of the collision properties of small spheres. *Phys. Fluids,*, **6**, 1108.

Gidaspow, D., Ding, J. and Jayaswal, U.K. (1990). Multiphase Navier-Stokes equation solver. Numerical Methods for Multiphase Flows, *FED* **91**, 47.

Gidaspow, D. (1994). *Multiphase Flow and Fluidization*, Academic Press, Boston, USA.

Gorham, D.A. and Kharaz, A.H., (1999). Results of particle impact tests, Impact Research Group Report IRG 13, The Open University, Milton Keynes, UK.

Hoffmann, A.C., Janssen, L.P.B.M. and Prins, J. (1993). Particle segregation in fluidised binary mixtures, *Chem. Engng Sci*., **48**, 1583.

Hoomans, B.P.B., Kuipers, J.A.M., Briels, W.J. and van Swaaij, W.P.M., (1996). Discrete particle simulation of bubble and slug formation in a two-dimensional gas-fluidised bed: a hard-sphere approach, *Chem. Engng Sci*., **51**, 99.

Kawaguchi, T., Tanaka, T. and Tsuji, Y., (1998). Numerical simulation of two-dimensional fluidized beds using the discrete element method (comparison between the two- and three-dimensional models), *Powder Technol*., **96**, 129.

Kuipers, J.A.M., van Duin, K.J. van Beckum F.P.H. and van Swaaij, W.P.M. (1992). A numerical model of gas-fluidized beds, *Chem. Engng Sci*., **47,** 1913.

Kumaran, V. and Koch, D.L. (1993). Properties of a bidisperse particle-gas suspension Part 1. Collision time small compared with viscous relaxation time, *J. Fluid Mech*., **247**, 623.

Manger, E. (1996). Modelling and simulation of gas/solids flow in curvilinear coordinates, *Ph.D. Thesis*, Telemark Institute of Technology, Porsgrunn, Norway.

Mathiesen, V., Solberg T. and Hjertager, B.H., (1998). A computational study of multiphase flow behavior in a circulating fluidized bed with realistic particle size distribution, *Proc. 3rd Int. Conf. On Multiphase Flow*, 8-12 June 1998, Lyon, France

Mikami, T., Kamiya, H. and Horio, M., (1998). Numerical simulation of cohesive powder behavior in a fluidized bed, *Chem. Engng Sci*., **53**, 1927.

Nienow, A.W. and Naimer, N.S. (1980). Continuous mixing of two particulate species of different density in a gas fluidised bed, *Trans IChemE*., **58**, 181.

Nienow, A.W., Naimer, N.S. and Chiba, T. (1987). Studies of segregation/mixing in fluidised beds of different size particles, *Chem. Eng. Comm*., **62**, 52.

Richardson, J.F. and Zaki, W.N., (1954). Sedimentation and fluidization: part I. *Trans. Inst. Chem. Eng*., **32**, 35.

Rowe, P.N., Nienow, A.W. and Agbim, A.J. (1972). The mechanism by which particles segregate in gas fluidised beds: binary systems of near-spherical particles, *Trans. Instn Chem. Engrs*, **50**, 310.

Schwarzer, S., (1995). Sedimentation and flow through porous media: Simulating dynamically coupled discrete and continuum phase, *Phys. Rev. E.* **52**, 6461.

Seibert, K.D. and Burns, M.A. (1998). Simulation of structural phenomena in mixed-particle fluidized beds, *AIChE J.* **44**, 528.

Tsuji, Y., Kawaguchi, T. and Tanaka, T., (1993). Discrete particle simulation of two dimensional fluidized bed, *Powder Technol.* **77**, 79.

Wang, Y. and Mason, M.T., (1992). Two-dimensional rigid-body collisions with friction. *J. Appl. Mech.*, **59**, 635.

Wen, C.Y. and Yu, Y.H., (1966). Mechanics of fluidization. *Chem. Eng. Prog. Symp. Ser.*, **62** (62), 100.

Wu, S.Y. and Baeyens, J. (1998). Segregation by size difference in gas fluidized beds, *Powder Technol.* **98**, 139.

Xu, B.H. and Yu, A.B., (1997). Numerical simulation of the gas-solid flow in a fluidized bed by combining discrete particle method with computational fluid dynamics. *Chem. Engng Sci*. **52**, 2785.

Chapter 7.

THE INFLUENCE OF COLLISION PROPERTIES ON THE FLOW STRUCTURE IN A RISER

Abstract:

A two-dimensional hard-sphere discrete particle model was used in order to simulate the gas-solid flow in the riser section of a circulating fluidised bed (CFB). The Newtonian equations of motion are solved for each individual particle in the system while taking into account the particle-particle and particle-wall collisions. The gas phase hydrodynamics is described by the spatially averaged Navier-Stokes equations for two-phase flow. The results proved to be very sensitive with respect to the collision parameters (i.e. coefficient of restitution (e) and coefficient of friction (m)). In the case of fully elastic and perfectly smooth collisions (e = 1.0, m = 0.0) hardly any clustering of particles could be observed as opposed to the case where these collision parameters were assigned realistic values (e = 0.94, m = 0.28). Particle-wall collisions turned out to have very little influence on the flow structure. A strong effect of the collision properties on the axial solids profile was found where a pronounced build-up of solids was observed in the simulation with realistic values for the collision parameters. In the simulation assuming fully elastic and perfectly smooth collisions no build-up of solids was observed. This result is supported by the experimental findings of Chang and Louge (1992) where a smaller pressure drop over the riser was found when glass particles were used to which a coating was applied in order to decrease the coefficient of friction. Lift forces acting on the suspended particles turned out to have a slightly redispersive effect on the flow structure which made the radial segregation of the solids a little less pronounced.

Parts of this chapter are based on the papers:

B.P.B. Hoomans, J.A.M. Kuipers and W.P.M. van Swaaij, (1998). Granular dynamics simulation of cluster formation in dense riser flow, *Third International Conference on Multiphase Flows 1998*, June 8-12, Lyon, France.

B.P.B. Hoomans, J.A.M. Kuipers and W.P.M. van Swaaij, (1999). Discrete particle simulation of cluster formation in dense riser flow, *Circulating Fluidized Bed Technology VI*, J. Werther (Ed.), p. 266.

1. Introduction

Cluster formation is a characteristic feature of dense gas solid flow in the riser section of a Circulating Fluidized Bed (CFB). Although a clear definition is lacking (Chen, 1995) clusters can be typified as regions of locally higher solid fraction. Since the existence of such clusters has a profound influence on the performance of a CFB unit as a chemical reactor they have been the subject of a number of studies. Kuipers *et al*. (1998) demonstrated that the radial solids segregation in a riser (*i.e*. core-annulus flow) has a negative effect on the performance of the riser as a chemical reactor. Radial solids segregation in a riser is largely due to the existence of clusters that tend to accumulate near the wall. Horio and Kuroki (1994) experimentally observed clusters in dilute riser flow using a laser sheet technique. They found that the clusters had a characteristic parabolic shape.

Tsuo and Gidaspow (1990) used a Two-Fluid approach with constant solids viscosity in order to simulate the riser section of a CFB. They reported the formation of cluster-like structures even though the spatial resolution in their simulation was rather low (computational cells of 7.62 mm width and 76.2 mm height) compared to typical cluster sizes. After time averaging the typical core-annulus flow structure where the average solids concentration is considerably higher near the wall was obtained. Other Two-Fluid approaches incorporating the kinetic theory of granular flow (Sinclair and Jackson (1989), Nieuwland *et al.* (1996)) did not focus particularly on cluster formation but more on the radial segregation of solids. This type of model possesses a peculiar dependency on the magnitude of the coefficient of restitution where a small deviation from unity causes the flow structure to change completely while the agreement with experimental findings deteriorates. This was (among others) pointed out by Hrenya and Sinclair (1997) who also reported that when particle phase turbulence was included in the model the aforementioned dependency became far less pronounced.

Tanaka *et al.* (1996) performed simulations of gas-solid flow in a vertical duct using the Lagrangian approach for the solid particles. They employed the Direct Simulation Monte Carlo (DSMC) method to describe the particle dynamics. In a later paper Tsuji *et al.* (1998) made a comparison between the work of Tsuo and Gidaspow (1990) and Tanaka *et al*. (1996). In the DSMC method the simulated particles actually represent a certain number of 'real' particles. A random number generator is invoked to determine the collision partners and the geometry of the collision. Hence this method does not account for actual particle-particle and particle-wall interaction in a direct way. Moreover the modified Nanbu method used in their work does not guarantee exact conservation of energy (Frezzotti, 1997). This can be an important drawback especially since the collision parameters, that determine how much energy is dissipated in collisions, turned out to be of key importance in their simulations. Recently Helland *et al.* (1999) and Ouyang and Li (1999) presented discrete particle approaches similar to the one used in this work but in their simulations collisions are detected at constant time intervals allowing the particles to slightly overlap. In this chapter a Eulerian-Lagrangian simulation technique for dense gas-solid two-phase flow in a riser is presented which features direct incorporation of the particle-particle and particle-wall interaction.

2. Model

Since a detailed description of the model is presented in Chapter 2 and Chapter 3, the key features will be summarised briefly here.

2.1 Granular dynamics

The collision model as originally developed by Wang and Mason (1992) is used to describe a binary, instantaneous, inelastic collision with friction. The key parameters of the model are the coefficient of restitution ($0 \leq e \leq 1$) and the coefficient of friction ($m \geq 0$). Foerster *et al.* (1994) have shown that also the coefficient of tangential restitution ($0 \leq b_0 \leq 1$) should be used in order to describe the collision dynamics more accurately. These

three collision parameters are all included in the model. In all simulations presented in this chapter, the coefficient of tangential restitution is assumed to be equal to zero.

In the hard-sphere approach a sequence of binary collisions is processed. This implies that a collision list is compiled in which for each particle a collision partner and a corresponding collision time is stored. A constant time step is used to take the external forces into account and *within* this time step the prevailing collisions are processed sequentially. In order to reduce the required CPU time neighbour lists are used. For each particle a list of neighbouring particles is stored and only for the particles in this list a check for possible collisions is performed. Since in riser flow the velocity differences between the particles is larger than in bubbling fluidised beds the neighbour list is chosen rather large ($D_{nblist} = 8\ D_p$) to ensure that all collisions are properly detected.

2.2 External forces

The equation of motion used for the simulations of riser flow is:

$$m_p \frac{d\mathbf{v}_p}{dt} = m_p \mathbf{g} + \mathbf{F}_{drag} + \mathbf{F}_{LG} + \mathbf{F}_{LM} \tag{7.1}$$

where m_p represents the mass of a particle and $\mathbf{v}_p$ its velocity. In equation 7.1 the first term on the right hand side is due to gravity and the second term is due to drag:

$$\mathbf{F}_{drag} = \frac{1}{8} p D_p^2 C_d r_g \left|\mathbf{u} - \mathbf{v}_p\right| \left(\mathbf{u} - \mathbf{v}_p\right) e^{-2.7} \tag{7.2}$$

In equation 7.2 r_g represents the density of the gas phase and **u** represents its velocity. It should be noted that the drag correction due to the presence of other particles has been accounted for via the well-known Richardson and Zaki (1954) correction factor. The drag coefficient for an isolated particle depends on the particle Reynolds number as given by Rowe and Henwood (1961):

$$C_d = \begin{cases} \dfrac{24}{\mathrm{Re}_p}\left(1+0.15\left(\mathrm{Re}_p\right)^{0.687}\right) & \mathrm{Re_p} < 1000 \\ 0.44 & \mathrm{Re_p} \geq 1000 \end{cases} \tag{7.3}$$

where the particle Reynolds number is defined as:

$$\mathrm{Re}_p = \frac{e\, r_g \left|\mathbf{u}-\mathbf{v}_p\right| D_p}{m_g} \ . \tag{7.4}$$

Gravity and drag force are implemented by default in all simulations shown in this work. The lift forces are not used by default but since an additional simulation was performed in order to test their influence the lift forces will be discussed in more detail here.

The second term on the right hand side of equation 7.1 is the lift force due to a velocity gradient. Following the lines of Tanaka *et al.* (1996) only the gradient in the x-direction is considered:

$$F_{LG,x} = \frac{1}{8} p D_p^2 C_{LG}\, r_g \left|\mathbf{u}-\mathbf{v}_p\right|^2 sign(c) \tag{7.5}$$

where χ denotes the velocity gradient $\partial(u_y\text{-}v_{p,y})/\partial x$.

The empirical relations used for the lift coefficient C_{LG} are summarised in table 7.1.

The third term on the right hand side in equation 7.1 is the lift force due to particle rotation, also known as the Magnus lift force:

$$\mathbf{F}_{LM} = \frac{1}{8} p D_p^2 C_{LM}\, r_g \left|\mathbf{u}-\mathbf{v}_p\right| \frac{\left(\mathbf{u}-\mathbf{v}_p\right)\times w_r}{\left|w_r\right|} \ . \tag{7.6}$$

where w_r is defined as follows:

$$w_r = w - \frac{1}{2}\nabla \times \mathbf{u} \tag{7.7}$$

The empirical relations used for the lift coefficient C_{LM} can be found in table 7.1.

Table 7.1. *Empirical relations for the lift coefficients*

$\frac{C_{LG}}{C_{LG,Sa}} = \left(1 - 0.3314 x^{1/2}\right)\exp\left(-\frac{\mathrm{Re}_p}{10}\right) + 0.3314 x^{1/2}$ $\mathrm{Re}_p \le 40$ (Mei, 1992)
$\frac{C_{LG}}{C_{LG,Sa}} = 0.0741\,\mathrm{Re}_c^{1/2}$ $\mathrm{Re}_p > 40$
with: $C_{LG,Sa} = 8.225\frac{\mathrm{Re}_c^{1/2}}{\mathrm{Re}}$ (Saffman, 1965), $x = \frac{D_p\lvert c\rvert}{2\lvert\mathbf{u}-\mathbf{v}_p\rvert}$ and $\mathrm{Re}_c = \frac{r_g\lvert c\rvert D_p^2}{4m_g}$
$C_{LM} = 2g$ $\mathrm{Re_p} < 10$ with: $g = \frac{D_p\lvert w_r\rvert}{2\lvert\mathbf{u}-\mathbf{v}_p\rvert}$
$C_{LM} = 3.8g\,\mathrm{Re}_p^{-1/2}$ $10 < \mathrm{Re_p} < 500$ (Oesterlé, 1994)
$C_{LM} = 0.40g$ $500 < \mathrm{Re_p}$ (Tsuji *et al.*, 1985)
$C_m = \frac{1}{p}\left(a\,\mathrm{Re}_w^{-1/2} + b\,\mathrm{Re}_w^{-1}\right)$ with: $\mathrm{Re}_w = \frac{r_g\lvert w_r\rvert D_p^2}{4m_g}$
a = 5.32; b = 37.2 $10 < \mathrm{Re}_\omega \le 20$
a = 6.44; b = 32.2 $20 < \mathrm{Re}_\omega \le 50$ (Dennis *et al.* 1980)
a = 6.45; b = 32.1 $\mathrm{Re}_\omega \ge 50$

The rotational velocity of particles is not only affected by collisions with the system walls or with other particles, but also by the torque exerted on them by the fluid:

$$I\frac{dw}{dt} = -\frac{1}{64}pD_p^5 C_m \rho_g |w_r| w_r \quad . \tag{7.8}$$

The empirical relations used for the rotational drag coefficient C_m are summarised in table 7.1.

For the integration of equation 7.1 as well as equation 7.8 a simple explicit first order scheme was used to update the velocities and positions of the particles.

2.3 Inlet and outlet conditions

In the riser section of a CFB there is a continuous transport of particles throughout the system that has to be taken into account in the simulation. Instead of simulating the entire riser section, including inlet and exit configurations, only the middle section was simulated. At the inlet of the simulated system particles were placed at random in the bottom row of cells ensuring that there is no overlap with other particles or walls. An initial axial velocity of 0.4 m/s was assigned to each particle fed to the system. At each time step a specific number of particles was fed to the riser duct in accordance with a specified solids mass flux (G_s). The cross sectional area in this (two-dimensional) case was assumed to be equal to the width of the system times the particle diameter. At the outlet particles which had crossed the upper boundary were simply removed from the system at each time step. The particles were only allowed to leave the system at the upper boundary.

2.4 Gas phase hydrodynamics

The calculation of the gas phase hydrodynamics mainly follows the lines presented by Kuipers *et al.* (1992). It is based on the numerical solution of the following set of partial differential equations that can be seen as a generalised form of the Navier-Stokes equations for a gas interacting with a solid phase as originally derived by Anderson and Jackson (1967).

Continuity equation gas phase:

$$\frac{\partial\left(\varepsilon_g \rho_g\right)}{\partial t} + \left(\nabla \cdot \varepsilon_g \rho_g \mathbf{u}\right) = 0 \ . \tag{7.9}$$

Momentum equation gas phase:

$$\frac{\partial\left(\varepsilon_g \rho_g \mathbf{u}\right)}{\partial t} + \left(\nabla \cdot \varepsilon_g \rho_g \mathbf{u}\mathbf{u}\right) = -\varepsilon \nabla p - \mathbf{S}_p - \left(\nabla \cdot \tau_g\right) + \varepsilon_g \rho_g \mathbf{g} \ . \tag{7.10}$$

In this work transient, two-dimensional, isothermal (T = 293 K) flow of air at slightly elevated pressure (p = 1.2 Bar) is considered. The constitutive equations and the boundary conditions used can be found in Chapter 3. Note that no turbulence modelling is included in the present description. The reasons for this can be summarised as follows. Firstly the main goal of this work is to study the influence of particle properties on the flow structure. Secondly the particles used in the simulations in this chapter are rather coarse (500 μm) and are therefore not much influenced by turbulent eddies as for instance is the case for FCC particles (70 μm). And last but not least there is no generally accepted and experimentally validated turbulence model for the type of two-phase flow that is the subject of study here. Helland *et al*. (1999) did include an additional term in the momentum equation of the gas phase in order to account for sub-grid scale effects of turbulent eddies. However this term was taken directly from a single-phase flow model without any modification for the presence of the particles. It cannot be denied that the assumption of laminar flow is questionable for the type of flow encountered in the simulations in this chapter but there is no doubt that the application of a single-phase flow turbulence model in this situation is questionable as well. The void fraction (ε) is calculated from the particle positions in the bed. There is one important modification with respect to the model of Hoomans *et al.* (1996) and that deals with the way in which the

two-way coupling between the gas-phase and the particle motion is established. In the present model the reaction forces to the forces exerted on a particle by the gas-phase per unit of volume is fed back through the source term $\mathbf{S}_p$ which has the dimension Nm^{-3}.

3. Results

As a first test case for the model the same system was chosen as was used by Tsuo and Gidaspow (1990) and Tanaka *et al*. (1996) in their simulations. The general parameter settings are summarised in Table 7.2. In all simulations a time step of 10^{-4} s was used together with a computational grid of 20 (NX) by 100 (NY) cells.

Table 7.2. *General parameter settings*

	particles	system		gas	
diameter, D_p	500 μm	width	0.08 m	temperature, T	293 K
density, r	2620 kg/m^3	height	2.00 m	pressure, p	1.2 Bar
solids mass flux, G_s	25 kg/m^{2}s			velocity, u_g	5.0 m/s

3.1 Effect of collision parameters

At first the influence of the collision parameters was examined. Tanaka *et al*. (1996) reported a strong dependency of the flow structure with respect to the coefficients of restitution (e) and friction (m). In the work of Hoomans *et al*. (1996) on bubbling and slugging fluidised beds these parameters also turned out to have a decisive influence on the flow behaviour. Therefore three different simulations were performed where the collision parameters were set according to the values presented in Table 7.3.

Table 7.3. *Settings for the collision parameters*

	e	m	e_w	m_w
Ideal	1.0	0.0	1.0	0.0
non-ideal	0.94	0.28	0.94	0.28
Ideal particles/ non-ideal walls	1.0	0.0	0.94	0.28

At first it was checked if each simulation had reached a steady state where the outlet solids mass flux was equal to the specified solids mass flux of 25 kg/m^{2}s. For the simulation with ideal collision parameters this steady state was reached within 10 s but for the simulation with non-ideal collision parameters it took more than 30 s before the outlet solids mass flux was equal to inlet solids mass flux. Once the steady state was reached the simulations were run for 10 s in order to obtain statistically reliable time averages. In Figure 7.1 the outlet solids mass flux is presented as a function of time for the simulation with the non-ideal collision parameters.

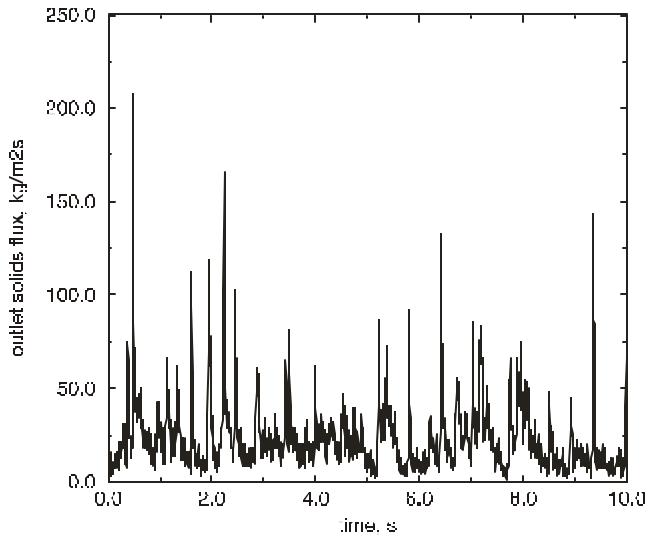

Figure 7.1. *Outlet solids flux as a function of time for the simulation with non-ideal collision parameters (e = 0.94, m = 0.28).*

Note that t = 0 s in this figure corresponds to the initial condition for the actual simulation of the system at steady state conditions. The solids flux during the time required to reach this steady state is not shown here. In Figure 7.1 it can be observed that the outlet solids mass flux has a very peaky nature but the time average value is equal to the specified mass flux (G_s = 25 kg/m^{2}s). It should be noted that in the simulations presented by Tsuo and Gidaspow (1990) and Tsuji *et al.* (1998) the time averaged outlet solids mass flux was by far not equal to 25 kg/m^{2}s and therefore their results do not apply to fully developed riser flow.Two snapshots of simulations with ideal (e = 1.0, m = 0.0) and non-ideal (e = 0.94 and m = 0.28) collision parameters are shown in Figure 7.2. These are snapshots of the middle section of the riser (1.0 to 1.2 m height).

In Figure 7.2 a typical cluster can clearly be observed in the case of non-ideal collision parameters. The snapshot of the simulation with the ideal collision parameters shows a much more homogeneous distribution of the particles.

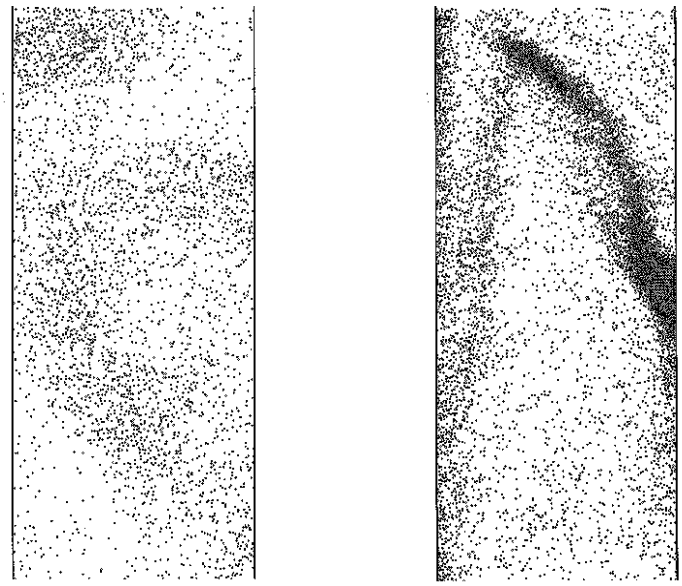

Figure 7.2. *Snapshots of a small section of the simulated riser (width = 0.08 m). Left: ideal collision parameters, e = 1.0, m = 0.0, Right: non-ideal collision parameters: e = 0.94, m = 0.28.*

From animations of the simulations it could be observed that in the simulation with the non-ideal collision parameters the clusters moved downward preferably along the walls and had a streaky, semi-parabolic shape. These clusters are rather dynamic in nature: they continuously form, grow and break up. Typical downward velocities for these clusters are in the order of magnitude of 1.0 m/s which is in agreement with the experimental findings of Tsuo and Gidaspow (1990). In the case of ideal collision parameters the flow was much more homogeneous and although locally slightly denser regions can be distinguished, these can hardly be identified as clusters. Similar results were obtained in a simulation with ideal collision parameters for particle-particle collisions but non-ideal parameters for particle-wall collisions.In Figure 7.3 the time averaged (10 s) radial solids profile at 1.0 m height is presented. For the case with non-ideal collision parameters the typical *core-annulus* flow structure can be observed where the solids fraction is relatively high near the wall and relatively low in the centre of the riser duct. In the other two cases the radial profile is flat. This result is a strong indication that the presence of clusters, which is clearly observed in the non-ideal case, causes the typical core-annulus structure since no cluster formation, and hence no core-annulus structure, could be observed in the other two cases where no energy was dissipated in particle-particle collisions.

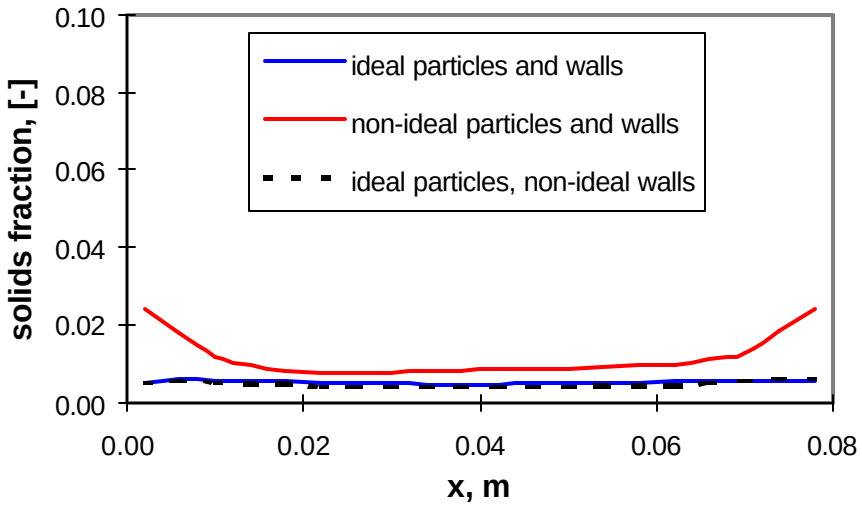

Figure 7.3. *Radial profile of the time averaged solids volume fraction at 1.0 m above the inlet of the simulated riser.*

It is also remarkable that the average solids hold-up is higher in the simulation with the non-ideal collision parameters than in the simulations with ideal particle-particle collisions. This suggests that there is an effect of the collision parameters on the axial solids profile in the riser.

3.2 Axial effects

The reason why it took the simulation with the non-ideal collision parameters much longer to reach a steady state turned out to be the build up of a solids profile in the riser. By the time the steady state was reached a total number of about 60,000 particles was found inside the system whereas in the simulations with ideal particle-particle collisions this number was about 25,000. This had also a pronounced effect on the CPU time. The simulation with non-ideal collision parameters required over 27 hours of CPU time per simulated second on a Silicon Graphics Origin200 server with a R10000 processor (180 MHz, 1 Mb cache).

Figure 7.4. *Snapshots of the bottom section of the simulated riser (width = 0.08 m) from 0.0 to 0.2 m. Left: ideal collision parameters, e =1.0, μ = 0.0, Right: non-ideal collision parameters: e = 0.94, μ = 0.28.*

The simulations with ideal particle-particle collisions required 2.5 hrs of CPU time per simulated second on the same machine. The reason for this huge difference is the total number of collisions that had to be processed in the simulations: 1 million collisions per second for the simulation with ideal collision parameters, 65 million collisions per second for the simulation with non-ideal collision parameters.Since clusters of particles move downward in the riser and the particles cannot leave the system at the bottom it can be understood that an axial solids profile will eventually be established. In Figure 7.4 a snapshot of the bottom section of the riser is presented for the simulations with ideal and non-ideal collision parameters. In this figure the same difference between ideal and non-ideal collision parameters can be observed as in Figure 7.2 but in the bottom section the difference is even more pronounced. Large strands of particles move down alongside the walls and then break up again after impinging on the bottom wall. In Figure 7.5 the time averaged (10 s) radial solids profile at 0.2 m above the bottom is presented for the three different cases.

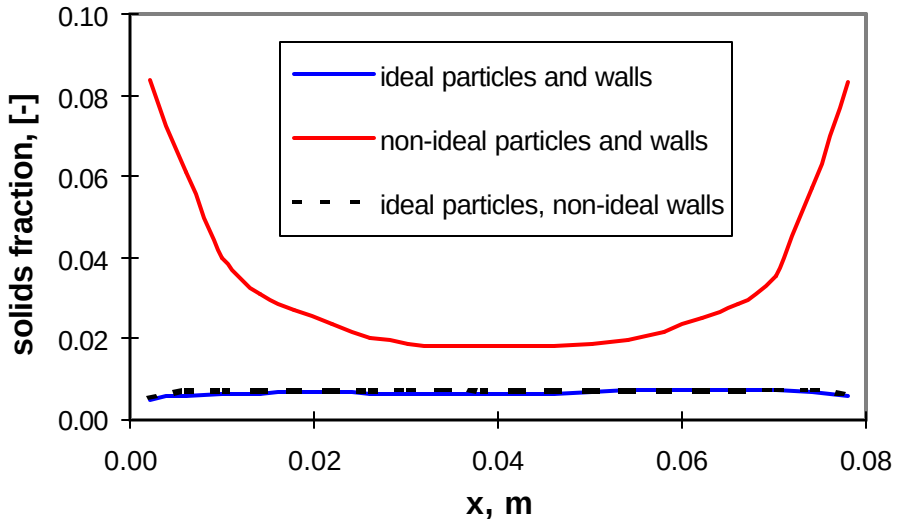

Figure 7.5. *Radial profile of the time averaged solids volume fraction at 0.2 m above the inlet of the simulated riser.*

Similar to the radial solids profiles presented in Figure 7.3 the core-annulus flow structure can be observed in the simulation with non-ideal collision parameters but not in the simulations with ideal particle-particle collisions. Again, hardly any difference could be observed between the simulation with both ideal particle-particle and particle-wall collisions and the simulation with ideal particle-particle but non-ideal particle-wall collisions indicating that particle-particle collisions dominate the flow behaviour. It is also clear that the average solids hold-up for the simulation with the non-ideal collisions at 0.2 m in the riser is higher than at 1.0 m (Figure 7.3). This suggests the existence of a non-uniform axial solids profile.

In Figure 7.6 the time averaged (10 s) axial distribution of the solids volume fraction in the riser are presented for the two cases mentioned above. For the non-ideal case clearly a build up of solids in the riser can be observed which is in agreement with the different total number of particles in the simulations reported earlier (app. 60,000 vs. 25,000). In this figure the results of the simulation with ideal particle-particle but non-ideal particle-wall collisions are not included for clarity reasons. However, these results are very similar to the results of the simulation with ideal collision parameters.

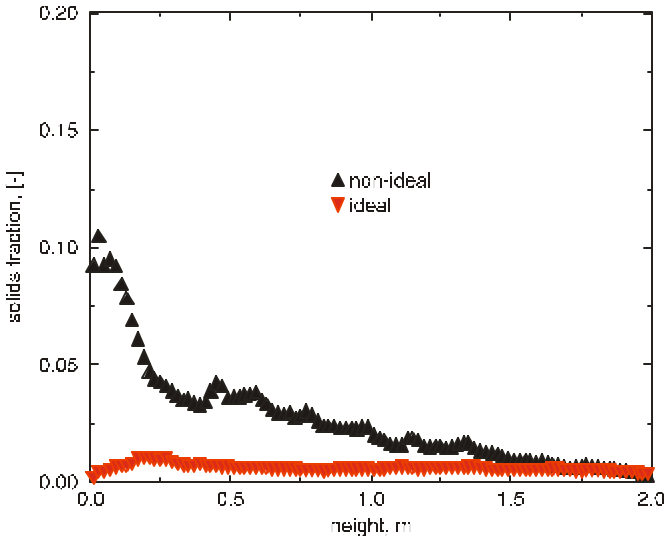

Figure 7.6. *Axial profile of the time-averaged solids volume fraction (non-deal: e = 0.94, m = 0.28, ideal: e = 1.0, m = 0.0)*

In Figure 7.6 it can clearly be observed that a build up of solids exists in the case of the simulation with non-ideal particle collisions whereas in the case of ideal collisions the axial solids distribution is nearly uniform. Chang and Louge (1992) reported results from experiments using a somewhat different system but operated at a rather similar mass loading and Froude number. They found a significant change in axial pressure profile in the riser when they applied a coating to glass particles in order to make them smoother. For the coated glass particles (*i.e.* lower coefficient of friction) the pressure drop over the riser was much less than for the non-coated glass particles indicating a lower solids hold up in the system. The results of the simulations presented above support the idea that the difference in the axial pressure profile found in these experiments is caused by the difference in particle-particle interaction in both cases. In the case where less energy is dissipated in collisions (*i.e.* the more ideal system: lower values for the coefficient of friction, higher values for the coefficient of restitution) less clusters are being formed and hence there is less internal solids circulation within the riser. This results in a lower solids hold up in the riser and hence a lower pressure drop.

Chang and Louge (1992) pointed out that these effects become less pronounced at higher solids fluxes. A simulation was performed with ideal collision parameters at a solids flux of 50 kg/m^{2}s in order to investigate this. Although the system appeared less homogeneous than at a solids flux of 25 kg/m^{2}s still the formation of clusters was far less pronounced than in the non-ideal case with a solids flux of 25 kg/m^{2}s. Obviously there is still a large difference between the simulated system with ideal collision parameters and the coated glass particles used in the experiments. Nevertheless the simulation results clearly show the important effect of the collision parameters on the flow structure in a riser and this result is supported by the experiments of Chang and Louge (1992). It is therefore of great importance that the collision parameters (*i.e.* coefficient of restitution and friction) are taken into account in the scale up as well as the design of riser reactors.

3.3 Influence of lift forces

By default the two lift forces in equation 7.1 and the effect of the gas flow on the rotation of the particles (equation 7.8) were not included in the simulations. However, an additional simulation was performed including all these effects in order to investigate their influence on the flow structure. The case with the non-ideal collision parameters and a superficial gas velocity of 5.0 m/s was chosen as a test case. The time averaged (10 s) radial distributions of the solids volume fraction at 0.2 m above the riser inlet are presented in Figure 7.7 for the two simulations.

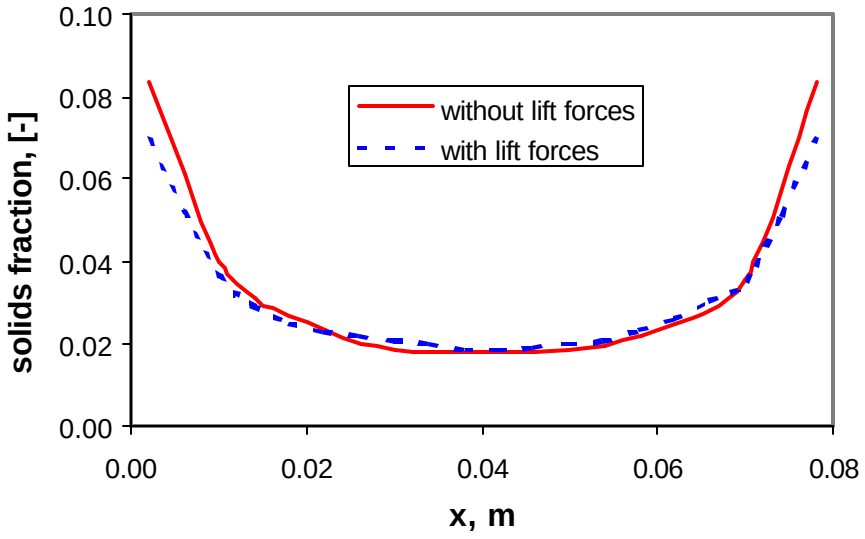

Figure 7.7. *Influence of the lift forces on the time-averaged radial distribution of the solids volume fraction at 0.2 m above the inlet of the simulated riser.*

From Figure 7.7 it is apparent that the lift forces did not have a significant influence on the flow structure. The radial segregation is slightly less pronounced when the lift forces are included in the equations of motion. This can be understood since the lift forces tend to move the particles toward the centre of the riser and therefore have a redispersive effect.

4. Conclusions

Granular Dynamics simulations of riser flow have been performed using a two-dimensional hard-sphere discrete particle model. Particles of 500 μm diameter and a density of 2620 kg/m^3 were introduced in a riser of 0.08 m width and 2.00 m height at a solids mass flux of 25 kg/m^{2}s. By default the superficial gas velocity was set equal to 5.0 m/s. The simulations turned out to be rather sensitive to the collision parameters, *i.e.* the coefficients of restitution (e) and friction (m). When these parameters were assigned non-ideal values (e = 0.94, m = 0.28) cluster formation was observed. When the collision parameters were set to ideal values (e = 1, m = 0) no cluster formation was observed. This was also the case in a simulation where only particle-wall collisions were considered non-ideal whereas particle-particle collisions were still taken to be ideal. The time averaged radial distribution of the solids volume fraction clearly revealed the typical core-annulus structure for the simulation with the non-ideal collision parameters. For the simulations with ideal particle-particle collisions the time averaged radial distribution of the solids volume fraction was rather flat. Particle-wall collisions turned out to have very little influence on the flow structure.

In the non-ideal case the solids hold-up in the riser was much higher than in the ideal case as could be observed from axial solids volume fraction profiles. These results are supported by the experimental findings of Chang and Louge (1992) where a large difference in axial pressure profile was found when a coating was applied to glass particles in order to change the surface roughness (*i.e.* decrease the coefficient of friction). In those experiments a smaller pressure drop (*i.e.* smaller solids hold-up) was found for the coated (smoother) particles which is in agreement with the trend observed in the simulations.

Finally the influence of the lift forces was investigated. These forces turned out to have a slightly redispersive effect on the flow structure which made the radial segregation of the

solids a little less pronounced. Since this was only a minor effect it could be regarded as a justification for the fact that the lift forces were neglected in the default simulations.

Notation

C_d	drag coefficient, [-]
C_m	rotational drag coefficient, [-]
e	coefficient of restitution, [-]
D_{nblist}	width of neighbour list square, m
D_p	particle diameter, m
I	moment of inertia, kgm^2
F	force, N
G_s	solids mass flux, kg/m^{2}s
g	gravitational acceleration, m/s^2
m_p	particle mass, kg
NX	number of computational cells in x-direction, [-]
NY	number of computational cells in y-direction, [-]
p	pressure, Pa
$\mathbf{S}_p$	momentum source term N/m^3
T	temperature, K
t	time, s
u	gas velocity vector, m/s
$\mathbf{v}_p$	particle velocity vector, m/s
V_p	particle volume, m^3
x	x coordinate, m
y	y coordinate, m

Greek symbols

a	coefficient in expression Magnus lift force (table 7.1), [-]
b	coefficient in expression Magnus lift force (table 7.1), [-]

b_0	coefficient of tangential restitution, [-]
χ	velocity gradient, 1/s
e	void fraction, [-]
m	coefficient of friction, [-]
m_g	gas viscosity, kg/ms
t	gas phase stress tensor, kg/ms^2
r	density, kg/m^3
ξ	dimensionless velocity gradient, [-]
w_p	particle rotation velocity, 1/s
w_r	relative rotation velocity gas/particle, 1/s

Subscripts

g	gas phase
LG	lift force due to velocity gradient
LM	Magnus lift force
p	particle
w	wall

References

Anderson, T.B. and Jackson, R., (1967). A fluid mechanical description of fluidized beds (equations of motion), *Ind. Eng. Chem., Fundam.*, **6**, 527.

Chang, H. and Louge, M.Y., (1992). Fluid dynamic similarity of circulating fluidized beds, *Powder Technol.*, **70**, 259.

Chen, J.C., (1996). Clusters (The Thomas Baron Plenary Lecture 1995), *AIChE Symp. Ser.* **92** (No. 313), 1.

Dennis, S.C.R., Singh, S.N., Ingham, D.B., (1980). The steady flow due to a rotating particle at low and moderate Reynolds numbers, *J. Fluid Mech*., **101** (2), 257.

Foerster S.F., Louge, M.Y., Chang,H. and Allia, K., (1994). Measurements of the collision properties of small spheres, *Phys. Fluids*, **6**, 1108.

Frezzotti, A., (1997). A particle scheme for the numerical solution of the Enskog equation, *Phys. Fluids*, **9**, 1329.

Helland, E., van den Moortel, T., Occelli, R., Tadrist, L., Hjertager, B.H., Solberg, T. and Mathiesen, V., (1999). Numerical/experimental study of gas-particle flow behaviour in a circulating fluidized bed, in *Circulating Fluidized Bed Technology VI*, J. Werther (Ed.), p. 261.

Hoomans, B.P.B., Kuipers, J.A.M., Briels, W.J. and van Swaaij, W.P.M. (1996). Discrete particle simulation of bubble and slug formation in a two-dimensional gas-fluidised bed: A hard-sphere approach, *Chem. Engng Sci*., **51**, 99.

Horio, M., Kuroki, H., (1994). Three-dimensional flow visualization of dilutely dispersed solids in bubbling and circulating fluidized beds, *Chem. Engng Sci.*, **49**, 2413.

Hrenya, C.M. and Sinclair, J., (1997). Effects of particle phase turbulence in gas-solid flows, *AIChE J*., **43**, 853.

Kuipers, J.A.M., van Duin, K.J., van Beckum, F.P.H. and van Swaaij, W.P.M., (1992). A numerical model of gas-fluidized beds, *Chem. Engng Sci*., **47,** 1913.

Kuipers, J.A.M., Hoomans, B.P.B. and van Swaaij, W.P.M., (1998). Hydrodynamic models of gas-fluidized beds and their role for design and operation of fluidized bed chemical reactors, in *Fluidization IX*, L.-S. Fan and T.M. Knowlton *eds*., p. 15

Nieuwland, J.J., van Sint Annaland, M., Kuipers, J.A.M. and van Swaaij, W.P.M., (1996). Hydrodynamic modelling of gas-particle flows in riser reactors, *AIChE J.*, **37**, 1009.

Mei, R., (1992). An approximate expression for the shear lift force on a spherical particle at finite Reynolds number, *Int. J. Multiphase flow*, **18**, 145.

Oesterlé, B., (1994). Une étude de l'influence des forces transversales agissant sur les particules dans les écoulements gaz-solide, *Powder Technol.*, **79**, 81.

Ouyang, J. and Li, J., (1999). Discrete simulations of heterogeneous structure and dynamic behavior in gas-solid fluidization, *Chem. Engng Sci*., **54**, 5427.

Richardson, J.F. and Zaki, W.N., (1954). Sedimentation and Fluidisation: Part I, *Trans. Inst. Chem. Engng*, **32**, 35.

Rowe, P.N. and Henwood, G.A., (1961). Drag forces in a hydraulic model of a fluidised bed-part I, *Trans. Instn Chem. Engrs*, **39**, 43.

Saffman, P.G., (1965). The lift on a small sphere in a slow shear flow, *J. Fluid Mech.*, **22(2)**, 385.

Sinclair, J. and Jackson, R., (1989). Gas-particle flow in a vertical pipe with particle-particle interactions, *AIChE J*., **35**, 1473.

Tanaka, T., Yonemura, S., Kiribayashi, K., Tsuji, Y., (1996). Cluster formation and particle-induced instability in gas-solid flows predicted by the DSMC method, *JSME Int. J. Series B,* **39**, 239.

Tsuji. Y., Morikawa, Y. and Mizuno, O., (1985). Experimental measurement of the Magnus lift force on a rotating sphere at low Reynolds numbers, *J. Fluids Eng*., **107**, 484.

Tsuji, Y., Tanaka, T. and Yonemura, S., (1998). Cluster patterns in circulating fluidized beds predicted by numerical simulation (discrete particle model versus two-fluid model), *Powder Technol.*, **95**, 254.

Tsuo, Y.P. and Gidaspow, D., (1990). Computation of flow patterns in circulating fluidized beds, *AIChE J.*, **36**, 885.

Wang, Y. and Mason, M.T., (1992). Two-dimensional rigid-body collisions with friction. *J. Appl. Mech.*, **59**, 635.

Chapter 8.

EXPERIMENTAL VALIDATION OF GRANULAR DYNAMICS SIMULATIONS OF GAS-FLUIDISED BEDS WITH HOMOGENOUS INFLOW CONDITIONS USING POSITRON EMISSION PARTICLE TRACKING

Abstract:

A hard-sphere Granular Dynamics model of a two-dimensional gas-fluidised bed was experimentally validated using Positron Emission Particle Tracking (PEPT). In the model the Newtonian equations of motion are solved for each solid particle while taking into account the particle-particle and particle-wall collisions. The gas phase hydrodynamics is described by the spatially averaged Navier-Stokes equations for two-phase flow. A quasi two-dimensional bed of 0.185 m width and 0.4 m height with homogenous inflow conditions at 1.5 u_{mf} was chosen as a test case. Glass particles (r_p = 2435 kg/m^3) with diameters ranging from 1.25 mm to 1.5 mm were used as the bed material. The collision parameters required in the simulation were obtained from separate, independent measurements. In the PEPT experiment the motion of a single tracer particle in the bed was tracked during the period of one hour. In the simulation the motion of 15,000 particles was tracked during a period of 45 s. The simulation data was time averaged over 45 s for each particle and subsequently ensemble averaged over all the particles in the simulation. The comparison was made on the basis of averaged velocity maps, occupancy plots and speed histograms. The results showed good agreement between experiment and simulation when the measured values for the collision parameters were used. When collisions were assumed to be fully elastic and perfectly smooth the agreement was much worse.

1. Introduction

Experimental validation of flow models for dense gas-fluidised beds, that form the basis for (amongst others) reactor models, is of crucial importance to arrive at models that can predict the performance of fluidised beds with confidence. The trend in both experiments and models is that systems can be studied in more and more detail with continuously increasing accuracy. It is not the objective to present a complete review of available experimental techniques in gas-fluidised beds here. A comprehensive review on measuring techniques in fluidised beds was presented by Werther (1999) whereas an extensive overview of existing techniques for the measurement of solids concentration and velocity was presented by Nieuwland *et al*. (1996).

With increasing computer power Granular Dynamics simulations have become a very useful and versatile research tool to study the dynamics of dense gas-particle flows. In these models the Newtonian equations of motion are solved for each individual granular particle in the system. The mutual interactions between particles and the interaction between particles and walls are taken into account directly. The discrete particle approach was pioneered by Tsuji *et al*. (1993) who used a soft-sphere model to describe the interaction between the particles. A three dimensional version of this model was later presented by Kawaguchi *et al*. (1998) whereas Mikami *et al*. (1998) extended the (2D) model in order to include cohesive forces between the particles. Hoomans *et al*. (1996) presented a hard-sphere approach where collisions are assumed to be binary and instantaneous. Xu and Yu (1997) developed a hybrid technique combining elements of both soft-sphere and hard-sphere techniques. In the studies on discrete particle simulation of gas-fluidised beds previously reported in the literature experimental validation has received little attention. This was partly due to the fact that proper experimental techniques were not widely available.

In Chapter 5 and Chapter 6 of this thesis experimental validation was performed by direct observation of transient phenomena that occurred in a transparent system by using a video camera. This is a very basic technique that nonetheless can provide useful information on for instance the formation of a single bubble at an orifice or the dynamics of segregation. In the latter case it is required that the segregating species

can be visually identified. However, the direct observation technique is limited to systems that allow for direct observation (*i.e.* transparent quasi two-dimensional set-ups) in contrast to for example X-ray techniques (Yates *et al.*, 1994). Furthermore the information that is obtained using direct observation covers macroscopic behaviour: Important quantities such as local solids volume fraction, local solids velocities etc. cannot be obtained using this technique.

Particle tracking techniques are non-invasive measurement techniques where the motion of a single tracer particle is tracked for a period of time. Such techniques are ideally suited to validate a discrete particle model since the motion of a single particle in the bed can be tracked and therefore it allows for relatively direct comparison between measured data and simulation results. Lin *et al.* (1985) presented a technique where a radioactive tracer particle was used that was made of scandium-46 (Sc-46). A total of 12 scintillation detectors were positioned around the fluidised bed to enable determination of the location of the particle. More recently Larachi *et al.* (1996) applied the tracking technique using Sc-46 tracers to gas-liquid-solid flows and Mostoufi and Chaouki (1999) applied the technique to liquid-fluidised beds.

In this work a cooperation between the University of Twente and the University of Birmingham was initiated in order to use the Positron Emission Particle Tracking (PEPT) technique developed at Birmingham to validate the granular dynamics model of a gas fluidised bed developed at Twente. PEPT has been developed at Birmingham since 1987 and was successfully applied to a large number of systems for solids processing including mixers and gas fluidised beds (Seville *et al.* 1995). A comprehensive introduction to PEPT can be found in Stein *et al.* (1997). Recently a PEPT system was also developed by Stellema *et al.* (1998). PEPT differs from other tracking techniques in the sense that it uses positron emitting radioisotopes which have the unique feature that their decay leads to simultaneous emission of a pair of back-to-back γ-rays. In a following section a more elaborate discussion of the PEPT technique will be presented.

2. Model

Since a detailed description of the model is presented in Chapter 2 and Chapter 3, the key features will be summarised briefly here.

2.1 Granular dynamics

The collision model as originally developed by Wang and Mason (1992) is used to describe a binary, instantaneous, inelastic collision with friction. The key parameters of the model are the coefficient of restitution ($0 \leq e \leq 1$) and the coefficient of friction ($\mu \geq 0$). Foerster *et al.* (1994) have shown that also the coefficient of tangential restitution ($0 \leq b_0 \leq 1$) should be used in order to describe the collision dynamics more accurately. These three collision parameters are all included in the model.

In the hard-sphere approach a sequence of binary collisions is processed. This implies that a collision list is compiled in which for each particle a collision partner and a corresponding collision time is stored. A constant time step is used to take the external forces into account and *within* this time step the prevailing collisions are processed sequentially. In order to reduce the required CPU time neighbour lists are used. For each particle a list of neighbouring particles is stored and only for the particles in this list a check for possible collisions is performed.

2.2 External forces

The incorporation of external forces differs somewhat from the approach followed by Hoomans *et al*. (1996). In this work the external forces are used in accordance with those implemented in the two-fluid model presented by Kuipers *et al.* (1992) where, of course, the forces now act on a single particle:

$$m_p \frac{d\mathbf{v}_p}{dt} = m_p \mathbf{g} + \frac{V_p \beta}{(1-\varepsilon)} \left(\mathbf{u} - \mathbf{v}_p \right) - V_p \nabla p \quad , \tag{8.1}$$

where m_p represents the mass of a particle, $\mathbf{v}_p$ its velocity, $\mathbf{u}$ the local gas velocity and V_p the volume of a particle. In equation (8.1) the first term is due to gravity and the third term is the force due to the pressure gradient. The second term is due to the drag force where β represents an inter-phase momentum exchange coefficient as it usually appears in two-fluid models. For low void fractions ($\varepsilon < 0.80$) β is obtained from the well-known Ergun equation:

$$\beta = 150\frac{(1-\varepsilon)^2}{\varepsilon}\frac{\mu_g}{D_p^2} + 1.75(1-\varepsilon)\frac{\rho_g}{D_p}\left|\mathbf{u}-\mathbf{v}_p\right| \quad , \tag{8.2}$$

where D_p represents the particle diameter, μ_g the viscosity of the gas and ρ_g the density of the gas. For high void fractions ($\varepsilon \geq 0.80$) the following expression for the inter-phase momentum transfer coefficient has been used which is basically the correlation presented by Wen and Yu (1966) who extended the work of Richardson and Zaki (1954):

$$\beta = \frac{3}{4}C_d\frac{\varepsilon(1-\varepsilon)}{D_p}\rho_g\left|\mathbf{u}-\mathbf{v}_p\right|\varepsilon^{-2.65} \quad . \tag{8.3}$$

The drag coefficient C_d is a function of the particle Reynolds number and given by:

$$C_d = \begin{cases} \dfrac{24}{\mathrm{Re}_p}\left(1+0.15\mathrm{Re}_p^{0.687}\right) & \mathrm{Re}_p < 1000 \\ 0.44 & \mathrm{Re}_p \geq 1000 \end{cases} , \tag{8.4}$$

where the particle Reynolds number (Re_p) in this case is defined as follows:

$$\mathrm{Re}_p = \frac{\varepsilon\rho_g\left|\mathbf{u}-\mathbf{v}_p\right|D_p}{\mu_g} \quad . \tag{8.5}$$

For the integration of equation (8.1) a simple explicit first order scheme was used to update the velocities and positions of the particles.

2.3 Gas phase hydrodynamics

The calculation of the gas phase hydrodynamics mainly follows the lines presented by Kuipers *et al.* (1992). It is based on the numerical solution of the following set of partial differential equations that can be seen as a generalised form of the Navier-Stokes equations for a gas interacting with a solid phase as originally derived by Anderson and Jackson (1967).

Continuity equation gas phase:

$$\frac{\partial\left(\varepsilon_g \rho_g\right)}{\partial t} + \left(\nabla \cdot \varepsilon_g \rho_g \mathbf{u}\right) = 0 \ . \tag{8.6}$$

Momentum equation gas phase:

$$\frac{\partial\left(\varepsilon_g \rho_g \mathbf{u}\right)}{\partial t} + \left(\nabla \cdot \varepsilon_g \rho_g \mathbf{u}\mathbf{u}\right) = -\varepsilon \nabla p - \mathbf{S}_p - \left(\nabla \cdot \varepsilon \tau_g\right) + \varepsilon_g \rho_g \mathbf{g} \ . \tag{8.7}$$

In this work transient, two-dimensional, isothermal (T = 293 K) flow of air at atmospheric conditions is considered. The constitutive equations can be found in Chapter 3. There is one important modification with respect to the model presented by Hoomans *et al.* (1996) and that deals with the way in which the two-way coupling between the gas-phase and the dispersed particles is established. In the present model the reaction force to the drag force exerted on a particle per unit of volume is fed back to the gas phase through the source term $\mathbf{S}_p$ which has the dimension of force per unit of volume N/m^3.

3. Positron Emission Particle Tracking

Positron Emission Particle Tracking (PEPT) is a technique that allows non-invasive observation of the motion of a single radioactive tracer particle. The PEPT technique is schematically represented in Figure 8.1.

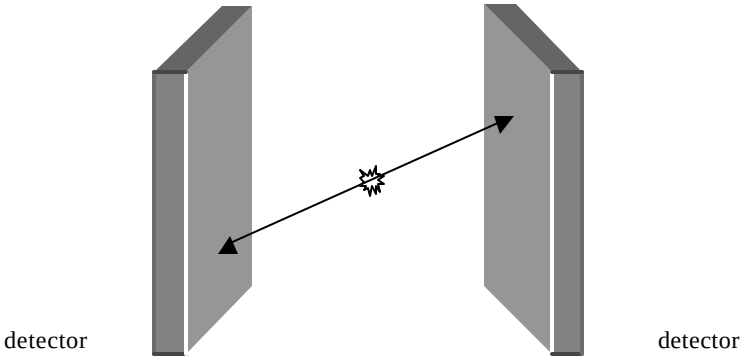

a) detection

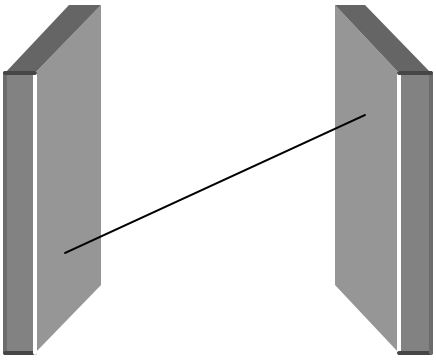

b) reconstruction

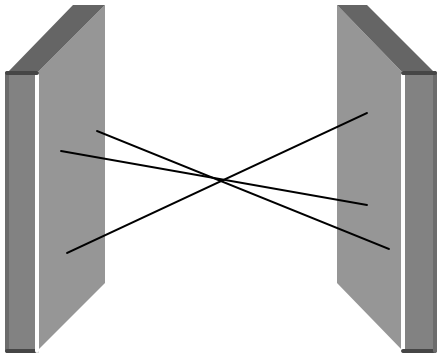

c) particle location

Figure 8.1. *The principle of the PEPT technique*

In the experiment reported here a glass particle taken from the sample of particles used in the fluidisation experiment was activated by direct irradiation in a cyclotron beam.

The glass particle was irradiated with the ^{3}He beam from a cyclotron to produce the positron emitter ^{18}F from reactions involving the oxygen on the glass. The decay of the ^{18}F isotope features the conversion of a proton to a neutron with the emission of a positron, the anti-particle of the electron. The positron then annihilates with an electron to produce a pair of back to back γ-rays. The γ-rays are detected by the positron cameras which consists of two position-sensitive γ-ray detectors that have an active area of 0.3 by 0.6 m. By using a reconstruction algorithm the position of the particle can be obtained as the intersection point of successive annihilation vectors. The algorithm employs an iterative scheme to discard corrupt annihilation vectors that can be caused by γ-ray scattering or random coincidences. When the tracer particle does not move the more annihilation vectors are used the more accurate the particle position can be determined. However, when the particle is moving the set of annihilation vectors should be large enough to locate the particle accurately but not so large that it has moved significantly during the time period over which the set was measured.

The technique was not optimised for the use of a quasi two-dimensional system and for the post processing the standard software was used. The instantaneous particle velocity is inferred from the difference between successive locations.

4. Comparison between PEPT data and simulation

The PEPT experiment as performed in this work renders the trajectory of a single particle during one hour. This time scale cannot be reached by means of simulation on modern day computers. Instead the motion of 15,000 particles is tracked during a shorter period of time (45 s). In fact considerably more data is generated in the simulation since 15,000 times 45 seconds is a far larger number than 1 times 3600 seconds. And since the 15,000 simulated particles cover the whole of the fluidised system, the simulation data does not suffer from poorly sampled regions in contrast with the experimental data.

It is assumed that it is justified to compare the simulation results with the time averaged experimental data by first time averaging the simulation data for each of the 15,000 particles and subsequently taking an ensemble average over all the 15,000 particles. By doing this there is a risk that rare events, which occur over a time scale close to or greater than the duration of a simulation, are poorly sampled. On the contrary, the chance that such a rare event is experienced by the tracer particle in the experiment is rather low as well.

The actual comparison is made on the basis of occupancy plots, velocity maps and speed histograms which are standard outputs of the PEPT software (Tin *et al.*, 1997) that was supplied by the University of Birmingham. To obtain an occupancy plot from the PEPT data the system is first divided into cells (10 mm width/height). In the occupancy plot the fraction of the total time that the tracer particle has spend in that particular cell is displayed using a colour code that is explained in the legend accompanying the plot. For the simulations a similar procedure was followed after all the individual particle trajectories were added together. In order to obtain the velocity maps the system was again divided into cells. The velocity vectors in the figure are averaged velocity for that particular cell. How the averages were obtained is explained above. Finally the PEPT data was compared with the results of the simulation using speed histograms. For the PEPT experiment the speed of the tracer particle was calculated on the basis of the 3 velocity components (x,y,z) at each instant. The histogram shows the speed distribution based on the data set covering the entire duration of the experiment of one hour. The speed histograms obtained from the simulation results are based on the two velocity components (x,y) taken into account in the simulations.

5. Results

As a test system for the experimental validation a gas-fluidised bed (0.185 m width, 20 mm depth) with homogeneous inflow conditions (u_g = 1.5 u_{mf}, u_{mf} = 0.9 m/s) was chosen. The parameter settings for the simulation are summarised in table 8.1. The bed was filled with the glass particles in such a way the static bed height was about 0.17 m.

In the simulation a total number of 15,000 particles was used to match the bed height encountered in the experiment. The bed used in the experiment was assembled using glass as the construction material. It was fitted with a porous plate distributor with a sufficiently high pressure drop to ensure homogeneous inflow conditions. In preliminary experiments a malfunctioning distributor plate was used which caused a strongly non-symmetrical solids flow pattern in the bed indicating a non-uniform gas distribution. The actual PEPT experiment used for the experimental validation was run for one hour in order to collect sufficient data to calculate statistically reliable averages.

Table 8.1. *Parameter settings for the PEPT simulation*

Particles:		Bed:	
Shape	spherical	Width	0.185 m.
density, ρ_p	2418 kg/m^3	Height	0.40 m
particle diameter, D_p	1.25-1.50 mm	Number x-cells, *NX*	37
		Number y-cells, *NY*	80
$e = e_w$	0.97	cell width, *DX*	5 mm
$\mu = \mu_w$	0.10	cell height, *DY*	5 mm
$\beta_0 = \beta_{0,w}$	0.33		
N_p	15,000	time step, *DT*	10^{-4} s

The particle-particle collision parameters presented in table 8.1 were independently measured by Gorham and Kharaz (1999) using the facility at the Open University at Milton Keynes described in Chapter 2. The particle-wall collision parameters were assumed to be equal to the particle-particle collision parameters. This is justified since earlier simulations (Chapter 4) showed that the influence of the particle-wall collision parameters were negligible compared to the influence of the particle-particle collision parameters. A log-normal particle size distribution about an average diameter of 1.375 mm was taken into account in the simulation. Particle diameters lower than 1.25 mm and greater than 1.50 mm were rejected in order to mimic the effects of sieving and hence match the particle size distribution encountered in the experiment.

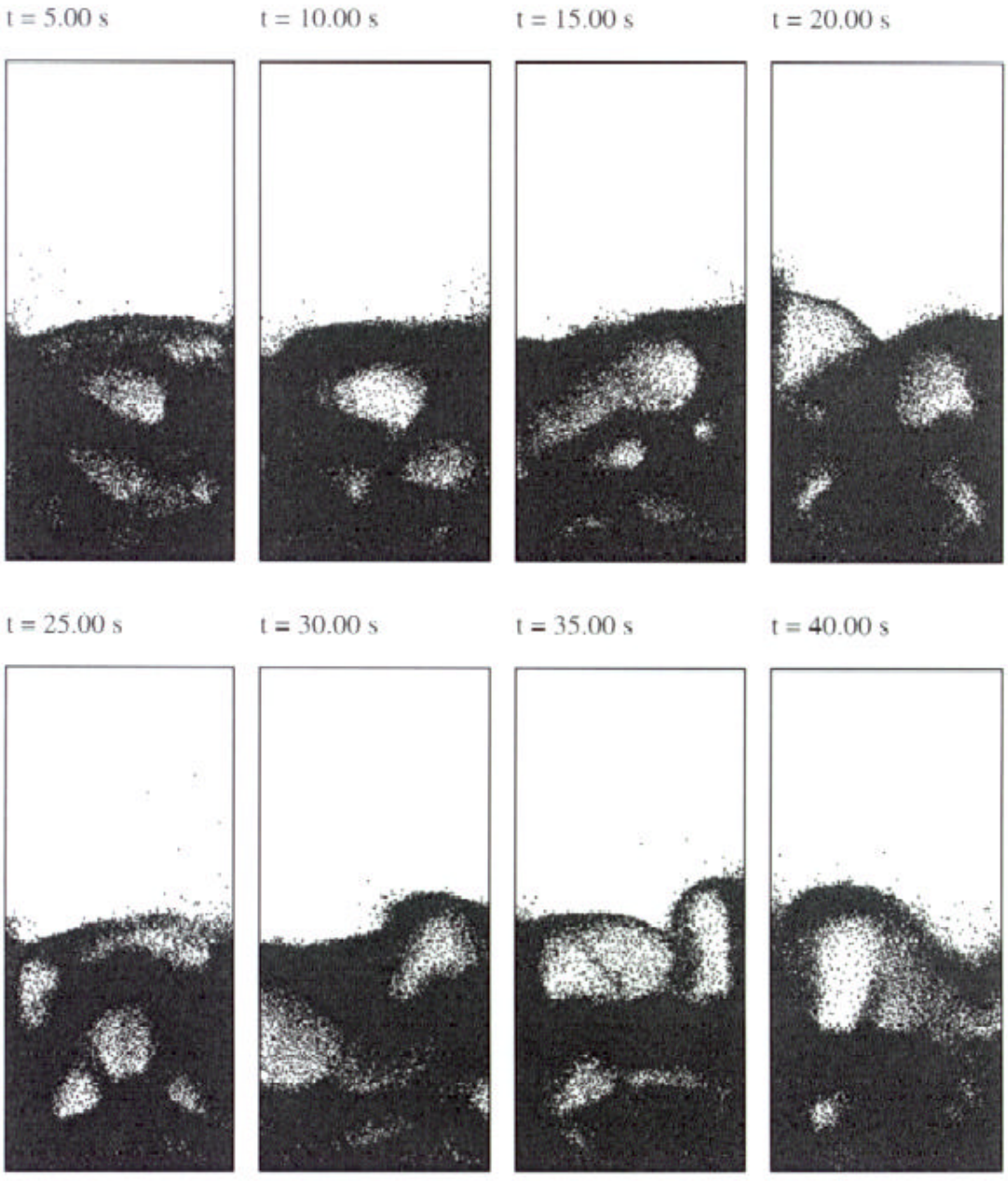

Figure 8.2. *Snapshots of particle configurations of the simulation.*

An initial simulation was performed first to ensure that the actual simulation would not suffer from any start-up effects. During this initial simulation the system was operated at a homogeneous gas inflow of 1.5 u_{mf} (u_{mf} = 0.9 m/s) with the parameter settings

presented in table 8.1. After this initial simulation the actual simulation (duration 45 s) was started and the required data (positions and velocities) was stored at time intervals corresponding to those used in the experiment. Snapshots of the simulation are presented in Figure 8.2. In this figure it can be observed that the bed is bubbling quite vigorously and this behaviour could also be visually observed during the PEPT experiment. In Figure 8.3 an example of the trajectory of one single (randomly chosen) particle in the simulation is presented. This trajectory covers the whole duration of the simulation of 45 s.

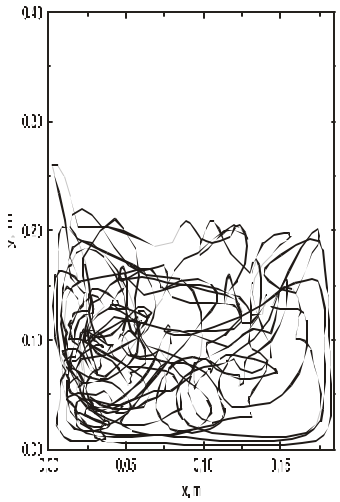

Figure 8.3. *Example of a trajectory of a single particle during the simulation.*

Although the figure above gives some insight into the motion of a particle in a fluidised bed it does not provide a solid basis for a comparison. Therefore averaging techniques were applied as discussed in the previous section which yield data that permit a comparison between the PEPT data and the simulation results.

In Figure 8.4 the velocity map obtained from the PEPT data is presented together with the velocity maps obtained from two simulations. In the centre the velocity map of the simulation using the measured values for the collision parameters (table 8.1) is presented and on the right the velocity map of a simulation assuming fully elastic, perfectly smooth collisions (e = 1, m = 0, also referred to as *ideal* collisions) is presented. A reference vector indicating the magnitude of the velocity is included in all of the three velocity maps. In velocity map of the PEPT data a circulation pattern

can be observed where particles rise in the centre of the bed and descend near the walls. Two circulation cells can be distinguished which together form a rather symmetric picture indicating that the gas inflow was indeed homogeneous.

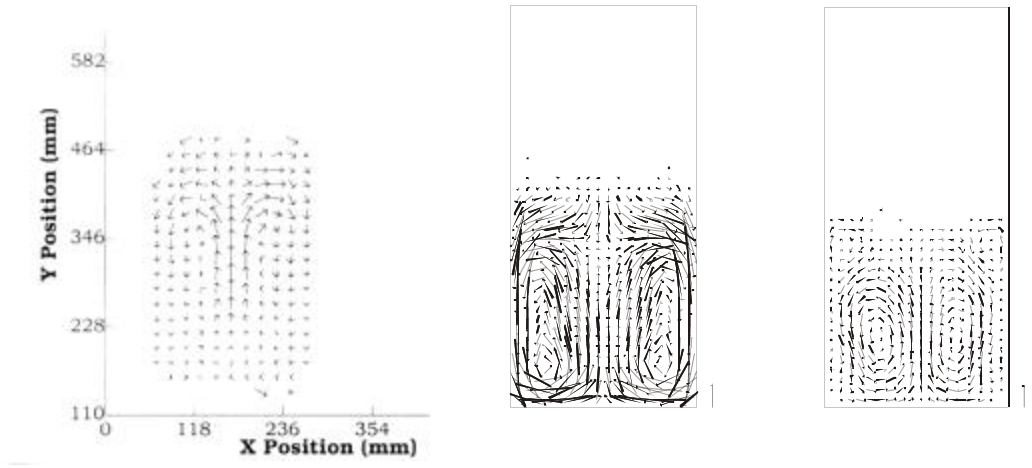

Figure 8.4. *Velocity map obtained from the PEPT data (left) compared with the velocity maps of the simulation using the measured collision parameters (centre) and the simulation assuming fully elastic, perfectly smooth collision (right)*

From the simulation with the measured collision parameters a very similar velocity map was obtained. Although not perfectly symmetric two circulation cells can be distinguished which is in good agreement with the PEPT data. The velocity map of the simulation assuming fully elastic, perfectly smooth collisions shows a somewhat different behaviour. The velocity vectors are smaller indicating lower speeds and also two additional circulation cells on top of the two main cells can be observed. These additional circulation cells rotate in the opposite direction and were not present in the PEPT experiment.

In Figure 8.5 the occupancy plots obtained from the PEPT data and the two simulations are presented together. In this figure it can be observed that in the PEPT data the occupancy was higher near the walls which was also the case in the simulation with the measured collision parameters. This indicates that the particles spend relatively more time near the walls. In the simulation assuming fully elastic, perfectly

smooth collisions the occupancy is almost the same at each position in the system. In other words the residence time of the particles is evenly distributed throughout the whole system. This is due to the absence of bubbles in the latter case which causes a very homogeneous type of fluidisation.

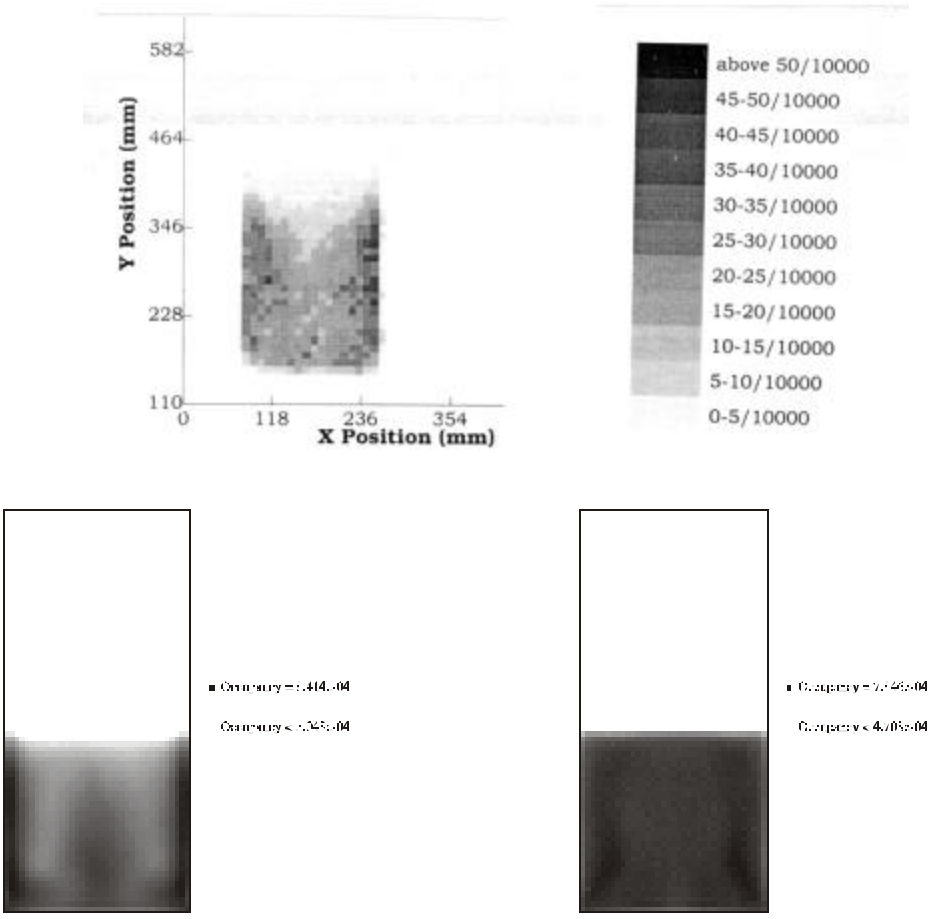

Figure 8.5. *Occupancy plots obtained from the PEPT data (above), the simulation using the measured collision parameters (left) and the simulation assuming fully elastic, perfectly smooth collisions (right)*

It should be noted that the occupancy plot obtained from the PEPT data is not as smooth as the ones obtained from the simulations. This is obviously due to the fact that in the experiment one single particle was tracked for one hour. This does not guarantee that the whole system is covered and therefore it can be understood that

some regions of the bed suffer from poor statistics. For the simulation results all the particles in the system were taken into account which renders a far smoother picture since the whole of the bed was automatically sampled.

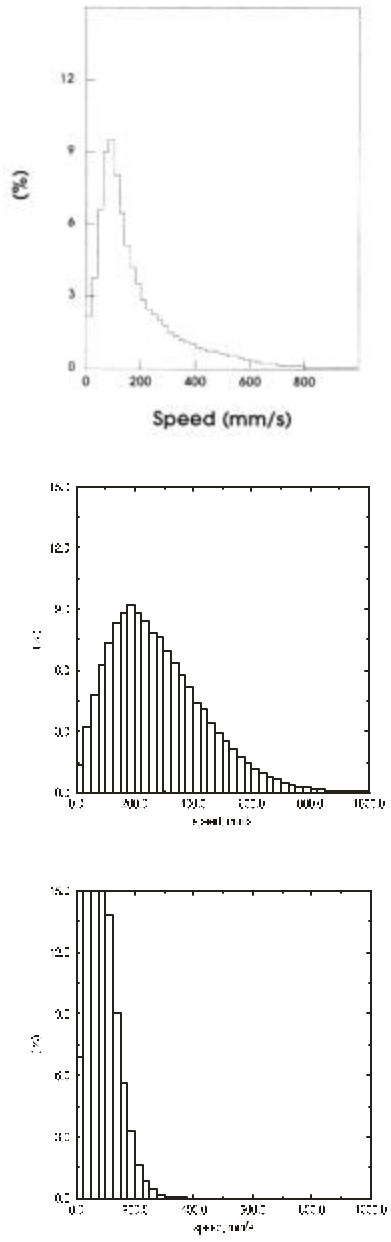

Figure 8.6. *Speed histogram obtained from the PEPT experiment (top) compared with the speed histograms obtained from the simulation using the measured collision parameters (left) and the simulation assuming perfectly smooth, fully elastic collisions (right)*

In Figure 8.6 the speed histogram obtained from the PEPT experiment is presented together with the speed histograms obtained from the two simulations. Where the velocity map and the occupancy plot provide a basis for a more qualitative comparison between simulation and experiment, the speed histogram offers the possibility for a quantitative comparison.

In Figure 8.6 it can be observed that the results of the simulation using the measured collision parameters compare rather well with results of the PEPT experiment. Although the simulation results show a somewhat higher average speed than the PEPT data (about 0.25 m/s in the simulation and 0.15 m/s in the experiment) the shape of the distribution is rather similar. The higher average speed is most likely due to the two-dimensional nature of the simulation. The absence of the front and back walls in the simulation implies that the particles in the simulation do experience a lower amount of wall friction that effectively results in a higher average speed. It is important to note that in both the experiment and the simulation particle speeds above 0.4 m/s are observed. Since these higher speeds are closely related to the bubbling behaviour in the bed it is important that good agreement between simulation and experiment is achieved on this matter. Although the speeds observed in the simulation are somewhat higher than the ones observed in the experiment for reasons discussed above, the agreement is encouraging.

The agreement between the results of the PEPT experiment and the simulation assuming fully elastic, perfectly smooth collisions is much worse in this respect. In the latter simulation the average speed (about 0.1 m/s) is actually closer to the average speed observed in the experiment but more importantly however, the distribution of speeds in the histogram is far more narrow: no speeds above 0.4 m/s were observed. The reason for this is the absence of bubbles in the simulation with ideal collision parameters since the particles attain their maximum speeds when they are accelerated into the wake of a bubble. This once again emphasises the profound influence that these collision parameters have on the dynamics of a gas-fluidised bed.

6. Conclusions

Granular dynamics simulations of gas-fluidised beds with homogeneous inflow conditions were experimentally validated using the Positron Emission Particle Tracking facility at the University of Birmingham. A quasi two-dimensional bed of 0.185 m width and 0.4 m height with homogenous inflow conditions at 1.5 u_{mf} was chosen as a test case. Glass particles (r_p = 2435 kg/m^3) with diameters ranging from 1.25 mm to 1.5 mm were used as the bed material. In the PEPT experiment the motion of a single tracer particle in the bed was tracked during the period of one hour. In the simulation the motion of 15,000 particles was tracked during a period of 45 s. The simulation data was time averaged over 45 s for each particle and subsequently ensemble averaged over all the particles in the simulation. The results showed good agreement between experiment and simulation when measured values for the collision parameters were used. The particle speeds observed in the simulation were somewhat higher than those observed in the experiment which is most likely due to the absence of the front and back wall in the simulation. When collisions were assumed to be fully elastic and perfectly smooth the agreement was worse. No speeds higher than 0.4 m/s were observed whereas in the experiment as well as in the simulation with the measured collision parameters speeds up to 0.8 m/s were found. This demonstrates the profound influence of the collision parameters on the bed hydrodynamics since these higher speeds are closely related to the presence of bubbles in the bed. From a direct comparison with an experiment it was therefore shown that the assumption of fully elastic, perfectly smooth collisions is not valid for fluidised bed simulations.

From this first comparison between granular dynamics simulations and a PEPT experiment it can be concluded that PEPT is a powerful tool for the experimental validation of these simulations. In future work it should not only be attempted to perform the validation on a more detailed level but also the simulation data can be used to verify the PEPT software. Since the simulation yields particle positions and corresponding velocities that are exact, the PEPT software should be able reproduce these results.

Notation

C_d	drag coefficient, [-]
e	coefficient of restitution, [-]
D_p	particle diameter, m
DT	time step, s
DX	horizontal computational cell dimension, m
DY	vertical computational cell dimension, m
$\mathbf{g}$	gravitational acceleration, m/s^2
m_p	particle mass, kg
N_p	number of particles, [-]
NX	number of computational cells in x-direction, [-]
NY	number of computational cells in y-direction, [-]
p	pressure, Pa
$\mathbf{r}$	position vector, m
$\mathbf{S}_p$	momentum source term N/m^3
T	temperature, K
t	time, s
$\mathbf{u}$	gas velocity vector, m/s
$\mathbf{v}_p$	particle velocity vector, m/s
V_p	particle volume, m^3

Greek symbols

b	volumetric interphase momentum transfer coefficient, $kg/(m^3s)$
b_0	coefficient of tangential restitution, [-]
e	void fraction, [-]
m	coefficient of friction, [-]
m_g	gas viscosity, kg/ms
t	gas phase stress tensor, kg/ms^2
r	density, kg/m^3

Subscripts

g	gas phase

mf	minimum fluidisation
p	particle
w	wall

References

Anderson, T.B. and Jackson, R., (1967). A fluid mechanical description of fluidized beds (equations of motion), *Ind. Eng. Chem., Fundam.*, **6**, 527.

Foerster S.F., Louge, M.Y., Chang,H. and Allia, K. (1994). Measurements of the collision properties of small spheres. *Phys. Fluids,*, **6**, 1108.

Gorham, D.A. and Kharaz, A.H., (1999). Results of particle impact tests, Impact Research Group Report IRG 13, The Open University, Milton Keynes, UK.

Hoomans, B.P.B., Kuipers, J.A.M., Briels, W.J. and van Swaaij, W.P.M., (1996). Discrete particle simulation of bubble and slug formation in a two-dimensional gas-fluidised bed: a hard-sphere approach, *Chem. Engng Sci.*, **51**, 99.

Kuipers, J.A.M., van Duin K.J., van Beckum, F.P.H. and van Swaaij, W.P.M., (1992). A numerical model of gas-fluidized beds, *Chem. Engng Sci.*, **47,** 1913

Larachi, F., Cassanello, M., Chaouki, J. and Guy, C., (1996). Flow structure of the solids in a 3-D gas-liquid-solid fluidized bed, *AIChE J.*, **42**, 2439.

Lin, J.S., Chen, M.M. and Chao, B.T., (1985). A novel radioactive particle tracking facility for measurement of solids motion in gas fluidized beds, *AIChE J*., **31**, 465.

Kawaguchi, T., Tanaka, T. and Tsuji, Y., (1998). Numerical simulation of two-dimensional fluidized beds using the discrete element method (comparison between the two- and three-dimensional models), *Powder Technol.*, **96**, 129.

Mikami, T., Kamiya, H. and Horio, M., (1998). Numerical simulation of cohesive powder behavior in a fluidized bed, *Chem. Engng Sci.*, **53**, 1927.

Mostoufi, N. and Chaouki, J., (1999). Prediction of effective drag coefficient in fluidized beds, *Chem. Engng Sci.*, **54**, 851.

Nieuwland, J.J., Meijer, R., Kuipers, J.A.M. and van Swaaij, W.P.M., (1996), Measurements of solids concentration and axial solids velocity in gas-solid two-phase flows, *Powder Technol.*, **87**, 127.

Richardson, J.F. and Zaki, W.N., (1954). Sedimentation and fluidization: part I. *Trans. Inst. Chem. Eng*., **32**, 35.

Seville, J.P.K., Simons, S.J.R., Broadbent, C.J., Martin, T.W., Parker, D.J. and Beynon, T.D., (1995). Particle velocities in gas-fluidised beds, Fluidization VIII, Engineering Foundation, Preprints Tours, 319.

Stein. M., Martin, T.W., Seville, J.P.K., McNeil, P.A. and Parker, D.J., (1997). Positron emission particle tracking: particle velocities in gas fluidised beds, mixers and other applications, in *Non-invasive monitoring of multiphase flows*, Chaouki, J., Larachi, F. and Dududkovic, M.P. (eds), Elsevier Science, Amsterdam, the Netherlands.

Stellema, C.S., Vlek, J., Mudde, R.F., de Goeij, J.J.M. and van den Bleek, C.M., (1998). Development of an improved positron emission particle tracking system, *Nucl. Instr. And Meth. In Phys. Res. A*, **404**, 334.

Tan, M., Parker, D.J. and Dee, P.R., (1997). PEPT data presentation software, manual, Birmingham University, UK.

Tsuji, Y., Kawaguchi, T. and Tanaka, T., (1993). Discrete particle simulation of two dimensional fluidized bed, *Powder Technol.* **77**, 79.

Wang, Y. and Mason, M.T., (1992). Two-dimensional rigid-body collisions with friction. *J. Appl. Mech.*, **59**, 635.

Werther, J., (1999). Measurement techniques in fluidized beds, *Powder Technol.*, **102**, 15.

Wen, C.Y. and Yu, Y.H., (1966). Mechanics of fluidization. *Chem. Eng. Prog. Symp. Ser*., **62** (62), 100.

Xu, B.H. and Yu, A.B., (1997). Numerical simulation of the gas-solid flow in a fluidized bed by combining discrete particle method with computational fluid dynamics. *Chem. Engng Sci*. **52**, 2785.

Yates, J.G., Cheesman, D.J. and Sergeev, Y.A., (1994). Experimental observations of voidage distribution around bubbles in a fluidized bed, *Chem. Engng Sci*. **49**, 1885.

Publications

1. B.P.B. Hoomans, J.A.M. Kuipers, W.J. Briels and W.P.M. van Swaaij, (1996). Discrete particle simulation of bubble and slug formation in two-dimensional gas-fluidised beds: a hard-sphere approach, *Chem. Engng Sci.*, **51**, 99.

2. B.P.B. Hoomans, J.A.M. Kuipers and W.P.M. van Swaaij, (1998). Discrete particle simulation of segregation phenomena in dense gas-fluidized beds, in *Fluidization IX*, L.-S. Fan and T.M. Knowlton (eds), 485.

3. J.A.M. Kuipers, B.P.B. Hoomans and W.P.M. van Swaaij, (1998). Hydrodynamic models of gas-fluidized beds and their role for design and operation of fluidized bed chemical reactors, in *Fluidization IX*, L.-S. Fan and T.M. Knowlton (eds), 15.

4. B.P.B. Hoomans, J.A.M. Kuipers and W.P.M. van Swaaij, (1998). Granular Dynamics Simulation of Cluster Formation in Dense Riser Flow, *Third International Conference on Multiphase Flows 1998*, June 8-12, Lyon, France.

5. B.P.B. Hoomans, J.A.M. Kuipers and W.P.M. van Swaaij, (1998). The influence of particle properties on pressure signals in dense gas-fluidised beds: a computer simulation study, *World Congress on Particle Technology 3*, July 7-9, Brighton, UK.

6. B.P.B. Hoomans, J.A.M. Kuipers, W.J. Briels and W.P.M. van Swaaij, (1998). Comments on the paper 'Numerical simulation of the gas-solid flow in a fluidized bed by combining discrete particle method with computational fluid dynamics' by B.H. Xu and A.B. Yu, *Chem. Engng Sci.*, **54**, 2645.

7. B.P.B. Hoomans, J.A.M. Kuipers and W.P.M. van Swaaij, (1998). The influence of a particle size distribution on the granular dynamics of dense gas-fluidized beds: a computer simulation study, *AIChE Symp. Ser. No. 318*, **Vol. 94**, 15.

8. B.P.B. Hoomans, J.A.M. Kuipers and W.P.M. van Swaaij, (1999). Discrete particle simulation of cluster formation in dense riser flow, *Circulating Fluidized Bed Technology VI*, J. Werther (Ed.), .

9. B.P.B. Hoomans, J.A.M. Kuipers and W.P.M. van Swaaij, (2000). Granular dynamics simulation of segregation phenomena in dense gas-fluidised beds, *Powder Technology* (in press).

Dankwoord (Ackowledgements)

En zo komt er een einde aan een promotie met ballen*. Een promotie die zeker niet het werk is van slechts één persoon. De mensen die een bijdrage hebben geleverd aan de totstandkoming van dit proefschrift wil ik op deze plek dan ook graag bedanken.

Allereerst gaat mijn dank uit naar mijn drie promotoren. Modellering van de hydrodynamica van meerfasenstromingen is een onderzoekslijn waarmee Hans Kuipers inmiddels wereldwijd een grote naam heeft opgebouwd. Hans, het was me een waar genoegen om deel uit te maken van jouw team. Ik ben je dankbaar voor het grote vertrouwen dat je in me had. Ook zonder Wim Briels was dit promotieproject niet van de grond gekomen. Zijn vermogen om formules te doorgronden en die vervolgens te manipuleren is ook de kwaliteit van dit proefschrift ten goede gekomen. Wim, ik denk met veel plezier terug aan de tijd die ik in jouw groep heb doorgebracht. Wim van Swaaij volgde het onderzoek weliswaar van wat grotere afstand maar wist op beslissende momenten een zet in de goede richting te geven. Wim, ik zal altijd onthouden dat je me een sleepkabel aanreikte toen ik met pech langs de weg stond.

Een vijftal afstudeerders heeft een zeer gewaardeerde bijdrage geleverd aan de diverse onderwerpen die in dit proefschrift aan bod komen. Robert Heijnen (segregatie, het idee voor het plaatje op de kaft van dit proefschrift is aan zijn brein ontsproten), Marco Stam (zachte ballen), Peter Schinkelshoek (riserstroming), Reneke van Soest-Seij (3-D harde ballen) en Jan Gerard Schellekens (segregatie): allemaal ontzettend bedankt !

Veel steun heb ik gehad aan mijn collega's Erik Delnoij, Mathijs Goldschmidt, Michiel Gunsing en Jie Li van de multi-phase flow crew van Hans Kuipers waar we dankbaar van elkaars kennis en vaardigheden gebruik konden maken.

De experimenten beschreven in hoofdstuk 5 waren niet mogelijk geweest zonder de hulp van Jelle Nieuwland, Patrick Huttenhuis en Olaf Veehof. Ik wil Bart Lammers bedanken voor het ontwikkelingswerk aan de visualisatiesoftware dat hij heeft uitgevoerd tijdens

* vrij naar Marco Stam, afstudeerverslag Universiteit Twente, 1996.

zijn afstudeeropdracht bij Erik. De video-animaties van mijn simulaties zijn inmiddels in alle werelddelen te zien geweest. Mathijs heeft een cruciale rol gespeeld bij de totstandkoming en het bedrijven van de opstelling die gebruikt is voor de experimenten beschreven in hoofdstuk 6. Hierbij werd hij technisch ondersteund door Gerrit Schorfhaar. Paul-Guillaume Schmitt voerde in het kader van zijn stage een deel van de metingen met deze opstelling uit (merci beaucoup !) en dank zij Siebren Mellema konden de videobeelden digitaal verwerkt worden. I wish Jie Li and Pranay Darda all the best with their continuation of the discrete particle work.

Professor Jonathan Seville and Dr. David Parker of the University of Birmingham are gratefully acknowledged for their support of the PEPT validation project reported in Chapter 8. I want to thank Matthias Stein, Mohamad Amran Mohd Salleh, Dennis Allen, and Aidan McCormack for their valuable contribution to this Birmingham-Twente project. The collision parameters required for the validation simulations in Chapter 6 and Chapter 8 were experimentally obtained by Dr. David Gorham and Ahmad Kharaz of the Open University at Milton Keynes.

Deze metingen werden financiëel ondersteund door het Unilever Research Laboratorium Vlaardingen. Ik wil Joop Olieman, Frank van de Scheur en Atze-Jan van der Goot bedanken voor de mogelijkheid die ze Mathijs en mij geboden hebben om te participeren in een groots opgezet internationaal Unilever onderzoeksprogamma. Dit heb ik als zeer leerzaam ervaren.

Met veel plezier denk ik terug aan de contacten met Silicon Graphics (tegenwoordig SGI). Met name de cursussen in het kader van de Powergroup en de directe interactie met experts op het gebied van supercomputing heb ik erg op prijs gesteld. Ruud van der Pas, Ronald van Pelt, Peter Michielse en Bart Mellenberg: bedankt !

Secretariële ondersteuning werd altijd vriendelijk en correct verzorgd door (in chronologische volgorde): Greet van der Voort-Kamminga, Bartie Bruggink, Gery Stratingh, Yvonne Bruggert, Nicole Haitjema, Annemiek Vos, Ria Stegehuis-de Vegte en

Brigitte Sanderink. Rik Akse zorgde voor een keurige afhandeling van de financiële zaken.

Ik wil Ben Betlem, Niels Kruyt, Ties Bos, Martin van der Hoef en Peter Roos hier nogmaals bedanken voor de bijdrage die ze geleverd hebben in de diverse afstudeercommissies binnen het promotieproject.

Ook buiten kantooruren om heb ik me altijd uitstekend vermaakt met mijn collega AIO's in Enschede. Met groot plezier denk ik terug aan de diverse borrels, kroegtochten en etentjes, het zaalvoetballen met Proceskunde en vooral ook het karten om de Briels trofee en De Dhont Cup met Computational Chemistry (nog altijd ongeslagen binnen CT !). Reinier, Harald, Johan, Frank, Roelof, Nico, Wouter, Hein, Wim, Margie en José, bedankt !

Een speciaal woord van dank is op zijn plaats voor mijn goede vriend en paranimf Martijn Oversteegen. Tinus heeft in de beginperiode een zeer belangrijke rol gespeeld door mij te attenderen op de simulatietechnieken uit de Moleculaire Dynamica. De basis voor dit proefschrift is in die periode gelegd. Verder is hij de afgelopen jaren altijd goed geweest voor veel gezelligheid, een luisterend oor en een kritische noot op zijn tijd. Tinus, het was me een groot genoegen !

Tot slot wil ik mijn ouders, Peter en Ine, en mijn broers (paranimf) Tom & Rick bedanken die samen een solide basis vormen waar ik altijd op kon terugvallen. Allemaal ontzettend bedankt !

Bob.

Levensloop

Bob Hoomans werd geboren op 2 augustus 1971 in Oldenzaal waar hij ook de lagere school bezocht. In 1989 behaalde bij het VWO diploma aan het Thijcollege te Oldenzaal.

In september 1989 werd begonnen met de studie Chemische Technologie aan de Universiteit Twente in Enschede. In het kader van deze opleiding liep hij van september 1993 tot maart 1994 stage bij het Joint Research Centre (JRC) in Ispra, Italië. In januari 1995 studeerde hij af bij de vakgroep Proceskunde op het onderwerp discrete deeltjessimulatie van gas-gefluïdiseerde bedden.

In juni 1995 trad hij in dienst als promovendus (AIO) bij de vakgroepen Chemische Fysica (later Computational Chemistry) en Proceskunde waar hij onderzoek verrichte op het gebied van granulaire dynamica van gas-vast tweefasenstromingen. De resultaten van dit onderzoek vormen de basis voor dit proefschrift.

In oktober 1999 trad hij in dienst als CFD engineer bij DSM Research in Geleen.